Universitat Autònoma de Barcelona

Controlled release systems for dental hypersensitivity. Study of Liposomes and novel Metal-Organic Frameworks as cannabinoids carriers

Jorge Rodríguez Martínez

Universitat Autònoma de Barcelona

Controlled release systems for dental hypersensitivity. Study of Liposomes and novel Metal-Organic Frameworks as cannabinoids carriers.

Jorge Rodríguez Martínez

Doctoral Thesis

PhD programme in Chemistry

Directors:

Prof. Manuel Valiente Malmagro

Dr. María Jesús Sánchez Martín

Department of Chemistry

Faculty of Sciences

2022

Universitat Autònoma de Barcelona

Doctoral Thesis

PhD programme in Chemistry

Controlled release systems for dental hypersensitivity. Study of Liposomes and novel Metal-Organic Frameworks as cannabinoids carriers.

Jorge Rodríguez Martínez

2022

This PhD thesis has been carried out in the Centre GTS (Grup de Tècniques de Separació en Química) at the Department of Chemistry of the Universitat Autònoma de Barcelona, under the supervision of Professor Manuel Valiente Malmagro and Dr. María Jesús Sánchez Martín.

Prof. Manuel Valiente Malmagro

Dr. María Jesús Sánchez Martín

Y si no es a la primera

Persevera, persevera.

Siempre recuerdo estas líneas de un poema titulado “Vuelve a intentarlo” de “The Children's Book of Virtues”. Mi tía Mari y mi abuela Amor me lo leían cuando era pequeño, y yo solía enrabietarme porque no todo sale siempre bien a la primera (más bien casi nada). Hoy me parece la frase perfecta para describir cualquier tesis, investigación científica o reto de la vida en general.

ACKNOWLEDGMENTS - AGRADECIMIENTOS

Nunca se me han dado bien estas cosas y siempre he odiado ese sentimiento cuando sabes que el momento de una despedida inevitable se acerca. Desde luego serán unas de las páginas más difíciles de toda la tesis, sino las que más.

Me mudé a Barcelona en marzo de 2018 y sin duda formará parte de mí para siempre. La tesis ya está llena de ciencia, por eso he querido hacer un pequeño homenaje en la portada a esta ciudad con un plano del Eixample, el barrio que ha sido mi casa durante esta etapa. Desde luego, lo que más valoro de estos años es el tiempo, los recuerdos, las lecciones y las personas con las que he vivido todos esos momentos. Estoy muy agradecido por como he evolucionado estos años y no hay suficientes palabras para expresarlo, pero he intentado hacerlo lo mejor posible en estas páginas. Gracias Barcelona.

Antes de nada: ¡¡¡PERDÓN POR SI ME DEJO A ALGUIEN!!!

La verdad que nunca fue mi sueño hacer el doctorado, pero ahora no me imagino no haber vivido y disfrutado esta experiencia y estos años en GTS. Gracias por crear un grupo donde desde el primer momento me sentí acogido, querido e incluido por todos. GTS no es sólo un grupo de investigación, ahora también es parte de la familia que se elige y me siento muy afortunado de formar parte de él.

Manolo gracias por confiar en este biotecnólogo descarrilado que no sabía cuestiones tan básicas como las leyes de Fick; tu pasión por la ciencia es contagiosa y eres un gran ejemplo e inspiración por el continuo aprendizaje y crecimiento tanto personal como profesional. Gracias por hacer de guía y de soporte todo este tiempo, a la vez que lo acompañabas de sentido del humor. Siempre alucinaré con tus historietas y batallitas (menos las que eran a las 19.00 horas de la tarde…), tu sistema de rombos o el cartelito totalmente cierto de “deadlines amuse me”, entre otras muuuuchas cosas (lo que pasa en los “dental hubs” se queda en los “dental hubs”). Y aunque haya que perseguirte siempre en busca de firmas y de correcciones, al final siempre sacas un hueco en tu apretada agenda y no se me ocurre un mejor director para dirigir la tesis. Ah, y por último y no menos importante ¡gracias por todo el delicioso jamón claro! Has dejado el nivel demasiado alto y ahora cualquiera que no sea el tuyo me parece malo…

Recuerdo perfectamente mi primer día en GTS, estaba muy nervioso, ciudad nueva, trabajo nuevo, gente nueva… Mari, fuiste la persona que me recibiste en la tabla periódica del departamento y a los cinco segundos de hablar contigo supe que estaría en buenas manos, y no me equivoqué. Gracias por hacer de mami científica y por todo el apoyo incondicional, sobre todo al principio cuando íbamos dando tumbos como pollo sin cabeza y no sabíamos ni como encarrilar esto. Gracias por estar ahí cuando lo necesitaba. Eres una crack y una luchadora, estoy seguro de que vas a llegar muy lejos y espero estar ahí para verlo. Aunque no todo iba a ser ciencia… las cervezas, las bravas y los viajecitos también nos han ayudado mucho. Tenemos que volver a Laponia a ver si esta vez hay más suerte con las auroras y pasamos un poco más de frío que la última vez.

Sandra, mi eterna BMQ (expired) y reina actual de acabados húmedos, fiel compañera de batallas y locuras. Creo que el primer día que llegué a Biomat con mis padres, mi madre se quedó tranquila cuando vio las pegatinas de minions en la puerta, sentí su mirada de alivio al reconocer que era el lugar indicado para mí. Desde luego esta tesis no habría sido posible sin ti y va a ser súper raro dejar nuestro reino. Tenerte como hermana de doctorado ha sido una de las mejores cosas de

esta etapa, haces que el trabajo sea menos trabajo y llenas la vida de la gente que te rodea de felicidad y locuras. A partir de ahora estaremos un poquito más lejos, pero no pienses que te vas a librar de mi tan fácilmente y por mucho que te pese, tendrás que venir de visita a verme a tu amado Madrid.

Mi querida Manuela, emérito visir del Reino de Biomat y jefe del ICP Hole. Fuiste una de las primeras personas que conocí cuando entré en GTS y siempre has estado ahí para todo. Ha sido un gusto haber podido trabajar contigo y he aprendido un montón de ti. Pero afortunadamente también hemos compartido otros momentos menos laboratoriosos como las discotecas, días de playa y montaña, viajes, muchas cervezas y bravas, las clases de bodyjump y las épocas eurovisivas y de manuvision. Con muchas ganas de nuestra próxima aventura en Turín y de todas las que nos quedan… Siempre tendrás un huequito en mi hogar para lo que necesites, sea donde sea (aunque a veces te quiera estrangular por tu infinita discreción y por no ser una cotilla mala).

Mis queridos minions: Paula, Óscar, Anna, Serena y Adrià. Desde luego que esta tesis os pertenece más que a mí. Una de las cosas más bonitas de esta etapa ha sido compartir con vosotros tantos momentos. Con que hayáis aprendido la mitad de todo lo que yo he podido aprender de cada uno de vosotros sería todo un logro. Paulita creo que tú confiabas mucho más en los MOFs que yo, gracias por todos esos afterworks en el Alaska y por siempre tener una sonrisa, incluso en los momentos más duros de la investigación. Aún nos quedan muchas fiestas pendientes. Oscarito, aún recuerdo tu primer día queriendo aparentar formalidad… te duró poco! Gracias por construir esta sana y bonita amistad y por incluirme en tu familia junto con tu nañi, espero vuestra visita. Ay mi Anna… estoy seguro de que por muchos kilómetros que nos separen siempre estaremos el uno para el otro, vales millones y vas a conseguir todo lo que te propongas, sabes que siempre estaré ahí para lo que sea y cuando sea. Serena, “my Italian girl”, I am missing you since you left GTS, you were always involved with us in the lab, but also in the rest and most important mandatory traditions of the group (tiramisu, coconut balls, Eurovision or Ana y los 7). I wish you the best in your new stage in Dublin, since we cannot meet you in Torino maybe we can visit you… Adrià, tú has vivido el estrés de la recta final. Como ya te dijo Sandra, desde el primer día apuntabas maneras. Siempre estuviste implicado en todo y te has apuntado a cualquier bombardeo, compaginando tus clases y exámenes. Queda pendiente ir al ruso de Terrassa…

Clara, contigo he pasado horas puliendo dientes, incluso manualmente… Fuiste la primera persona conocida (no conviviente) que vi tras el confinamiento, todavía me acuerdo de tu mascarilla de Batman. Me he reído demasiado, a la vez que he aprendido mucho de tu creatividad y de tu don de gentes innato. Aunque al final esta tesis no haya sido de blanqueamiento dental, siempre lo llevaré en mi corazoncito. No puedo no mencionar los momentos épicos que nos dieron los lefosomas y el sodium chloride. Aún nos quedan pendientes la inauguración de tu pisazo, más escapadas como la de Bilbao y muuuuuuchas cervezas.

Gracias a Gorka, Bicpig, demás unicornios y mascotas, plantas y decoración de Biomat. Hacéis que el reino sea un lugar más ameno donde trabajar, espero que las próximas incorporaciones os sepan cuidar bien.

Iris, Stone Queen por excelencia. Dices que soy como un gato porque puedo ser adorable y rancio al mismo tiempo, y tienes razón. Gracias por salvarme siempre y resolver dudas químicas a tu biotecnólogo de confianza. Porque, aunque estés muy liada y vayas con mil cosas, siempre eres capaz de sacar un rato para ayudar a la gente. Pase lo que pase siempre seremos Ginfaxi team, cada uno con sus locuras, nadie puede arrebatarnos ese espléndido fika. Perdóname por ese

“primavera trompetera” en los micro-CT de tus amadas piedras. Espero que los franceses te estén tratando como te mereces y en algún momento habrá que planear una visita a Pau. No te deseo suerte porque no la necesitas, eres una investigadora nata, te gusta y se nota.

Mon, lo primero que me dijiste mi primer día cuando entré en tú despacho fue: ¿te gusta comer? Y a los pocos días entendí todo y después de más de cuatro años lo entiendo aún más… Un pilar fundamental de GTS, comprensiva y profesional, dispuesta a ayudar a todo el mundo cuando lo necesita. Pero, además, una pieza clave en el buenrollismo y en la cohesión del grupo. Siempre dispuesta a cualquier plan, desde un té de apoyo en la ofi, a cervezas y bravas, karaokes, pádel o escapadas de fin de semana con Soplica. Estoy deseando vivir Eurovisión en directo a tu lado, muchas más ediciones de calendarios y mil momentos más juntos.

Las actuales y dignas sucesoras de plantas, Marcia y Marilyn. Desde el domingo que nos animasteis a beber chupitos en la playa supe que erais unos buenos fichajes de GTS. Marcia, compañera de rotavapor y liposomas, gracias por esa deliciosa yuca y esos magníficos aguacates cubanos. Siempre ayudándonos el uno al otro en todo lo que podemos. Marilyn, una super mamá científica, corriendo de un lado para otro y siempre con una botella de tequila en el bolso. Que deciros que no sepáis ya, me encantáis y hemos pasado grandes momentos juntos y muuuuchas risas. Aun nos quedan muchas fiestas pendientes y muchos chupitos que beber. Os deseo lo mejor tanto en GTS y en la tesis, como en vuestra vida personal, porque os lo merecéis. Espero estar a vuestro lado en todos vuestros logros y momentos.

Thanks to my dear Chinese colony. Jing Jing, I have enjoyed a lot with you from the beginning, Miranda trip, your Spanish wedding or in the club with Ting Ting. I still remember you mixing zurracapote in your office like your own baby. My unconditional Tintina, I am missing you from the day that you finished your PhD stage, and you came back to China. We shared so many moments together in the UK during your experiment, but also after that in SAF for the “chicha”, learning Chinese and Spanish with songs and bad words, drinking beers and eating Manolo potatoes, and much more. You are my Chinese soulmate. Thanks also to your husband Wei for his support in the SAF and for always being one of our team. Lou, we were PhD candidates of the same year and we have been moving forward in parallel with our own research like brothers. You are a great person and a hard worker, but also very funny and we have laughed a lot with you, as your one finger moment. I always wish you the best and I hope that we can all meet soon in China, in Spain or in any place, I am missing you, Chinese colony (I want to meet your pets). My dear Dong, the coolest Chinese. We have enjoyed a lot these years and I am sure that we will still have more moments together. I wish you the best in your last year of PhD stage and I hope that you can stay in Europe with your cute girlfriend after that some years more to keep you close by.

Nithya, synchrotron queen. Thanks for all your delicious and a little spicy (according to you…) Indian food and for being the only one that knocked Biomat door. I wish you the best and I hope that everything in India is going well, and we could visit you some day.

Júlia, mira que Manu había dejado el listón muy alto, pero tú no te quedas atrás. Estoy tranquilo porque el Reino de Biomat se queda en buenas manos contigo. Espero que eches buenas broncas a todo aquel que intente desordenar o robar material del reino. Gracias por todas esas gestiones a las que me has ayudado desde la distancia mientras estaba estos últimos meses en Suecia.

Laia, aún recuerdo que a los dos días de entrar en GTS te apuntaste sin dudarlo a participar en la primera edición del sexy calendar y te trajiste todo tu arsenal de maquillaje y corsés. Gracias por esa deliciosa repostería, mucho ánimo y fuerza con lo que te queda, ya eres la siguiente.

Víctor siempre recordaré nuestras “peleas” por conseguir la bomba de vacío y por los primeros intentos frustrantes con el AF4 y HPLC. Mucha suerte en la nueva etapa que empiezas como doctorando, estoy seguro de que te irá genial.

Reihan, el nuevo fichaje. Mucha suerte tanto dentro como fuera de GTS, eres toda una caja de sorpresas y siempre muy agradecida. Espero que te apuntes al calendario el año que viene y a enseñarnos tus habilidades con los tatuajes.

Montse López, la elegancia de GTS. Siempre con una sonrisa y un porte envidiables. Me acompañaste y apoyaste los primeros días de mi primera aventura sueca. Tus mails y gestiones como Reina de la Unidad de Química Analítica siempre serán los mejores. Gracias por preocuparte por ver cómo estaba, sobre todo en esta recta final.

Gus, el chico para todo. Gracias por ese enfoque “get out of the building” y por hacerme pensar más allá de la investigación básica, aunque cuando hables con tantas siglas sea difícil seguirte. Gracias también por tu humor característico y por las lecciones de vino (cuando tenga dudas te seguiré preguntado).

Roberto, el rey de los sincrotrones, otro descarrilado como yo en un grupo de químicos. Gracias por todo el apoyo, consejos y ayuda con los MOFs, y por poner siempre lo mejor de ti y el mayor esfuerzo en que las proposals sean perfectas y los experimentos se planeen con cabeza. Gracias también por tener siempre tiempo para preguntarme cómo iba todo, te deseo lo mejor.

Alba y Mª Dolors gracias por vuestra gran labor y gestiones, siempre persiguiendo a Manolo para conseguir firmas y hacer que todo vaya de la mejor manera posible.

Gracias a toda la gente que ha pasado por GTS con secondments de diferentes proyectos y otro tipo de estancias, es imposible enumerar a todos. Especial mención a todo el equipo cubano, sobre todo a Toky por esos deliciosos aguacates, por su dulzura y por siempre preocuparse de todos nosotros. También gracias a toda la gente que ha venido de Argentina y nos ha traído un pedacito de su cultura.

Gracias por dejarme participar en el proyecto NEOSETAC donde me he sentido más en mi salsa de biotecnólogo que en la propia tesis. Gracias a este proyecto he podido conocer a nuestras compis de CliniSciences, fieles seguidoras de nuestro calendario solidario. Gracias también por hacerme ese training para refrescar los cultivos celulares antes de irme Suecia en 2019. Thanks to the rest international members who have been participating in this project during these years, especially to the Swedish team in Karolinska Intitutet. Thanks to Professor Moustapha Hassan and his research group for welcoming and taking care of me for six months. Gracias también a la chupipandi de mis primeros meses en Suecia, especialmente a Inés, Alicia y Silvia.

Gracias a todo el equipo de la UIC que ha hecho posible esos ensayos clínicos, digamos que mi nueva aventura profesional tras la tesis está influenciada en parte por este proyecto. Gracias también por prestarnos vuestro estupendo colorímetro en los últimos ensayos *in vitro* cuando el de GTS ya había pasado a mejor vida. He aprendido mucho sobre la aplicabilidad de los productos dentales con vuestro punto de vista odontológico.

Gracias al equipo del proyecto Dentalytics, ya llevamos más de dos años detrás de ello y aunque aún no sabemos cómo va a continuar esta aventura, he aprendido un montón de todo lo que hemos hecho durante este tiempo, así como ver la ciencia desde distintos puntos de vista y como una tecnología que empezó en el laboratorio puede convertirse en algo aplicable.

Gracias también a todos los minions que han pasado por GTS estos años. Al igual que a los secondments, es imposible nombrar a todos porque han sido muchos. JT, tú serás el minion de plantas adoptado por dientes preferido, zalamero nato, siempre liándola, dispuesto a apuntarse a todo y a hacer pasar un buen rato a la gente. Indira, my partymate and Voll-Damm lover, it was sad to say goodbye, but now you are again in Barcelona, I hope we can meet more. Gracias también a las otras minions de dientes, Anna por enseñarme a pulir y Mariona por cortar mandíbulas hasta las diez de la noche. María (Manu) por ser vecina de la Carrasco, Fa, Greek team (how to forget o Spanish pirula), Montsito, Marco, Taraneh, Joan, Veroniki, Sergi, Alejandro, Shazra, Nereida, Raquel… y muchos más!

José Amigo gracias por hacer de la Quimiometría una herramienta útil y entendible, sin tu curso no habría sido capaz de tratar los datos del experimento del sincrotrón. Gracias también por ser el mejor anfitrión que alguien puede tener en Bilbao, aún recuerdo el primer día en el Tegobi o el txangurro y el chuletón de la última vez.

Lucía, primero de todo gracias por aceptar el marronazo de leerte esta tesis, espero que lo hayas disfrutado al menos un poquito. Nos conocimos en época prepandémica y ahora nos volvemos a reencontrar. Un alma libre, siempre dispuesta a cualquier plan. Te deseo lo mejor en tu nueva etapa en Barcelona y espero que algún día me puedas enseñar Argentina. Nunca olvidaré tu chocotorta.

Gracias al resto de compis de la planta de Analítica por todos los favores, la ayuda y las risas. Mucha suerte en la nueva etapa a todos los que habéis acabado y mucha fuerza a los que estáis a nada de terminar.

Gracias a toda la gente de la secretaría del Departamento de Química por hacer posible todas las gestiones, especialmente a Elena. Gracias también al equipo de conserjería norte por todos los paquetes recogidos y por alegrarte los días siempre con sus sonrisas y mejor humor.

Gracias a toda la gente de los servicios de análisis del SAQ, ICN2 y especialmente al equipo de microscopía. Martí, Cris y Emma con vosotros el análisis de muestras siempre fue más divertido. Gracias también a Ibraheem por todo el soporte, ayuda y paciencia en la beamline de MIRAS en ALBA sincrotrón.

Gracias a todos los participantes del Sexy Calendar. Como una idea que surgió en una fiestónoma lleva ya casi cuatro años y cada vez llega a más gente. Nos lo pasamos bien y disfrutamos, a la vez que destinamos los beneficios a una buena causa.

Gracias también a todo el personal de cafeterías y bares que nos ayudaban a evadirnos de la ciencia. Sobre todo, al equipo de la cafetería de Ingeniería, porque gracias a vosotros siempre se empieza el día con buen pie.

Gracias a todas las personas que estaban en GTS cuando empecé, pero que terminaron a los pocos meses de llegar yo. Sergi, tú fuiste el RRPP encargado de hacerme el tour por GTS. Gracias por recibirme, incluirme y acogerme en Biomat de la mejor forma. Gracias por toda la cerveza, por ser del team Barcelona, por el finde en tu pueblo, por toda la comida casera, por ser una cotilla mala más, por las fiestas de Sants y por siempre querer café por las mañanas. Aunque seas un rancio y ni grabases un vídeo para la madre de tu hijo, se te quiere mucho. Vero, recuerdo el día que nos presentaron, tú acababas la beca y yo la empezaba. Gracias por darme mucha fuerza y ánimos, parece que han servido porque aquí estamos. Espero que podamos repetir pronto un fin de semana como el del carnaval del vino prepandemia. ASU, aún no te hemos ido a ver a Pau, pero tranquila que lo haremos. Fuiste mi primer ejemplo de tesis, parece que fue ayer… Gracias

por estar siempre dispuesta a desconectar con unas cervezas y a apuntarte a cualquier escapada, aunque tengas que coger el coche y venirte desde Francia.

Gracias a los exGTS que he podido conocer en este tiempo y toda la gente del grupo de cerveceros. Marta creo que nunca me perdonarás lo de Portaventura, tampoco he puesto la frase de la Pantoja en la tesis, lo nuestro no tiene solución. Gracias por todo el pádel, las cervezas y bravas after pádel y todas las escapadas llenas de risas y aventuras. Javi Muro, gracias por todos esos chistes malos. Elena, desde el COVID nos hemos visto poquísimo, gracias por esas cervezas entre semana y por todos esos planes de findes, incluido el viaje Miranda-Haro-San Sebastián. Albert, después de mucho hablar de ti por fin te conocí hace unos meses, gracias por ser el mejor compañero de kayak y por hacer una barbacoa deliciosa.

Borjita, no te libras… Gracias por los stickers, por las ofertas de chollómetro, por buscar siempre un sitio de bravas digno, por hacer de guía en nuestras expediciones, por hacerme reír tanto, por ser Doña Ruperta y por quejarte de todo. Aunque a veces seas un rancio (como yo), es parte de tu encanto y sello personal, gracias por ser como eres. Aunque te cueste admitirlo, siempre estás deseoso de que os haga visitas a vuestro pueblo pijo. No te flipes al leer esto, pero serás una de las personas a las que más eche de menos sin ninguna duda. Espero que ya estés al tanto de los mejores bares y restaurantes de Madrid porque espero tu visita. Recuerda mirar siempre casas con una habitación extra…

Gracias a los padres de Sandra, gracias por acogernos siempre de la mejor manera posible y por alimentarnos con las delicias de Miranda. Gracias también por venir de visita a Barcelona y acogerme en vuestros planes, me siento uno más de la familia. Alberto tus delgadillas son dignas de estrella michelín, admiro tu creatividad y vitalidad. Mar, mi alma gemela del 25 de octubre, siempre estaremos ahí apoyándonos el uno al otro mientras el resto hace locuras, como saltar desde un puente.

Mis fieles compis de piso en Barcelona, Silvia y Alba. Después de mis padres, sois las personas que más años habéis aguantado una convivencia conmigo. Desde luego, tras 4 años lo que empezó siendo una convivencia se ha convertido en una gran amistad. Aunque somos muy distintos, nos hemos compaginado demasiado bien y hemos vivido muchas cosas juntos: mudanzas, viajes, fiestas, confinamientos, dramas, risas… pero la verdad es que todo han sido muy buenos momentos. No os imagináis la pena que me da que en cierto modo se acabe. Aunque eso no quita para que nos queden mil cosas pendientes como Lisboa o los pueblos negros, ahí lo dejo…

No puedo pensar en estos años en Barcelona sin acordarme de Calzone. Gracias por adoptarme y acogerme de la mejor manera como uno más del máster. Porque esta etapa no hubiese sido igual sin esos días de playa y Costa Brava, sin el Camino de Ronda, sin los buffets libres de sushi, sin las noches de Almo2bar, sin las cervezas afterwork en el Gato Negro, sin las empanadillas y calimochos de Xao, sin las celebraciones de cumpleaños, sin la Chococochurros, sin el descubrimiento de Elyella en Razz, sin el concierto de La Raíz en el pueblo maldito, sin la casa rural, sin los pelotazos del vermut de Sagrades Tannines, sin la escapada a Xeraco, sin el arroz al horno “digestivo” en pleno verano, sin la Red Velvet o la Carrot Cake del Mercadona o sin los días de salir a tomar algo y que luego se lie como la última vez en Perros Mediterráneos. Estoy seguro de que seguiremos viviendo más momentos como estos en el futuro.

Echando la vista atrás no puedo no acordarme de mi etapa en Valencia. Fue mi primer año de independencia, en el que creamos la pequeña familia de Putupiso en nuestra Miraculosa. Esta ciudad nos marcó a todos… Toda la gente que conocimos, el grupo de tardes del máster TEQ,

todas las experiencias que vivimos, todo lo que aprendimos y lo bien que lo pasamos. Desde entonces siempre llevo un pedacito de terreta dentro de mí. Tenemos pendiente una escapa para rememorar nuestras tardes en el Molino, en las fallas con sus mascletás, en las escaleras de la lonja, en las happy hours del Redcap, una noche en Piccadilly o pretendiendo aparentar ser señoras de bien en el Café de las horas con una buena sangría de vino blanco.

Estos agradecimientos tampoco tendrían sentido sin la gente de Biotec de la ULE y más especialmente sin mis Calostrochos, "once a lion always a lion". Juntos empezamos nuestra vida científica y este 2022 es el décimo aniversario desde que nos conocemos. Una de las mejores etapas de mi vida sin ninguna duda, porque, aunque teníamos que estudiar y hacer horarios imposibles entre trabajos grupales, prácticas de laboratorio y biblioteca, siempre había hueco para muchas risas, jueves de espichas, tardes de cortos, chambelanes, rutas de limonada, fiestas de Villafañe y mezclas de alcoholes (con un poquito de azúcar claro). Cada vez que nos reunimos es como si no pasara el tiempo y eso pasa con muy poca gente. Gracias por seguir ahí después de tantos años y por esos reencuentros navideños, espero que este diciembre los podamos retomar.

No puede faltar una mención especial a Estos/Estos./estos/estos., lleváis diez años estando ahí siempre, para la bueno y lo malo, aguantando mis borderías y particular forma de ser. Puedo decir sin dudarlo que sois las personas con las que más confianza tengo y con las que más me puedo reír del mundo. Ojalá nos pudiésemos ver más a menudo, aunque de momento no lo estamos haciendo nada mal. Dicen que los amigos de la universidad son para toda la vida y estoy seguro de que es nuestro caso. Hay que ir buscando una nueva lectura a la altura de Holden para nuestras próximas vacaciones de calas inaccesibles, madrugones y achicharramientos bajo el sol.

Siguiendo este viaje atrás en el tiempo, siempre recuerdo muy buenos momentos de mi etapa preuniversitaria y toda la buena gente que conocí en IES Lancia, IESO Astura y Pedro Aragoneses Alonso. Gracias a ese grupo de Cumpleaños atrasado porque después de tantos años ahí seguimos, y siempre que coincidimos y nuestras apretadas agendas lo permiten, sacamos un hueco para vernos.

Ya casi para terminar, pero no por ello menos importante, tengo que dar las gracias a toda la gente de mi tierra leonesa y de mi pueblo Villafañe. Mis raíces, el lugar donde crecí, no me imagino una infancia mejor que la vivida en un pueblo. Mi eterno e incondicional Grupo Entrañable, nos conocemos desde que tenemos memoria y hemos pasado por todas las etapas de la vida juntos, niñez, adolescencia y edad adulta (por mucho que nos pese ya…). Éramos felices con muy poco, tardes de bicicleta por el canal, noches de escondite en la plaza, días enteros en la piscina de Merche, noches en el Cueto viendo las estrellas, días en el bar de Jose comiendo Jumpers y helados, cuando nuestra mayor preocupación era que con qué vasos íbamos a causar tendencia en las fiestas de los pueblos o que teníamos que participar sí o sí en cada actividad organizada en las fiestas de Villafañe. Hemos vivido muchas "primeras veces" juntos y si empiezo a enumerar, esto sería más largo que toda la tesis. Porque, aunque los caminos de la vida de cada uno nos separen kilómetros, siempre estamos y estaremos ahí.

Por último, mil gracias a toda mi familia. A mis abuelos, la que aún está (y esperemos que por muchos años más) y los que no, porque siempre fui el mimado de la familia y me dabais todos mis caprichos. Tita, Nano, Luisa y Jandro, gracias por el chicharro guisado, por las patatas amarillas, las canciones, los potajes, por cuidar de mí siempre y por seguir haciéndolo, el niño ya no es tan niño… Gracias a mis tíos, sobre todo a mi madrina Yoli por siempre hacerme reír y mi tía Mari por todos los momentos vividos juntos. Gracias a mis premos por siempre reservarme un hueco para salir por ahí y hacer excursiones de los nuestras, como la última con los enanitos

de Blancanieves. Gracias a Leo, el pequeño de la familia, por estar cargado de energía y hacernos reír mucho. Gracias a Zeus por haber sido el compañero más fiel. Gracias a mis padres por la educación que he tenido y porque nunca me ha faltado de nada. Gracias por dejarme estudiar y encarrilar mi vida según lo que yo quería hacer, por ayudarme en cada mudanza, por ir a buscarme a Villanubla cada vez que iba de Barcelona a León, por todos los festines y manjares para coger reservas, por las tortillas, por los botillos, por los tomates de la huerta… se acaba una aventura y empieza otra, ahora un poco más cerca de casa.

Cuando al principio de los agradecimientos decía que iban a ser unas de las páginas más difíciles de toda la tesis, sino las que más, no mentía. Estoy feliz por cerrar esta etapa y tengo muchas ganas de mi nuevo proyecto, pero también estoy muy triste por terminar algo que ha sido tan bonito y enriquecedor.

Con todo mi cariño y siempre en mi corazón,

JRM

FINANCIAL SUPPORT

This doctoral stage has been developed with public funding through:

- FI-2018 scholarship, Fons Social Europeu and Agència de Gestió d'Ajuts Universitaris i de Recerca (AGAUR, Generalitat de Catalunya).

- Pre-doctoral grant in Chemistry Department, Universitat Autònoma de Barcelona (UAB).

- CHEMNEXUS, CTM2015-65414-C2-1-R, Ministerio de Economía y Competitividad de España (MINECO).

- Synchrotron granted proposals in ALBA Synchrotron and Diamond Light Source.

- NEOSETAC project (GA778325), H2020-MSCA-RISE-2017, European Union funding for Research & Innovation, Marie Curie Actions.

SHORT-TERM STAYS

Different short-term stays have been carried out during the period of this doctoral stage, where valuable collaborations have taken place, along with the acquirement of novel insights in several areas of knowledge:

- 15/05/2018 – 20/05/2018. Synchrotron IR microspectroscopy study to characterize the effect of novel whitening treatment into dental hydroxyapatite; CELLS - ALBA Synchrotron, Cerdanyola del Vallès (Barcelona).
- 06/09/2018 – 10/09/2018. Study of selenium speciation and distribution of Se, Mo, V, W in Se-enriched wheat plants treated with plant biostimulants; DIAMOND, Didcot (United Kingdom).
- 11/01/2019 – 10/04/2019. Karolinska Cell Therapy Center, Karolinska Institutet and Karolinska University Hospital, Stockholm, Sweden. Under the European Union funded H2020-MSCA-RISE-2017 project NEOSETAC (New Selenium-based Targeted Nanocapsules to treat Breast Cancer).
- 12/06/2019 – 13/06/2019. Influence of amelogenin in the dental remineralization process; ALBA Synchrotron, Cerdanyola del Vallès (Barcelona).
- 14/06/2019 – 02/07/2019. Karolinska Cell Therapy Center, Karolinska Institutet and Karolinska University Hospital, Stockholm, Sweden. Under the European Union funded H2020-MSCA-RISE-2017 project NEOSETAC (New Selenium-based Targeted Nanocapsules to treat Breast Cancer).
- 27/09/2019 – 07/10/2019. Karolinska Cell Therapy Center, Karolinska Institutet and Karolinska University Hospital, Stockholm, Sweden. Under the European Union funded H2020-MSCA-RISE-2017 project NEOSETAC (New Selenium-based Targeted Nanocapsules to treat Breast Cancer).
- 29/10/2019 – 01/11/2019. Study of the synergistic effects of Se-compounds and stablished anti-cancer drugs on breast cancer cells; CELLS - ALBA Synchrotron, Cerdanyola del Vallès (Barcelona).
- 28/11/2020 – 29/11/2020. Synchrotron IR microspectroscopy analysis of tooth remineralization process assisted by amelogenin; CELLS - ALBA Synchrotron, Cerdanyola del Vallès (Barcelona).

- 01/12/2020 – 02/12/2020. Synchrotron IR microspectroscopy study: potential analgesic delivery systems loaded with cannabinoids for oral health; CELLS - ALBA Synchrotron, Cerdanyola del Vallès (Barcelona).
- 21/01/2022 – 20/03/2022. Karolinska Cell Therapy Center, Karolinska Institutet and Karolinska University Hospital, Stockholm, Sweden. Under the European Union funded H2020-MSCA-RISE-2017 project NEOSETAC (New Selenium-based Targeted Nanocapsules to treat Breast Cancer).

ARTICLES AND PATENT NOT INCLUDED IN THIS THESIS

- Review article: "Tooth whitening: From the established treatments to novel approaches to prevent side effects" **Jorge Rodríguez-Martínez**, Manuel Valiente, María-Jesús Sánchez-Martín; August 2019 (Published), *Journal of Esthetic and Restorative Dentistry* (https://doi.org/10.1111/jerd.12519).
    - Top downloaded paper 2018-19 in *Journal of Esthetic and Restorative Dentistry*.
- Research paper: "Flash Tooth Whitening: A Friendly Formulation Based on a Nanoencapsulated Reductant" Clara Babot-Marquillas, Maria-Jesús Sánchez-Martín, **Jorge Rodríguez-Martínez**, Joan Estelrich, Maria-Antònia Busquets, Manuel Valiente; November 2020 (Published), *Colloids and Surfaces B: Biointerfaces* (https://doi.org/10.1016/j.colsurfb.2020.111241).
- **Jorge Rodríguez-Martínez** was acknowledged for his support in the following research paper: "Combination of Two Synchrotron Radiation-Based Techniques and Chemometrics to Study an Enhanced Natural Remineralization of Enamel" Sandra Diez-García, María-Jesús Sánchez-Martín, José Manuel Amigo, Manuel Valiente; March 2022 (Published), *Analytical Chemistry* (https://doi.org/10.1021/acs.analchem.1c05498).
- Patent: "Tooth Whitening Composition" (application number 1916023.3 and EP19382958.7) Manuel Valiente Malmagro, María Jesús Sánchez Martín, Clara Babot Marquillas and **Jorge Rodríguez Martínez**; PCT requested 03/11/2020.

RESUMEN

La hipersensibilidad dental o dentinaria se define como un dolor corto y agudo en respuesta a diferentes estímulos. Aunque existen numerosos tratamientos para combatir esta molestia, ninguno es totalmente eficaz, por lo que es necesario desarrollar nuevas estrategias. Un potencial candidato es el cannabidiol gracias a sus propiedades terapéuticas y moduladoras sobre determinados receptores ubicados en la cavidad oral que están involucrados en la respuesta de este dolor. Sin embargo, el cannabidiol también presenta desventajas, como su baja estabilidad química y su escasa solubilidad en soluciones acuosas. Por este motivo, los sistemas de administración controlada de fármacos pueden emplearse para encapsular este compuesto, evitando así estas dificultades. En este aspecto, las redes organometálicas de γ-ciclodextrina han ganado protagonismo en el ámbito de la biomedicina, debido a sus prometedoras características. Otro ejemplo más conocido y estudiado en el ámbito de la odontología son los liposomas de dipalmitoilfosfatidilcolina. Una limitación adicional del cannabidiol, además de la inestabilidad química, es su elevado coste. Por ello, otros compuestos homólogos o precursores como el olivetol pueden usarse como análogos en ciertos enfoques experimentales.

En esta tesis doctoral se pretende desarrollar una nueva formulación con potencial efecto analgésico basada en cannabidiol encapsulado en dos sistemas de liberación controlada de fármacos como una nueva perspectiva en el tratamiento de la hipersensibilidad dentinaria. Los sistemas de liberación controlada seleccionados fueron las redes organometálicas de γ-ciclodextrina y los liposomas de dipalmitoilfosfatidilcolina.

Las redes organometálicas de γ-ciclodextrina fueron sintetizadas utilizando el microondas analítico a partir de diferentes fuentes de potasio (KOH, KCl y KNO_3). Se investigó la encapsulación del olivetol como análogo de cannabidiol usando el método de impregnación y de co-cristalización. En cuanto a las propiedades estructurales, las redes organometálicas mostraron los típicos cristales cúbicos cuando se utilizó KOH, y morfologías trigonales al emplear KCl y KNO_3. El contenido de olivetol fue significativamente más alto cuando se emplearon KCl o KNO_3 en combinación con el método de co-cristalización, mientras que la encapsulación utilizando KOH y el método de impregnación fue muy pobre. Por lo tanto, se estableció una metodología basada en la síntesis usando el microondas y fuentes de potasio

como KCl o KNO_3, junto con el método de co-cristalización para la obtención de olivetol encapsulado en redes organometálicas de γ-ciclodextrina.

En el caso de los liposomas de dipalmitoilfosfatidilcolina, se estudió la encapsulación del olivetol como análogo del cannabidiol usando el método de hidratación en capa fina y dispersión mecánica empleando un rotavapor y la sonicación respectivamente. Ambas formulaciones de liposomas, con y sin olivetol, mostraron una morfología similar y una distribución de tamaño por debajo de 200 nm, a pesar de que el compuesto es encapsulado en la bicapa lipídica. Además, el contenido de olivetol fue cuantificado, haciéndolos adecuados como portadores del compuesto y para su aplicación *in vitro*.

Posteriormente, para evaluar la aplicación de las formulaciones sobre los dientes, se planteó un estudio *in vitro* usando dientes bovinos como modelo. Para ello, se realizó un análisis de espectroscopía infrarroja de fuente de sincrotrón sobre la estructura dental. Los datos obtenidos se trataron mediante el análisis de componentes principales que agrupó las muestras según la presencia del fármaco y/o la presencia de un sistema de administración controlada, revelando que ambos sistemas dirigieron el transporte del compuesto de forma eficiente, a pesar de que la carga de olivetol en las formulaciones de redes organometálicas fue menor que en los liposomas.

Teniendo en cuenta estas diferencias en términos de encapsulación entre ambos sistemas, la metodología desarrollada previamente para obtener las formulaciones de redes organometálicas se optimizó para explorar las mejores condiciones de síntesis. Para ello, se utilizó un diseño de experimentos basado en una metodología de superficie de respuesta para optimizar la encapsulación del olivetol y el rendimiento de la reacción. Se estableció un modelo cuadrático para el rendimiento de la reacción y un modelo de interacción de dos factores para la encapsulación del fármaco, en ambas fuentes de potasio (KCl y KNO_3). Con las condiciones óptimas, los valores experimentales para ambas respuestas mejoraron los resultados previos de forma significativa. Además, se demostró que las nuevas condiciones no comprometían sus propiedades estructurales.

Finalmente, para validar el uso del olivetol como análogo en las redes organometálicas, se llevó a cabo la metodología optimizada empleando el cannabidiol. Estas formulaciones mostraron las mismas propiedades estructurales que cuando se usó olivetol, a pesar de una pequeña pérdida de cristalinidad. Además, los resultados del rendimiento y los valores de encapsulación del cannabidiol fueron comparables a los del olivetol. Por lo tanto, la

sustitución del olivetol por cannabidiol en las redes organometálicas de γ-ciclodextrina no alteró los resultados previos, validando el uso del olivetol como análogo.

Teniendo en cuenta los resultados obtenidos, una metodología para el desarrollo de una nueva formulación basada en cannabidiol encapsulado en redes organometálicas de γ-ciclodextrina fue establecida y optimizada, validando el uso de olivetol como análogo de este compuesto. Además, la aplicación *in vitro* de esta nueva formulación mostró resultados prometedores, así como en la formulación de liposomas. Por lo que ambos sistemas de liberación controlada emergen como una nueva perspectiva para combatir la hipersensibilidad dentinaria.

RESUM

La hipersensibilitat dentinària es podria definir com un dolor curt i agut en resposta a diferents estímuls. Tot i que hi ha nombrosos tractaments per combatre aquesta molèstia, cap és totalment eficaç, per la qual cosa cal desenvolupar noves estratègies. Un candidat potencial és el cannabidiol gràcies a les seves propietats terapèutiques i moduladores de determinats receptors ubicats a la cavitat oral que es troben involucrats en la resposta d'aquest dolor. No obstant això, el cannabidiol també presenta desavantatges, així com la seva baixa estabilitat química i escassa solubilitat en solucions aquoses. Per aquest motiu, els sistemes d'administració controlada de fàrmacs es poden fer servir per encapsular aquest compost, evitant així aquestes dificultats. En aquest aspecte, les xarxes organometàl·liques de γ-ciclodextrina han guanyat protagonisme en l'àmbit de la biomedicina, degut a les seves característiques prometedores. Un altre exemple més conegut i estudiat en l'àmbit de l'odontologia són els liposomes de dipalmitoilfosfatidilcolina. Una limitació addicional del cannabidiol, a més de la inestabilitat química, n'és el cost elevat. Per això, altres compostos homòlegs o precursors com l'olivetol es poden fer servir com un anàleg en determinats enfocaments experimentals.

En aquesta tesi doctoral es pretén desenvolupar una nova formulació amb un potencial efecte analgèsic basada en cannabidiol encapsulat en dos sistemes d'alliberament controlat de fàrmacs com una nova perspectiva en el tractament de la hipersensibilitat dentinària. Els sistemes d'alliberament controlat seleccionats van ser les xarxes organometàl·liques de γ-ciclodextrina i els liposomes de dipalmitoilfosfatidilcolina.

Les xarxes organometàl·liques de γ-ciclodextrina van ser sintetitzades utilitzant el microones analític a partir de diferents fonts de potassi (KOH, KCl i KNO_3). Es va investigar l'encapsulació de l'olivetol com un anàleg del cannabidiol utilitzant el mètode d'impregnació i de co-cristal·lització. Pel que fa a les propietats estructurals, les xarxes organometàl·liques van mostrar els típics cristalls cúbics quan es va utilitzar KOH, i morfologies trigonals amb la utilització del KCl i KNO_3. El contingut d'olivetol va ser significativament elevat quan es van emprar KCl o KNO_3 en combinació amb el mètode de co-cristal·lització, mentre que l'encapsulació utilitzant KOH i el mètode d'impregnació va ser molt pobre. Per tant, es va establir una metodologia basada en la síntesi utilitzant el microones i fonts de potassi com el KCl o KNO_3, juntament amb el mètode de co-cristal·lització per a l'obtenció d'olivetol encapsulat en xarxes organometàl·liques de γ-ciclodextrina.

En el cas dels liposomes de dipalmitoilfosfatidilcolina, es va estudiar l'encapsulació de l'olivetol com un anàleg de cannabidiol utilitzant el mètode d'hidratació en capa fina i dispersió mecànica emprant un rotavapor i la sonicació respectivament. Ambdues formulacions de liposomes, amb olivetol i sense, van mostrar una morfologia similar i una distribució de mida per sota de 200 nm, malgrat que el compost és encapsulat a la bicapa lipídica. A més, el contingut d'olivetol va ser quantificat, fent-los adequats com a portadors del compost i per a la seva aplicació *in vitro*.

Posteriorment, per avaluar l'aplicació de les formulacions sobre les dents, es va plantejar un estudi *in vitro* utilitzant dents bovines com a model. Per fer-ho, es va fer una anàlisi d'espectroscòpia infraroja de font de sincrotró sobre l'estructura dental. Les dades obtingudes es van tractar mitjançant l'anàlisi de components principals que va agrupar les mostres segons la presència del fàrmac i/o la presència d'un sistema d'administració controlada, revelant que els dos sistemes van dirigir el transport del compost de forma eficient, malgrat que càrrega d'olivetol en les formulacions de xarxes organometàl·liques va ser menor que en els liposomes.

Tenint en compte aquestes diferències en termes d'encapsulació entre tots dos sistemes, la metodologia prèviament desenvolupada per obtenir les formulacions de xarxes organometàl·liques es va optimitzar per explorar les millors condicions de síntesi. Per fer-ho, es va utilitzar un disseny d'experiments basat en una metodologia de superfície de resposta per optimitzar l'encapsulació de l'olivetol i el rendiment de la reacció. Es va establir un model quadràtic per al rendiment de la reacció i un model d'interacció de dos factors per a l'encapsulació del fàrmac, a les dues fonts de potassi (KCl i KNO_3). Amb les condicions òptimes, els valors experimentals per a totes dues respostes van millorar els resultats previs de forma significativa. A més, les formulacions optimitzades van mostrar que les noves condicions òptimes no comprometien les propietats estructurals.

Finalment, per validar l'ús de l'olivetol com un anàleg a les xarxes organometàl·liques, es va dur a terme la metodologia optimitzada fent servir el cannabidiol. Aquestes formulacions van mostrar les mateixes propietats estructurals que quan es va fer servir l'olivetol, malgrat una petita pèrdua de cristal·linitat. Addicionalment, els resultats del rendiment i els valors d'encapsulació del cannabidiol van ser comparables als de l'olivetol. Per tant, la substitució de l'olivetol per cannabidiol a les xarxes organometàl·liques de γ-ciclodextrina no va alterar els resultats previs, validant així l'ús de l'olivetol com un anàleg.

Tenint en compte els resultats obtinguts, una metodologia per al desenvolupament d'una nova formulació basada en cannabidiol encapsulat en xarxes organometàl·liques de γ-ciclodextrina va ser establerta i optimitzada, validant l'ús d'olivetol com un anàleg d'aquest compost. A més, l'aplicació *in vitro* d'aquesta nova formulació va mostrar resultats prometedors, així com la formulació de liposomes. Per això ambdós sistemes d'alliberament controlat emergeixen com una nova perspectiva per combatre la hipersensibilitat dentinària.

SUMMARY

Dental or dentin hypersensitivity is known as a short and sharp pain in response to a variety of dental stimuli. Although numerous treatments exist to combat this discomfort, none of them are fully effective, so new strategies need to be developed. One potential candidate is cannabidiol due to its therapeutic and modulatory properties on certain receptors located in the oral cavity and involved in the pain response. However, cannabidiol also has some drawbacks, such as its low chemical stability and poor solubility in aqueous solutions. Taking into account these constraints, controlled drug delivery systems can be used to overcome such limitations by encapsulating this compound. In this respect, γ-cyclodextrin metal-organic frameworks have gained prominence in the biomedical field, due to their promising characteristics. Another example, better known and studied in the field of dentistry, are dipalmitoylphosphatidylcholine liposomes. An additional limitation of cannabidiol besides the chemical instability is its high cost. Therefore, other homologous compounds or precursors such as olivetol can be used as an analogue in experimental approaches.

In this doctoral thesis we aim to develop a new formulation with potential analgesic effect based on cannabidiol encapsulated in two controlled release drug delivery systems as a new perspective in the treatment of dentin hypersensitivity. The selected controlled release systems were γ-cyclodextrin metal-organic frameworks and dipalmitoylphosphatidylcholine liposomes.

γ-Cyclodextrin metal-organic frameworks were synthesized using analytical microwave from different potassium sources (KOH, KCl and KNO_3). The encapsulation of olivetol as a cannabidiol analogue was investigated using the impregnation and co-crystallization method. In terms of structural properties, the metal-organic frameworks showed typical cubic crystals when KOH was used, and trigonal morphologies when KCl and KNO_3 were employed. The olivetol content was significantly higher when using KCl or KNO_3 in combination with the co-crystallization method, while the encapsulation using KOH and the impregnation method was very poor. Therefore, a methodology based on the synthesis using microwave and potassium sources such as KCl or KNO_3, together with the co-crystallization method was established for obtaining olivetol loaded in γ-cyclodextrin metal-organic frameworks.

In the case of dipalmitoylphosphatidylcholine liposomes, the encapsulation of olivetol as a cannabidiol analogue was studied using the method of thin-film hydration and mechanical dispersion using a rotary evaporator and sonication, respectively. Both liposome

formulations in presence and absence of olivetol, showed similar morphology and size distribution below 200 nm, despite the drug is encapsulated in the lipid bilayer. Furthermore, the olivetol content was quantified, making them suitable as carriers of the drug and for *in vitro* application.

Subsequently, to evaluate the application of the formulations over the teeth, an *in vitro* study using bovine teeth as a model was carried out. For this purpose, synchrotron source infrared spectroscopy analysis of the dental structure was performed. Generated data were treated by principal component analysis that grouped the samples according to the presence of the drug and/or the presence of a controlled delivery system, revealing that both systems conducted the transport of the compound efficiently, even though the olivetol loading in the metal-organic frameworks formulations was lower than in the liposomes.

Taking into account these differences in terms of encapsulation between the two systems, the methodology previously developed to obtain the metal-organic frameworks formulations was optimized to explore the best synthesis conditions. For this purpose, a design of experiments based on a response surface methodology was used to optimize olivetol encapsulation and reaction yield. A quadratic model for reaction yield and a two-factor interaction model for drug encapsulation were established for both potassium sources (KCl and KNO_3). Under the optimal conditions, the experimental values for both responses significantly improved the previous results. Furthermore, it was shown that the new conditions did not compromise their structural properties.

Finally, to validate the use of olivetol as an analogue in these metal-organic frameworks, the optimized methodology was carried out using cannabidiol. These formulations showed the same structural properties as the observed with olivetol, despite a small loss of crystallinity. Furthermore, the reaction yield results and encapsulation values of cannabidiol were comparable to those of olivetol. Therefore, the substitution of olivetol for cannabidiol in γ-cyclodextrin metal-organic frameworks did not alter the previous results, validating the use of olivetol as an analogue.

Taking into account the indicated results, a methodology for the development of a new formulation based on cannabidiol loaded in γ-cyclodextrin metal-organic frameworks was established and optimized, validating the use of olivetol as an analogue of this compound. Furthermore, the *in vitro* application of this new formulation showed promising results, as

well as in the formulation of liposomes. Thus, both controlled release systems emerge as a new perspective to combat dentin hypersensitivity.

GLOSARY

2FI	Two-factor interaction
Δ^8-THC	Δ^8-Tetrahydrocannabinol
Δ^9-THC or THC	Δ^9-Tetrahydrocannabinol
γ-CD-MOF	γ-Cyclodextrin metal-organic framework
γ-CD-MOF KCl	γ-CD-MOF preparing with KCl as potassium source
γ-CD-MOF KNO_3	γ-CD-MOF preparing with KNO_3 as potassium source
γ-CD-MOF KOH	γ-CD-MOF preparing with KOH as potassium source
ANOVA	Analysis of variance
ATR-FTIR	Attenuated total reflectance Fourier transform infrared
APD	Avalanche photodiode detector
CCD	Central Composite Design
CB1	Cannabinoid receptor 1
CB2	Cannabinoid receptor 2
CBD	Cannabidiol
CBDV	Cannabidivarin
CBG	Cannabigerol
CD	Cyclodextrin
COD	Crystallography Open Database
Cryo-TEM	Cryo-transmission electron microscopy
d	Interplanar distance

DDS	Drug delivery systems
DLS	Dynamic light scattering
DoE	Design of Experiments
DPPC	Dipalmitoylphosphatidylcholine
ECS	Endocannabinoid system
EDX	Energy-dispersive X-ray
FE-SEM	Field emission scanning electron microscope
HAP	Hydroxyapatite
HEPES	2-[4-(2-hydroxyethyl)piperazin-1-yl]ethanesulfonic acid
MCT	Mercury-Cadmium-Telluride
MLVs	Multilamellar vesicles
MOFs	Metal-organic frameworks
MPD	Material Powder Diffractometer
OLV	Olivetol
PBS	Phosphate-buffered saline
PC	Phosphatidylcholine
PC1	Principal component 1
PC2	Principal component 2
PCA	Principal component analysis
PEG 20000	Polyethylene glycol 20000
PI	Prediction interval

RSM	Response surface methodology
SEM	Scanning electron microscopy
SWOT Analysis	Strengths, Weaknesses, Opportunities, and Threats Analysis
T_c	Phase transition temperature
TRP channels	Transient receptor potential cation channels
TRPA channels	Transient receptor potential cation ankyrin channels
TRPC channels	Transient receptor potential cation canonical channels
TRPM channels	Transient receptor potential cation melastatin channels
TRPML channels	Transient receptor potential cation mucolipin channels
TRPN channels	Transient receptor potential cation no mechanoreceptor potential C channels
TRPP channels	Transient receptor potential cation polycystic channels
TRPV channels	Transient receptor potential cation vanilloid channels
XRD	X-Ray diffraction
XRPD	X-Ray powder diffraction

TABLE OF CONTENTS

1. INTRODUCTION

Oral diseases are one of the most common diseases across the globe according to the World Health Organization. Everybody wants a good oral health free of pain or discomfort as the one caused by dentin hypersensitivity. This is a widely studied topic since hundreds of research articles about this problem could be found, because the science and the mechanisms behind it are still not fully understood. Besides, the economic interests are also presented since the current available treatments against dentin hypersensitivity are not effective and the demand for oral health products is increasing. Hence, companies are looking for new and effective strategies to achieve a competitive advantage in the market of oral health that moves large sums of money every year.

1.1. TOOTH STRUCTURE

Teeth are one of the hardest and resistant structures in the human body [1]. Teeth are located inside the oral cavity, attached to the mandible and maxilla bones of vertebrates [2]. These structures have different functions, since they are involved in the mechanical digestion of food, in oral communication for the articulation of sounds and in aesthetic dentistry [3].

The tooth is divided in two main parts: the crown and the root (Fig. 1). The crown is the visible and external part located above the gums or gingival tissue, while the root is the inner part below the gums allowing the attachment of the tooth in the oral cavity [4]. The crown is covered with a hard outer layer called enamel [5]. Underneath, there is the dentin tissue and the pulp chamber. The latter contains blood vessels and nerves, in order to maintain the tooth irrigated with nutrients and being able to receive and transmit stimulus [6]. The root is also covered by the dentin and an outer layer similar to the enamel but thinner and softer called cementum [7]. In the inner part of the root, root canals contain blood vessels and nerves, connecting the pulp chamber of the crown with the rest of the body [8]. Therefore, teeth are mainly composed of four dental tissues: Enamel, dentin and cementum that are considered hard tissues and the soft tissue is that which refills the pulp chamber and the root canals, which contains blood vessels and nerves [9].

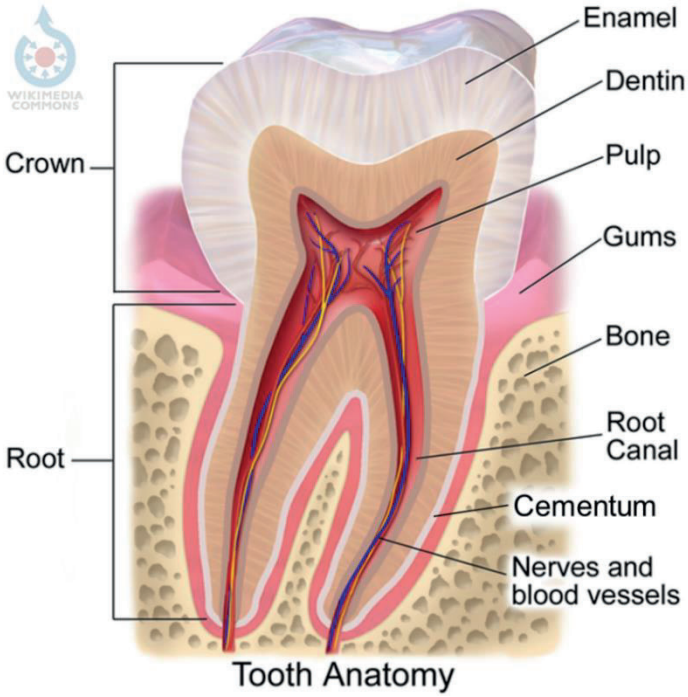

Figure 1: Anatomy of the tooth showing the two main parts (*the crown and the root), the hard tissues (enamel, dentin, and cementum) and the soft tissue (blood vessels and nerves)* [10].

These three hard tissues are connected through interfacial regions that separate two mineralized tissues with different compositions and biomechanical properties [11]: cemento-enamel junction or neck, dentino-enamel junction and dentino-cemental junction. The first one is the interface between the crown and the root, while the last two prevent crack propagation to dentin [12]. There is also another junction called junctional epithelium that attaches the connective tissue of the gingival tissue to the tooth surface providing a firm attachment [13].

Another part of the tooth is the acquired dental pellicle. It consists in adsorbed proteins and biopolymers from the oral environment that form a film coating the enamel surface after its eruption [14]. First, these molecules are adsorbed due to electrostatic forces with the enamel surface charges and then, due to the own interactions with the already adsorbed proteins [15]. The formation of this film is a dynamic process since it is removed during the brushing or chewing and built after that continuously [16]. This pellicle favours the lubrication of the tooth, regulates the bacterial adherence and protects the tooth surface against damage and demineralization, among others [17].

1.1.1. COMPOSITION AND STRUCTURE OF ENAMEL AND DENTIN

Enamel and dentin are the main tissues that comprise the teeth. Enamel is the hardest tissue in vertebrates and without the ability to regenerate itself since it is an acellular and avascular structure [9,18]. Enamel provides the resistant outer layer of the dental crown that protects the tooth from physical, thermal, and chemical forces that could damage the rest of the tissues that conforms the teeth. This hardness is due to the fact that it is a highly mineralized and densely packed tissue [19]. Enamel consists of inorganic material (96%) mainly carbonated calcium-deficient hydroxyapatite (HAP) [20]. The remaining 4% is a mixture of water and organic molecules, mostly glycoproteins such as amelogenins that are involved in the formation and organization of hydroxyapatite crystals during enamel formation [18]. The carbonated calcium-deficient HAP is a hexagonal crystalline calcium phosphate [$Ca_{10}(PO_4)_6(OH)_2$] and carbonates impurities [CO_3^{2-}] [21]. There is a typical carbonate content gradient along the enamel tissue, decreasing from the outer to the inner enamel, which involves a loss in the crystallinity [22]. Besides, these carbonates could substitute two anion phosphate groups or two hydroxyl groups in HAP structure, being B-type or A-type carbonated apatites, respectively [23]. The lattice parameters of HAP structure are modified due to the different size of the substitute anions [24]. The packing of the HAP crystals in the enamel in a parallel aligned orientation confers to this tissue its mechanical properties such as the extreme hardness, stiffness, and resilience [25]. This characteristic organization form the basic units of the enamel called rods and, between them, there are interprismatic spaces with organic matter called interrods [19,26].

The dentin is the major tissue of the tooth. It gives the tooth its colour and is softer and more elastic than the enamel [27]. The dentin acts as a protective layer and supports the crown of the tooth by giving it greater elasticity. These properties are explained because of its composition and organization. The dentin consists of more organic material than the enamel, being less mineralized. It is composed of inorganic material (70%) mainly carbonated calcium-deficient HAP as in the enamel and, organic molecules (20%), mostly collagen and water (10%) [28]. Besides, this tissue is organized in characteristic dentinal tubules filled with dentinal fluid that connect the enamel with the pulp chamber and the cementum with the root canals in the crown and in the root, respectively [29]. This fact confers less packing to the crystals of the dentin being a porous structure more similar to the composition of bones, explaining its different properties in comparison to the enamel [30].

In general, it is important to note that the composition and structures of these tissues are not constant and depend on many aspects, such as the age, diet, environmental factors or the species [31,32]. Therefore, it is important to consider these differences when chemical or physical studies are performed using tooth samples.

1.1.2. BOVINE TEETH AS AN *IN VITRO* MODEL

Although mammalian teeth are similar, tooth composition and structure could vary [11,31]. To perform *in vitro* tooth experiments, the ideal samples are usually human teeth free of any defect or without previous treatments. In general, this kind of samples are difficult to obtain since the dentist will remove a tooth when something is going wrong [33].

Bovine tooth is used as a substitute for human tooth in *in vitro* studies [34]. These teeth are easily to obtain from a slaughterhouse, or a butcher shop and they usually have a large surface without caries or defects. Besides, these samples are more homogeneous than human ones since bovines have a similar diet and lifestyle [35,36]. Moreover, ethical review is not necessary when bovine teeth are used for *in vitro* experiments and they are accepted as a valid model in several International Organization for Standardization (ISO) guides, for example ISO 29022:2013 or ISO 28399:2021 [37,38]. Therefore, bovine teeth are extensively employed as a model in dental *in vitro* studies for different applications, such as tooth whitening, dental erosion, or bonding/adhesive strength [39,40]. Nevertheless, human, and bovine teeth have some slight differences, such as the calcium content or the fracture resistance that are higher and lower in bovine samples, respectively (Table 1). These differences are due to the different crystal organization [41]. Thus, this variability should be considered especially when the obtained results of *in vitro* studies using bovine samples want to be extrapolated to human teeth.

Table 1: Comparison between human and bovine teeth [34].

		Human teeth	Bovine teeth
Enamel	Average diameter of crystallites	Smaller	Larger
	Calcium content	Lower	Higher
	Calcium distribution	More heterogeneous	More homogenous
	Carbonate content	No significant differences	
	Demineralization	No significant differences	
	Caries progression	Slower	Faster
	Microhardness	Higher	Lower
Dentin	Diameter of dentinal tubules	No significant differences	
	Number of dentinal tubules	Higher	Lower
	Stain removing	More difficult	Easier
	Caries progression	No significant differences	
	Diffusional water flux	No significant differences	
	Wear induced by erosion	Higher	Lower

1.2. DENTIN HYPERSENSITIVITY

Nowadays, dentin hypersensitivity is a very common clinical condition that has not yet been properly resolved. Dentin hypersensitivity, also known as dental hypersensitivity or cervical dentin sensitivity, is defined as pain arising from exposed dentin in response to chemical, thermal, tactile or osmotic stimuli that cannot be explained as arising from any other dental defect or disease, varying between individuals due to differences in pain tolerance, environmental factors and emotional state [42,43]. Although it does not represent a serious health problem, it is a common need in patients as it causes a very unpleasant and unwanted sensation, usually described as a brief and sharp repetitive pain [44].

The prevalence of this hypersensitivity varies between 4% and 57% [43]. This wide range is due to the differences between the populations studied, as well as the different study methods that have been conducted. Most studies have reported that, in terms of gender, there is more incidence in women than in men (Fig. 2) [45,46], although there is not enough

scientific evidence to support this fact [47]. Regarding the age, it has been reported that there is a higher incidence in the 30-40 age range with a prevalence of 30%, although all age groups can suffer it [47]. This could be explained by the decrease in dentin permeability over the years [48].

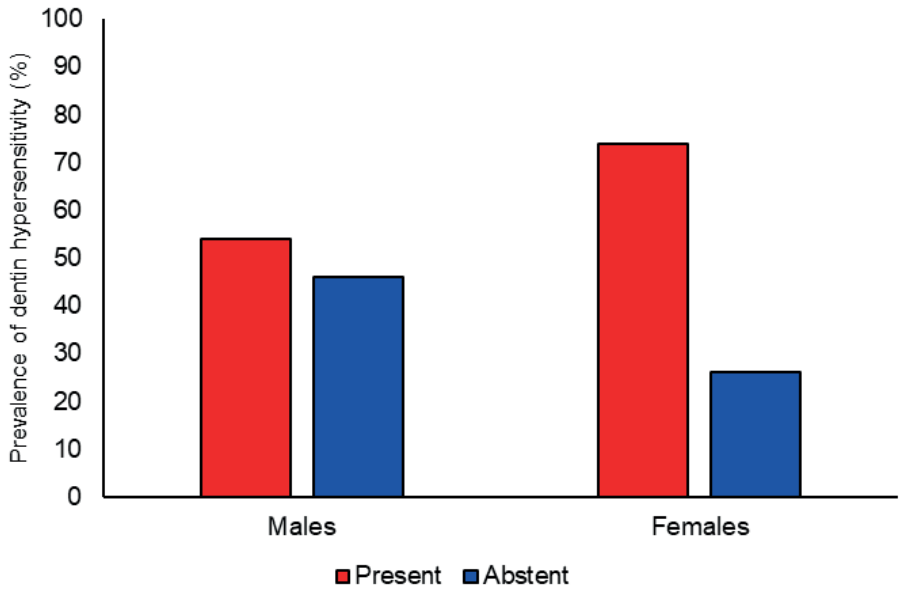

Figure 2: Prevalence of dentin hypersensitivity among the respondents showing the differences in terms of gender [46].

There are many causes that can lead to the development of dental hypersensitivity. In young patients, the main cause is dental erosion [49]. On the other hand, periodontal diseases and their associated treatments cause hypersensitivity in 85% of affected patients [50]. Other reasons that can lead to periodontal disease include gingival recession due to improper brushing, excessive smoking, tooth whitening treatments or excessive flossing [47,51].

Therefore, this high prevalence of hypersensitivity is an important issue that needs to be addressed in order to prevent or eliminate the pain.

1.2.1. THEORIES AND MECHANISMS

Although the origin of dentin hypersensitivity remains unclear, there are three accepted theories that explain the mechanism by which this pain occurs (Fig. 3).

- Brannstrom's hydrodynamic theory [48,52,53]

This is the most accepted theory at present and is based on the fact that when an external stimulus reaches the exposed dentinal tubules, a pressure change occurs, causing the fluid contained in the tubules to move. In this way, the nerve endings located at the inner ends of these tubules or in the outer layers of the pulp are stimulated and depolarised, thus generating a nerve impulse to the brain that translate into pain. Depending on the external stimulus, the movement of the fluid within the tubule's changes. For example, if the stimulus is thermal, heat will cause the fluid to expand and move. Conversely, cold will act in the opposite way. However, both excitations will result in the production of pain.

- Odontoblast transduction theory [52,54]

This theory assumes that odontoblasts transmit external stimuli through exposed dentinal tubules, and these external signals are transferred to nerves causing a neuronal signalling cascade translated into pain. However, at present, there is no experimental scientific basis to test the theory.

- Neural theory [43,52]

It argues that external stimuli directly affect the nerve endings of the dentinal tubules via the pulpal nerve fibres. Currently, there is no strong evidence to support this theory.

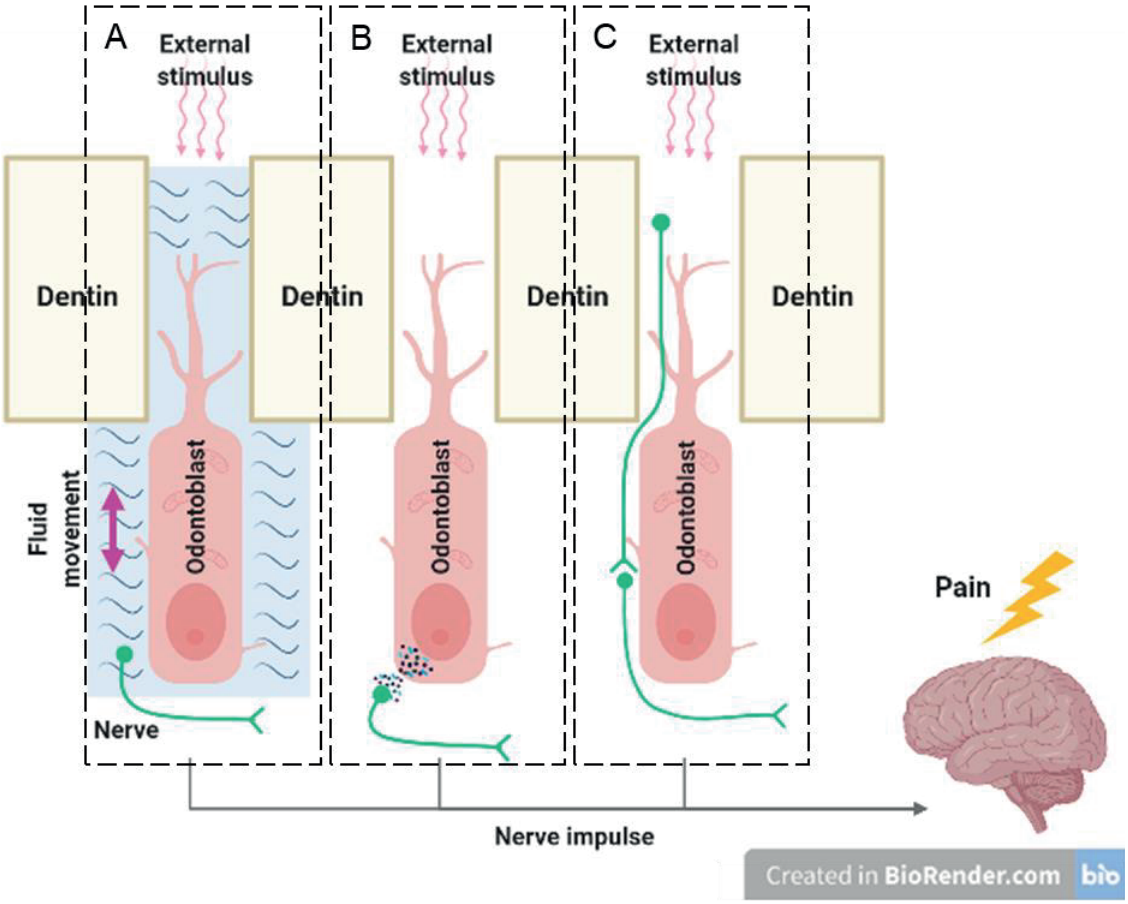

Figure 3: Theories that explain the dentin hypersensitivity mechanism: Brannstrom's hydrodynamic theory (A), odontoblast transduction theory (B), and neural theory (C) [43].

1.2.2. CURRENT TREATMENTS

At present, there are three main strategies currently available for the treatment of dentin hypersensitivity, which employ different mechanisms to avoid this pain (Fig. 4).

-Nerve desensitization agents

The base of these treatments consists of the use of potassium nitrate in order to desensitize the pulpal sensory nerves reducing its response to stimulation and blocking the signalling pathway that would ultimately be transformed into pain [55]. However, the specific mechanism of action of this potassium salt is not well known. The most accepted theory is that the depolarizing activity of the potassium ions reduces the neuronal activity [56]. A study showed that using 5% of potassium nitrate in toothpastes was more effective than the control without this salt, reducing the dentin hypersensitivity for four weeks [57].

- Dentinal tubules occlusion agents

This kind of treatments follow the Brannstrom's hydrodynamic theory. There are many agents used to plug the dentinal tubules, but their exact mechanisms are not fully understood, but several hypotheses have been formulated to explain how each compound works. In general, these treatments cover the exposed tubules through mechanical formation of a natural layer and/or forming insoluble materials that precipitate in the tubules and on the surface [48]. Such compounds include strontium acetate, sodium fluoride, stannous fluoride, and sodium monofluorophosphate [58]. These agents, among other salts are usually added to toothpastes and they act blocking the dentinal tubules through chemical precipitation onto the dentine surface decreasing dentin permeability. To improve its effect, lasers could be applied to promote this precipitation process [59]. Another example is the use of formaldehyde and glutaraldehyde that occlude the tubules promoting the precipitation of salivary proteins [58]. Dentinal adhesives are also employed as dentin sealers and soft tissue grafts to cover exposed tubules due to gingival recession using surgery [57].

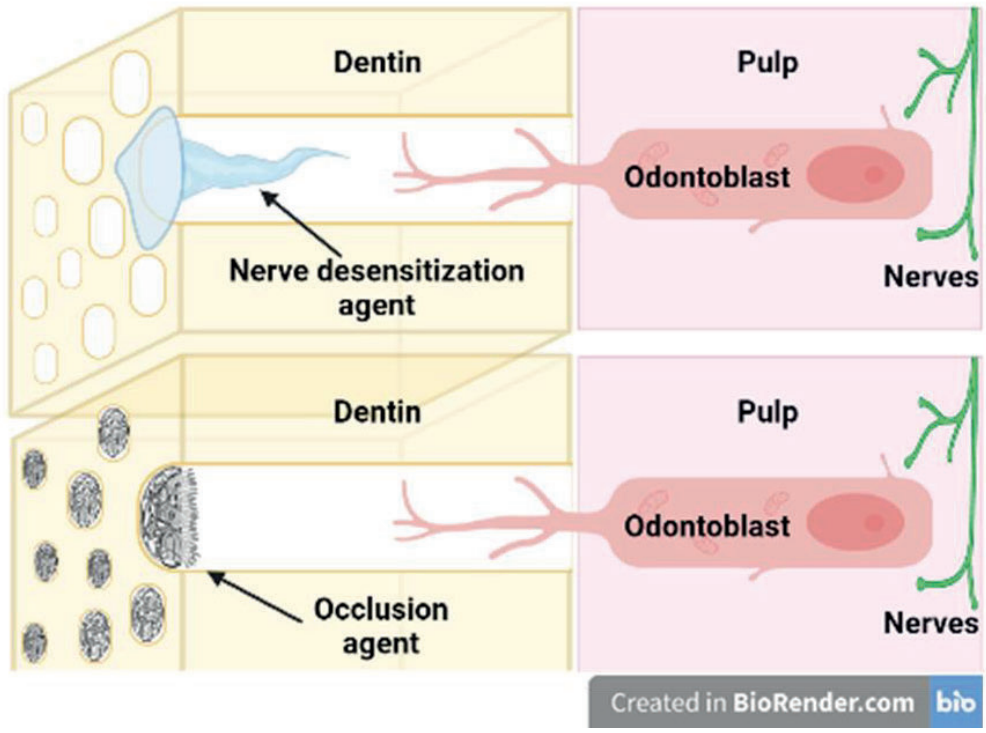

Figure 4: Nerve desensitization and dentinal tubules occlusion agents as current treatments to avoid dentin hypersensitivity [43].

-Analgesics and anti-inflammatory agents

An analgesic is any member of the group of drugs used to achieve analgesia, the relief and reduction of pain. Analgesic drugs act at different levels of the nervous systems and there is a wide selection of these drugs depending on the pharmacochemical properties and the action mechanism. In dentin hypersensitivity the drugs used for pain relief correspond to two main groups: non-narcotic analgesics (non-opioids) and opioids [60].

Some examples of non-narcotic analgesics employed in dentin hypersensitivity are ibuprofen, etodolac, dipyrone and acetaminophen. Ibuprofen may help to reduce dentin hypersensitivity during some treatments but not after them [61]. Besides, the perioperative use of this drug was not able to avoid the pain but reduced its intensity up to one hour [62]. The combination of ibuprofen and acetaminophen may decrease dentin hypersensitivity as data from a clinical experiment revealed [61]. Other medicine used as preventive treatment on dentin hypersensitivity is etodolac. However, a single dose preventive administration of this compound did not affect either risk of dentin hypersensitivity or level of pain reported by patients, during or after the procedure [63]. Topical dipyrone had the same lack of effect as etodolac in a clinical trial reported by Rezende *et al.* [64].

Opioids are administrated to treat very intense pains as they are considered very powerful analgesics [65]. The mostly used opioid in the dental field is codeine in combination with acetaminophen (non-opioid), without promising results [66]. Furthermore, the use of opioids in this field is not recommended since they are considered very potent compounds and they can produce a high amount of side effects [67].

Another group of drugs was found to treat inflammation and pain in dentistry: corticosteroids. These agents have been used topically for their anti-inflammatory effects, but are not particularly effective [53]. An example is dexamethasone, but it did not reduce the risk and intensity of dentin hypersensitivity [68].

As a conclusion, even though there are a great number of possible strategies to be applied in the treatment of the dentin hypersensitivity, up to date any treatment has yet been found to be entirely efficient for all patients. Therefore, more research is still being performed with the objective of finding an effective and long-lasting treatment able to reduce dentin hypersensitivity without significant side effects [69].

1.3. CANNABINOIDS

Cannabinoids are a type of active chemical compounds that are naturally found in the stems and flowers of the *Cannabis sativa* plant [70]. Among the more than 500 known constituents of *C. sativa*, more than 100 belong to cannabinoids. This plant belongs to family *Cannabaceae* and it is native to Asia [71]. *C. sativa* has been used for recreational, industrial and medicinal purposes for thousands of years due to the properties of cannabinoids [72]. These compounds are secreted in a resin by glandular hairs in male and female plants, being the female preferred since they produce more amount of this cannabinoid-rich resin [73].

Cannabinoids represent a group of C21 or C22 (for the carboxylate forms) hydrophobic compounds [74]. Chemically, they are terpenophenolic compounds and the most important cannabinoids are Δ^9-tetrahydrocannabinol (Δ^9-THC or THC), famous for its psychotropic effect, Δ^8-tetrahydrocannabinol (Δ^8-THC), cannabidiol (CBD), cannabigerol (CBG) and cannabidivarin (CBDV) (Fig. 5) [75].

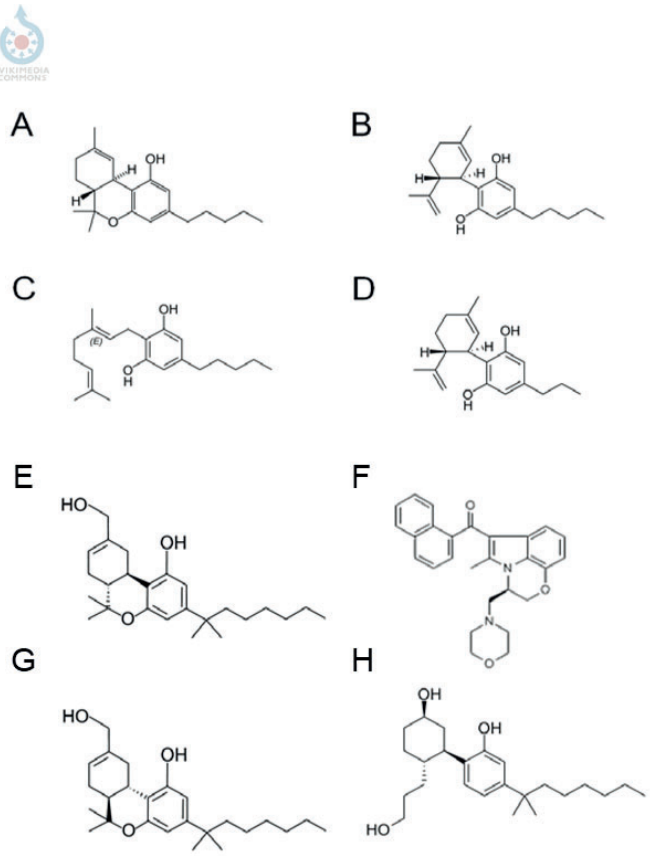

Figure 5: Cannabinoid chemical structures: Δ^9-tetrahydrocannabinol (Δ^9-THC or THC) (A), cannabidiol (CBD) (B), cannabigerol (CBG) (C), cannabidivarin (CBDV) (D) and synthetic cannabinoids (E-H) [76].

These compounds act on the endocannabinoid system (ECS), which consists of a group of endogenous cannabinoid receptors located in the central and peripheral nervous systems [77]. The ECS regulates various physiological processes through these receptors such as appetite, memory, pain or immune response [78]. The two more important receptors are cannabinoid receptor 1 (CB1) and cannabinoid receptor 2 (CB2). Meanwhile CB1 is mainly expressed in the brain and therefore involved in cognition and brain function, CB2 is more present in the immune and hematopoietic system [79]. After the modulation of these receptors, specific signalling pathways induce multiple actions in organism showing the final effect.

1.3.1. CANNABIDIOL

Cannabidiol is the main non-psychotropic cannabinoid of *C. sativa* and it is the component responsible of most of the medical benefits of this plant [80]. CBD is not psychoactive and antagonizes the psychotomimetic and other psychotropic effects of THC. Although THC and CBD show similar structures, the fact that THC exists in planar configuration meanwhile CBD presents a non-planar configuration, determines their difference in terms of the psychotropic activity [81]. Furthermore, cannabidiol has powerful therapeutic characteristics in several health fields, such as antioxidant, anti-inflammatory and immunomodulatory effects [82]. All these properties together with the absence of psychotropic effects and its minimal side effects, make CBD safe for its use in biomedicine. This compound has shown promising results in the control of serious diseases such as epilepsy, Alzheimer, multiple sclerosis, chronic pain, diabetes and in the treatment of various types of cancer [83,84]. Therefore, CBD is considered the main non-psychotropic compound with a remarkable relevance in scientific applications due to its medical benefits [85].

The effects of cannabidiol, as well as the rest of cannabinoids, occur when they act on their corresponding endocannabinoid receptors (CB1 and CB2). However, other distinctive characteristic of cannabidiol is the fact that it can interact with more receptors, explaining its wide spectrum of action [86]. For example, CBD can modulate transient receptor potential cation channels (TRP channels), which mediate a variety of sensations such as pain or temperature [87].

Nevertheless, cannabidiol is also known for other less attractive characteristics. This compound is soluble in organic solvents but not in aqueous media, being a disadvantage specially when CBD is used in biomedicine since the physiological media is an aqueous solution [88]. Moreover, cannabidiol shows low chemical stability and high degradation easiness, being oxidized under alkali conditions [89]. Therefore, some strategies could be developed to protect CBD and avoid these difficulties when this compound is wanted to be employed in biomedicine, such as the use of appropriate drug delivery systems (DDS) [90]. Furthermore, other important aspect to take into account of cannabidiol is the price of this compound, since it can reach 1,400 €/g or more, making more difficult its use in experimental research approaches.

1.3.2. CANNABIDIOL IN ORAL HEALTH

The use of cannabidiol in dentistry has been scarce studied, and its effects in the treatment of oral diseases are not well-known. Nonetheless, considering its properties, mechanisms of action and favourable results in treating other complex diseases, it is believed that it can exert a positive therapeutic effect on some pathologies that are still challenging in oral health such as dentin hypersensitivity [91].

There are few studies about cannabidiol in dentistry. One of them tested the effects of CBD in a periodontitis experimental model in rats. The results indicated that CBD may be useful to control bone resorption during progression of experimental periodontitis in these animals [92]. Cuba *et al*. considered the possibility of the use of CBD for the prevention and treatment of oral mucositis. This study demonstrated that cannabidiol is safe to use and possesses antioxidant, inflammatory and analgesic properties [91]. Other cannabis products and devices have been patented by companies such as Axim Biotech, Incannex, APIRx or Cannaderm. For example, a delivery system of oil infused cannabis is disclosed to be used in toothpastes and gummies to help strength the root of teeth [93]. Other application discloses oral care compositions based on toothpastes, toothpowders or mouthwashes that contain cannabinoids, preferably cannabidiol and/or cannabigerol to be used to treat oral infectious diseases, including periimplantitis, periodontitis, oral mucositis, and dental pain [94]. A toothpaste with a mixture of different cannabinoids led a pain relief transferring these compounds in contact with the gums [95].

Besides, some commercial products with cannabidiol developed to combat dental pain are available in the market [96]. CBD chewing gum increases production of saliva, reducing decay thanks to the antibacterial, antiseptic and analgesic properties of this compound, preventing biofilm attachment. Toothpaste infused with CBD, made of baking soda, peppermint oil, organic coconut oil and CBD oil, relieves hypersensitivity and heals the gums, removing the plaque. CBD hemp oil tincture for adding few drops in the toothpaste to maintain the oral environment free of bacteria and it could reduce hypersensitivity. CBD capsules are appropriated for use as analgesics after surgery or to combat hypersensitivity, and also, CBD oral spray and tea infused with cannabidiol provide pain relief.

1.3.3. CANNABIDIOL AS TREATMENT OF DENTIN HYPERSENSITIVITY

As it was previously explained, CBD not only interacts with the most common cannabinoid receptors, but also this compound could act through transient receptor potential cation channels (TRP channels) [87].

TRP ion channel family comprises seven classes of nonselective cation channels: TRPA (ankyrin), TRPC (canonical), TRPM (melastatin), TRPML (mucolipin), TRPP (polycystic), TRPN (no mechanoreceptor potential C) and TRPV (vanilloid) [97]. These classes include several subfamilies with at least 28 sequenced members. They are able to alter the membrane potential of the cells modifying the intracellular concentration of different cations such as calcium, magnesium and sodium [98]. This fact activates a signalling pathway that has a key role in pain response and other sensations. The modulation of these channels takes place through several signals including thermal, mechanical and chemical stimuli [99].

To date, the presence of several members of the TRPV, TRPM, TRPC and TRPA classes have been reported in dental tissues, including odontoblasts and the nerves in the pulp chamber [54,100]. The mechanism of action of these channels in the transduction of dental pain starts when the exposed dentin suffers the application of an external stimuli (Fig. 6). This signal induces the movement of the dentinal fluid, activating the TRP channels of the odontoblasts and the nerves. This activation increases the calcium concentration in the odontoblasts, activating them. The activated odontoblasts release neurotransmitters to the nerves, such as glutamate and adenosine triphosphate through glutamate permeable and pannexin channels, respectively. This release activates the nerves in the pulp chamber that promote a

signal in the neurons giving a final response in form of pain [54,101]. Therefore, TRP channels may serve as potential drug targets for the development of pharmacological strategies to manage dental pain [102].

Moreover, CBD has been shown to interact with these TRP channels by desensitising them, regulating calcium entry into odontoblasts and dental pulp nerves, blocking the signalling pathway described above, thus decreasing the pain response [98,103]. For this reason, CBD emerges as a promising candidate for the treatment of dentin hypersensitivity [96].

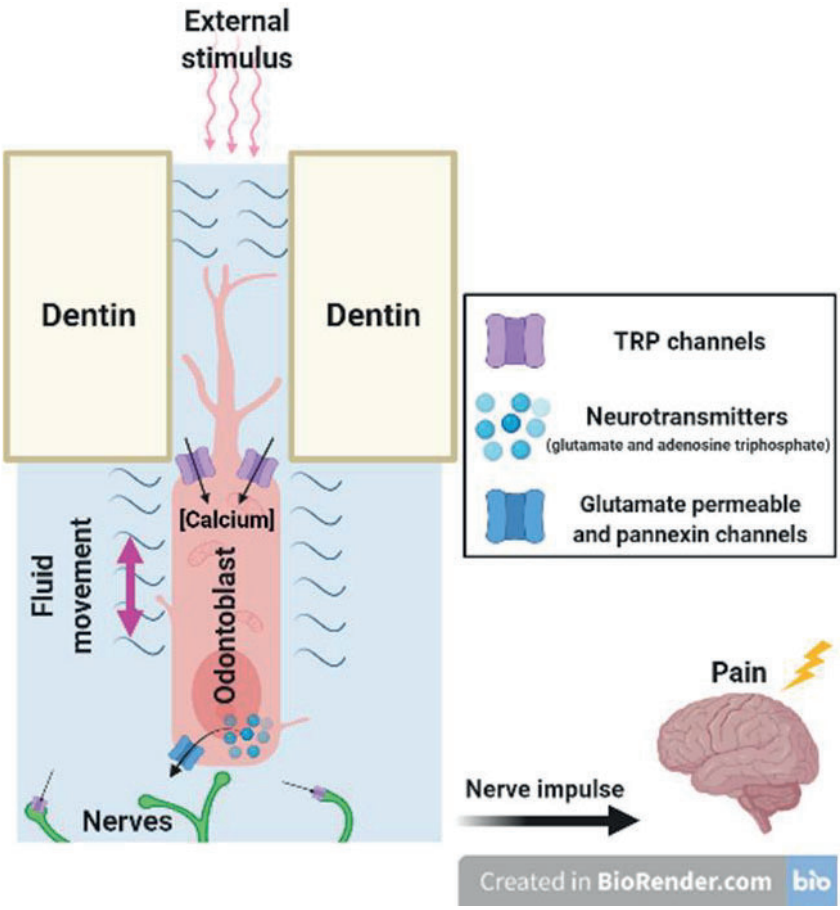

Figure 6: Mechanism of action of transient receptor potential cation channels in the transduction of dental pain [54].

1.3.4. OLIVETOL (OLV)

Olivetol, also known as 5-pentyl-1,3-benzenediol or 5-pentylresorcinol, is a phenolic compound naturally present in several plants such as lichens or wheat. It is also produced by various insects as pheromone, antiseptic or repellent agent [104]. OLV is a precursor of

cannabinoids in its synthesis, as its chemical structure is included in the chemical structure of these compounds including cannabidiol (Fig. 7). It makes olivetol an important metabolite in cannabinoid biosynthesis [105]. Thus, OLV is defined as an experiential model of the n-pentyl resorcinol sector of cannabinoids and it is used to produce synthetic analogues of these compounds [106]. Besides, olivetol has some of the interesting properties of CBD, such as the antioxidant effect by reducing free radical production [104]. A distinctive aspect of OLV in comparison with the rest of cannabinoids is its price, that is around 30 €/g, being 50 times cheaper than CBD.

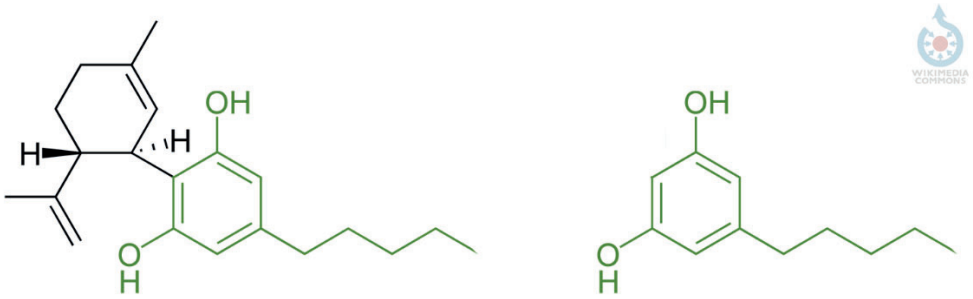

Figure 7: Chemical structure comparison between cannabidiol (left) and olivetol (right), olivetol structure is highlighted in green.

Although they cannot be considered as analogue compounds, OLV could be employed as a more affordable alternative in some experimental approaches since it may mimic cannabidiol chemical behaviour due to the common characteristics.

1.4. DRUG DELIVERY SYSTEMS (DDS)

Nowadays, there are many limitations to the direct administration of the active compounds responsible of the therapeutic effect. For example, efficacy could be reduced due to difficulties with the drug itself, as is the case of CBD (explained in section 1.3.1). To overcome these difficulties, controlled drug delivery systems (DDS) have been developed [107]. This controlled delivery aims to release drugs in a defined concentration, to target its transport to the specific site and in the desired time [108,109].

Drug transport using these DDS has several benefits over the direct administration [110]:

- ✓ Improves the efficiency of the release.
- ✓ Minimises undesirable side effects of the drug.
- ✓ Reduces the toxicity of the administered drug.
- ✓ Protects the drug against degradation or elimination by the body.
- ✓ Can reach tissues and organ locations non reachable by labile molecules

Because DDS have a final application in biomedicine, a very important aspect they have to fulfil is that they should offer safety, efficiency, optimal bioavailability, biocompatibility, stability, non-toxicity, non-immunogenicity and the ability to be site-specific [111]. Drug delivery systems appeared in 1952 for the first time and they have been quite developed [110]. Different structures have been tested as DDS, such as liposomes, dendrimers, carbon nanotubes or metal-organic frameworks (MOFs) (Table 2) [112]. These DDS have been employed as treatments of different diseases including cancer or diabetes, among others [113]. Moreover, these materials are included in pharmaceutical products that generate more than 100 billion € in annual revenues [114]. Thus, these facts show the clinical and commercial importance of DDS in biomedicine. Nevertheless, although different methodologies have been proposed for a controlled drug administration process, the perfect DDS has not yet been developed.

As it was explained before, cannabidiol presents some limitations since it is a hydrophobic compound, showing poor aqueous solubility. This fact is particularly important in biomedicine applications since the physiological media is an aqueous solution. Besides, CBD has low chemical stability. Therefore, suitable DDS could be employed for cannabidiol encapsulation in order to protect this compound from its degradation and to improve its biodistribution [90].

Table 2: SWOT (Strengths, Weaknesses, Opportunities, and Threats) analysis of different drug delivery systems [115–124].

DRUG DELIVERY SYSTEM	STRENGTHS	WEAKNESSES	OPPORTUNITIES	THREATS
Dendrimers	Biodegradable and biocompatible Encapsulation of hydrophobic and hydrophilic drugs	Aggregation *in vivo*	Application as diagnostic reagents High control over the size, branch density and surface functionality	Adverse effects after long-term use A chemical modification is required to avoid its elimination by body
Carbon nanotubes	Excellent mechanical, electrical and surface properties *In vivo* monitoring in real time due to its intrinsic spectroscopic properties	Insoluble in water Aggregation in most solvents Cytotoxicity	Functionalization can reduce its aggregation and increase the solubility	Biosecurity disputes
Micelles	Biodegradable and biocompatible Spontaneously self-assemble in water	Drug loading and release depending on the molecular weight of the carrier	Easy size and morphology modulation Easy to synthesize at large scale	Fast degradation and drug release
Quantum dots	Monitoring in real time due to its fluorescent properties Encapsulation of hydrophobic and hydrophilic drugs	Low biocompatibility and physiological stability Aggregation	Surface modification to increase its effectiveness	Possible loss of its fluorescent and effectiveness
Metal-organic frameworks (MOFs)	Structural versatility Large surface areas and high porosity	Toxicity depending on the components	Carriers for gaseous therapeutics Biocompatible with the previous selection of its components	Low stability in aqueous medium Long synthetic procedures
Liposomes	Encapsulation of hydrophobic and hydrophilic drugs Biodegradable and biocompatible	Possible drug leakage Low stability in the body High production cost	High variety of vesicle Easy size control	Hydrophobic drugs encapsulation is dependent on the solubility of the drug in the bilayer

1.4.1. METAL-ORGANIC FRAMEWORKS (MOFs)

Metal-organic frameworks (MOFs) are crystalline materials made of metal ions (or metal clusters) linked through coordination bonds to organic ligands into one, two, or three-dimensional extended periodic network structures (Fig. 8) [125]. MOFs present extraordinary properties such as high surface areas, ultrahigh porosity, and thermal stability [126]. These structural characteristics are determined by the metal-organic combination. Besides, MOFs are editable materials since their properties could be modulated like porous size or surface characteristics through the modifications of their components, and the different possibilities during their synthesis procedures or the encapsulation process [127]. For instance, if the organic ligand is flexible, the MOF will experience some flexibility. Therefore, MOFs can be developed and properly adjusted modifying these factors depending on targeted applications [128].

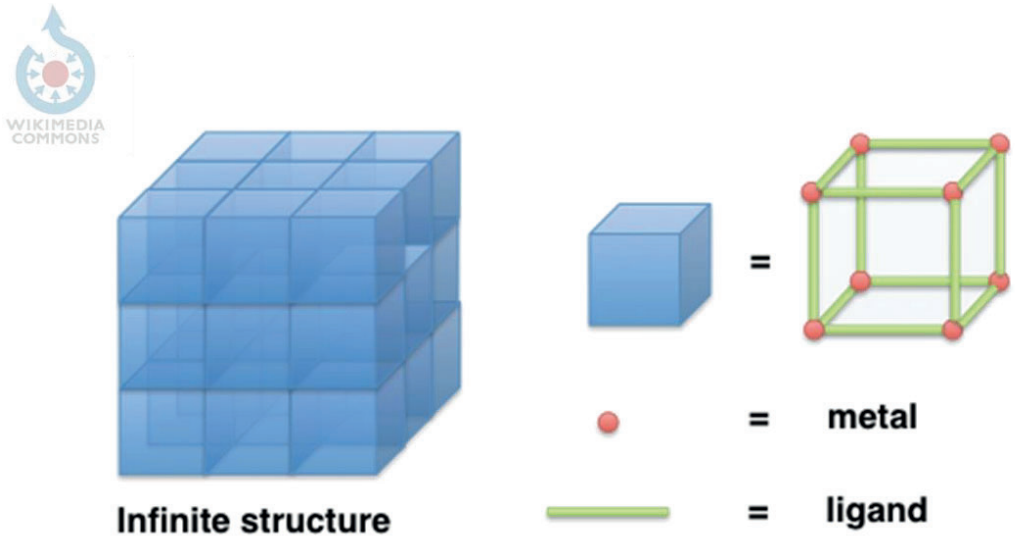

Figure 8: Components of metal-organic frameworks including the metal ion and the organic ligand.

In order to obtain these materials, different synthesis methods can be followed, including vapor diffusion, solvothermal/hydrothermal, or microwave assisted methods [129]. Meanwhile, the guest compounds can be loaded employing several encapsulation methodologies, such as impregnation, grinding and co-crystallization methods [130]. The selection of the appropriate encapsulation technique should be considered in order to ensure that it does not affect MOF properties neither the guest compound. For instance, the pH of

the media where the encapsulation process is taking place could degrade the guest compound [131,132].

Due to the benefits of MOFs, these materials have emerged in plenty applications, including catalysis, gas storage, pollutant-removal agents or as drug delivery systems [133–135]. Indeed, the number of publications about this new class of crystalline materials has been gaining attention in many scientific fields over the last years (Fig. 9) [136]. In biomedical field, the use of MOFs as DDS has increased since they have been downsized to micro and nanoscale, being efficient drug delivery systems for different compounds [133]. In this context, an important aspect to consider is the biocompatibility of the materials constituting the MOFs, since they should show low toxicity and safety for *in vivo* applications [137]. In this regard, it is fundamental to use harmless precursor materials like calcium or potassium metal linkers or biocompatible organic ligands such as nucleobases, amino acids, polypeptides, proteins and cyclodextrins (CDs) [138]. Thus, the materials that follow these aspects are ideal host structures for the encapsulation of different compounds such as drugs with therapeutic interest [139]. A biocompatible type of MOF that is being widely used in biomedicine in recent years is γ-cyclodextrin metal-organic framework (γ-CD-MOF) [140].

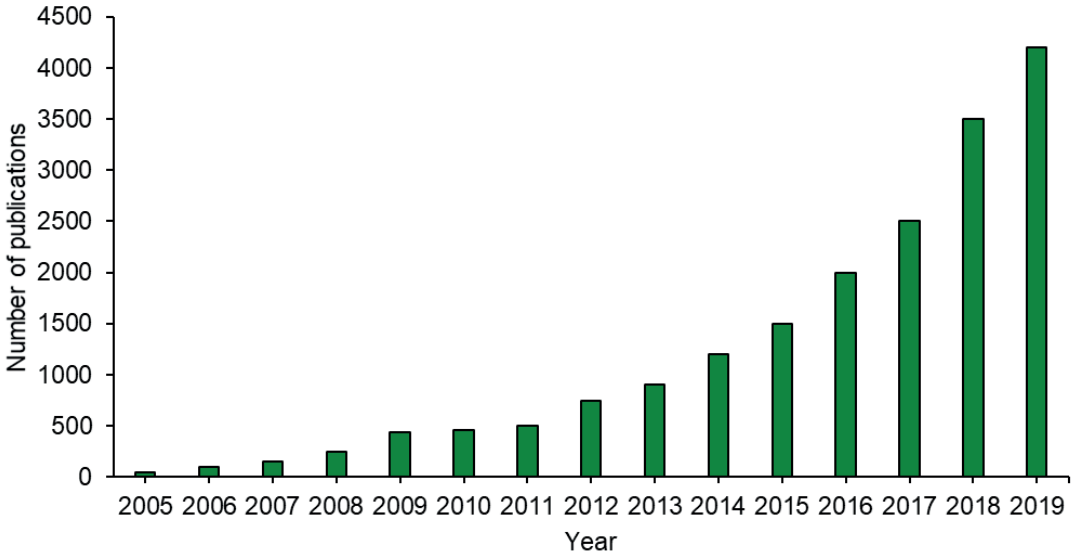

Figure 9: Number of publications related to metal-organic frameworks per year from 2005 to 2019 [136].

1.4.1.1. γ-CYCLODEXTRIN METAL-ORGANIC FRAMEWORKS (γ-CD-MOFs)

γ-Cyclodextrin metal-organic frameworks (γ-CD-MOFs) are a type of biocompatible MOFs made of γ-CD as organic ligand and alkali-metal cations as metal linker such as potassium, rubidium, and caesium [141].

CDs are natural cyclic oligosaccharides formed by D-glucopyranose units linked by a α-1,4-glycosidic bond [142]. There are three main cyclodextrins depending on the number of glucopyranose units: α-CD, β-CD and γ-CD with 6, 7 and 8 glucopyranose units, respectively (Fig. 10) [126,138].

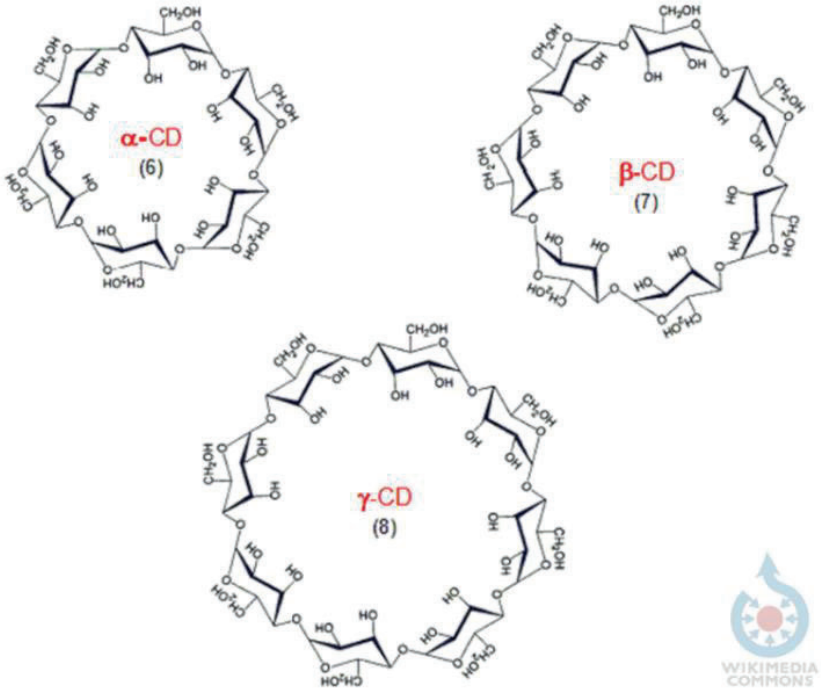

Figure 10: Chemical structure of α-, β-, and γ-cyclodextrins showing the glucopyranose units.

Cyclodextrins have a truncated cone-shaped structure due to the chair conformation of the glucopyranose units (Fig. 11) [143]. Meanwhile its outer surface is hydrophilic because of the hydroxyl groups, the inner cavity is hydrophobic due to the carbons and oxygens of the glucopyranose residues [126]. This structure allows cyclodextrins to encapsulate hydrophobic compounds in its inner cavity through non-covalent interactions (hydrogen bridges, Van der Waals and electrostatic forces) and to deliver them in aqueous solution due to its hydrophilic surface [144]. However, drug loading in this cavity is limited. Thus,

cyclodextrins could be combined with many molecules, both organic and inorganic, to create novel and biocompatible materials with higher drug loading capacity, including MOFs [138].

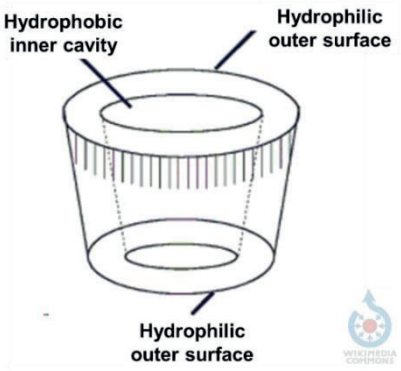

Figure 11: Truncated cone-shaped structure of cyclodextrins showing the hydrophilic outer surface and the hydrophobic inner cavity.

Among the three types of cyclodextrins, γ-CD has been used to prepare biocompatible and non-toxic MOFs due to the presence of more -OCCO- binding groups in the primary and secondary faces, which can be used to form complexes with alkali-metal cations [141]. Calcium, iron, zinc and titanium ions have been considered biologically acceptable, but potassium ions from potassium hydroxide are one of most used to obtain these CD-MOFs [145]. The crystal structure of these typical CD-MOFs corresponds to body-centered cubic crystals of space group *I*432 (Fig. 12) [146]. However, other space groups and structures have been also reported for these MOFs when metal sources different from KOH have been employed [147].

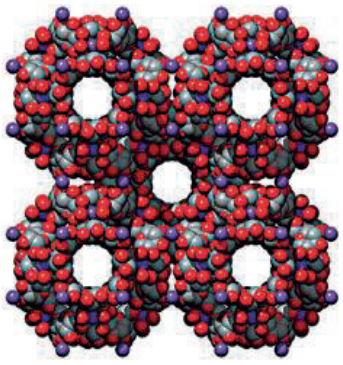

Figure 12: Space-filling representation of the extended solid-state structure of the typical γ-CD-MOFs corresponds to body-centered cubic crystals of space group I432.

These CD-MOFs can be synthetized using the different methods listed above for any MOF, being vapor diffusion crystallization the classical method. This method consists in mixing the reagents in a precipitant solution (not concentrated) into a sealed environment with the same precipitant solution (concentrated). This action allows to reach an equilibrium since vapours from the concentrated solution starts to migrate to the unconcentrated one. Then, reagents start to react forming the crystals due to the concentration gradient created [148]. Nevertheless, this method is not suitable to mass production and industrial use since the process to obtain the crystals takes several weeks and the size remains heterogeneous. To overcome these difficulties, new synthesis methods are emerging such as the use of analytical microwave-assisted technique as a fast and efficient process [127]. The synthesis of CD-MOFs using the analytical microwave allows to control and modulate the size of the crystals being more homogeneous [149]. Besides, only some hours are needed to obtain the MOFs instead of weeks and the reaction yield is also improved [150]. Another advantage of these γ-CD-MOFs is their editability since hydroxyl groups of CDs will allow a surface functionalization, so post-modification methodologies could be performed after the synthesis with different purposes such as to improve their stability in aqueous medium [126,151].

Regarding the encapsulation process, different methods can also be used, being the impregnation technique the most common. It consists in the immersion of the synthesized CD-MOFs in a solution where the guest molecules are dissolved. However, the solvent plays a critical role in the efficiency of encapsulation, as well as the time, temperature and ratio between the drug and the MOF [126]. Co-crystallization method has also been employed for drug encapsulation in CD-MOFs. In this process, the drug is in the same solution with the reagents that will comprise the final MOF and the encapsulation takes place at the same time as the crystal formation [152]. In this case, it must be considered that the synthesis process does not alter the drug.

In this context, CD-MOFs are promising candidates as DDS and they have already been employed in biomedicine for the encapsulation of different compounds such as ibuprofen or lansoprazole [153,154]. Thus, they would show potential as DDS in oral health.

1.4.2. LIPOSOMES

Liposomes are concentric spherical-shaped vesicles typically based on one or more phospholipid bilayers surrounding an aqueous core (Fig. 13) [155]. Liposomes present the ability to encapsulate different substances. Meanwhile hydrophilic drugs are encapsulated in the aqueous core of the liposomes, hydrophobic compounds are encapsulated in the bilayers [156]. Besides, liposomes are non-toxic, biocompatible, and biodegradable and they can fuse with the cell membrane and release the encapsulated drug [157]. For this reason, liposomes have been widely employed as DDS to transport several drugs in the treatment of different diseases, such as cancer, multiple sclerosis, or even COVID-19 [158,159].

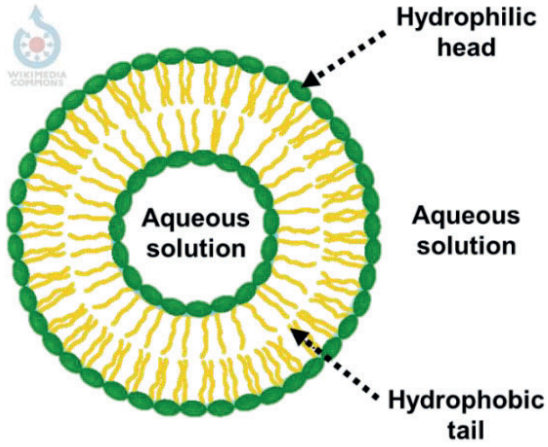

Figure 13: Scheme of a liposome showing phospholipid bilayer surrounding an aqueous interior and excluding an aqueous exterior environment.

The major structural components of the liposomes are phospholipids. Phospholipids are amphipathic molecules with a hydrophilic polar head group and hydrophobic hydrocarbon chains [160]. A parameter that is involved in the stability of the liposomes is the phase transition temperature (T_c) of the phospholipid or phospholipids that constitute the vesicles. This temperature defines the fluidity changes of each phospholipid and is directly proportional to the length of the hydrophobic chains [161]. The longer the chain of the phospholipid is, the higher its T_c will be and more rigid will be the bilayer. This parameter could affect important factors of the liposomes such as its stability, aggregation, and permeability [162].

For liposomes synthesis, the most well-known process is the thin-film hydration method. It consists in drying down the phospholipids from organic solvents in the bottom of a round flask using the rotary evaporator and then its mechanical dispersion in the aqueous media [163]. Meanwhile, the drug encapsulation for hydrophobic compounds takes places during the drying process, hydrophilic drugs are loaded in the mechanical dispersion through the aqueous medium [164]. Nevertheless, depending on the type of vesicle and drug, the technique may vary.

There are different types of liposomes according to the number of concentric bilayers, the size and the phospholipids that comprise the formulation [165]. Other important characteristic of these systems is the easy control of all these variables as well as the surface functionalization [166]. Therefore, liposomes could be modulated depending on its final application.

1.4.2.1. DIPALMITOYLPHOSPHATIDYLCHOLINE (DPPC) LIPOSOMES

The most common phospholipid used for liposome synthesis, due to its stability and its ability to act against changes in pH, is phosphatidylcholine (PC) [167]. PC has phosphocholine as polar head group and two acyl hydrocarbon chains (Fig. 14). Among PCs, dipalmitoylphosphatidylcholine (DPPC) has been widely studied as DDS since it is a phospholipid naturally present in human body, and its T_c (41 ºC) is similar to the human body temperature [168]. DPPC is a fully saturated phospholipid with high stability and encapsulation efficiency [169]. Furthermore, DPPC liposomes have been already applied in dentistry as tooth whitening treatment since they are able to be adsorbed to hydroxyapatite [40].

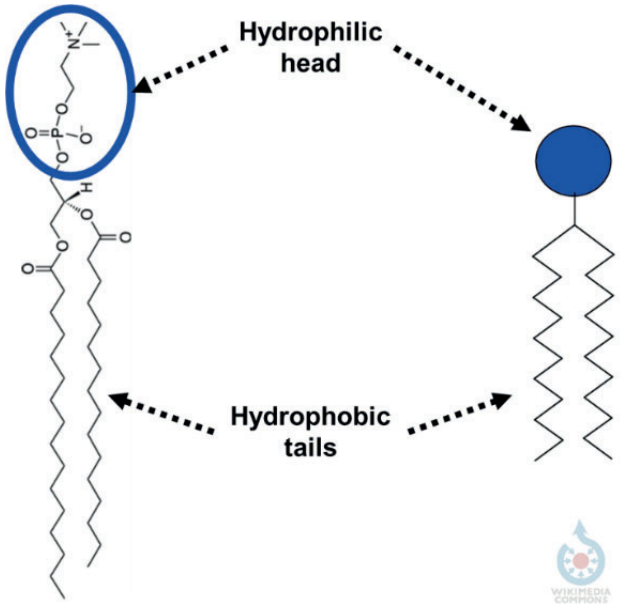

Figure 14: Chemical structure of dipalmitoylphosphatidylcholine showing the hydrophilic head and the hydrophobic tails.

Therefore, as DPPC liposomes are a well-known and highly reported model applied in several fields including oral health, they can be good candidates as DDS for dentin hypersensitivity treatments.

2. OBJECTIVES

Since there is not any current totally effective treatment to combat dentin hypersensitivity, finding a suitable alternative for this problem is a challenge. The main objective of this doctoral thesis is to develop a new formulation with potential analgesic effect based on cannabidiol delivery systems as a treatment for dentin hypersensitivity. This objective was planned to be accomplished by carrying out the following specific tasks:

- To develop a suitable synthesis for a novel encapsulation methodology to obtain cannabinoids loaded in γ-CD-MOFs using olivetol as a cannabidiol analogue.
- To implement a suitable preparation of dipalmitoylphosphatidylcholine liposomes to encapsulate cannabinoids by using olivetol as a cannabidiol analogue.
- To assess the penetration pattern of the drug loaded in each drug delivery system (γ-CD-MOFs or DPPC liposomes) along the tooth structure by an *in vitro* study that includes a bovine tooth model, the use of synchrotron-source infrared spectroscopy and principal component analysis (PCA) for data treatment.
- To optimize the γ-CD-MOFs synthesis and encapsulation methodology in terms of reaction yield and drug encapsulation by using a particular design of experiments (DoE).
- To validate the use of olivetol as a cannabidiol analogue using the optimal conditions in MOFs' formulations.

3. EXPERIMENTAL SECTION

3.1. EXPERIMENTAL TECHNIQUES

3.1.1. ANALYTICAL MICROWAVE

Microwave chemistry is the science of applying microwave radiation that acts as high frequency electric fields and it is able to heat any material containing mobile electric charges. Unlike conventional heating, microwave radiation produces uniform and fast heating of the target compounds since it is possible to control and follow the different parameters that are involved in the process such as time, temperature, power, and pressure. In this context, analytical microwave allows to save time and energy [170].

Figure 15: CEM corporation MARS 5 digestion analytical microwave system (CEM Corporation Matthews, North Carolina, USA) used in the present studies.

Analytical microwave technique has been employed for different purposes such as the digestion of elemental metals using acids or in extraction processes to obtain analytes from a sample matrix into an organic solvent [171]. In this work, this technique was used to perform the MOFs synthesis as offers the advantages of being a simple, rapid, inexpensive, relatively green, and efficient method. The instrument used was the analytical microwave Mars 5 (CEM Corporation Matthews, North Carolina, USA) (Fig. 15).

3.1.2. ULTRAVIOLET–VISIBLE (UV-VIS) SPECTROPHOTOMETRY

Ultraviolet-visible spectrophotometry is a type of absorption spectroscopy involving photons whose wavelengths are from the ultraviolet to visible range. The energy of these photons can promote the excitation of an electron from the ground state into a higher energy orbital.

When a sample is irradiated by a light source with a specific intensity (I_0) in the ultraviolet and visible range, the sample partially absorbs it, and the intensity of the transmitted light (I) can be measured as absorbance by a suitable detector (Fig. 16). The more molecules contains the solution, more radiation will be absorbed [172].

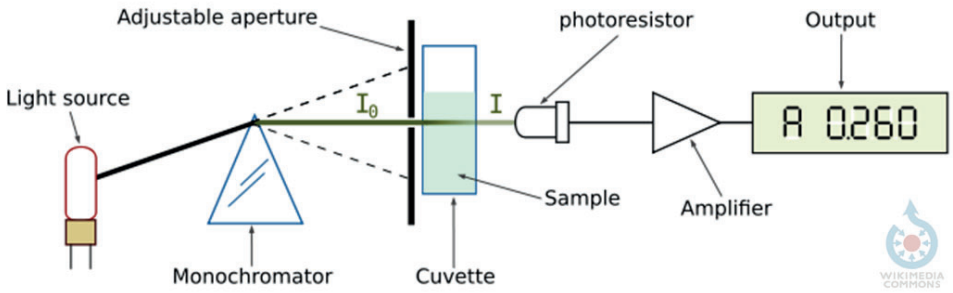

Figure 16: Essential parts of a spectrophotometer including the light source, the monochromator and the sample.

Thus, in this characterization technique there is a linear relationship between absorbance and absorber concentration through Lambert-Beer law, being very useful for quantitative analysis [173]. Moreover, each molecule has its own absorption spectrum.

In this work, this technique was applied to quantify the drug content in the drug delivery systems since cannabidiol and olivetol present a characteristic absorption peak at 275 nm. The instrument used was a UNICAM, model UV-2 200 (USA) double-beam spectrophotometer (Fig. 17).

Figure 17: UNICAM UV-2 200, UV double-beam spectrophotometer used in present studies.

3.1.3. SCANNING ELECTRON MICROSCOPY (SEM)

Scanning electron microscopy uses electrons instead of light to form an image. The electron beam is produced by an electron gun, and it interacts with the surface of the sample creating the image with the electrons generated from this interaction (Fig. 18). This technique gives information about the surface characteristics of the sample, including shapes, textures, morphology, and orientation of the materials [174]. The electron beam is focused using vacuum and multiple condenser lenses. These high-energy electrons hit the sample and the different electrons generated from this interaction are collected by each detector that builds the image depending on the equipment. Backscattered electrons are produced when an electron in the beam collides with the nucleus of an atom in the sample, generating images with different brightness depending on the surface chemical composition, but with lower resolution. Secondary electrons are produced when an electron in the beam passes very close to the nucleus of an atom in the sample, providing enough energy to one or more of the inner electrons to jump out of the sample. These electrons provide detailed topographical information of the sample. It is important to notice that the conductive samples are less altered by the electron beam and images could be directly obtained. Non-conductive samples had to be coated with a conductive material like gold or carbon tape. Another approach is to remove the electrons accumulated on the sample surface using a gentle flux of nitrogen gas to prevent overcharging [175].

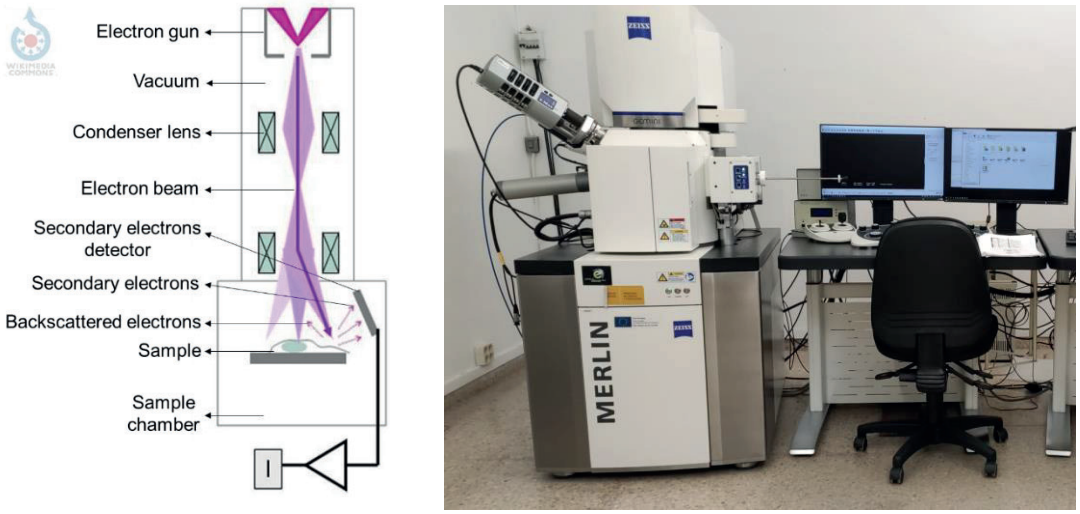

Figure 18: Scanning electron microscope set up (left) and a Zeiss Merlin SEM equipment (right) used in present studies.

In the present work, the morphology of the MOFs samples was analysed by SEM with a Zeiss Merlin SEM equipment (Fig. 18).

3.1.4. ENERGY-DISPERSIVE X-RAY (EDX) SPECTROSCOPY

This analytical technique is used for quantitative or qualitative elemental analysis and chemical characterization of samples. A high-energy beam of charged particles hits the sample, an electron is excited by this beam and kicked out. Then, other electron from a higher energy state fills this gap, releasing the difference of energy between the two states as X-ray (Fig. 19). Since each element has a characteristic atomic structure, this X-ray emission is also different allowing the elemental analysis [176].

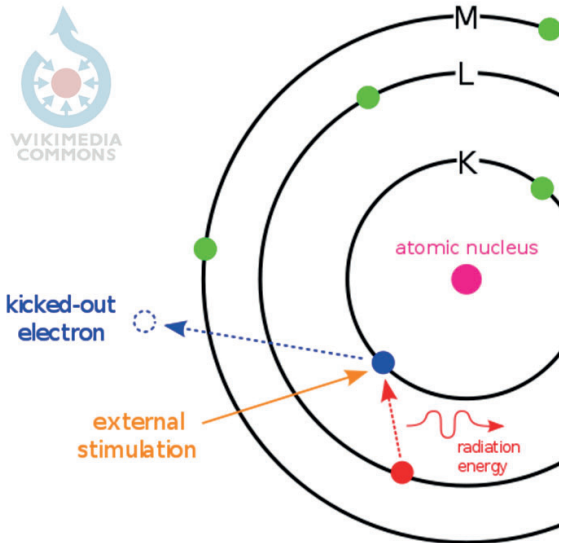

Figure 19: Principle of EDX spectroscopy, the external stimulation beam of charged particles excites an electron and other electron from a high-energy state fills this gap releasing energy.

In this work, the presence of the metal linker in the MOFs samples was qualitatively determined using the EDX Oxford INCA X-Max Detector coupled to the scanning electron microscope.

3.1.5. X-RAY DIFFRACTION (XRD)

The basis of diffraction techniques is the interaction of the crystalline structure of a substance with a source of X-rays. This structure has infinite parallel planes separated by a certain distance called the interplanar distance (d). When an X-ray beam goes to one plane, it is diffracted with an angle θ and it will be also diffracted with the same θ angle by the second plane. If these waves have constructive interference the diffracted beam is not cancelled and is detectable. This occurs when the path length difference between the waves is a multiple (n) of the wavelength (λ), following the Bragg's law condition (Fig. 20). As each family of planes has a distance d, planes at different angles will be detected and the results will differ depending on the structure. Thus, the crystalline phases could be characterized based on the different diffraction peaks which are the reflections of the planes of each phase, and each reflection is assigned by Miller indices represented by (hkl) values [177].

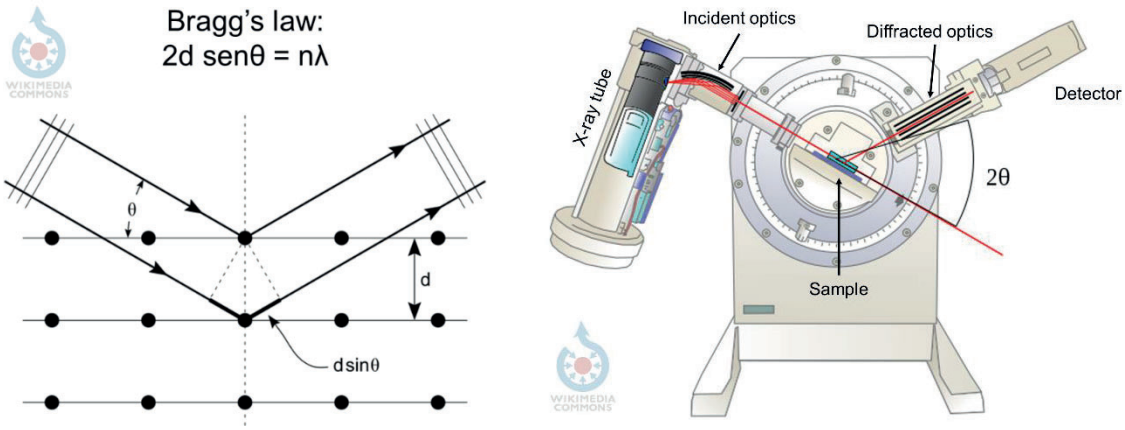

Figure 20: Bragg diffraction from a cubic crystal lattice (left) and XRD diffractometer (right).

In the present work, the crystallinity of the MOFs samples was characterized by X-ray powder diffraction (XRPD) using a Malvern Panalytical X'Pert PRO MPD (Material Powder Diffractometer) (Fig. 21). The MPD is suitable for the analysis of polycrystalline samples at room temperature. This diffractometer has a vertical theta-theta goniometer (240 mm radius).

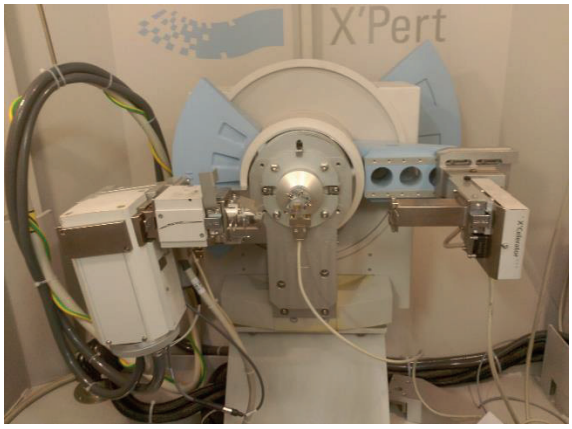

Figure 21: Malvern Panalytical X'Pert PRO MPD (Material Powder Diffractometer) used in this study.

3.1.6. FOURIER TRANSFORM INFRARED (FTIR) SPECTROSCOPY

This spectroscopy is based on the absorption of infrared radiation by vibrating molecules. A molecule will absorb the energy of an infrared light beam and if this energy is enough, the atoms that form the molecule will vibrate in a certain way because of this energy supplied. Two basic categories of vibrations can be distinguished such as stretching and bending vibrations. Stretching vibrations are changes in the interatomic distance along the axis of the bond between two atoms and they can be symmetric (in-phase) and antisymmetric (out-of-phase). Meanwhile, bending vibrations are caused by changes in the angle formed by two bonds. Each molecule has its own infrared spectrum, so this technique is widely used to study the chemical composition of materials [178]. Fourier transformed infrared (FTIR) spectroscopy is based on the interference of radiation between two beams. The light from an infrared source is divided into two beams through a splitter placed at 45º from the source. One of the beams travels to a stationary mirror, and the other to a moving mirror. Then, they are reflected to the splitter where they are combined again. The new single beam interacts with the sample and then the resulting signal is converted in the infrared spectrum by Fourier transformation. In FTIR spectroscopy there are different sample measurement techniques such as transmission or specular reflectance. Another mode of measurement is the attenuated total reflectance (ATR), in which the infrared light beam is incident on a crystal, and it is reflected at least once on its surface in contact with the sample. The light undergoes multiple internal reflections in the crystal which are extended into the sample and finally, the light beam is collected by the detector (Fig. 22) [179].

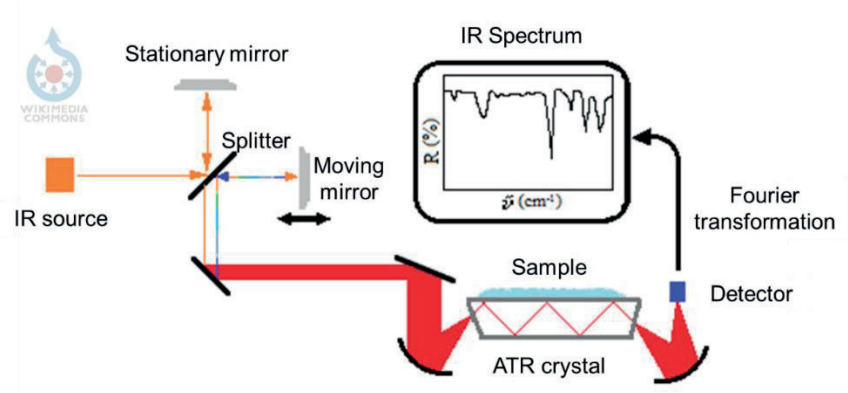

Figure 22: Essential parts of a Fourier transform infrared spectrophotometer with ATR sample measurement technique.

In the present work, infrared spectroscopy spectra of samples were obtained using an Infrared Spectrophotometer Tensor 27 equipped with an Attenuated Total Reflectance module Specac Golden Gate (ATR-FTIR, Bruker, Ettlingen, Germany) (Fig. 23). The ATR accessory allows direct recording of samples, thus, facilitating the recording of IR spectra on liquid or solid samples regardless of their physical nature.

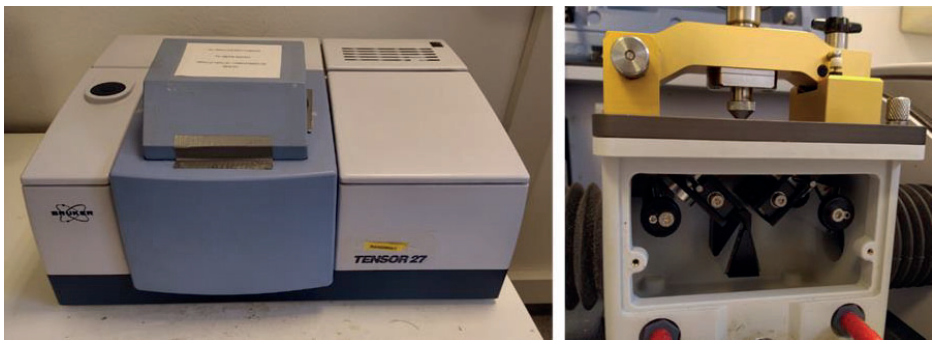

Figure 23: Infrared Spectrophotometer Tensor 27 (left) equipped with an Attenuated Total Reflectance module Specac Golden Gate (right) used in the present studies.

3.1.7. CRYO-TRANSMISSION ELECTRON MICROSCOPY (CRYO-TEM)

Transmission electron microscopy uses electrons instead of light to form an image. In this technique, the electrons cross the sample, so it should be very thin. Thus, TEM gives information about the internal structure of the sample, including its morphology, composition, and crystalline structure [180].

The electron beam is focused using vacuum and multiple condenser lenses to the sample. These high-energy electrons interact with the sample, since they are negatively charged, and they are repelled by the electrons in the orbital of atoms. This interaction causes the electrons of the beam to scatter and a contrast is generated. This contrast will be greater the more electrons have the atoms around their nucleus, since more electrons of the beam will be scattered. After the sample, the objective lenses focus the scattered electrons, and the projector lenses magnify the image and project it on to the detector, building the image (Fig. 24). Due to the vacuum environment, samples should be protected to avoid its dehydration. This could be done by rapid freezing using liquid nitrogen (Cryo-TEM) [181].

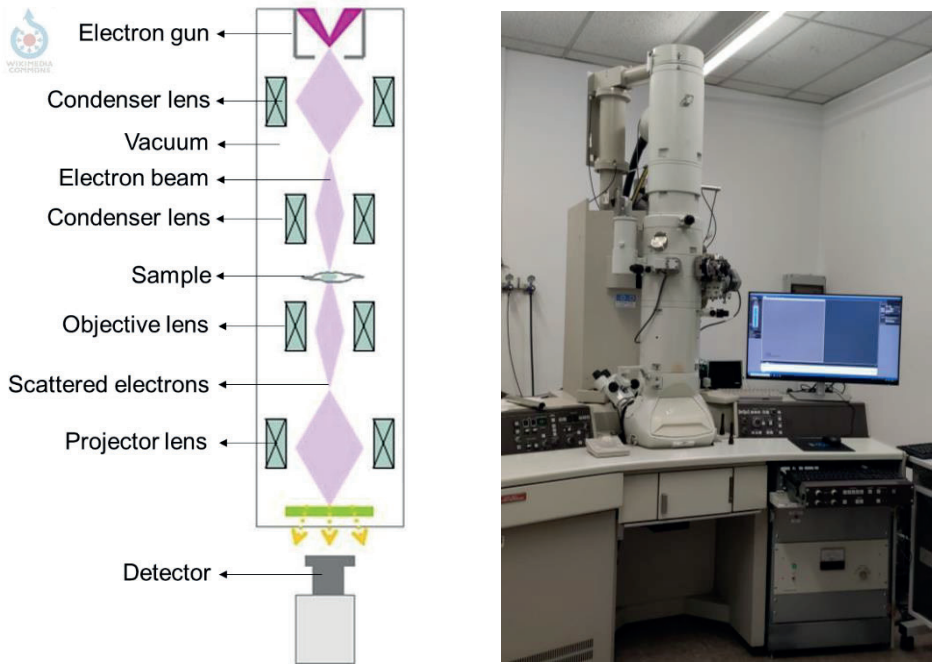

Figure 24: Transmission electron microscope set up (left) and cryo-TEM JEM-2011 equipment (right) used in the present studies.

This technique has been applied to characterize liposomes dispersions in terms of size and morphology using a JEM-2011 (Jeol, Japan) (Fig. 24).

3.1.8. DYNAMIC LIGHT SCATTERING (DLS)

Dynamic light scattering is a technique for measuring the size distribution of molecules and particles that have been scattered or dissolved in a liquid. This technique correlates the

Brownian motion of particles with their size by illuminating the sample with a laser beam, analysing the intensity of the fluctuations of the scattered light at a known scattering angle using a detector (Fig. 25). An important feature of this motion is that larger particles move more slowly than smaller particles, and the relationship between the particle size and its velocity due to Brownian motion is defined by the Stokes-Einstein equation [182].

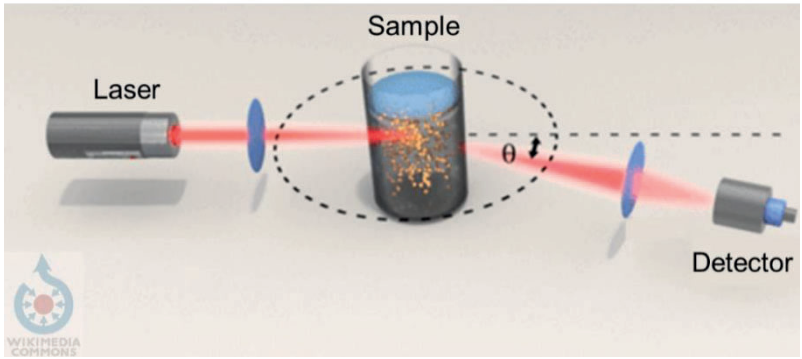

Figure 25: Dynamic light scattering set up including the laser beam, the sample, and the detector.

In the present work, liposome dispersions size distributions were characterized by dynamic light scattering (DLS). This analysis was performed with ZetaSizer Nano ZS (Malvern Panalytical, Netherlands, and United Kingdom) and sensitive avalanche photodiode detector (APD) (Fig. 26).

Figure 26: ZetaSizer Nano ZS equipment (Malvern Panalytical, Netherlands, and United Kingdom) for DLS analysis carried out in present studies.

3.1.9. SYNCHROTRON RADIATION

Synchrotron light is electromagnetic radiation generated by the acceleration of charged particles such as electrons, circulating inside an accelerator in a circular orbit, maintained by magnetic fields. Electrons are emitted from a hot metal filament in the electron gun. Then, the particles are accelerated to 100 MeV by a linear accelerator, and they travel to the booster ring where the electrons are further accelerated to almost the speed of light. Following this, the electrons are periodically injected from the booster ring to the storage ring. The storage ring is a polyhedron with bending magnets in each vertex. These magnets force the electrons to deviate from their straight trajectory, producing radiation in a broad spectrum of photon energy [183]. This photon energy is emitted tangentially to the beamlines where it is used for different analysis. To compensate these energy losses during the emission, radio-frequency cavities feed energy to the electrons in the storage ring. Beamlines are mainly divided in optical and experimental hutches and control cabin. In the optical hutch, the beam is focused to select the energy radiation desired depending on the analysis [184]. Meanwhile, in the experimental hutch the samples are located for the analysis and in the control cabin each experiment is monitored (Fig. 27).

The advantage of using the synchrotron light is that the beam is highly collimated since it is emitted in the forward direction and tangentially to the circular orbit. This fact gives that the brightness of synchrotron light is trillions of times greater than conventional laboratory sources. This property leads to better signal-to-noise ratio that means lower noise in the spectral data, thus increasing the spectral resolution. Besides, the highly collimated source allows to have a thinner beam, achieving high spatial resolution and analysing small areas.

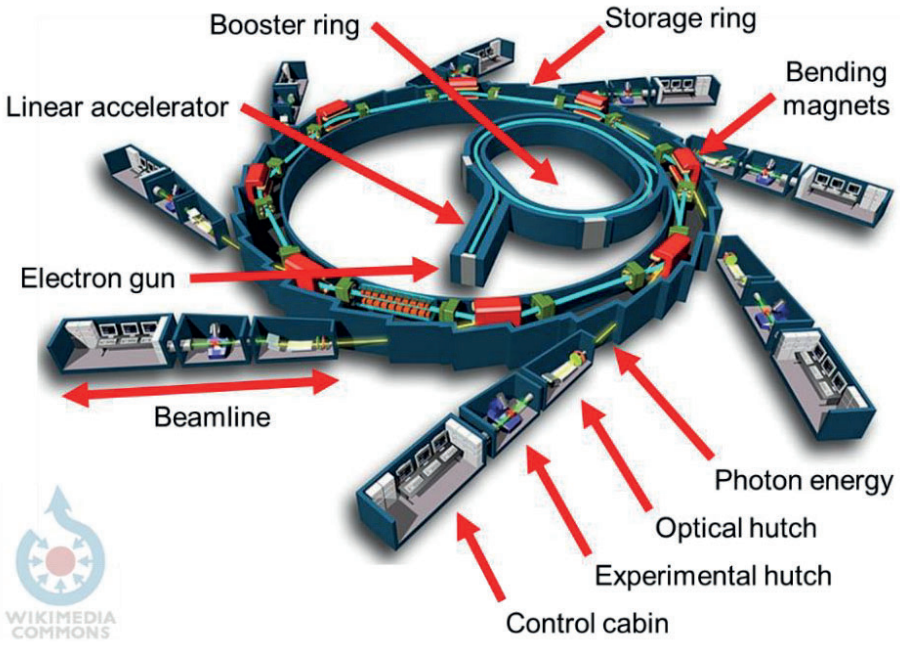

Figure 27: General diagram of a synchrotron facility, specifically Synchrotron Soleil.

Thus, depending on the radiation energy selection in the optical hutch, the beamlines are designed for different techniques such as infrared, soft X-rays or hard X-rays. In the present work, the technique used with synchrotron radiation was infrared microspectroscopy. The addition of a synchrotron radiation light source to FTIR technique provides the high intensity, the spectral purity, the spatial and the energy resolution necessary to study the dental structure at micro and nano levels.

In this work, tooth samples were analysed by FTIR microscope in the reflection mode at MIRAS beamline of ALBA synchrotron (Cerdanyola del Vallès, Spain) (Fig. 28). Hyperion 3000 microscope coupled to a Vertex 70 spectrometer (Bruker, Germany) and an HgCdTe (MCT) detector was used.

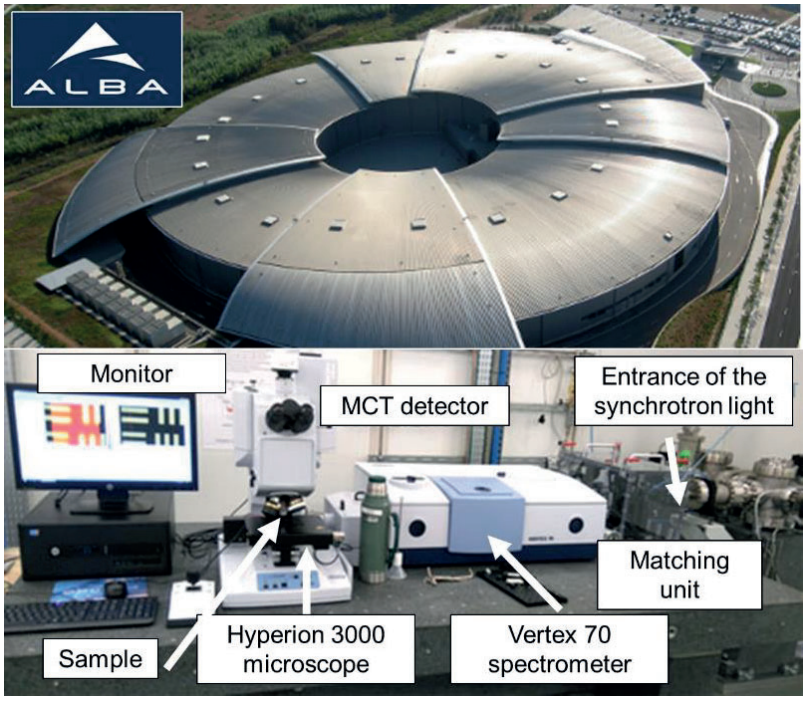

Figure 28: ALBA synchrotron (top) and MIRAS beamline (bottom) in Cerdanyola del Vallès, Spain (source: https://www.albasynchrotron.es/es).

3.2. CHEMOMETRIC TECHNIQUES

The use of instrumental techniques for analytical purposes along with the continuous technological progress create large amounts of complex data in a fast way. Nevertheless, obtaining data does not mean understand the information that the data have. Thus, these data should be processed and interpreted in order to convert it into useful information. In this context, chemometric techniques appear as a promising tool for chemical data evaluation and interpretation.

Chemometrics is the chemical discipline that uses mathematical, statistical, and other methods to design or select optimal measurement procedures and experiments, and to provide maximum relevant chemical information by analysing data [185]. For these reasons, chemometrics is an interdisciplinary field. Although its methods and tools come from other disciplines, the aims of chemometrics are linked to chemistry. Besides, chemometrics is improving several aspects in analytical chemistry today such as speed, lower costs, miniaturisation, or transportability.

Chemometrics is not a single tool but a range of methods including basic statistics, signal processing, factorial design, calibration, curve fitting, factor analysis, detection, pattern

recognition, and neural network [186]. In the present work, design of experiments (DoE) and principal component analysis (PCA) were applied as chemometrics tools.

3.2.1. DESIGN OF EXPERIMENTS (DoE)

In analytical chemistry, optimization is a critical stage that allows to find the experimental conditions which produce the best possible response and, therefore, the best possible analytical performance. Design of Experiments (DoE) has become one of the best-known statistical techniques that allows to maximize information derived from complex experimental data though the full control of the variables under examination, the relations between them and the responses which have to be optimized [187]. Furthermore, it can lead to a more efficient use of the resources, a reduction of process development times and a greater process reliability in the experimental procedures.

To develop a suitable DoE, the investigated experimental area or experimental domain should be properly defined. Thus, all the experimental variables or factors that may influence the process must be carefully identified and examined, as well as the levels or values of each one (generally represented by a normalized scale in the interval between -1 and +1 for each factor). The properties that are the object of the optimization or responses should be also selected. It is important to consider that the more factors, levels and/or responses have the DoE, the more experiments will be carried out, so it is necessary to find a compromise [188].

Choosing the most appropriate design is also a key aspect since associated with the design there will be a mathematical model that relates the factors to the responses. The required model will be defined by the proper purpose of the experimentation. There are different experimental design models, but one of the most relevant and used is the response surface methodology (RSM)RSM is a multivariate statistical method that has been widely applied to the optimization of complex processes since it reduces the number of experiments, and it considers the interactions between the studied factor at the same time. In this context, RSM provides a detailed description of the system with a flexible, higher-order equation and a more accurate optimization. Because of its versatility, the RSM has been widely used not only in analytical applications but also in the industrial field as well as in the pharmaceutical and medical processes [189].

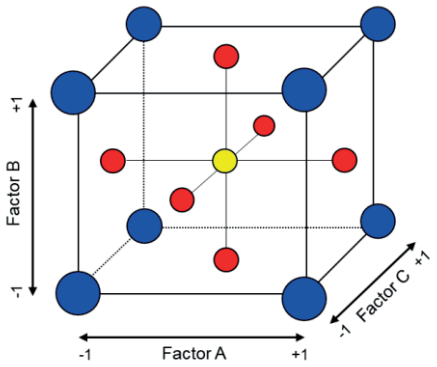

Figure 29: Example of a face-centered Central Composite Design experimental domain with three factors.

The face-centered Central Composite Design (CCD) is the most used in this model. This design requires three levels of each factor (-1, 0 and +1) since there are center points and points at the center of each face of the experimental domain (Fig. 29) [190].

After this selection and the performance of the experiments, the data will be analysed considering the chosen experimental domain, the experimental values of the responses and its comparison with the predicted ones. This evaluation will build the model, establishing cause-and-effect relationships between the factors and the responses. Besides, it will be able to predict new values for the responses by introducing changes in the factors, validating the designed model. In this work, a design of experiments (DoE) has been developed to optimize the reaction yield and drug encapsulation in CD-MOFs. Response surface methodology (RSM) based on a Central Composite Design (CCD) was selected for the optimization strategy.

3.2.2. PRINCIPAL COMPONENT ANALYSIS (PCA)

Principal component analysis (PCA) is one of the most frequently employed chemometric method. It is a multivariate method that can find intrinsic relationship or patterns (latent variables) between different samples by using the variables in an easy and visual way by using all the information available for each sample simultaneously. These latent variables will be the principal components that are going to explain the variability in the data. The main objective of PCA is to simplify and reduce the number of chemical variables of the original data identifying trends and patterns more easily, preserving the maximum information [191].

PCA follows different steps. First, it represents the data in a space that has the same dimensions that the number of new variables and where each sample is represented by a point. Each sample is a point in the space of a specific number of variables. Then, the analysis looks for the latent variables or principal components where the principal component 1 (PC1) will explain the direction of the maximum variability of the data and principal component 2 (PC2) will explain the maximum variability that the PC1 has not explained before. An important aspect is that the principal components are constrained to be orthogonal and to cross the origin (Fig. 30). To interpretate the PCA there are several plots. Scores plots stablish the relationship between the samples (points) with the new components though the distance of the projected samples to the axes. Meanwhile, loadings plots relate the new components with the old variables [192].

Before performing a PCA, the samples should be as most homogeneous as possible since PCA is scale-dependent and numerically larger variables appear to be more important. This problem could be solved using pre-processing techniques that help to remove noise and normalize the variables improving the quality of the analysis. One of the most common pre-processing methods to normalize continuous variables is the mean centering. This technique calculates the mean of each variable and subtracts this from each variable [193].

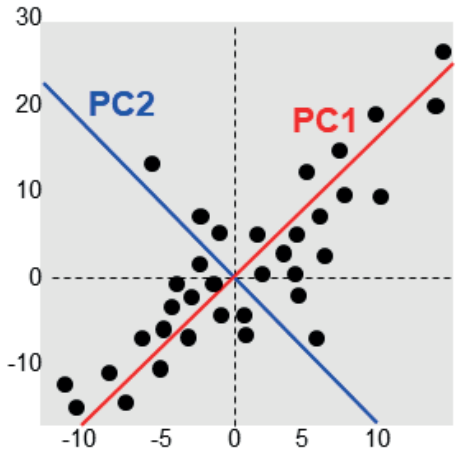

Figure 30: Principal components 1 and 2 explaining the two first directions with the maximum variability of the data.

In the present work, PCA was applied to process the infrared spectroscopic data from *the in vitro* experiment using synchrotron radiation to assess the penetration pattern of the drug in bovine teeth by both delivery systems.

3.3. EXPERIMENTAL PROCEDURES

3.3.1. REAGENTS

Chloroform (99.9%), sodium chloride (99%), disodium phosphate (99%), potassium hydroxide (85.5%) and potassium nitrate (99.2%) were purchased from VWR BDH Chemicals (Oud-Heverlee, Belgium). Potassium chloride (99.0%), sodium azide (99.5%), 2-[4-(2-hydroxyethyl)piperazin-1-yl]ethanesulfonic acid (99.5%, HEPES) and magnesium chloride (99%) were purchased from Sigma-Aldrich (St. Louis, MO, USA). 1,2-Dipalmitoyl-sn-glycero-3-phosphocholine (99%, DPPC) was purchased from Avanti Polar Lipids (Alabaster, AL, USA). Cannabidiol (99%) was purchased from Tocris Bioscience (Bristol, United Kingdom). Methanol (99.8%) and acetic acid (99.9%) were purchased from Fisher Scientific (Madrid, Spain). Ethanol (96%) and dichloromethane (99.5%) were purchased from Scharlau (Sentmenat, Spain). Potassium dihydrogen phosphate (99.5%) and calcium chloride (78%) were purchased from Panreac (Barcelona, Spain). Polyethylene glycol 20000 was purchased from Merk (Darmstadt, Germany). Olivetol (95%) and γ-cyclodextrin (98%) were purchased from Carbosynth Ltd (Compton, United Kingdom). MilliQ water was purified through a Millipore purification system from Millipore (Milford, MA, USA).

3.3.2. SYNTHESIS AND ENCAPSULATION METHOD OF OLV LOADED γ-CD-MOFs

The first experimental procedure was to establish a suitable synthesis and encapsulation methodology to obtain cannabinoids loaded γ-CD-MOFs using olivetol as CBD analogue. For that purpose, several potassium sources and different drug encapsulation methodologies were employed.

3.3.2.1. PREPARATION OF OLV LOADED γ-CD-MOFs

A fast synthesis of γ-CD-MOFs was performed using a microwave irradiation method [127] with some modifications. This reported method offers the advantages of simple, rapid,

inexpensive, relatively green, and efficient non-conventional heating and high yield [126]. Briefly, γ-CD (324 mg) and KOH (112 mg) were mixed in milliQ water (10 mL). The molar ratio of KOH to γ-CD was 1:8. Then, 6 mL of methanol were added. This initial solution was treated at 50 ºC in the analytical microwave (CEM Corporation Matthews, North Carolina, USA) for 10 min and a power of 600 w. After that process, 256 mg of PEG 20000 were added for one hour to trigger the precipitation of the crystals at room temperature. In order to remove the unreacted material, crystals were washed first with 10 mL of methanol and then with 10 mL of ethanol in a centrifuge at 3000 rpm for 5 min. Next, γ-CD-MOFs were left under vacuum and dried overnight at 50 ºC. Herein, preliminary alkaline γ-CD-MOFs (pH = 12) were obtained. Since cannabinoids get oxidized in alkali media, a neutralization of the γ-CD-MOFs was needed. For this step, crystals were treated with a mixture of 5.2 mL of ethanol and 0.8 mL of acetic acid. The suspension was then shaken at 290 rpm for 2 hours and the precipitates were collected by centrifugation (3000 rpm for 5 min). Once again, the powder was left to dry overnight under vacuum at 50 ºC. Afterwards, an activation of the γ-CD-MOFs was performed using a solvent exchange method with dichloromethane in order to remove guest molecules from chemicals used in the synthetic procedure. γ-CD-MOFs were mixed with 10 mL of dichloromethane at 290 rpm for 3 days. Every 24 hours the solvent was replaced by centrifugation (3000 rpm for 5 min). Finally, the samples were dried overnight under vacuum at 50 ºC. γ-CD-MOFs were kept under vacuum at room temperature until its use and the reaction yields were also calculated following equation 1:

$$\text{Reaction yield } (\%) = \frac{\text{Real MOF sample weight without drug (mg)}}{\text{Theorical MOF sample weight without drug (mg)}} \cdot 100 \quad [1]$$

Impregnation and co-crystallization methods were performed to load olivetol into γ-CD-MOFs. In case of impregnation, 30.8 mg of MOF samples were added to 20 mL of OLV 360 mg/mL solution in ethanol in order to obtain a 1:2 molar ratio of γ-CD-MOFs:OLV respectively (Fig. 31). Suspensions were incubated for 24 hours at 37 ºC under stirring conditions (290 rpm). After the incubation time, crystals were washed with 10 mL of ethanol in a centrifuge at 3000 rpm for 5 minutes in order to remove the drug that did not interact with the γ-CD-MOFs. Finally, the samples were dried and kept under vacuum at room temperature until their use.

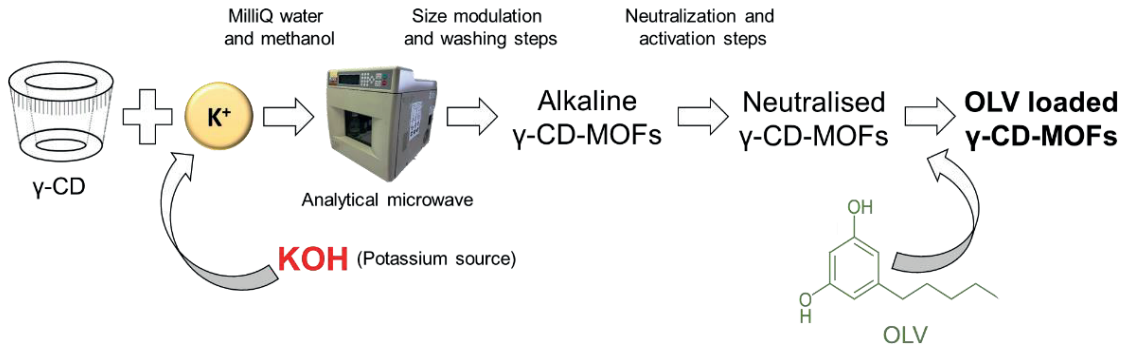

Figure 31: Synthesis of γ-CD-MOFs with microwave irradiation and OLV encapsulation using the impregnation method diagram.

The co-crystallization method is similar to that described before (Fig. 32). In this case, the potassium sources were KCl or KNO_3 instead of KOH, adding 149 mg or 202 mg respectively, to maintain the 1:8 molar ratio. The change in the potassium source is because in the co-crystallization the drug is loaded on the initial solution, where the synthesis takes place, and the pH of the medium must be neutral from the beginning to avoid olivetol oxidation. Additionally, 30 mg of OLV were also diluted in the initial solution. This amount of drug was selected in order to keep the same molar ratio between MOF and olivetol as in the impregnation method. In this method the incubation time with PEG 20000 was 24 hours instead of one hour, but the neutralization and activation steps were not needed. Finally, the washes were the same as described before, and the resultant samples were left overnight under vacuum at 50 ºC and kept in a desiccator under vacuum at room temperature until its use. It should be noted that MOFs were not obtained when KCl or KNO_3 were employed following the same synthesis procedure as for KOH.

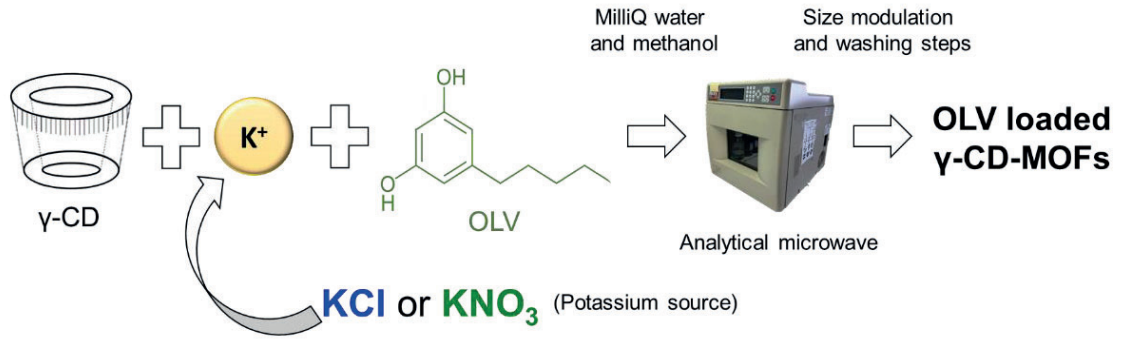

Figure 32: Synthesis of γ-CD-MOFs with microwave irradiation and OLV encapsulation using the co-crystallization method diagram.

The γ-CD-MOFs loaded by impregnation method were named as γ-CD-MOF KOH, loaded or not with OLV. In the case of co-crystallization technique OLV loaded MOFs were named as γ-CD-MOF KCl and γ-CD-MOF KNO_3, for KCl and KNO_3 as potassium sources respectively.

3.3.2.2. OLIVETOL LOADING QUANTIFICATION

The quantification of the drug encapsulation into the MOFs was determined as follows: 15 mg of MOF sample were added to 5 mL of a mixture of milliQ water and ethanol (1:1, v/v). The mixture was incubated at room temperature under stirring conditions (290 rpm) for 24 hours to promote the degradation of the crystals and release the encapsulated OLV. To determine the amount of olivetol, the solution was measured by UV-Vis spectrophotometry (Thermo Fisher Scientific, Massachusetts, USA). The UV detection was performed at 275 nm, where OLV presents a maximum of absorbance, and the reference was a mixture of milliQ water and ethanol (1:1, v/v). A calibration curve of different known concentrations of olivetol in milliQ water: ethanol (1:1, v/v) was also performed from 0 to 100 mg/L of the drug to determine the concentration of olivetol in the samples.

The drug loading for each MOF was calculated following equation 2:

$$\text{Drug loading } (\%) = \frac{\text{Encapsulated OLV into the carrier (mg)}}{\text{Total Weight of OLV loaded carrier (mg)}} \cdot 100 \quad [2]$$

All determinations of the loaded drug in each MOF sample were performed by triplicate.

3.3.2.3. CHARACTERIZATION OF THE SAMPLES

The morphology and elemental composition of the MOFs' samples were analysed by Scanning Electron Microscopy (SEM) and Energy Dispersive X-ray Spectroscopy (EDX). The images were taken with the Secondary Electron Detector with a low voltage of 1 - 2 kV and the EDX measurements were taken at 10 kV. This microscope has a unique charge compensation system that allows the high-resolution imaging of non-conductive samples, electrons which accumulate on the sample surface are swept away by a fine jet of nitrogen. All the experiments were performed at room temperature.

The crystallinity of the MOFs' samples was characterized by X-ray powder diffraction (XRPD). This analysis was carried in transmission mode using a capillary spinner and the sample were filled inside borosilicate glass capillaries with outer diameter of 0.7 mm. A focusing mirror was used for the incident beam and a lineal X'Celerator detector for the diffracted beam. The samples were irradiated with a ceramic X-ray tube with Cu Kα anode (l = 1.5406 Å), tube voltage of 45 kV, tube current of 40 mA in a step size scan mode (0.03° min^{-1}) and analysed over a 2θ angle range of 2.5 - 35°.

In the Infrared Spectroscopy analysis, to measure the powder samples 64 scans were carried out in wavenumber from 4000 cm^{-1} to 600 cm^{-1} at a resolution of 4 cm^{-1} and at room temperature. For the background the own diamond window of the equipment was used.

3.3.3. SYNTHESIS AND ENCAPSULATION METHOD OF OLV LOADED LIPOSOMES

The next experimental procedure was to establish a suitable synthesis and encapsulation methodology to obtain cannabinoids loaded DPPC liposomes with olivetol as CBD analogue. For that purpose, the thin-film hydration method using a rotary evaporator and the mechanical dispersion with sonication were employed.

3.3.3.1. PREPARATION OF OLV LOADED DPPC LIPOSOMES

DPPC liposomes were obtained by hydration and mechanical dispersion [40]. Briefly, DPPC was dissolved in chloroform/methanol (2:1, v/v) at 100 mM. 0.25 mL of the DPPC solution and a volume of the chloroform/methanol mixture were introduced in a bottom round flask until a final volume from 4 to 7 mL. Then, the evaporation took place using a rotary evaporator (Büchi, Flawil, Switzerland) maintaining the temperature of the bottom round flask above the phase transition temperature (T_c) of the phospholipid. In this study, this value is 41 ºC for DPPC. When the monolayer of DPPC was obtained on the inside surface of the flask, 5 mL of HEPES buffer solution 20 mM (pH = 7.4) was added to the flask. Then, the suspension was sonicated for 15 minutes to obtain multilamellar vesicles (MLVs), maintaining the temperature of the bottom round flask above the T_c. All liposomal preparations were stored at 4 ºC until its use and the final concentration of DPPC was 5 mM. A molar ratio of DPPC liposomes loaded with olivetol were prepared, 2:1 respectively. In this case, 3.75 mL of a mother solution of olivetol 600 mg/L in methanol were added with the DPPC solution into

the bottom round flask in order to get the final desired concentration of the drug (2.5 mM for 2:1 ratio). Then, solutions were treated as described above.

3.3.3.2. OLIVETOL LOADING QUANTIFICATION

The encapsulation of the drug was determined adapting a method previously described [194]. 0.167 mL of liposome suspension were added to 0.834 mL of ethanol (1:5, v/v). The mixture was sonicated for 5 minutes and mixed to promote the disruption of the liposomes and release the encapsulated olivetol.

The resultant solutions were measured by UV-Vis spectrophotometry at 275 nm where the characteristic peak of OLV could be found as in previous section. The reference was the same solution where each carrier was dissolved and a calibration curve of different known concentrations of OLV in the same solution was prepared from 0 to 100 mg/L for each carrier. All determinations were performed by triplicate following equation 2 (section 3.3.2.2).

3.3.3.3. CHARACTERIZATION OF THE SAMPLES

Liposome dispersions were characterized by Cryo-transmission electron microscopy (Cryo-TEM) and Dynamic light scattering (DLS). Cryo-TEM images were taken using 5000x of magnification and samples were prepared by depositing 3 µL on a copper grid covered with a carbon reinforced holey polymer film. Thin sample films (30 - 300 nm) were blotted with a filter paper and immersed into liquid ethane. Samples were kept below -179 °C and protected from atmospheric conditions during the whole process. All sample preparations were performed in a room at 25 °C and 70% relative humidity.

Dynamic light scattering is used to measure particle size and molecular size. Measurements were made in disposable folded capillary cells (R.I.: 1.450 and absorption coefficient: 0.01) at 20 ºC using a laser with λ_0 = 632.8 nm and 175º angle. The viscosity of water was taken as 1.0031 cP and 1.330 of R.I.

3.3.4. *IN VITRO* STUDY USING SYNCHROTRON-SOURCE INFRARED SPECTROSCOPY

Then, to assess the penetration pattern of the drug loaded in liposomes and in γ-CD-MOFs along the enamel tooth, an *in vitro* experiment was carried out using bovine tooth as a sample model, application of synchrotron-source infrared microspectroscopy for samples analysis and principal component analysis (PCA) to treat the generated spectral data.

3.3.4.1. TOOTH SAMPLES PREPARATION

Bovine incisors were cut by separating them from the roots using a diamond saw. Then, the specimens were cleaned and preserved in sodium azide solution (0.8%). Teeth were embedded in self-curing acrylic resin (Paladur, Germany) leaving the frontal enamel free of resin. Specimens were cut in half and its lateral surface was polished down to 1 µm particle size in order to obtain good reflection properties for the measurements using a sequence of silicon carbide paper. Then, teeth were treated with 0.1 mL of each treatment 3 times per day for 5 days, making sure that only the frontal enamel was in contact with each solution and not with the lateral surface (Table 3, Fig. 33). Since MOFs' treatments are the only ones which are in powder, 1 mg of each MOF formulation was mixed with 15 µL of HEPES buffer and then, the resultant solution was applied over the teeth.

Table 3: List with the different treatments applied over the dental samples.

Treatment's list
Control (HEPES buffer)
Cannabidiol (10 mg/mL)
Olivetol (10 mg/mL)
DPPC liposomes
DPPC liposomes loaded with olivetol
CD-MOFs KCl loaded with olivetol
CD-MOFs KNO_3 loaded with olivetol

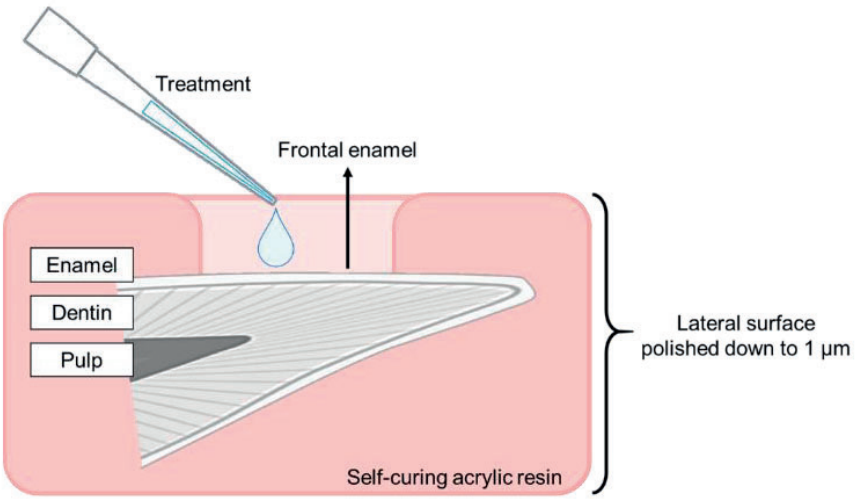

Figure 33: Sample preparation and treatment application over the teeth diagram.

3.3.4.2. SYNCHROTRON SOURCE INFRARED SPECTROSCOPY MEASUREMENTS

The 36x Schwarzschild magnification objective and condenser were used to focus the infrared light on the sample. A mapping of 300 x 1000 µm (wide x length) was made per each sample in the lateral surface from the outside of the enamel to the dentin. In each mapping, 250 spectra were measured having 5 spectra wide and 50 spectra length (Fig. 34). For each spectrum, 64 scans were carried out from 4000 cm^{-1} to 600 cm^{-1} with 4 cm^{-1} of spectral resolution and at room temperature, using 10 x 10 μm^2 of aperture size. The background was measured with a gold mirror reference. OPUS 7.5 (Bruker, Germany) was used to collect the spectra.

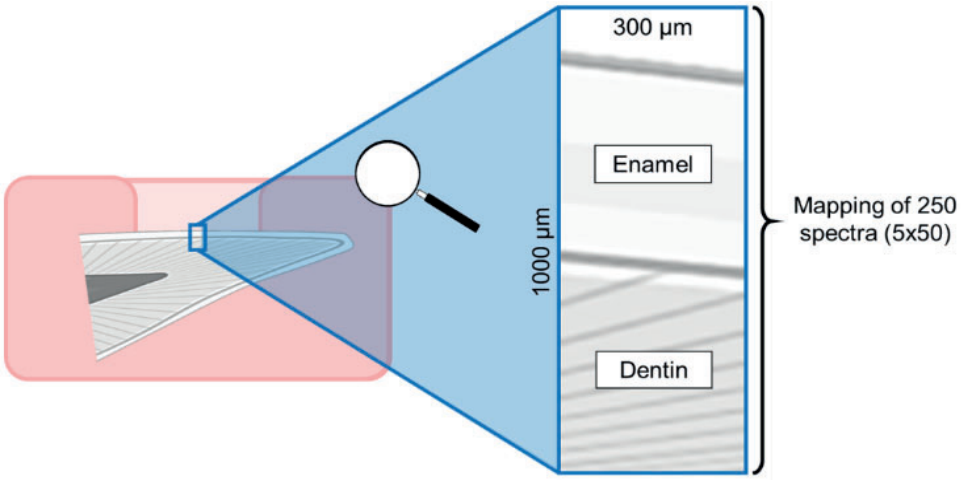

Figure 34: Synchrotron source infrared spectroscopy measurements procedure.

3.3.4.3. PRINCIPAL COMPONENT ANALYSIS

PCA was applied to process the data using PLS toolbox 8.2.1 (20559) for its use with MATLAB 9.1 (R2016b). This chemometric tool is able to extract the main variability correlating it with the chemical compounds that are in the sample and their distribution. In the spectral data obtained for this study, enamel and dentin are the two regions well differentiated in the mappings, being the most intense peak the ν_3 PO_4^{2-} for both regions. Due to the high variability of biological samples, the big mapping per sample were limited to two smaller mappings of 30 spectra having 5 spectra wide and 6 spectra length, one in the inner enamel and another in the inner dentin. The wavenumber range was also limited from 1600 to 700 cm^{-1} where the main bands of HAP are located. Before PCA, mean centering pre-processing was applied to all the spectra. Besides, in each region of the tooth, enamel and dentin, liposomes and MOFs treatments were analysed separately.

3.3.5. REACTION YIELD AND DRUG ENCAPSULATION OPTIMIZATION IN MOFs

Once the methodology for MOFs' formulations was already established, the next step was the optimization of this process in terms of reaction yield and drug encapsulation to explore the best conditions using design of experiments (DoE).

3.3.5.1. EXPERIMENTAL DESIGN AND OPTIMIZATION

A face-centered Central Composite Design (CCD) was used for applying the response surface methodology (RSM). The effect of four independent variables (input factors) on two dependent variables (output responses) was estimated. The central point value and the range of the four independent variables studied are shown in Table 4. These ranges were defined from a preliminary screening study (not shown).

Table 4: List of independent variables and their corresponding levels.

Independent variables	Unit	Symbol	Levels		
			-1	0	+1
Incubation temperature	ºC	A	20	25	30
Incubation time	hours	B	5	15	25
Methanol content	%	C	20	30	40
Olivetol concentration	mg/mL	D	1.3	2.2	3.1

The design consisted of 27 experiments including three central points (Table 5). The design was performed two times, one per potassium salt (KCl and KNO_3) as implicit factor, and the experiments were randomly performed. Reaction yield (%) and drug encapsulation (%) were selected as dependent variables (Y_1 and Y_2 respectively).

Table 5: Experimental design matrix.

Run	Coded variables			
	A	B	C	D
1	20	25	20	1.3
2	30	25	20	3.1
3	25	15	30	2.2
4	30	5	40	1.3
5	20	5	20	1.3
6	20	15	30	2.2
7	20	5	20	3.1
8	25	15	30	2.2
9	20	5	40	1.3
10	25	15	30	1.3
11	30	5	20	1.3
12	25	25	30	2.2
13	20	25	40	3.1
14	30	25	20	1.3
15	25	15	40	2.2
16	30	25	40	1.3
17	25	15	20	2.2
18	20	5	40	3.1
19	25	15	30	2.2
20	30	5	40	3.1
21	30	15	30	2.2
22	25	5	30	2.2
23	20	25	40	1.3
24	30	25	40	3.1
25	30	5	20	3.1
26	20	25	20	3.1
27	25	15	30	3.1

The experimental results were fitted with a quadratic model for reaction yield response, and two-factor interaction (2FI) model for drug encapsulation response, in both potassium salts. These multiple factorial regression analyses are based in the following equations (eq. 3-4):

$$Y_{1\,(Quadratic)} = \beta_0+\beta_1A+\beta_2B+\beta_3C+\beta_4D+\beta_5AB+\beta_6AC+\beta_7AD+\beta_8BC+\beta_9BD+\beta_{10}CD+\beta_{11}A^2+\beta_{12}B^2+\beta_{13}C^2+\beta_{14}D^2 \quad [3]$$

$$Y_{2\,(2FI)} = \beta_0+\beta_1A+\beta_2B+\beta_3C+\beta_4D+\beta_5AB+\beta_6AC+\beta_7AD+\beta_8BC+\beta_9BD+\beta_{10}CD \quad [4]$$

Where Y_1 and Y_2 are the dependent variables analysed (Y_1 reaction yield and Y_2 drug encapsulation); β_0 is a constant coefficient; β_1, β_2, β_3 and β_4 are the coefficients for linear effect; β_5, β_6, β_7, β_8, β_9 and β_{10} are the coefficients for interaction effect; β_{11}, β_{12}, β_{13} and β_{14} are the coefficients for quadratic effect; and A, B, C and D are the independent variables. The linear terms evaluate the effect of one factor over the response, the interaction terms analyse the effect of two factors at the same time and the quadratic terms determine a non-linear response. Statistical analysis for experimental data was performed through Design Expert Software version 11.1.0.1 (Stat-Ease Inc., Minneapolis, USA). The best fitting for each design was selected through comparison of different statistical parameters including multiple correlation coefficient (R^2), adjusted R^2, predicted R^2 and lack-of-fit. The level of significance was considered at p-value < 0.05.

To optimize the formulation of γ-CD-MOFs, reaction yield and drug encapsulation responses were maximized, in order to improve the results of previous studies with these MOFs, where reaction yield was around 31% and 35% and drug encapsulation 5.8% and 4.1%, for KCl and KNO_3 respectively.

3.3.5.2. PREPARATION OF OLV LOADED γ-CD-MOFs

For the preparation of OLV loaded γ-CD-MOFs, a synthesis method using microwave irradiation and the encapsulation using a co-crystallization technique were performed in a similar way as in the previous section 3.3.2.1.

The methodology was adapted in terms of the independent variables selected for the experimental design and their levels (Table 4). Briefly, 149 mg or 202 mg of KCl or KNO_3 respectively, were added with 324 mg of γ-CD. These compounds were mixed in 16 mL of an initial solution based on milliQ water and methanol, varying the percentage of organic solvent (20, 30 and 40%). Besides, different amounts of OLV were also diluted in this initial solution to have three final concentrations of the drug (1.3, 2.2 and 3.1 mg/mL). This initial solution was treated in the analytical microwave as described in section 3.3.2.1. During the incubation with PEG 20000, three different incubation times (5, 15 and 25 hours) and at three different incubation temperatures (20, 25 and 30 ºC) were tested. Finally, the washes and the storage were the same as in section 3.3.2.1. This methodology was repeated with the selected optimal conditions with two independent replicates per salt to verify the designs.

Reaction yields were calculated as before in section 3.3.2.1 (eq. 1).

After that, the quantification of the OLV content into the MOFs was performed following the same procedure described in section 3.3.2.2. This quantification was repeated with the samples prepared using the optimal conditions after the optimizations with DoE. Besides, SEM, XRPD and ATR-FTIR analysis with the same conditions as in section 3.3.2.3 were performed to verify if the new optimal conditions after DoE could compromise OLV loaded γ-CD-MOFs.

3.3.5.3. DRUG RELEASE STUDY

For the preparation of the OLV loaded γ-CD-MOFs the same synthesis procedure as in section 3.3.5.2 using the new optimal conditions from DoE was performed.

To study the release of the drug in an aqueous media from the γ-CD-MOFs, the next procedure was followed. 100 mg of OLV loaded γ-CD-MOFs were mixed with 50 mL of phosphate-buffered saline at pH 7.5. This solution was incubated at 36 ºC and under stirring conditions (150 rpm). Several aliquots of 1.5 mL at different times were taken: 0 min, 7 min, 15 min, 30 min, 60 min, 90 min, 120 min, 19 h, 24 h and 48 h. These aliquots were centrifuged for 5 min at 13000 rpm and the supernatants were kept. After removing each aliquot, 1.5 mL of fresh phosphate-buffered saline were replaced in the initial solutions in order to maintain the same total volume during the whole analysis.

To determine the amount of olivetol in the supernatants, solutions were measured by UV-Vis spectrophotometry (Thermo Fisher Scientific, Massachusetts, USA). The UV detection was performed at 275 nm and the reference was phosphate-buffered saline. A calibration curve of different known concentrations of olivetol in phosphate-buffered saline was also performed from 0 to 100 mg/L of the drug to determine the concentration of olivetol in the samples.

The released olivetol at the different times was calculated following equation 5:

$$\text{Released drug (\%)} = \frac{\text{Released OLV per time (mg/L)}}{\text{Total drug loading (mg/L)}} \cdot 100 \qquad [5]$$

All determinations of these release experiments were performed by triplicate per potassium salt.

3.3.6. VERIFY THE USE OF CBD USING THE OPTIMAL CONDITIONS IN MOFs

Finally, to validate the hypothesis that olivetol could be used as a cannabidiol analogue, the preparation of the CBD loaded γ-CD-MOFs using the optimal conditions obtained after DoE implementation, the quantification of the drug encapsulation into the MOFs and the characterization of the samples were performed.

For the preparation of CBD loaded γ-CD-MOFs the same procedure as in section 3.3.5.2 was followed using the new optimal conditions after DoE. The only difference was the amount of cannabidiol added since it was adjusted to maintain the same molar ratio as employed with olivetol.

The quantification of the CBD content into the MOFs was performed following the same procedure as in section 3.3.2.2, with the same UV detection at 275 nm that is the characteristic peak of CBD, and the reference was a mixture of milliQ water and ethanol (1:1, v/v). A calibration curve of different known concentrations of cannabidiol in milliQ water and ethanol solutions (1:1, v/v) was also performed from 0 to 100 mg/L of the drug to determine the concentration of cannabidiol in the samples. All determinations were performed by triplicate.

SEM, EDX, XRPD and ATR-FTIR analysis with the same conditions as in section 3.3.2.3 were performed to verify if the use of CBD instead of OLV could compromise or alter the previous properties of γ-CD-MOFs.

4. RESULTS AND DISCUSSION

4.1. DEVELOPMENT OF OLV LOADED γ-CD-MOFs AND DPPC LIPOSOMES

Following the different procedures for synthesis and olivetol encapsulation of these drug delivery systems, its characterization and drug content were studied to stablish the methodology to obtain these formulations.

4.1.1. CHARACTERIZATION OF γ-CD-MOFs

The crystal morphology and element distribution of different γ-CD-MOFs compared with native γ-CD were determined by SEM and EDX analysis. In case of γ-CD-MOF KOH, the final morphology of the crystals matched very well with the previously reported morphology of the same material (Fig. 35A) [195]. In the case of olivetol loaded γ-CD-MOF KOH, similar size and cubic shape were observed in comparison with the unloaded ones (Fig. 35B). Therefore, the morphology of the MOF structures was stable after the encapsulation with the drug.

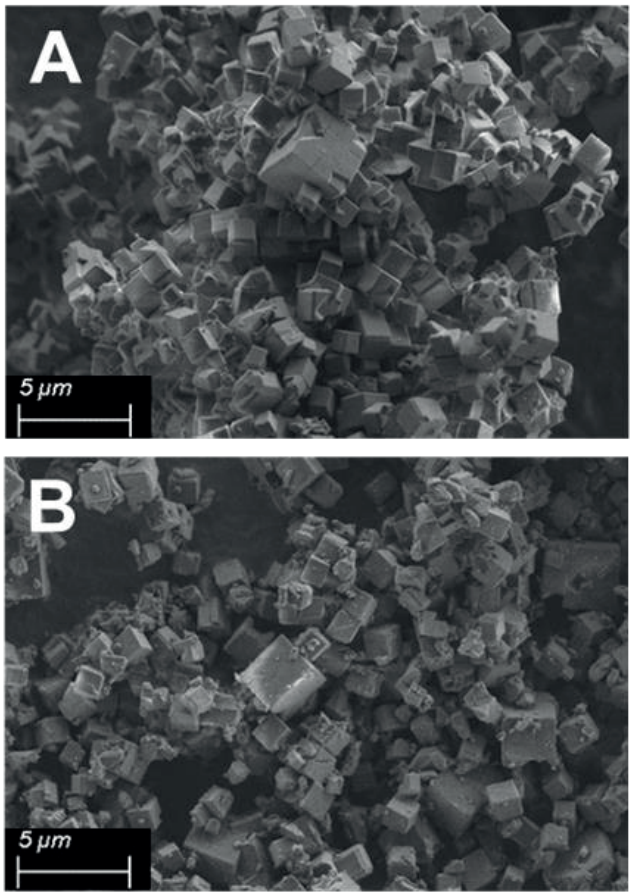

Figure 35: Scanning electron microscopy images of unloaded γ-CD-MOF KOH (A) and olivetol loaded γ-CD-MOF KOH (B) with a low voltage of 2 kV, 5000x of magnification and a working distance of 4.7 mm.

The SEM images of γ-CD-MOF KOH showed that they presented cubic-shaped with an average size of 2 µm, while the morphology of the raw γ-CD alone was completely different when the same technique was performed (Fig. 36).

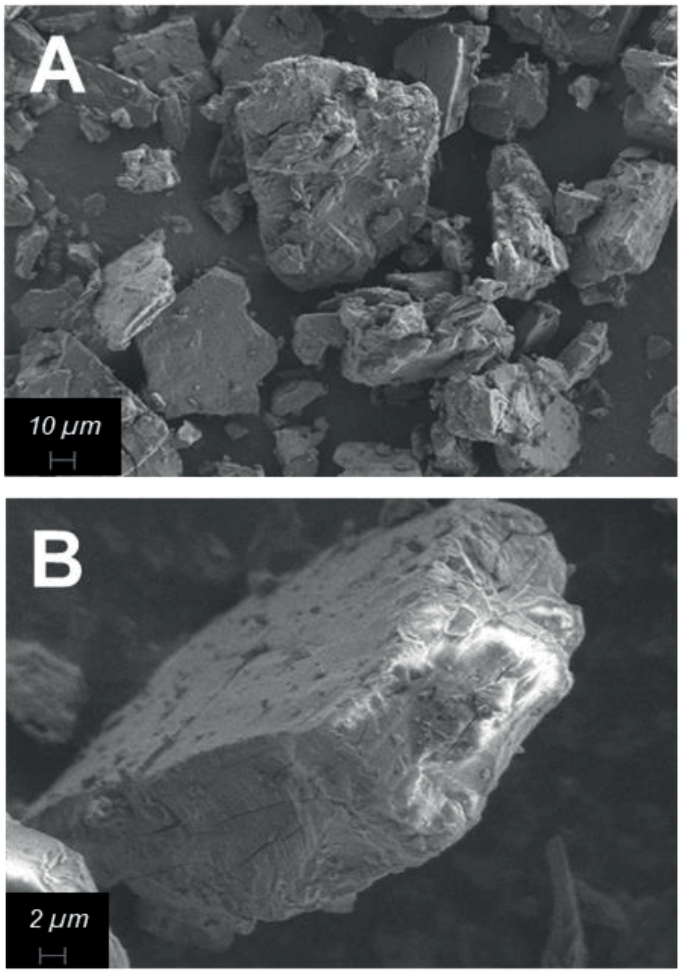

Figure 36: Scanning electron microscopy images of raw γ-CD with a low voltage of 2 kV, 1000x (A) and 5000x (B) of magnification and a working distance of 5.6 mm.

Moreover, the EDX detector in the SEM equipment was used for the elemental qualitative analysis of γ-CD-MOF KOH and it confirmed the presence of potassium in the cubic structures (Table 6). Thus, the cubic crystals were the material of interest. Furthermore, the average size of the structures was reduced in comparison with the γ-CD-MOFs obtained with conventional methodologies, such as vapor diffusion method. This fact demonstrated the high capabilities of the microwave technique to achieve narrow size distributions and control

of the morphology in the MOFs synthesis. Indeed, this is a key point when the final application of the structures is as drug delivery systems.

Table 6: Qualitative analysis of potassium using energy-dispersive X-ray spectroscopy in γ-CD-MOF KOH, γ-CD-MOF KCl, and γ-CD-MOF KNO_3 samples.

MOF sample	Atomic percentage of potassium (%)
γ-CD-MOF KOH	6
γ-CD-MOF KCl	5
γ-CD-MOF KNO_3	5

In case of γ-CD-MOF KCl and γ-CD-MOF KNO_3, the resultant crystals presented a different morphology when they were compared with γ-CD-MOF KOH and the reported ones. Co-crystallization of γ-CD-MOFs with OLV showed a rectangular shape as elongated prims and a bigger and less homogeneous size than in the synthesis with KOH (Fig. 37). The differences in size and homogeneity may be due to the incubation time with PEG during the synthesis process. Since in γ-CD-MOF KOH the incubation time was 1 hour, in the co-crystallization it took 24 hours to get the precipitation of the crystals. It was reported that if enough time is allowed for crystallization, larger particles will be obtained but also small ones because synthesis during a short time may be also possible [196]. Differences observed in shape between MOFs obtained by co-crystallization (γ-CD-MOF KCl and γ-CD-MOF KNO_3) and γ-CD-MOF KOH may be due to the use of the potassium salts instead of KOH as metal source. The change of this reagent modifies an important solution parameter such as pH. For γ-CD-MOF KOH, the pH of the initial solution was 12 while in the co-crystallization the pH was 7. It is reported that the control of the reaction medium pH in MOFs synthesis allows to control the size and the morphology of the resulting crystals [197]. Moreover, the totality of studies that synthetize γ-CD-MOF use alkali media in order to get the classic cubic shapes regardless of the metal source. The fact that both KCl and KNO_3 led to the same elongated prisms morphologies supports this pH-dependent theory. Besides that, EDX analysis also showed the presence of potassium in the MOFs obtained by co-crystallization (Table 6), confirming the interaction between the metal ion and the organic ligand to form this material.

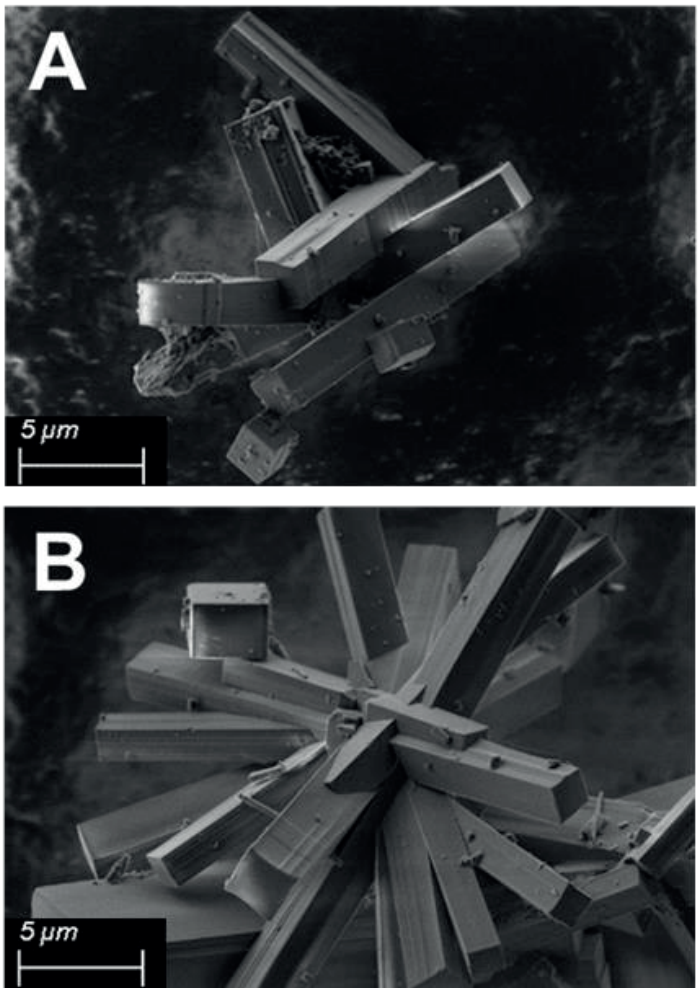

Figure 37: Scanning electron microscopy images of γ-CD-MOF KCl (A) and γ-CD-MOF KNO_3 (B) with a low voltage of 2 kV, 5000x of magnification and a working distance of 4.7 mm.

Further characterization was performed using X-ray diffraction. The crystallinity of γ-CD-MOF KOH before and after the encapsulation experiments with the drug was measured by XRPD. According to reported studies about the synthesis of γ-CD-MOFs using KOH, the characteristic peaks in X-ray diffraction patterns of these materials are located in the next angles: 4º, 5.7º, 7º, 13.3º and 16.6º (Fig. 38) [198]. These positions correspond to body-centered cubic crystals of space group *I*432. XRPD results showed that the diffractogram of the unloaded MOFs presented the same peaks in comparison with the standard reference of these crystals (Fig. 39).

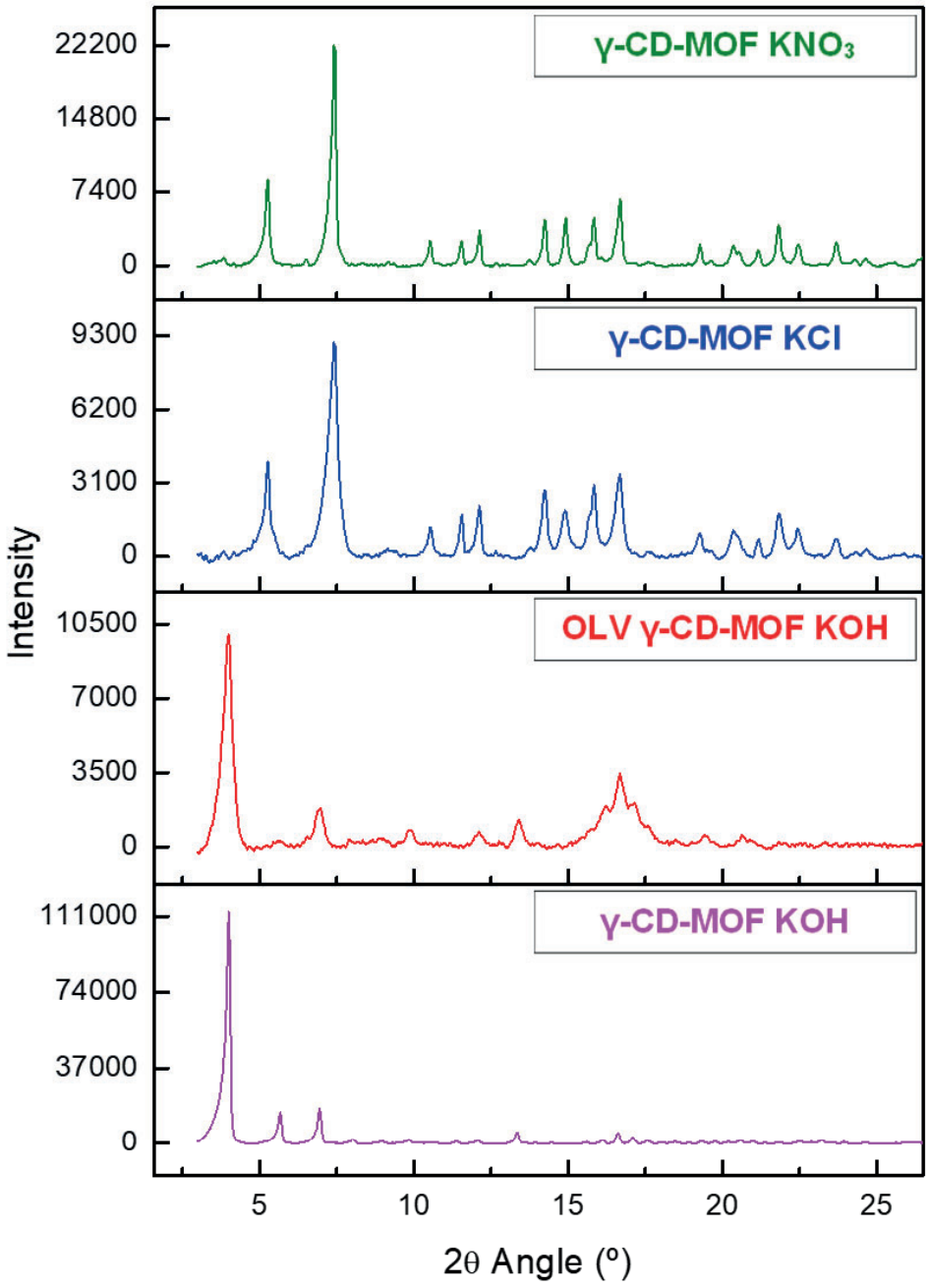

Figure 38: X-ray powder diffraction patterns of unloaded γ-CD-MOF KOH (pink), olivetol loaded γ-CD-MOF KOH (red), γ-CD-MOF KCl (blue) and γ-CD-MOF KNO_3 (green).

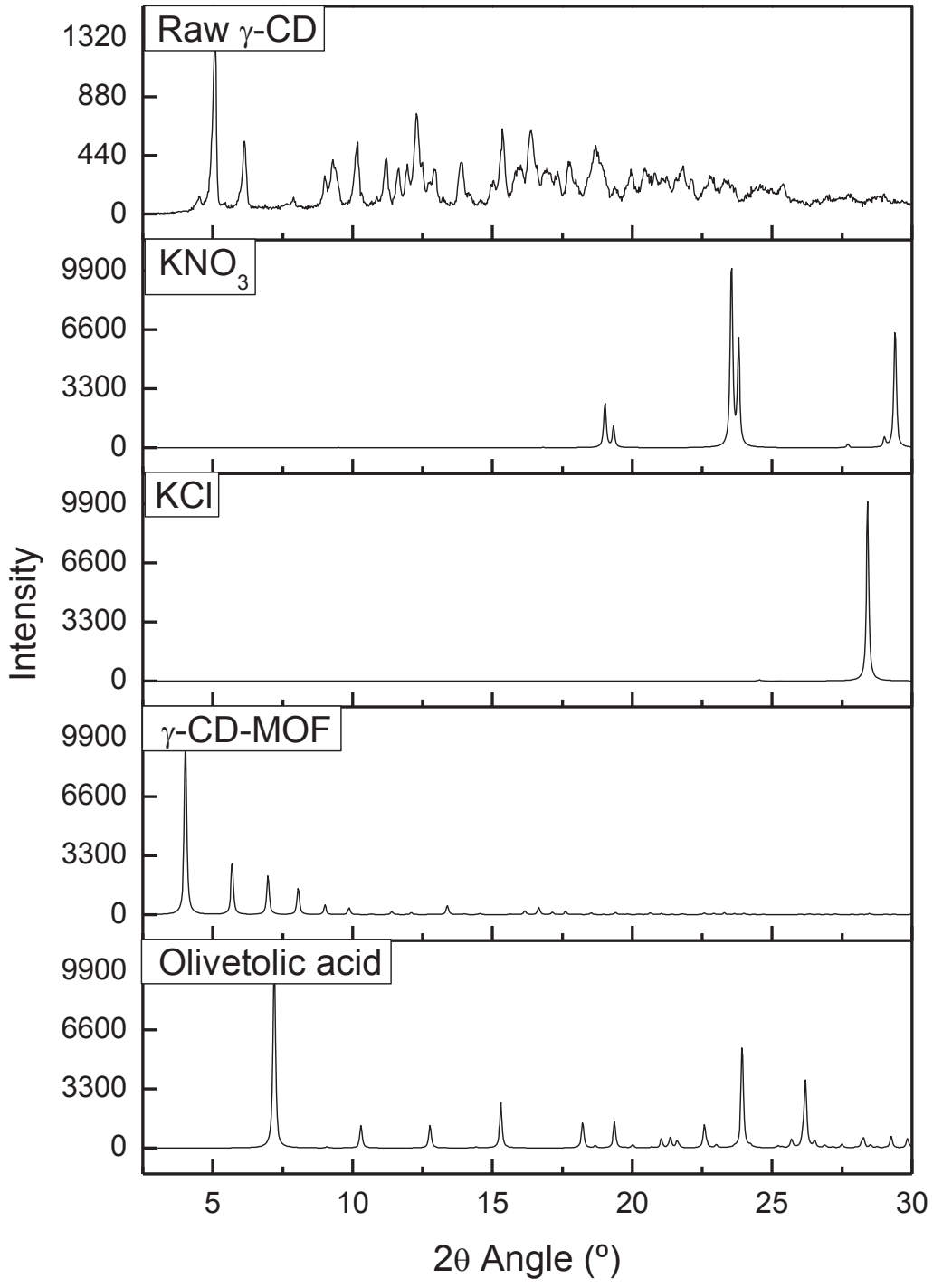

Figure 39: X-ray powder diffraction pattern of raw γ-CD and simulated references of olivetolic acid, γ-CD-MOF, KCl and KNO_3 from Crystallography Open Database (COD) [199–205].

Therefore, the crystalline phase obtained for γ-CD-MOF KOH coincided with the typical cubic unit of these materials. Comparing the data before and after the encapsulation experiment with olivetol, the crystallinity of MOFs loaded with the drug changed with respect to the unloaded crystals. The intensity of the peaks of the γ-CD-MOF KOH with OLV was significantly reduced compared to those of the unloaded MOFs (Fig. 38). This partial loss of crystallinity may result from the filling of pores with olivetol, the high degree of disorder of the drug and the presence of a low percentage of water in the ethanol solution used in these experiments [206]. However, the peak positions in the diffractograms were similar in both cases indicating that MOF crystals were stable after the encapsulation with olivetol [207]. Moreover, no new diffraction peaks appeared into the olivetol loaded MOFs, suggesting that the encapsulated drug is in an amorphous state. Taking into account SEM and XRPD results, we can conclude that the morphology of the γ-CD-MOF KOH was stable after the encapsulation with the drug, in spite of the partial loss of crystallinity. For γ-CD-MOF KCl and γ-CD-MOF KNO_3, important changes were observed in the diffraction patterns (Fig. 38). The partial loss of crystallinity was observed again in the co-crystallization MOFs with a similar intensity in the diffraction peaks as in the previous case of OLV loaded γ-CD-MOF KOH, probably due to the encapsulation of the drug. Furthermore, the characteristic position peaks were located in different angles: 5.3º, 7.4º, 10.5º, 11.5º, 12.1º, 14.2º, 14.9º, 15.8º and 16.7º. These peaks did not correspond with the diffraction pattern described before for the conventional CD-MOFs synthetized with KOH, despite the metal linker has not changed. Moreover, they did not match with the peaks of raw γ-CD or any simulated references (Fig. 39). A possible explanation for that is the pH of the initial solution during the MOF synthesis, as described before for SEM results. Since for γ-CD-MOF KOH the pH of the initial solution was around 12 due to the use of potassium hydroxide, for γ-CD-MOF KCl and γ-CD-MOF KNO_3 the potassium salts led the initial solution to a neutral pH. It is reported that the body-centered cubic CD-MOFs were grown from solutions of basic salts, such as hydroxides and carbonates. Although this alkali media is not enough to deprotonate the hydroxyl groups of γ-CD, it seems to facilitate the growing of this type of crystals [208]. Moreover, previous studies about CD-MOFs have reported trigonal crystals with several space groups (*R*32, *I*4, *P*1 or *P*32) different from *I*432 [147,208]. In these CD-MOFs, the metal sources were not the typical potassium hydroxide. Therefore, the metal linker and the pH of the initial solution could be causes of the different morphology and diffraction pattern observed for the CD-MOFs. This fact would explain the new diffraction patterns in γ-CD-MOF KCl and γ-CD-MOF KNO_3 that did not match

with the cubic space group *I*432 correlating the trigonal morphology observed in their respective SEM images.

Regarding reaction yield, these values matched well with the values described in reported studies in the synthesis process of the γ-CD-MOF KOH [126,146]. Nevertheless, in co-crystallization synthesis (γ-CD-MOF KCl and γ-CD-MOF KNO_3) similar reaction yields were obtained but much lower than for the γ-CD-MOF KOH (Table 7). These differences are due to the pH change, as typical cubic CD-MOFs growing is favoured in alkali solutions [208]. As it was reported before, γ-CD-MOF KCl and γ-CD-MOF KNO_3 presented different morphology and diffraction pattern, so the kinetics for crystals precipitation should not be the same as for the γ-CD-MOF KOH crystal formation because of the different pH values due to the alternative potassium sources. In fact, this could also explain the absence of MOFs using KCl or KNO_3 when the conventional synthesis with KOH was followed.

Table 7: Reaction synthesis yield of γ-CD-MOF KOH, γ-CD-MOF KCl and γ-CD-MOF KNO_3 with their respective standard deviations.

MOF sample	Reaction yield (%)	σ
γ-CD-MOF KOH	59.44	0.03
γ-CD-MOF KCl	30.98	0.06
γ-CD-MOF KNO_3	34.65	0.04

FTIR spectroscopy is a useful tool to detect the bonding changes between functional groups of the MOFs, the drug and the resulting interactions of both components. There were characteristic peaks in all γ-CD-MOF samples at 1078 cm^{-1}, 1152 cm^{-1}, 1336 cm^{-1}, 2700 – 2995 cm^{-1} and 3000 – 3670 cm^{-1} (Fig. 40A). These peaks were in agreement with previous reported literature of γ-CD-MOFs [107,209–211]. Moreover, these regions in the MOF spectra also coincided with the characteristic peaks in the γ-CD spectrum, showing the presence of the organic linker in the crystals. At 1078 cm^{-1}, an antisymmetric stretching vibration mode derived from the C–O–C groups in aliphatic ethers can be observed. These ether groups are presented in the γ-CD structure. The units of γ-CD are α-d-glucopyranose molecules with intra-monomeric ether bonds 1 → 5. These units are linked to each other through inter-monomeric ether bonds 1 → 4. The peak at 1152 cm^{-1} was assigned to the stretching vibration between carbon and oxygen atoms in C–OH groups of the two secondary alcohols that are in each unit of α-d-glucopyranose. The peak at 1336 cm^{-1} was related to the

contribution of alkane groups and the band from 2700 – 2995 cm^{-1} were the contributions of the C–H antisymmetric and symmetric stretching vibrations of CH_2 and CH_3 in aliphatic compounds. These regions may come from the CH_2 group in the hydroxymethyl side chain in each α-d-glucopyranose unit of γ-CD. A wide band ranging from 3000 – 3670 cm^{-1} was assigned to stretching vibrations of the hydroxyl groups, the ones that are secondary alcohols groups but also the primary alcohol in the hydroxymethyl side chain in each α-d-glucopyranose unit. In addition to these characteristic bands of γ-CD-MOFs, the peak observed at 1640 cm^{-1} may be due to the hydroxyl groups of water molecules that still remained into the cavities of the MOFs after the drying process. The spectrum of olivetol showed the characteristic peaks of this drug according to the literature at 690 cm^{-1}, 830 cm^{-1}, 1145 cm^{-1}, 1210 cm^{-1}, 1310 cm^{-1}, 1376 cm^{-1}, 1477 cm^{-1}, 1600 cm^{-1}, 1628 cm^{-1}, 2858 cm^{-1}, 2929 cm^{-1} and 3240 cm^{-1} (Fig. 40A) [212–214]. At 690 cm^{-1} and 830 cm^{-1} wavenumbers, two peaks from C–H out of plane deformations were observed because of the triple substitution in one, three and five carbon positions in the benzene ring of the OLV. The four peaks at 1145 cm^{-1}, 1210 cm^{-1}, 1310 cm^{-1} and 1376 cm^{-1} corresponded to the stretching vibrations between the carbon and oxygen atoms of the two C–OH groups that are presented in the drug molecule. Moreover, phenols absorb near 1350 cm^{-1} due to the OH deformation and give a second band due to C–OH stretching near 1210 cm^{-1}, and in this case, the two hydroxyl groups are in the benzene ring of the drug. At 1477 cm^{-1} and the double peak at 1600 and 1628 cm^{-1}, two regions of stretching vibrations derived from the interactions between the carbon atoms in the aromatic ring of the olivetol structure and the skeletal stretching vibration of -C=C- could be observed. The peaks at 2858 cm^{-1} and 2929 cm^{-1} were related to the antisymmetric stretching vibrations of C–H bond of CH_2 and CH_3 groups that are present in the pentyl chain of the molecule. The wide peak at 3240 cm^{-1} was assigned to stretching vibrations between oxygen and hydrogen atoms of the two hydroxyls groups in the aromatic ring. A direct comparison between the infrared spectra of OLV and γ-CD-MOF KOH before and after the encapsulation process with the drug did not show any differences (Fig. 40A). This could be due to the poor encapsulation of the drug in γ-CD-MOF KOH which was not enough to observe perceptible changes. Nevertheless, γ-CD-MOF KCl and γ-CD-MOF KNO_3 spectra showed, instead of the peak at 1640 cm^{-1}, a double peak at 1600 and 1628 cm^{-1} corresponding to the skeletal stretching -C=C- vibration of OLV (Fig. 40B). It was observed that the 1640 cm^{-1} peak in MOFs is partially occluded by this OLV signal. These results confirmed the interaction between γ-CD-MOFs and olivetol in the co-crystallization, because

if this interaction did not take place, OLV would have been removed during the washing steps with the organic solvents. Moreover, this interaction in γ-CD-MOF KCl and γ-CD-MOF KNO_3 was in agreement with the quantification of the drug described before, that showed a high OLV encapsulation in the co-crystallized samples. In accordance with previous literature, the interaction between OLV and γ-CD-MOFs may take place through the two phenolic hydroxyl groups of the olivetol structure and the inner cavity of the γ-CD molecules. It has been described that cyclodextrin molecules provide their cavities as a non-polar field, in which OLV is complexed through its hydroxyl groups and non-covalent interactions [215]. Furthermore, a study that encapsulates curcumin in γ-CD-MOFs to improve the stability of this compound concluded that the interaction between curcumin and the MOFs is through the phenolic hydroxyl group of the curcumin [216]. Therefore, based on the infrared results of this investigation and previous studies, the interactions between olivetol and γ-CD-MOFs may be due to intermolecular forces such as Van der Waals forces between the different atoms of the olivetol structure and the inner parts of the non-polar MOF cavities. This fact was also supported since there were not significant shifts in the spectra, meaning that there were not changes on vibrations through the molecules.

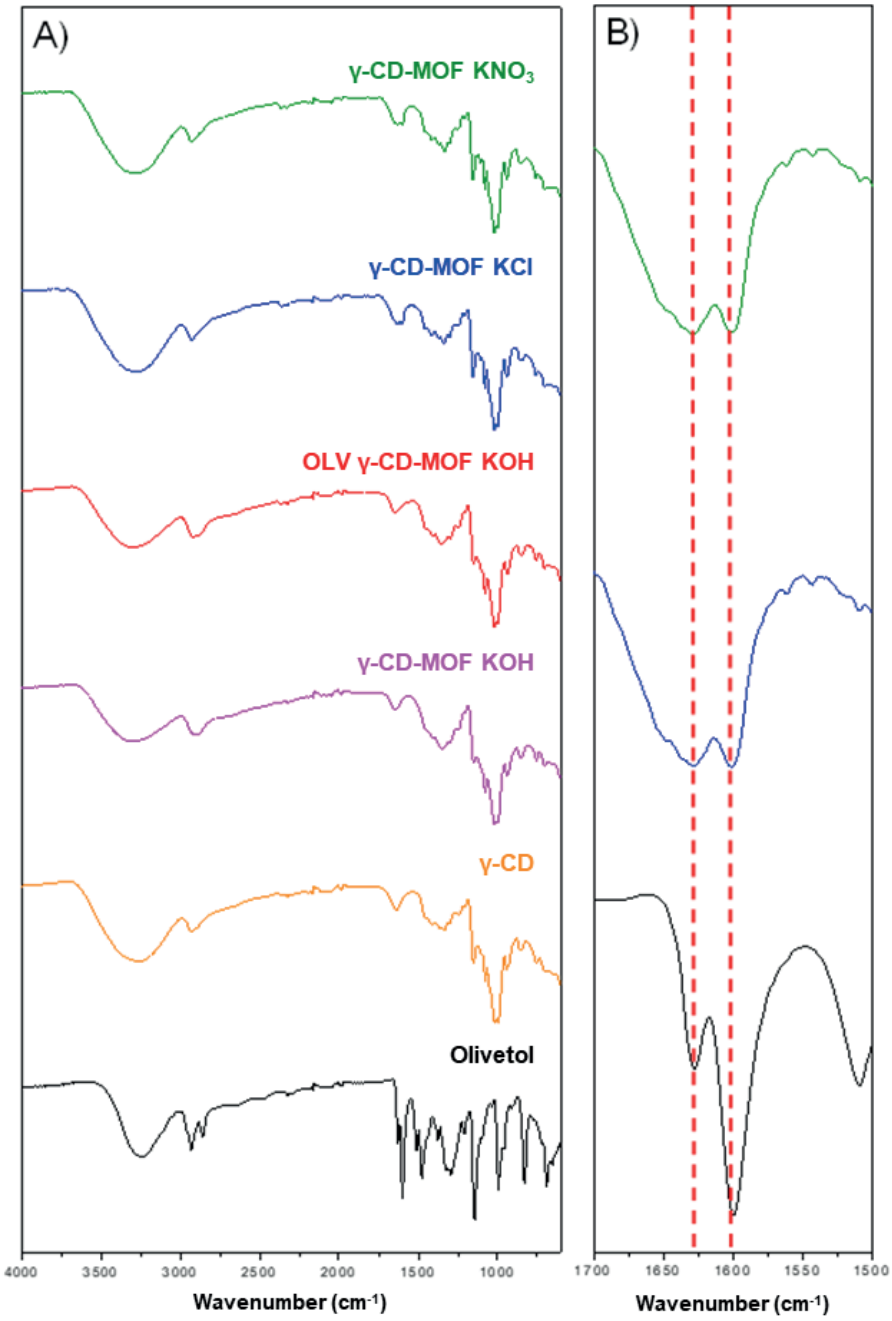

Figure 40: Attenuated Total Reflection-Fourier Transform Infrared Spectroscopy spectra of: olivetol (black), γ-CD (orange), unloaded γ-CD-MOF KOH (pink), olivetol loaded γ-CD-MOF KOH (red), γ-CD-MOF KCl (blue) and γ-CD-MOF KNO_3 (green) from 4000 cm^{-1} to 600 cm^{-1} (A). Magnified comparison of olivetol (black), γ-CD-MOF KCl (blue) and γ-CD-MOF KNO_3 (green) spectra (B) in the region of interest from 1700 cm^{-1} to 1500 cm^{-1} showing the double peak at 1600 and 1628 cm^{-1} assigned to olivetol.

4.1.2. CHARACTERIZATION OF DPPC LIPOSOMES

The size distribution is a key aspect to consider, even more when the final application is as drug delivery systems [217]. In order to get information about the size of DPPC liposomes

and the physical stability of these systems after the encapsulation of olivetol, DLS and cryo-TEM analysis were performed. DPPC formulations loaded with the drug showed more polydispersity than empty DPPC liposomes with wider and more asymmetric peaks in DLS results (Fig. 41).

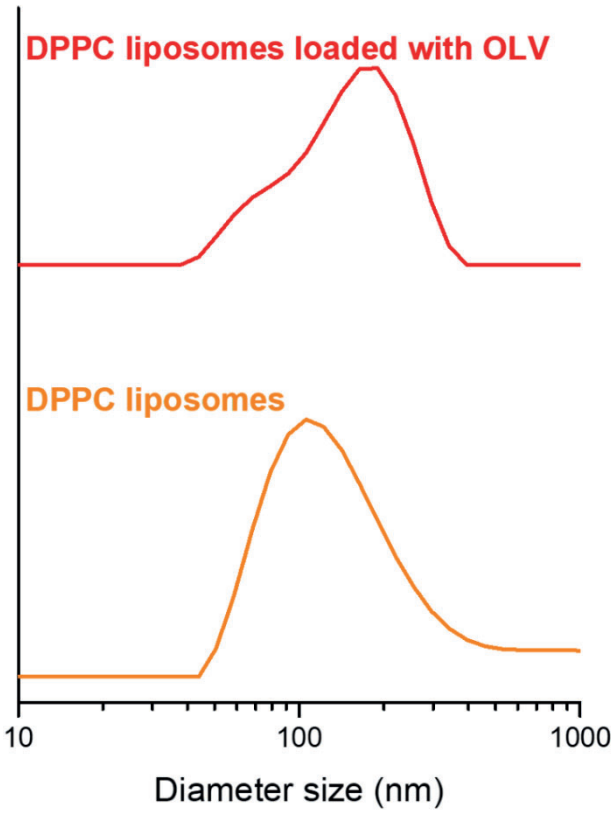

Figure 41: Size distribution by intensity of DPPC liposomes (orange) and OLV loaded DPPC liposomes (red).

These results were in agreement with cryo-TEM analysis, where bigger liposomes with several concentric lipidic bilayers could be observed in the samples with OLV (Fig. 42). The mean diameter of the liposomes was below 200 nm: 125 ± 52 nm for DPPC liposomes and 159 ± 67 nm for DPPC liposomes loaded with OLV. Mean diameter and standard deviation were similar in both liposomes' formulations. However, the size distribution observed in the liposomes without drug was closer to a normal distribution than the formulations with OLV, as well as the polydispersity index values were lower in the empty liposomes (0.3) than in the loaded ones (0.9). This fact means that the samples with low polydispersity index had an homogeneous distribution of the vesicles with similar diameters without aggregates [218]. It

could be explained since olivetol is an organic compound and it is encapsulated in the bilayer increasing the rigidity of liposomes, such as the effect of cholesterol addition [219]. Cryo-TEM analysis corroborated these results. The synthesis method was found to be useful for producing stable DPPC liposomes with and without olivetol of relatively controllable particle size.

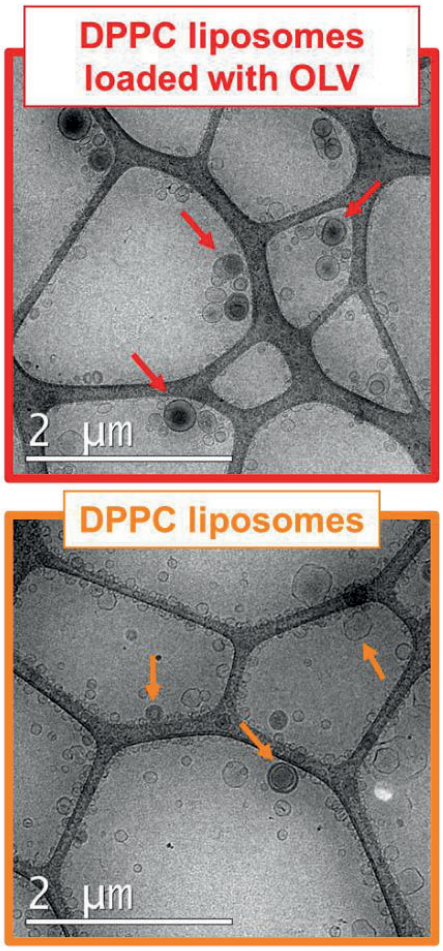

Figure 42: Cryo-TEM images of DPPC liposomes (orange) and OLV loaded DPPC liposomes (red).

4.1.3. OLIVETOL CONTENT IN γ-CD-MOFs AND DPPC LIPOSOMES

To determine the OLV content in the samples the next calibration curves of different known concentrations of olivetol were performed from 0 to 100 mg/L (Fig. 43). MilliQ water and ethanol (1:1, v/v) or HEPES buffer and ethanol (1:5, v/v) were used for MOFs and DPPC liposomes respectively.

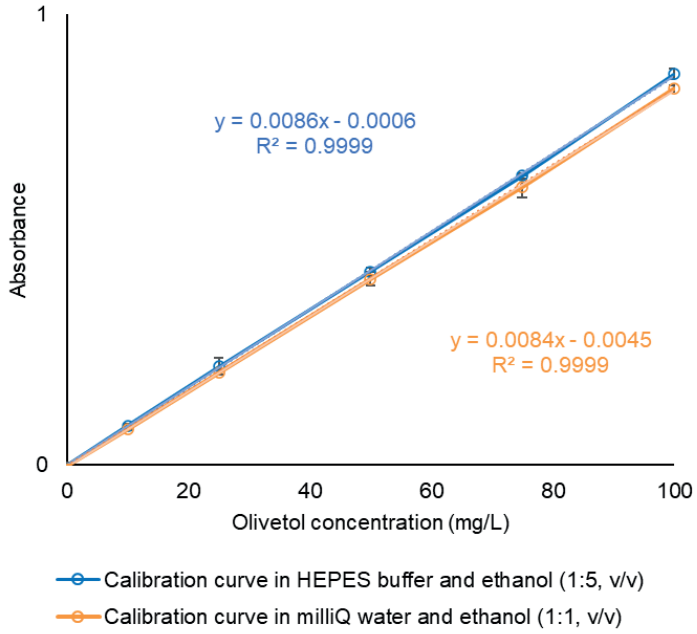

Figure 43: Calibration curves of different known concentrations of olivetol from 0 to 100 mg/L in HEPES buffer and ethanol (1:5, v/v) (blue) and milliQ water and ethanol (1:1, v/v) (orange) media for the quantification of the olivetol in DPPC liposomes and MOFs, respectively (n = 3). The calibration line was calculated by linear regression.

Regarding MOFs, not only reaction yields changed depending on the potassium source but also on the drug loading content. For OLV γ-CD-MOF KOH the drug content was very low using the impregnation method to perform the encapsulation (Fig. 44). This could be explained because of the hybrid polarity behaviour of OLV. Olivetol dissolves perfectly in organic solvents but it is partially miscible in aqueous solutions. According to that, OLV would tend to be more comfortable on a hydrophobic environment like the inner cavities of the MOFs, than in the ethanol solution used for the encapsulation, that is a relatively polar organic solvent. However, this hybrid polarity behaviour may cause that olivetol could interact with both hydrophobic and hydrophilic environments and the drug is not strongly attracted to the inner cavities of the MOFs, affecting its encapsulation efficiency. In the case of the co-crystallization process, the drug loading was higher than the impregnation method, showing γ-CD-MOF KCl slightly more OLV content than γ-CD-MOF KNO_3 (Fig. 44). This efficiency in the co-crystallization could be explained by the formation of crystals itself. γ-CD-MOF KCl and γ-CD-MOF KNO_3 precipitation may directly trap the drug into the MOF cavities, regardless the hybrid polarity behaviour of OLV. Moreover, drug loading values of co-crystallization synthesis were in agreement with reported studies about γ-CD-MOFs obtaining encapsulation percentages from 2% to 10% for different compounds [220–222].

For liposomes formulation, OLV encapsulation percentage was higher than the values for MOFs (Fig. 44). These percentages could not be compared between MOFs and liposomes, since the values are expressed in terms of mass and the weight of each carrier is different [147,220]. In any case, the drug could be quantified in DPPC liposomes, γ-CD-MOF KCl and γ-CD-MOF KNO_3 formulations, making them suitable as carriers for olivetol and for their application over the tooth structure.

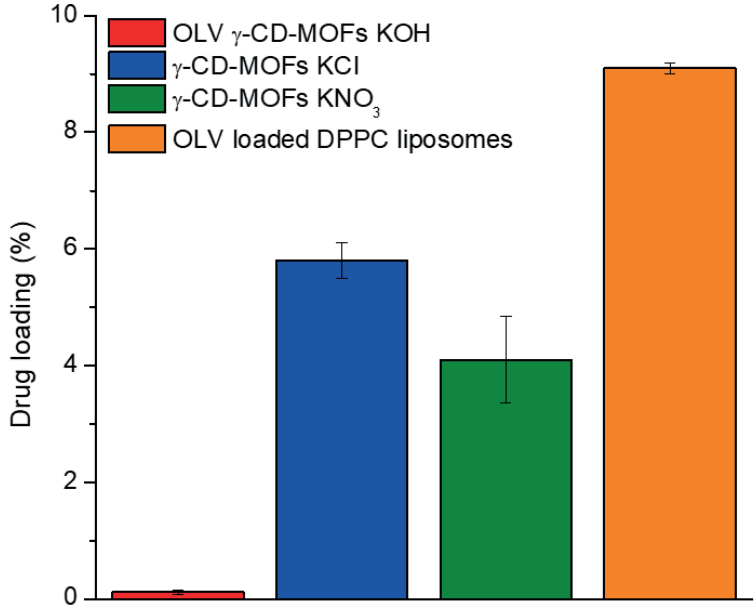

Figure 44: Drug loading percentage of olivetol in γ-CD-MOF KOH, γ-CD-MOF KCl, γ-CD-MOF KNO_3 and DPPC liposomes with their respective standard deviations.

4.2. *IN VITRO* STUDY USING SYNCHROTRON-SOURCE INFRARED SPECTROSCOPY

Then, an *in vitro* study of the drug penetration pattern using the previous DDS efficiently loaded with olivetol (DPPC liposomes, γ-CD-MOF KCl and γ-CD-MOF KNO_3 formulations) was carried out. This study was performed combining synchrotron-source infrared spectroscopy and principal component analysis (PCA) using bovine tooth as a model.

In order to verify if the amount of drug applied over the teeth in liposomes and MOFs formulations was comparable, the OLV amount per application was calculated based on the sample preparation process (section 3.3.4.1) and the drug encapsulation percentages in each formulation. This amount was of the same order for the three carriers (Table 8). Besides, the

amount of drug applied without carrier as positive control (OLV or CBD) was extremely high to study the efficiency when the carrier was used.

Table 8: Drug amount per application over the teeth for each formulation in comparison with the drugs alone (OLV and CBD).

	Drug amount per application (µg)
DPPC liposomes with olivetol (molar ratio 2:1)	36.8 ± 0.5
γ-CD-MOFs KCl loaded with olivetol	24 ± 3
γ-CD-MOFs KNO_3 loaded with olivetol	16 ± 2
CBD or OLV (10 mg/mL)	1000

4.2.1. PEAKS ASSIGNMENT OF ENAMEL AND DENTIN

Enamel and dentin are the main tissues that comprise the teeth. Enamel is composed of 96% of mineral content, while in the dentin it is reduced to approximately 70%. Regarding the organic matter, the enamel presents only 2% and in the dentin it increases to 20%, predominating cross-linked type I collagen. The inorganic mineral that mainly composes both tissues is the carbonated calcium-deficient hydroxyapatite (HAP), which is a crystalline calcium phosphate [$Ca_{10}(PO_4)_6(OH)_2$] and carbonates impurities [CO_3^{2-}] [21]. These carbonates could substitute two anion phosphate groups or two hydroxyl groups in HAP structure, being B-type or A-type carbonated apatite, respectively [23]. Bovine enamel and dentin reflection spectra are shown in figure 45 between 1600 and 700 cm^{-1} where the bands of carbonates and phosphates groups of HAP could be observed. Due to the high degree of crystallinity of the enamel, bands corresponding to this mineral matrix are more intense than in the dentin tissue which has a low crystallinity, and the peaks appear weakly [223]. Antisymmetric stretching vibration of phosphates groups (v_3 PO_4^{3-}) appears as a wide band in the 1200-900 cm^{-1} region, in both enamel and dentin tissues with a maximum at 1045 and 1028 cm^{-1} respectively. These broad bands are attributed to triply degenerated v_3 PO_4^{3-} and its deconvolution is described as secondary phase vibrations of Ca-O-P, P-O, Ca-O and O-Ca-O vibrations, but they are not fully resolved [224]. The shoulder at 956 cm^{-1} corresponds to the symmetric stretching vibration of the same group (v_1 PO_4^{3-}) in both tissues, despite the band being more saturated in the enamel than in the dentin [225]. Peaks at 1403 and 1442 cm^{-1} match with antisymmetric stretching vibration of carbonate groups (v_3 CO_3^{2-}) and the one at 867 cm^{-1} with symmetric angular deformation (v_2 CO_3^{2-}) in both tissues. These peaks correspond to a mixture of A-type and B-type carbonated apatites, being B-type the one with

more contribution since it is the predominant type in biological apatite [23]. Besides, organic matter (amide II) is detected at 1540 cm^{-1} in the dentin, since its percentage in this tissue is higher than in the enamel [226].

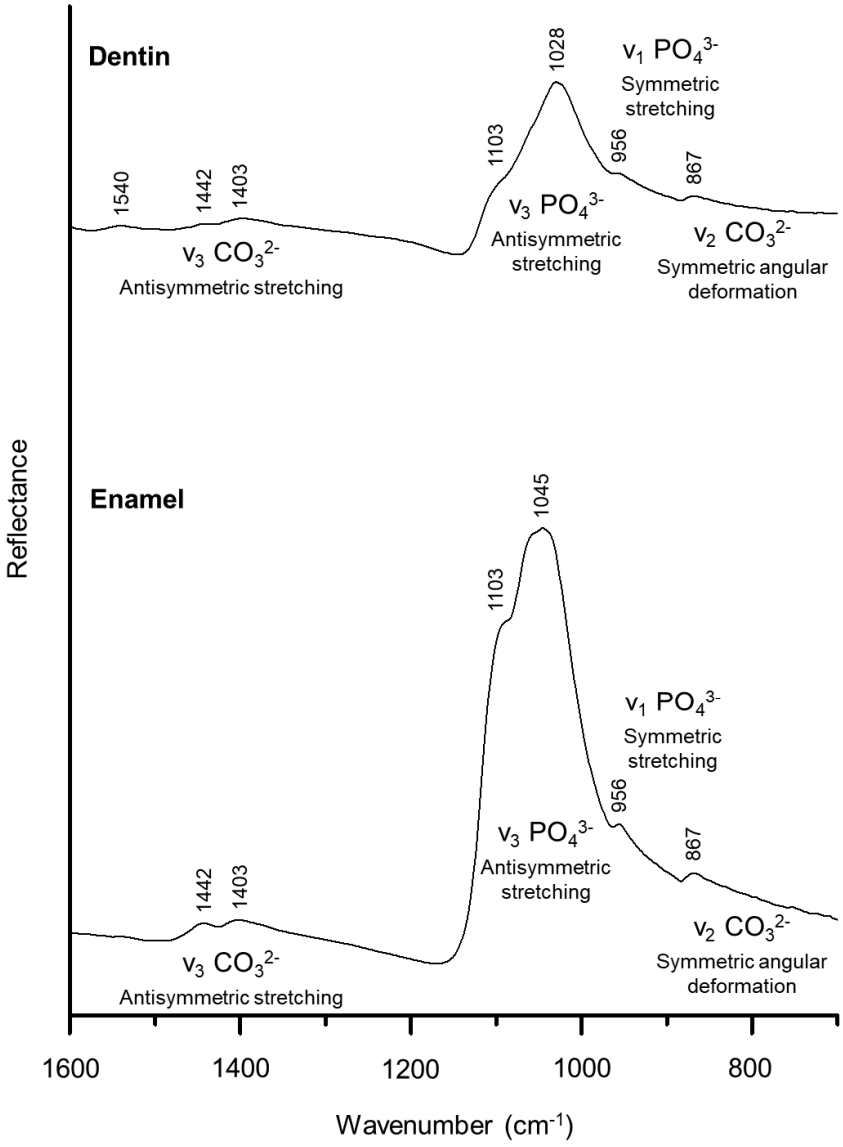

Figure 45: Average of the specular reflectance FTIR spectra of control enamel and dentin of bovine tooth and band assignment numbers (n = 30).

Taking into account the enamel structure properties, no contribution of drugs, liposomes or MOFs vibration peaks were expected to be distinguished, since their signals are not significant in comparison with the signal of the inorganic material of the enamel [227]. Thus,

only changes over HAP structure could be noted. The treatments with drug (CBD, OLV, OLV loaded liposomes and MOFs) produced the decrease of the bands of carbonates and phosphates groups of HAP in comparison with the average of the spectra of the samples without drug, especially in the antisymmetric stretching vibration v_3 PO_4^{3-} (Fig. 46). This fact could be explained due to the organic matter increment in the samples treated with drug, because the crystallinity of the enamel in these samples was worse detected than in the ones without any drug, since they have better reflective properties, and its infrared signal is higher [228]. Besides, shifts were not detected in the average spectra of the samples with and without drug for both carriers, so the treatments did not compromise carbonates and phosphates groups of HAP [229].

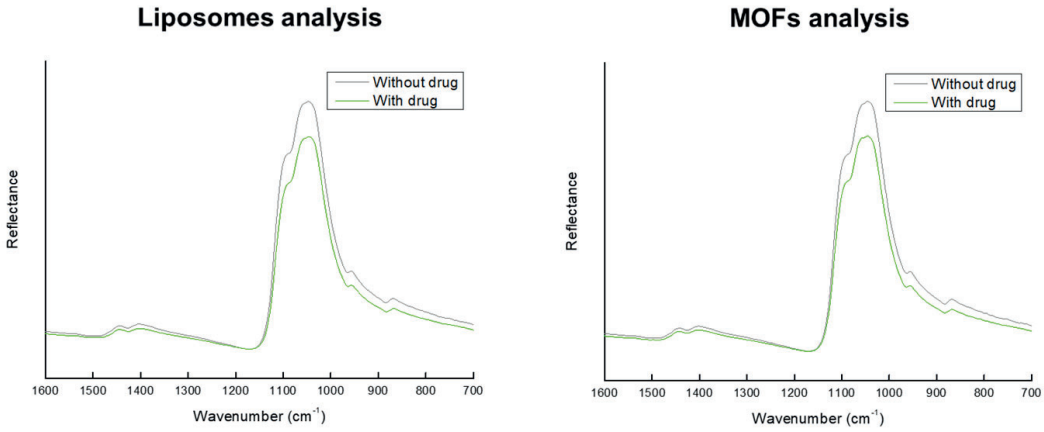

Figure 46: Average of the spectra of the groups with and without drug for liposomes and MOFs in the enamel.

In the dentin, the comparison between the average of the spectra without drug with the average of the spectra with drug (CBD, OLV, OLV loaded liposomes and MOFs) revealed a reduction in the intensity of all the bands, related to a higher organic matter content that decreased the crystallinity and the signal of the bands (Fig. 47) [21]. The only band that did not decrease is the one at 1540 cm^{-1} in case of the liposomes analysis, since this vibration may be related to the NH_3^+ deformation from the DPPC structure avoiding the loss of intensity of this peak despite the decrease in crystallinity due to the drug presence [230]. However, the main vibrations did not shift, so the chemical structure of the dentin was not changed.

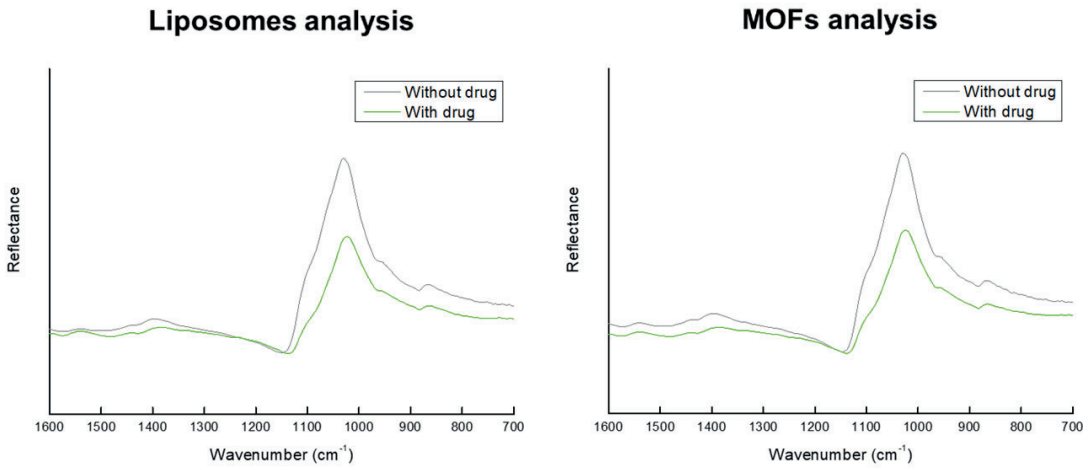

Figure 47: Average of the spectra of the groups with and without drug for liposomes and MOFs in the dentin.

4.2.2. TREATMENTS EFFECTS OVER THE ENAMEL ANALYSED BY PCA

In the present study, the enamel FTIR spectra of the different samples were analysed by PCA, where the weights of the main components were concentrated in the components 1 and 2 (PC1 and PC2) for both carriers. Liposomes and MOFs analysis had a PC1 of 95.20% and 96.01% *versus* PC2 of 3.39% and 2.43% accounting for a total of 98.59% and 98.44% of the variance, respectively (Fig. 48). Both carriers' analysis had a similar distribution in the enamel, and only two groups could be distinguished along PC1 according to drug presence (Fig. 48). This distribution agreed with the decrease of the bands reported in the previous section (Fig. 46) since the group with drug is in the negative part of the component (less intense signal) and the group without drug in the positive part (more intense signal).

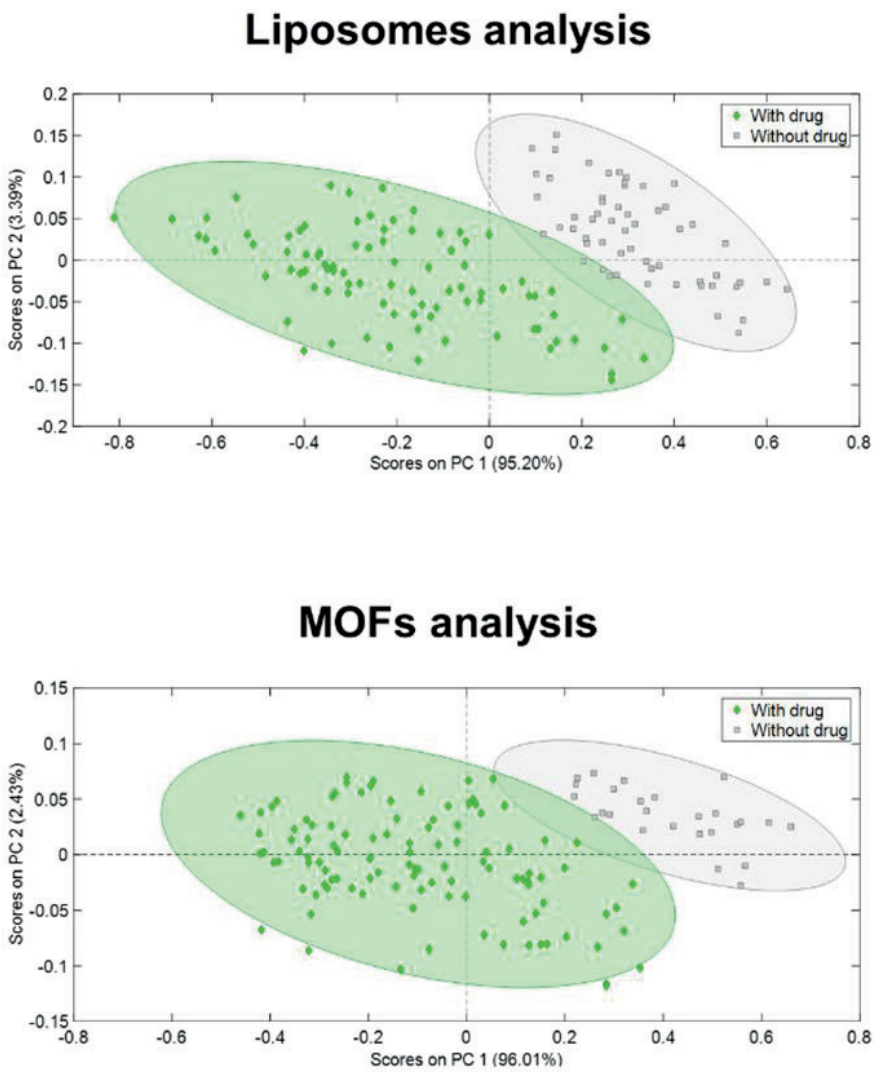

Figure 48: Principal Component Analysis of liposomes and MOFs in the enamel, scores plots grouping according to the drug presence. The group with drug included CBD, OLV and OLV loaded liposomes or MOFs (depending on the carrier analysis) and the group without drug comprised HEPES control for both carriers and also unloaded liposomes for liposomes analysis.

The group with drug included CBD, OLV and OLV loaded liposomes or MOFs (depending on the carrier analysis) and the group without drug comprised HEPES control for both carriers and also unloaded liposomes for liposomes analysis. Therefore, it revealed that both OLV loaded carriers may transport the drug, since these treatments were in the same group as CBD and OLV control treatments. Nevertheless, the separation between the groups that contained or not drug was not perfectly clear. This fact could be explained due to the large inorganic material content and high crystallinity of the enamel [231]. Because of these enamel properties, the signal of carbonates and phosphates groups of HAP was too high, overlapping the possible vibrations peaks of organic material that can be present in the

enamel, as well as the drugs and carriers employed in the treatments of this study [232]. For this same reason, no more differences related with the treatments could be observed between groups, since spectra were distributed according to the depth in the enamel structure along PC2 (Fig. 49).

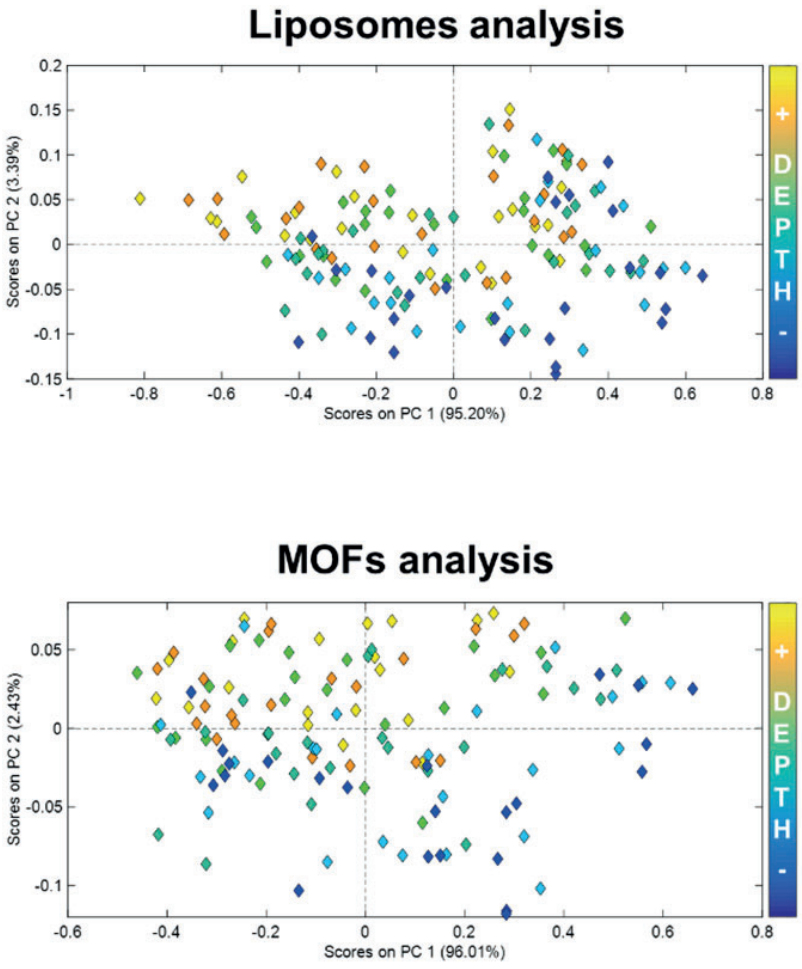

Figure 49: Principal Component Analysis of liposomes and MOFs in the enamel, scores plots showing the distribution across the enamel depth.

Regarding the loading graphs (Fig. 50), PC1 comprised all the bands of carbonates and phosphates groups of HAP previously assigned for both liposomes and MOFs analysis in the positive part of the graphs. PC2 loadings profiles revealed in the positive part of the graphs v_3 CO_3^{2-} and v_2 CO_3^{2-} peaks of carbonate groups from 1475 to 1380 cm^{-1} and 867 cm^{-1} respectively (Fig. 50). A secondary phase vibration of v_3 PO_4^{3-} at 1113 cm^{-1} was observed. This vibration contributes to the shoulder at 1103 cm^{-1} of the peaks assignment, and it is related

with the bandwidth [233]. Meanwhile, the maximum peak of v_3 PO_4^{3-} was in the negative part. This profile was in agreement with the distribution of the scores according to the depth in the enamel structure (Fig. 49). Enamel tissue presents heterogeneous distribution of the inorganic material, since its carbonate content increases from the outer to inner enamel, the phosphates decrease showing more crystallinity and more packing in the outer part [9,22,234]. Therefore, the fact that the scores in the positive part of the graph correspond to the inner parts of the enamel and the ones in the negative part to the outer region matched with the PC2 loading profiles for both carriers. This information is in accordance with the typical mineral gradient of the enamel, verifying that PC2 distributes the samples following the depth in this tissue.

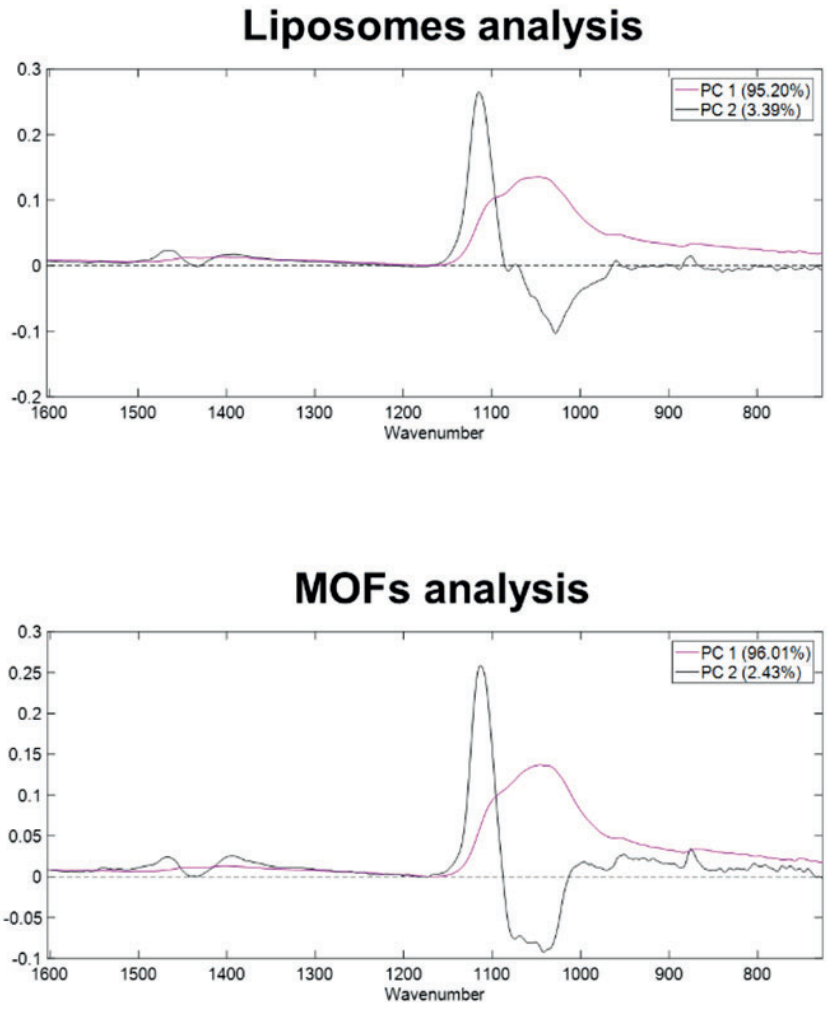

Figure 50: Principal Component Analysis of liposomes and MOFs in the enamel, loadings profiles of PC1 and PC2.

4.2.3. TREATMENTS EFFECTS OVER THE DENTIN ANALYSED BY PCA

The analysis of the dentin was also performed using PCA for the different treatments. As in the enamel results, the weights of the main components were in the components 1 and 2 (PC1 and PC2) for both carriers. Liposomes and MOFs analysis had a PC1 of 87.68% and 86.30% *versus* PC2 of 8.43% and 9.39% accounting for a total of 96.11% and 95.69% of the variance, respectively (Fig. 51). In comparison to the enamel analysis, the separation between the groups in the dentin was much better, and more consistent information could be obtained. This better separation of the different groups in the dentin may be due to the less mineral content and less crystal packing in this tissue, having the organic matter of the drug stronger presence improving the sample grouping [223]. Therefore, the signal of carbonates and phosphates groups of HAP decreases and the vibrations of the organic material could be distinguished. All the groups in both carriers' analysis had similar distribution in the scores graphs along PC1 and PC2 (Fig. 51). Loaded liposomes and MOFs groups were closer to the samples treated with only drug (CBD and OLV) than the samples without treatment or unloaded carrier. Thus, it means that both carriers led the drug transport until the dentin tissue efficiently increasing the diffusion process, despite the drug concentration per application was much lower than in the CBD and OLV control groups (Table 8) [40]. Furthermore, CBD and OLV control groups are completely overlapped in this analysis, confirming that OLV could be used as CBD analogue in this experiment. Dentin analysis also revealed differences related to the presence of liposomes or MOFs along PC2. Meanwhile, groups without any carrier were in the positive part of PC2, the groups with carrier were in the negative part of this component regardless the drug presence. Therefore, PC1 may group the samples according to the drug presence and PC2 according to the carrier presence in the dentin tissue. Moreover, these results from the dentin analysis verified and supported the previous results of the enamel.

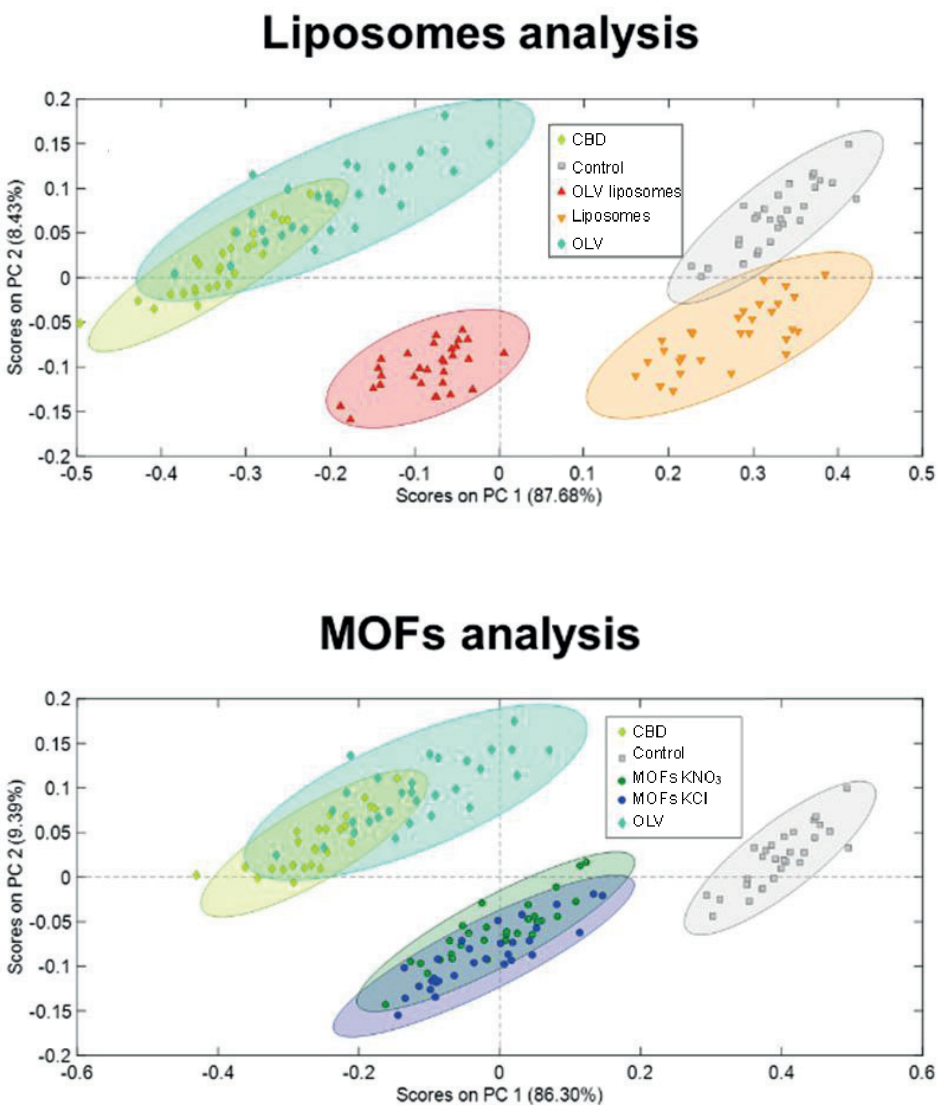

Figure 51: Principal Component Analysis of liposomes and MOFs in the dentin, scores plots grouping according to the drug presence and carrier presence.

PC1 loadings graphs included all the characteristic vibrations previously assigned in the dentin tissue for both carriers in the positive part of the profile (Fig. 52). As in the enamel analysis, drug vibrations did not appear since the contribution of the inorganic material was much more significant that the contribution of the drug. The loading profiles of PC1 were in agreement with the scores' graphs since the samples without drug were in the positive part of this component (more intense signal) and the samples with drug were in less positive values (less intense signal).

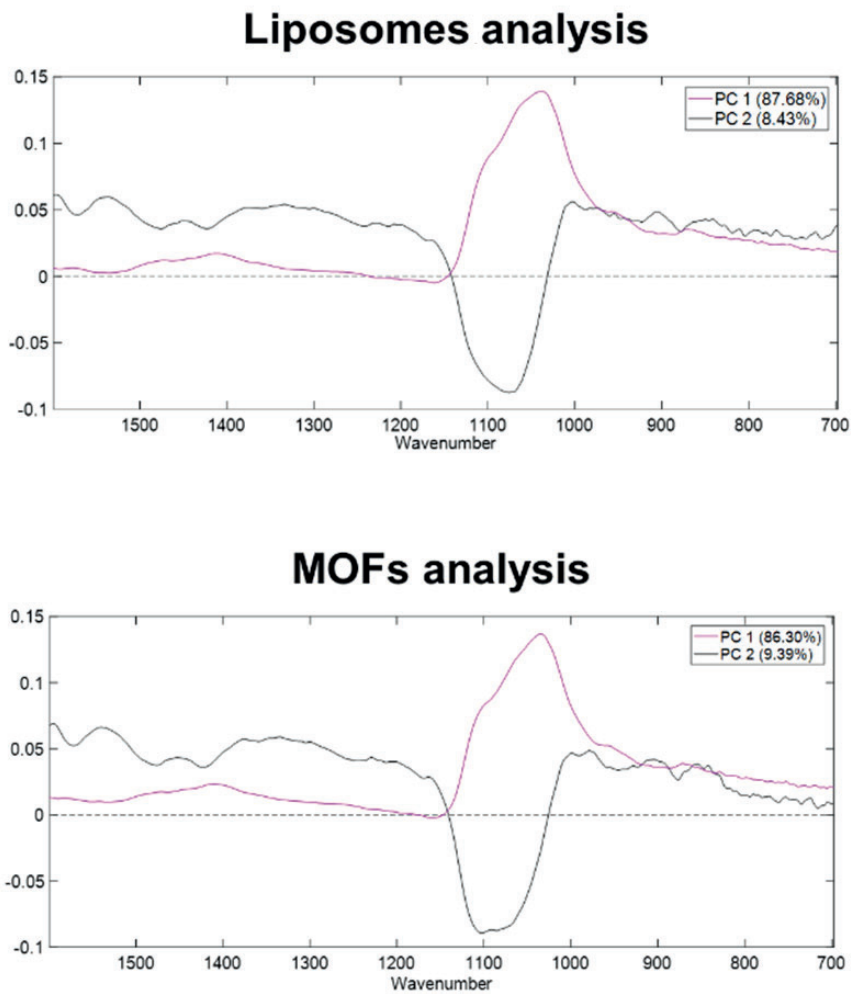

Figure 52: Principal Component Analysis of liposomes and MOFs in the dentin, loadings profiles of PC1 and PC2.

PC2 profiles comprised the wide band of the antisymmetric stretching vibration v_3 PO_4^{3-} in the negative part emphasising the shoulder at 1103 cm^{-1} of the peaks' assignment, while the rest of the peaks were in the positive half of this component (Fig. 52). This negative band gives information about the bandwidth and the groups that were in the more negative part of the scores graphs correspond to treatments with liposomes and MOFs that contributed with the increase of the organic material in the dentin tissue, reducing the crystallinity and making the mentioned phosphate band widder when these groups were compared to the ones without any carrier [233]. This information agreed with scores distribution along PC2 where the samples without carrier were in the positive part and the samples with carrier in the negative half. The fact that rest of the bands were in the positive part means that the presence of any carrier did not affect these vibrations.

4.3. REACTION YIELD AND DRUG ENCAPSULATION OPTIMIZATION IN MOFs

γ-CD-MOFs' formulations using KCl and KNO_3 provided comparable results to liposomes' formulation in the previous *in vitro* study, even though the drug loading was lower. Considering that fact, the methodology to obtain these MOFs' formulations based on the use of these alternative potassium sources and the co-crystallization technique for the olivetol encapsulation was optimized in terms of reaction yield and drug encapsulation using design of experiments (DoE).

4.3.1. MODEL FITTING

A total of 27 runs were performed per potassium salt, varying the four inputs factors at three different levels. Reaction yield (Y_1) and drug encapsulation (Y_2) were the two studied responses for this experimental design. The design layout with the experimental values of the responses is shown in Table 9.

Table 9: Experimental values of reaction yield and drug encapsulation responses for each potassium salt. Highlighted runs were removed from the analysis.

Run	Response values			
	KCl		KNO_3	
	Reaction yield (%)	Drug encapsulation (%)	Reaction yield (%)	Drug encapsulation (%)
	Y_1	Y_2	Y_1	Y_2
1	35.9	5.6	36.5	4.5
2	60.6	6.3	67.4	3.8
3	30.5	5.0	48.3	5.3
*4**	*0.2*	*0.4*	*0.3*	*0.3*
5	30.2	2.6	33.4	2.7
6	53.8	3.4	57.5	3.5
7	62.8	3.5	65.6	2.5
8	40.7	4.7	39.6	4.7
9	0.1	4.8	1.2	1.1
10	9.9	7.1	8.5	5.8
11	10.3	7.7	12.3	6.8
*12**	*44.2*	*6.5*	*44.5*	*7.1*
13	44.1	5.8	56.8	4.4
14	25.1	7.1	32.4	5.0
15	10.8	6.8	14.0	5.9
*16**	*0.2*	*1.1*	*0.5*	*1.9*

17	54.5	5.4	52.4	5.6
18	34.6	4.9	21.3	4.4
19	29.0	7.2	36.4	5.0
20*	*0.5*	*4.5*	*0.6*	*13.5*
21	11.6	8.2	29.0	7.4
22	18.8	6.8	25.6	6.5
23	5.0	4.3	2.7	2.0
24	2.4	7.2	14.6	6.8
25	40.4	6.8	39.6	6.0
26	72.7	5.1	75.5	5.4
27	54.0	5.5	57.9	5.6

Runs 4, 12, 16 and 20 were removed from the analysis. In case of runs 4, 16 and 20 not enough product could be obtained from the reaction due to the experimental conditions and the values of the responses were not consistent. For run 12, the values did not fit with the design. Excluding these mentioned four runs, reaction yield and drug encapsulation values varied from 0.1% to 75.5% and from 1.1% to 7.7%, respectively. These data were employed for the experimental design analysis using Design Expert Software. ANOVA statistical analysis was performed for the calculation of coefficients of the polynomial equations. Results showed that quadratic and 2FI models could be used to represent the data for the reaction yield (Y_1) and drug encapsulation (Y_2) respectively in both potassium salts. The equations for the responses (eq. 6-9) explain their interactions with the independent variables (incubation temperature, A; incubation time, B; methanol content, C and olivetol concentration, D). In all cases, the terms of the equations that presented a non-significant p-value (p-value > 0.05) were removed from the final equations in order to improve the fitting. Here below, the final reduced equations in terms of coded factors with only significant model terms are shown:

For potassium chloride:

$$Y_{1\,(\text{Reaction yield})} = 32.76-16.21A+5.98B-22.15C+18.13D+2.52AB-7.45AC-12.40B^2 \quad [6]$$

$$Y_{2\,(\text{Drug encapsulation})} = 6.06+1.62A-0.0958B+0.5353C-0.6819AB-0.4832BC \quad [7]$$

For potassium nitrate:

$$Y_{1\,(\text{Reaction yield})} = 41.07-12.96A+8.66B-21.25C+18.30D-5.37AC+4BD-8.56C^2-8.58D^2 \quad [8]$$

$$Y_{2\,(\text{Drug encapsulation})} = 5.33+1.85A-0.5220B+0.5917C+0.3250D-1.17AB+1.04AC-0.4231AD-0.5622BC+0.5289CD \quad [9]$$

The equations in terms of coded factors can be used to make predictions about the response for given levels of each factor. These equations are useful for identifying the relative impact of the factors by comparing the factor's coefficients. A positive value in the coefficients means that there is a synergistic effect on that response, and a negative value indicates an antagonistic effect [235,236].

In all models for both responses, statistic parameters showed a good fitting with the experimental results (Table 10).

Table 10: Statistics summary of the quadratic and 2FI response surface models for reaction yield and drug encapsulation responses in each potassium salt.

	Response			
	KCl		KNO_3	
	Reaction yield	Drug encapsulation	Reaction yield	Drug encapsulation
Model	Quadratic	2FI	Quadratic	2FI
F-value	92.89	11.79	31.19	23.34
Model p-values	< 0.0001	< 0.0001	< 0.0001	< 0.0001
R^2	0.9775	0.7762	0.9469	0.9417
Adjusted R^2	0.9669	0.7103	0.9165	0.9014
Predicted R^2	0.9561	0.6487	0.8507	0.7851
Adequate precision	31.92	11.97	21.10	16.99
Lack of fit p-values	0.9477	0.9651	0.5966	0.2461

The significance of the factors was determined based on the F-values and/or p-values with 95% confidence level. The obtained F-values implied that selected models were significant and there was only a 0.01% of chance that these F-values could occur due to noise. The coefficient of determination values (R^2) were close to unity indicating a good fitting of the model to experimental results. Besides, the predicted R^2 were in agreement with the adjusted ones, since in all the cases the difference between these two values was less than 0.2. In case of drug encapsulation for KCl, the R^2 values were lower, but they were accepted taking into account all other statistical parameters. Predicted *versus* actual values distributions (Fig. 53) also show a high compatibility of these data, since points are closely following the diagonal. Moreover, the adequate precision value measures the signal-to-noise ratio and a ratio greater than four is desirable, in order to use the model to navigate in the design space. The lack of fit expresses the residual error compared to the pure error. Non-significant lack of fit (p-value > 0.05) for the selected models indicated their accuracy and low

error. Therefore, based on the statistical analysis, the effect of the factors on responses could be explained using a quadratic polynomial model and a 2FI model for reaction yield and drug encapsulation, respectively.

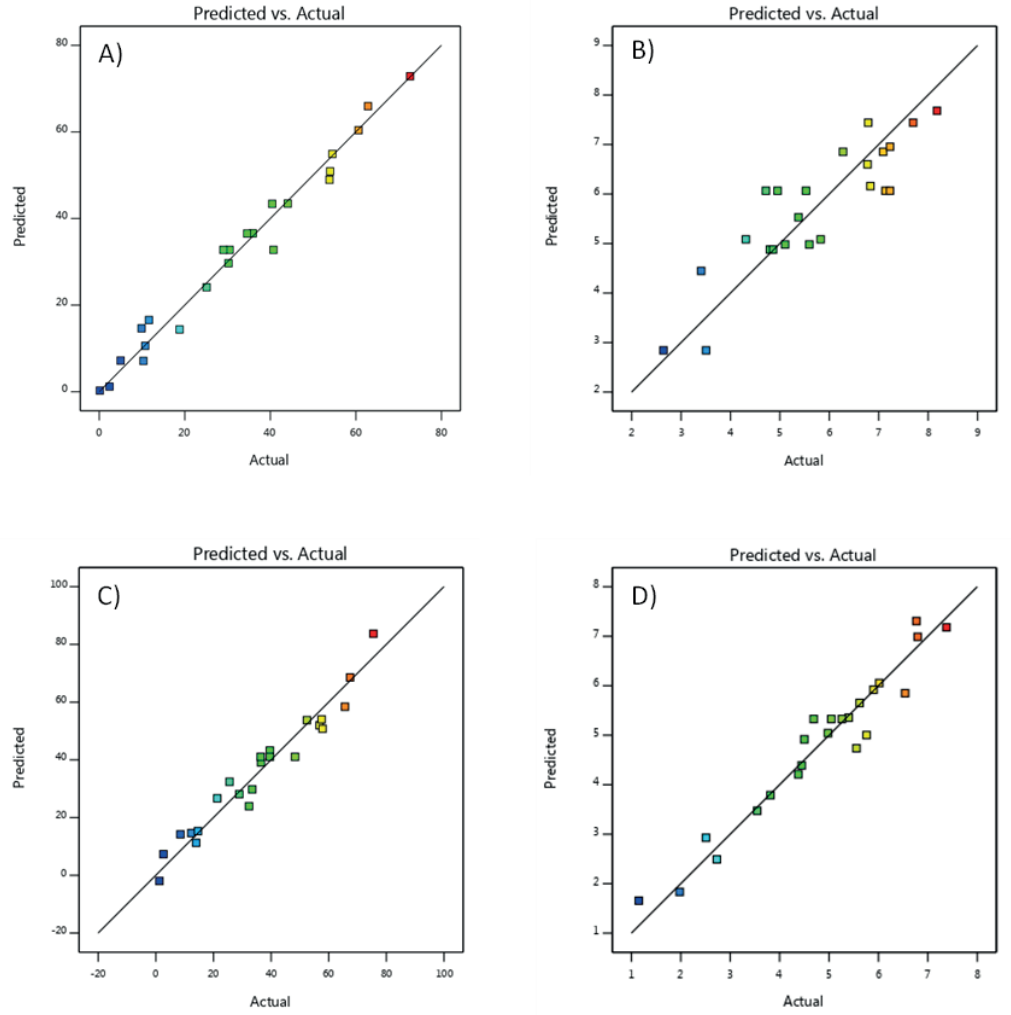

Figure 53: Predicted versus actual values for KCl reaction yield and drug encapsulation (A and B) and for KNO_3 reaction yield and drug encapsulation (C and D).

Furthermore, the residuals were studied to validate the adequacy of the different models through the analysis of the normal plots and the residuals *versus* the predicted responses graphs (Fig. 54). The difference between the real response and the predicted one determines the residual value. In all the cases, residuals were distributed in a straight line according to their normal probability. In figure 54, the distribution of the residuals *versus* predicted responses was totally random suggesting that the models were suitable, and they showed independence and constant variance assumption.

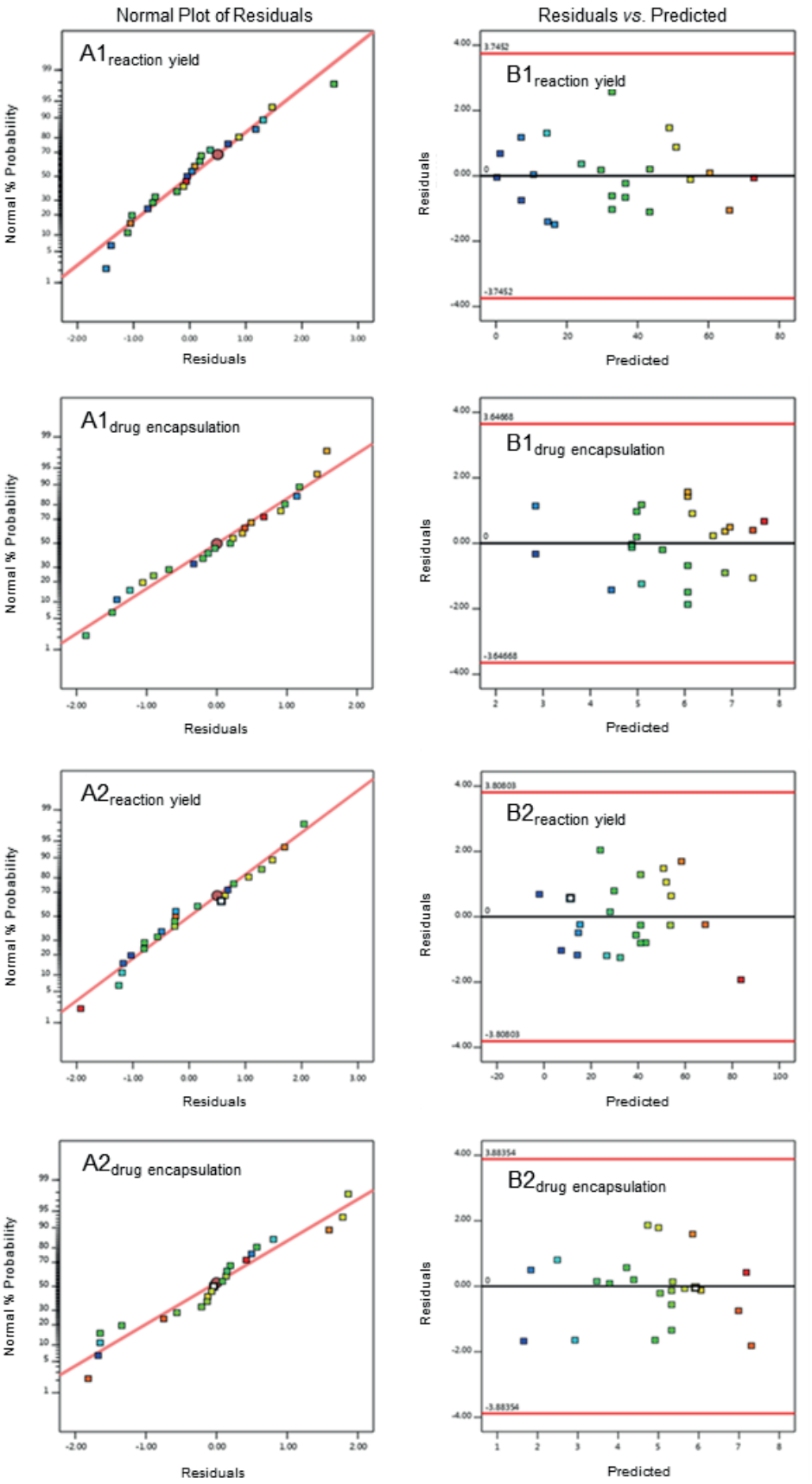

Figure 54: Normal probability plots of the residual (A) and residual versus predicted response graphs (B) for KCl (1) reaction yield and drug encapsulation and for KNO_3 (2) reaction yield and drug encapsulation.

4.3.2. REACTION YIELD

The selected factors in this study were adjusted following a quadratic polynomial for reaction yield response in both potassium salts (eq. 6 and 8). After removing non-significant terms, it could be observed that the linear contributions of all the factors presented the same behaviour for KCl and KNO_3. The incubation time (B) and olivetol concentration (D) increased the reaction yield. Meanwhile, the incubation temperature (A) and methanol content (C) showed an antagonistic effect. For KCl, the interaction of A with B increased this response, but the one of A with C and the quadratic contribution of B reduced the reaction yield. For KNO_3, the interaction of B with D showed an agonistic effect, whereas the interaction of A with C and the quadratic contributions of C and D minimised this response. Some of these main and interactions effects are shown using contour plots and three-dimensional response surface plots (Fig. 55). These plots give a visual representation of this response and its relationship with the different factors.

The increment of incubation time (B) and olivetol concentration (D) increased the reaction yield. The first parameter could be explained based on crystallization kinetics, as nucleation and crystal growth [237]. These parameters are time-dependent and if the time is too short, crystal formation could not occur [238]. Therefore, the MOFs reaction yield is increasing in function of time with the development of the crystallization process. The fact that the concentration of the drug had a positive effect in the reaction yield may be due to an increase in the solute's concentration of the initial solution, promoting its supersaturation. The supersaturation is directly proportional to the concentration. Therefore, if the concentration is higher than the solubility, the solution is supersaturated, and the crystallization process takes place [239]. The increment of olivetol could contribute to reach the supersaturation point of the initial solution, obtaining more precipitate. On the other hand, incubation temperature (A) and methanol content (C) presented a negative effect over the reaction yield. The concept of supersaturation could be also useful to explain the antagonistic effect of the incubation temperature. This parameter also depends on solubility, being inversely proportional. Increasing the temperature, the solubility also increases, decreasing the supersaturation [239]. Hence, the solution becomes under-saturated, and the crystallization process does not occur. The fact that the methanol content has a negative effect over the reaction yield may be related to olivetol solubility. Since olivetol is an organic compound, it is more soluble in organic solvents than in aqueous solutions. Therefore, the higher the

methanol content, the greater the amount of soluble drug in the same mixture, keeping it away from the supersaturation and making more difficult the crystallization process.

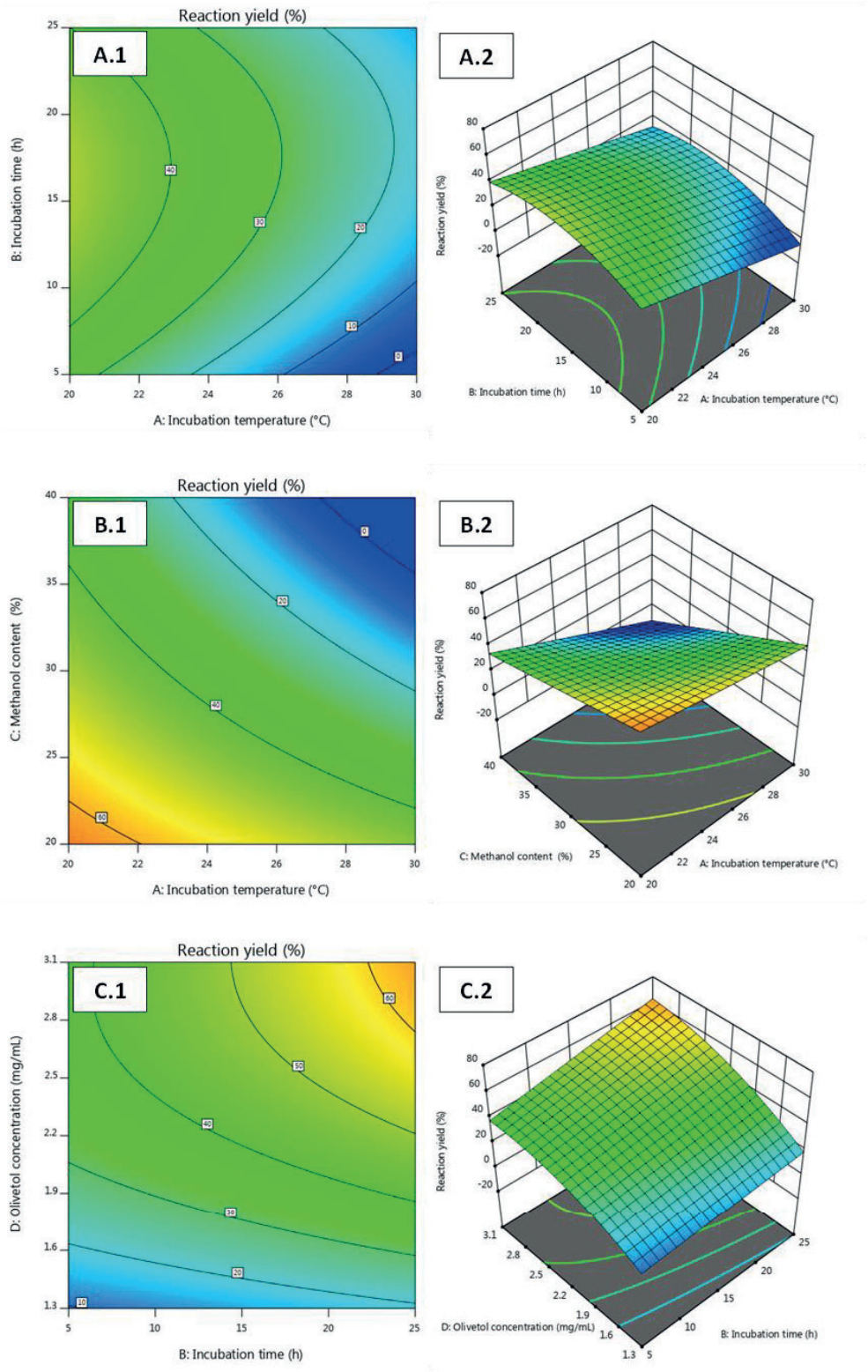

Figure 55: Contour plots (1) and three-dimensional response surface plots (2) for reaction yield response in both salts: KCl (A and B) and KNO_3 (C).

4.3.3. DRUG ENCAPSULATION

The effects of the factors on the drug encapsulation were studied through a 2FI polynomial for both potassium salts (eq. 7 and 9). After eliminating non-significant terms for KCl, the linear contribution of incubation temperature (A) and methanol content (C) increased the drug encapsulation. However, these responses were reduced due to the antagonistic effects observed by the linear contribution of incubation time (B) and by the interactions of A with B and B with C. In case of KNO_3, same contributions described before for KCl were observed presenting the same behaviour. Besides, the linear contribution of olivetol concentration (D), the interactions of A with C and C with D showed an agonistic effect, while the interaction of A with D decreased the drug encapsulation. Some of these main interactions' effects are shown using contour plots and three-dimensional response surface plots (Fig. 56). These plots give a visual representation of this response and its relationship with the different factors.

Incubation temperature (A), methanol content (C) and olivetol concentration (D) have a positive effect over the drug encapsulation. The behaviour of these factors could be described in terms of diffusion. The first state of Fick's law relates diffusion to concentration. This law postulates that the flux goes from a region of high concentration to regions of low concentration, being proportional to the concentration gradient [240]. Thus, olivetol molecules diffuse from the solution to the MOFs pores due to drug concentration gradient. According to Fick, diffusion is also directly proportional to the diffusion coefficient and this coefficient depends on the temperature. The relationship between this coefficient and the temperature could be explained by the Einstein equation, where a positive effect in temperature increases the thermal energy of molecules, raising its diffusion rate [241]. Besides, diffusion process is closely related to solute dissolution rate, when the dissolution rate is higher, diffusion also increases [242]. Thus, raising the methanol content of the initial solution, more olivetol molecules will be dissolved due to the non-polar behaviour of the drug. In this way, more olivetol will be available for diffusion into the pores, increasing the encapsulation process. The incubation time (B) contributes with a negative effect for drug encapsulation. Within the time, the diffusion process is taking place from the solution where the drug is highly concentrated to the empty pores of the MOFs. However, when the drug concentration is higher in the carriers than in the medium, the diffusion transport starts in

the opposite direction, trying to reach the equilibrium and decreasing the drug encapsulation [243].

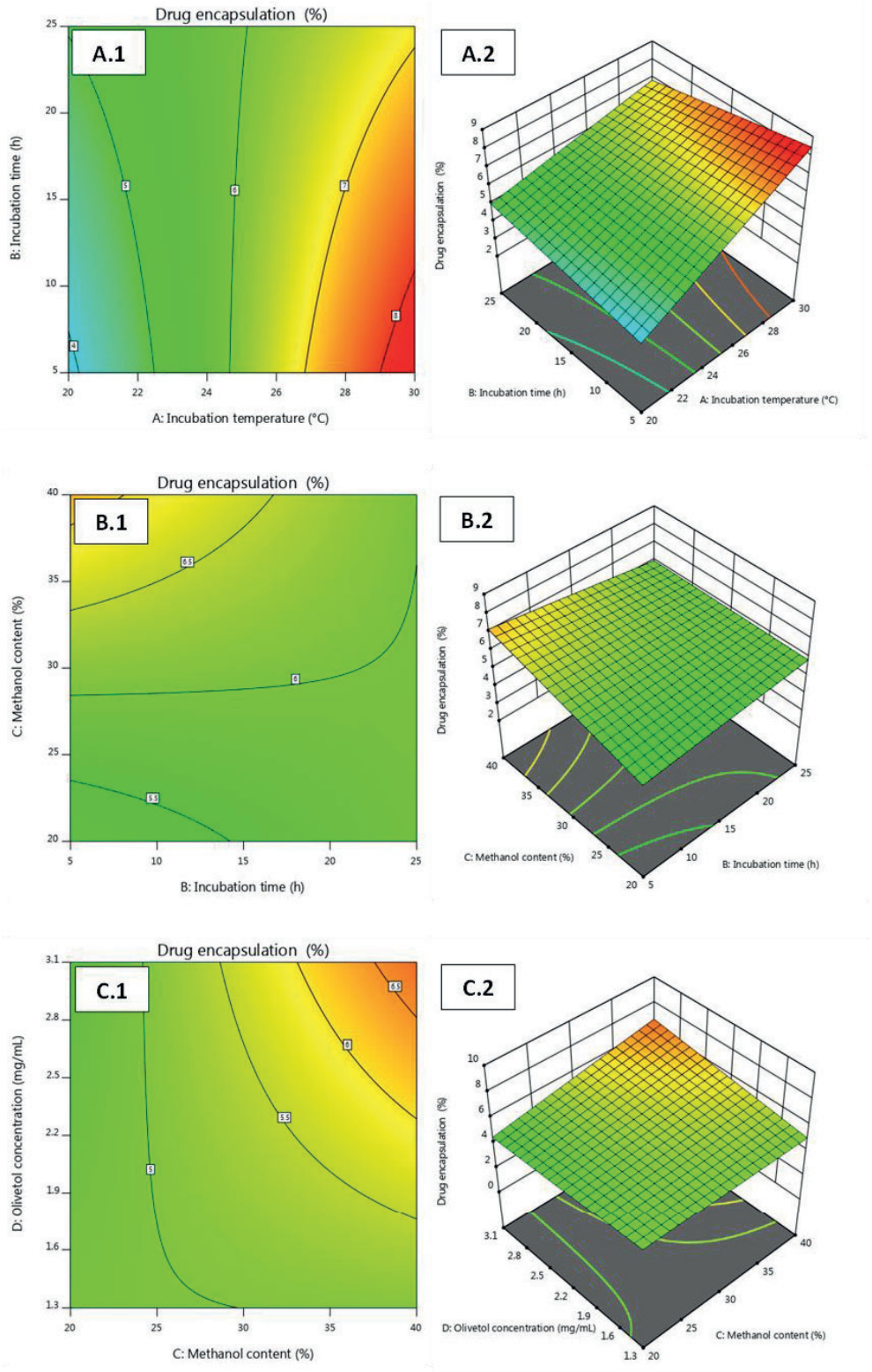

Figure 56: Contour plots (1) and three-dimensional response surface plots (2) for drug encapsulation response in both salts: KCl (A and B) and KNO_3 (C).

4.3.4. REPONSES OPTIMIZATION AND VERIFICATION OF THE MODELS

Optimization of the independent variables was done by setting goals for each response using Design Expert software. All four independent variables were incorporated in the optimization at their design space, except the incubation time for KCl. This variable was targeted to 15 hours, considering the practical experimental conditions. The challenge of this study was to maximize both responses. However, since their behaviour was the opposite, reaction yield response was targeted to 55% to be able to maximize the encapsulation. This value was selected to improve previous results of reaction yield of these CD-MOFs, which was around 35%. Besides, this number is like the one obtained when the conventional KOH is employed as potassium source. Numerical optimization values were selected using desirability function (D), where D values ranging between 0 and 1, being 0 for low desirable conditions and 1 for high desirable ones. Following this criteria, different solutions of optimal conditions were obtained with different desirability values. The solution that showed the highest desirability value was selected as the optimized synthesis conditions for each potassium salt (Table 11).

Table 11: Optimized synthesis conditions for each potassium salt with its desirability value.

Potassium salt	Incubation temperature (ºC)	Incubation time (hours)	Methanol content (%)	Olivetol concentration (mg/mL)	Desirability
KCl	30	15	23.1	3.1	0.945
KNO_3	26.9	18.6	27.9	3.1	0.815

Considering the practical experimental conditions, the conditions were set to 30 ºC, 15 hours, 23% and 3.1 mg/mL for KCl and 27 ºC, 18.5 hours, 28% and 3.1 mg/mL for KNO_3. The selected optimal conditions were verified by performing the experiments under these conditions in two independent replicates per salt. The results are shown in Table 12. Validation of the experimental design was done by comparing predicted and experimental values. The obtained data were inside the limits of the 95% prediction interval in all the cases and the values of the errors found to be within an acceptable range. This means that the experimental results were comparable to the predicted results that illustrate the preciseness of the design. Moreover, the experimental results for reaction yield were even better than the predicted values. Therefore, the generated models showed sufficient accuracy and predictability for optimizing the reaction yield and drug encapsulation in the experimental conditions

mentioned above. Besides, the values of both responses have been improved for both potassium salts in comparison with previous experimental results. Reaction yield values have doubled, while drug encapsulation has increased by 20% for KCl and 46% for KNO_3.

Table 12: Experimental and predicted values of both responses at optimized conditions for each salt (PI = prediction interval).

Potassium salt	Response	Predicted value	Experimental value	95% PI low	95% PI high	Error
KCl	Reaction yield (%)	55	60 ± 2	46	64	5
	Drug encapsulation (%)	7.3	7.0 ± 0.7	5.5	9.1	0.3
KNO_3	Reaction yield (%)	55	69 ± 3	39	71	14
	Drug encapsulation (%)	5.6	6.0 ± 0.4	4.4	6.7	0.4

4.3.5. CHARACTERIZATION OF THE OPTIMAL FORMULATIONS

The morphology and the crystallinity of the optimal formulations were studied using SEM and PXRD analysis (Fig. 57). Both γ-CD-MOFs formulations showed a rectangular shape as elongated prims. The length of most of the crystals was around 2 to 50 µm, but there were also crystal sizes out of this range. This fact may be due to the long time during the incubation step that was 15 and 18.5 hours for KCl and KNO_3, respectively. It was reported that if enough time is allowed during a crystallization process, the size of the resulting crystals would not be homogeneous [196]. Concerning the diffraction patterns, both formulations showed the same characteristics peaks that were in different angles: 5.3º, 7.4º, 10.5º, 11.5º, 12.1º, 14.2º, 14.9º, 15.8º and 16.7º. Besides, the sharp peaks in the diffraction patterns revealed a high crystallinity of the MOFs, despite the improvement in the drug encapsulation following the optimal conditions. These peaks' positions may correspond to a triclinic, tetragonal o trigonal space groups such as *R*32, *I*4, *P*1 or *P*32, that were already reported in CD-MOFs where the metal sources were not the typical potassium hydroxide [147]. These diffraction patterns would be correlated to the rectangular prism morphologies observed in their respective SEM analysis. Considering these SEM and PXRD results, it is remarkable to mention that the new optimal conditions did not compromise the morphology and the crystallinity of these γ-CD-

MOFs. Moreover, these results were in agreement with the previous obtained morphology and crystallinity characterization in section 4.1.1 (before the optimization).

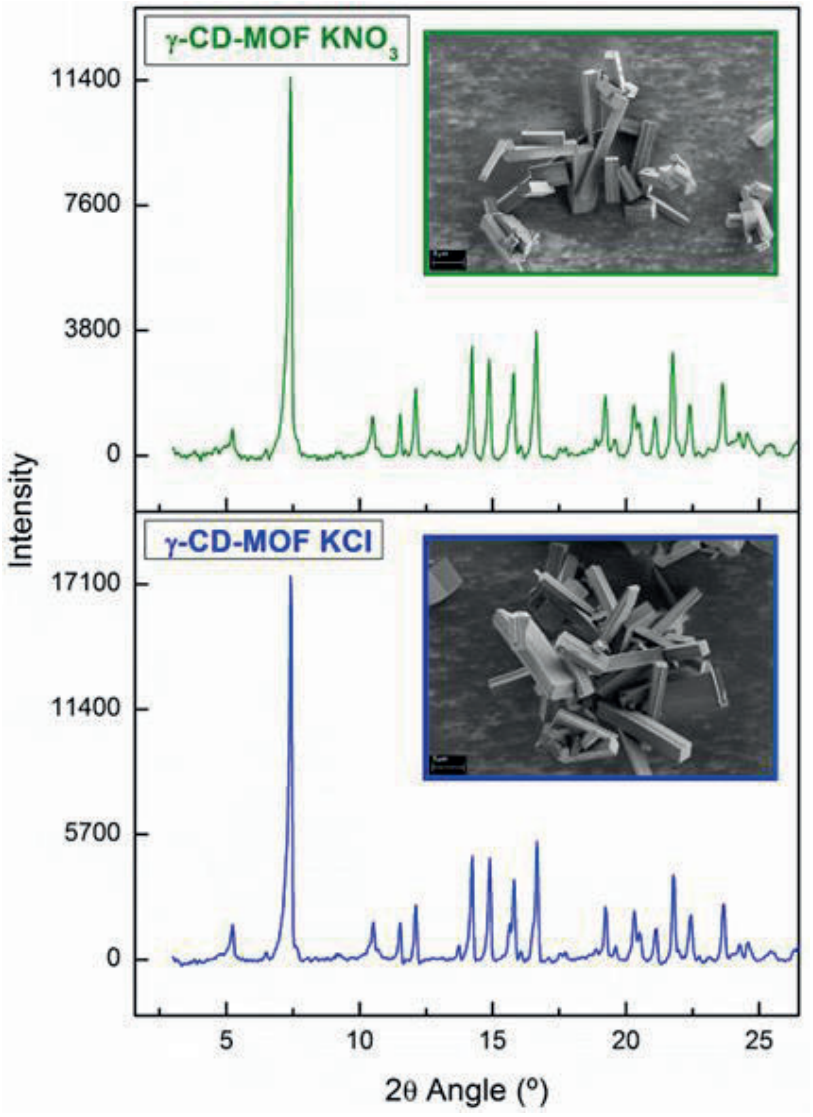

Figure 57: Scanning electron microscopy images and X-ray powder diffraction patterns of optimal γ-CD-MOF formulations using KCl (blue) and KNO_3 (green) as potassium sources.

FTIR analysis showed the characteristic peaks in both γ-CD-MOF formulations at 1078 cm^{-1}, 1152 cm^{-1}, 1336 cm^{-1}, 2700 – 2995 cm^{-1} and 3000 – 3670 cm^{-1} (Fig. 58). These peaks were in agreement with previous reported studies of these MOFs, and they matched with the characteristic peaks in the γ-CD spectrum, confirming the presence of the organic ligand in the crystals [107]. At 1078 cm^{-1} and 1152 cm^{-1}, stretching vibrations derived from -C-O-C- and C–OH bonds in cyclodextrin sugars could be observed, respectively. The peak at 1336 cm^{-1}

and the band from 2700 – 2995 cm^{-1} were related to the contributions of alkane groups. The wide band from 3000 – 3670 cm^{-1} was assigned to stretching vibrations of the hydroxyl groups from the cyclodextrin molecules. Besides, the peak observed at 1640 cm^{-1} could be due to the water molecules that remained into the cavities of the MOFs after the drying process. The spectrum of olivetol showed its characteristic peaks according to the literature at 3240 cm^{-1}, 2929 cm^{-1}, 2858 cm^{-1} and a double peak at 1628 cm^{-1} and 1600 cm^{-1}. These peaks correspond to the -OH stretching vibration, -CH symmetric and antisymmetric stretching in the aliphatic chain and the -C=C- stretching vibration from the aromatic ring respectively (Fig. 58) [212]. A direct comparison between the infrared spectra of OLV and both γ-CD-MOFs revealed that the single peak at 1640 cm^{-1} showed a double peak at 1600 and 1628 cm^{-1} that it was not in the raw γ-CD spectrum, and it may correspond to the skeletal stretching -C=C- vibration of the drug (Fig. 58). It means that olivetol is interacting with the γ-CD-MOFs as it is also reported in the results for the drug encapsulation response. These interactions could occur through intermolecular forces, as there were not significant shifts in the spectra. These results also agreed with previous infrared analysis for these MOFs before optimization in section 4.1.1.

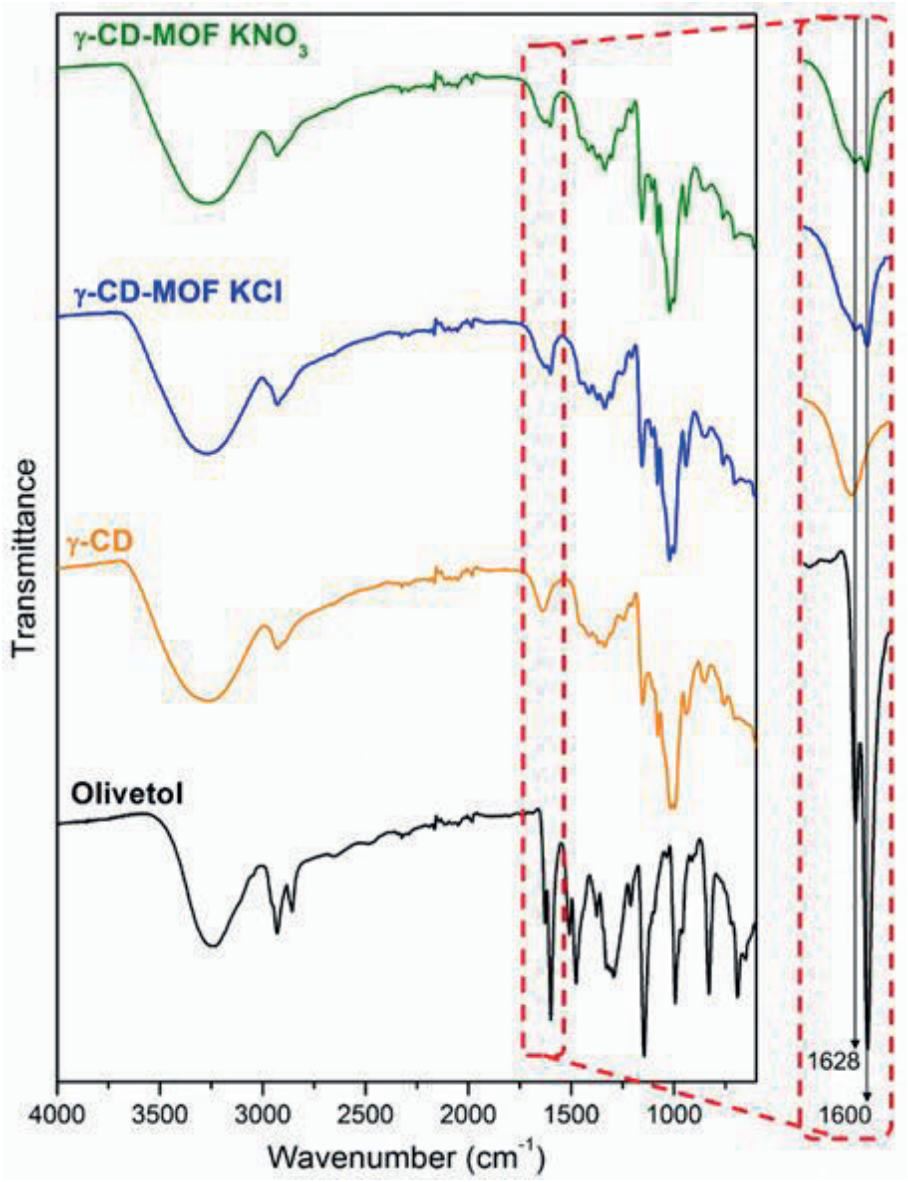

Figure 58: Attenuated Total Reflection-Fourier Transform Infrared Spectroscopy spectra of olivetol (black), γ-CD (orange), optimal γ-CD-MOF formulations using KCl (blue) and KNO_3 (green) as potassium sources from 4000 cm^{-1} to 600 cm^{-1}, showing a magnification of the double peak at 1600 and 1628 cm^{-1}.

4.3.6. DRUG RELEASE *IN VITRO* STUDY

To determine the released OLV from the optimal formulations after the optimization with DoE, a calibration curve of different known concentrations of olivetol in PBS from 0 to 100 mg/L was performed (Fig. 59).

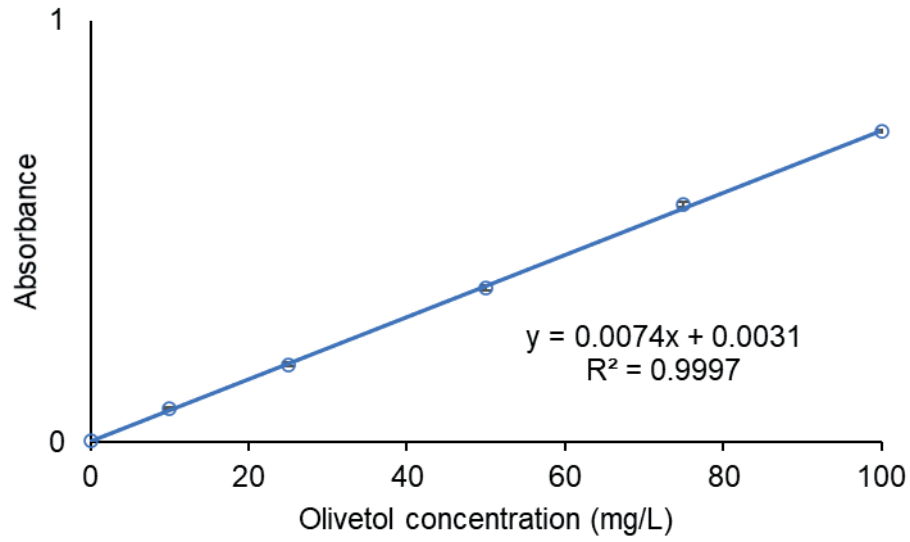

Figure 59: Olivetol calibration curve in PBS from 0 to 100 mg/L of the drug measured at 275 nm with the equation and the linear regression coefficient. The calibration line was calculated by linear regression (n = 3).

In order to study if the optimal formulations after DoE could release the drug over a period of time, the cumulative release of the olivetol from the MOFs was studied *in vitro* in PBS at pH 7.5 (Fig. 60). The release of the drug was quite fast in both formulations showing a continuous release over the first hour. After this time, the 75% of olivetol was released in γ-CD-MOFs KCl, while the formulation containing KNO_3 released the 50% of the drug. Then, the accumulative release of olivetol reached 89% after 19 hours and 96% after 48 hours in γ-CD-MOFs KCl, and only the 65% of olivetol was quantified after 48 hours for γ-CD-MOFs KNO_3. Thus, the formulation with KNO_3 needs more time to release all the drug content. It should also be mentioned that 40% of olivetol was released within the first hour from both γ-CD-MOFs. And the gradual release of the drug continued over this time. Therefore, these results indicated that γ-CD-MOFs could help in controlling the release of olivetol, since the diffusion of the free drug would be much faster. Moreover, these results were in agreement with previous release *in vitro* studies using these γ-CD-MOFs with other compounds [244–247]. In any case, thanks to the MOFs' adaptability, the functionalization of these materials could be performed in order to modify the drug release behaviour depending on the final application. Some studies have already modified this fast release through the functionalization with fullerene or cholesterol among others, to modulate drug release over the time [151,248–250]. Therefore, further investigations would be carried out in the future work.

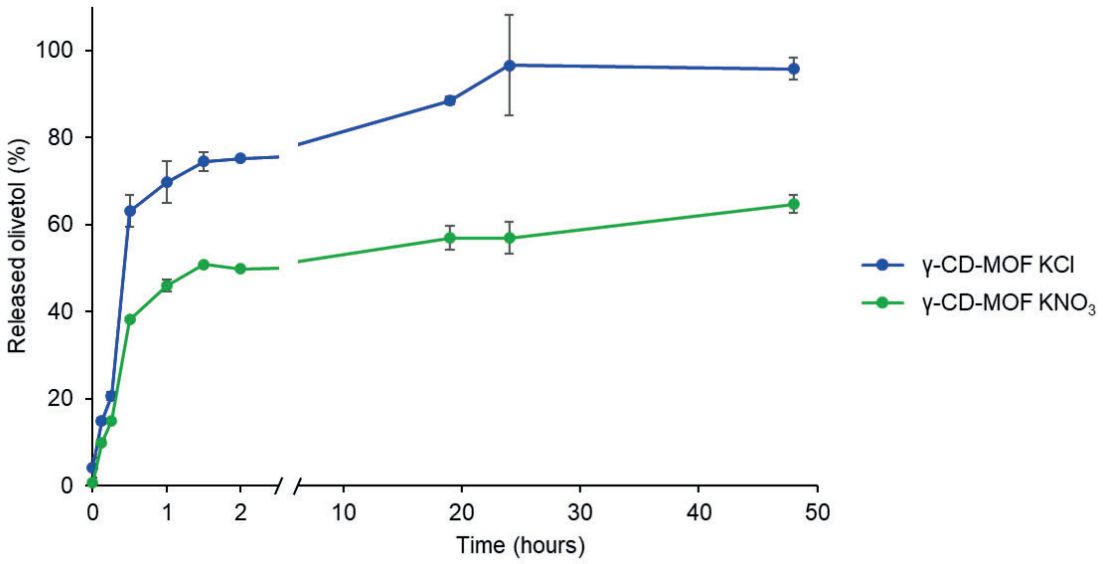

Figure 60: Release in vitro study of olivetol from the optimal MOF formulations in PBS buffer at pH 7.5 (n = 3).

4.4. VERIFY THE USE OF CANNABIDIOL IN MOFs USING THE OPTIMAL CONDITIONS

Finally, after the optimization using DoE, olivetol was substituted by cannabidiol in the process using the optimal conditions to explore if this change alter the properties of the formulations, validating the use of OLV as an analogue for CBD studies.

4.4.1. STRUCTURAL PROPERTIES OF γ-CD-MOFs

The morphology and the crystallinity of the cannabidiol formulations were studied using SEM and PXRD analysis. Both γ-CD-MOFs formulations (KCl and KNO_3) showed the same rectangular shape as elongated prims as the MOFs loaded with olivetol (Fig. 61). Furthermore, the EDX detector in the SEM equipment was used for the elemental qualitative analysis of these γ-CD-MOFs and it confirmed the presence of potassium in these structures (Table 13).

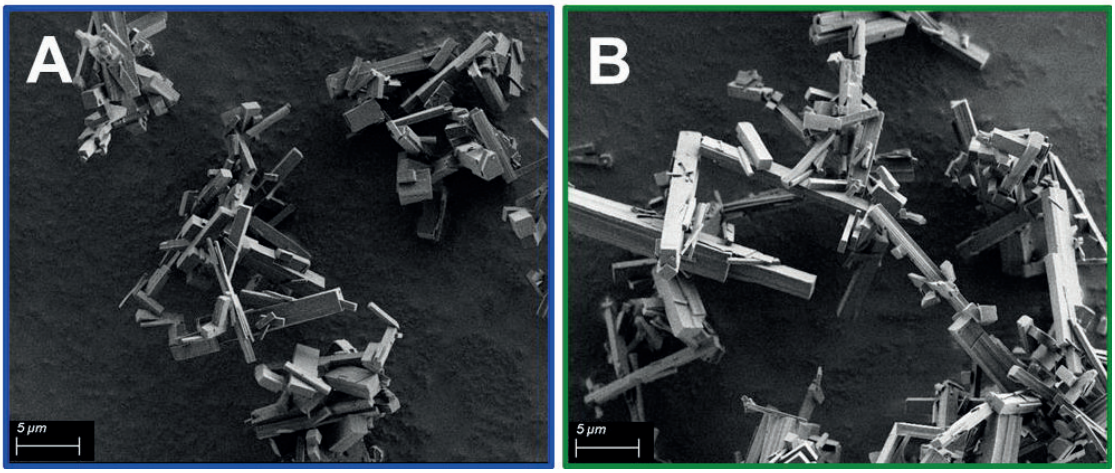

Figure 61: Scanning electron microscopy images of cannabidiol loaded γ-CD-MOF KCl (A) and γ-CD-MOF KNO_3 (B) with a low voltage of 2 kV, 5000x of magnification and a working distance of 4.7 mm.

Table 13: Qualitative analysis of potassium using energy-dispersive X-ray spectroscopy in cannabidiol loaded γ-CD-MOF KCl and γ-CD-MOF KNO_3 samples.

MOF sample	Atomic percentage of potassium (%)
γ-CD-MOF KCl	5
γ-CD-MOF KNO_3	7

Concerning the diffraction patterns, both formulations using CBD showed the same characteristics peaks that were in the same angles as before: 5.3º, 7.4º, 10.5º, 11.5º, 12.1º, 14.2º, 14.9º, 15.8º and 16.7º (Fig. 62). Thus, these peak positions may correspond to a triclinic, tetragonal o trigonal space groups such as *R*32, *I*4, *P*1 or *P*32, that were already reported in CD-MOFs where the metal sources were not the typical potassium hydroxide [147]. Nevertheless, the intensity of these peaks was significantly lower than the γ-CD-MOFs loaded with olivetol. This partial loss of crystallinity could be explained due to the more encapsulation amount of CBD filling the pores in comparison with the previous results with OLV. These findings are in accordance with previous reports that also observed this decrease [206,251,252]. In any case, these diffraction patterns would be correlated to the rectangular prism morphologies observed in the SEM analysis. Considering these results, it is remarkable to mention that the substitution of olivetol by cannabidiol did not compromise the morphology and the crystallinity of these γ-CD-MOFs using potassium chloride and potassium nitrate, despite the partial loss of crystallinity.

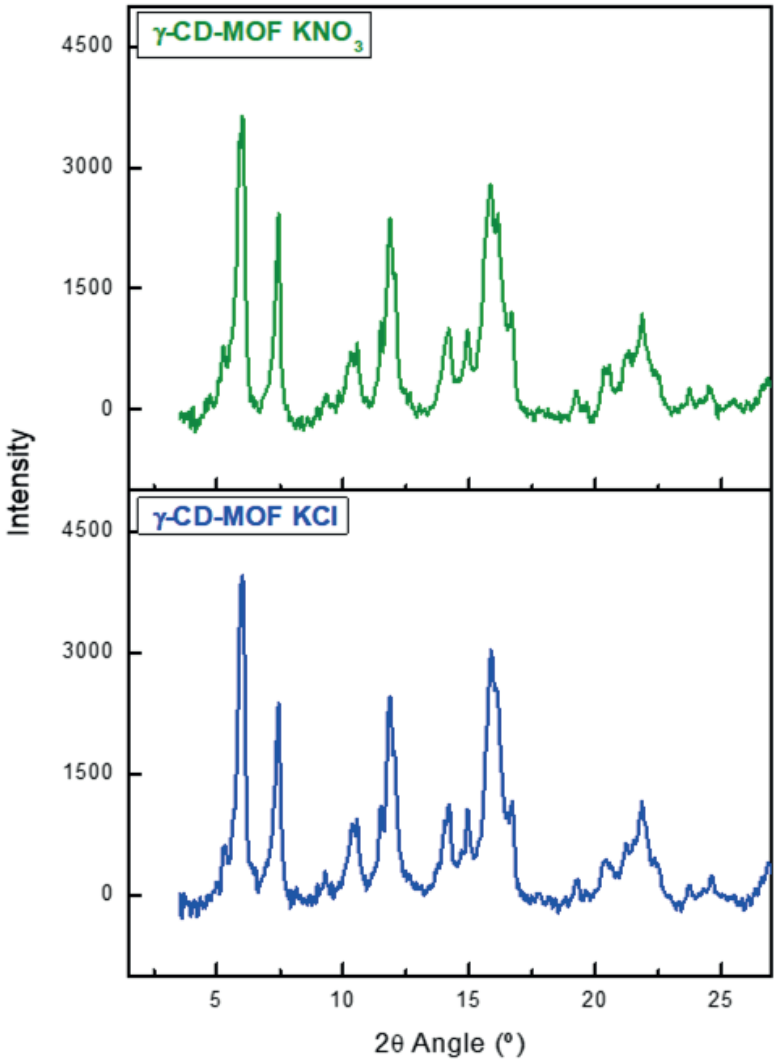

Figure 62: X-ray powder diffraction patterns of cannabidiol loaded γ-CD-MOF KCl (blue) and γ-CD-MOF KNO_3 (green) samples.

4.4.2. REACTION SYNTHESIS YIELD AND CANNABIDIOL CONTENT IN γ-CD-MOFs

The reaction yield values followed the predictions of the values from DoE when olivetol was used for the optimization of the formulations (section 4.3.4) (Table 14). Thus, the optimal conditions achieved before did not compromise the results when OLV is substituted by CBD in terms of reaction yield. Besides, these experimental results were even better than the predicted values, especially for γ-CD-MOFs KCl. The reaction yield was improved in comparison with previous results before the optimization, reaching values of the same order as the typical γ-CD-MOFs KOH when analytical microwave technique was employed.

Table 14: Reaction synthesis yield of cannabidiol loaded γ-CD-MOF KCl and γ-CD-MOF KNO_3.

MOF sample	Reaction yield (%)	
	Experimental value	Predicted value from DoE
γ-CD-MOF KCl	75	55
γ-CD-MOF KNO_3	65	55

To determine the CBD content in the samples a calibration curve of different known concentrations of cannabidiol in milliQ water:ethanol solutions (1:1, v/v) was performed from 0 to 100 mg/L (Fig. 63).

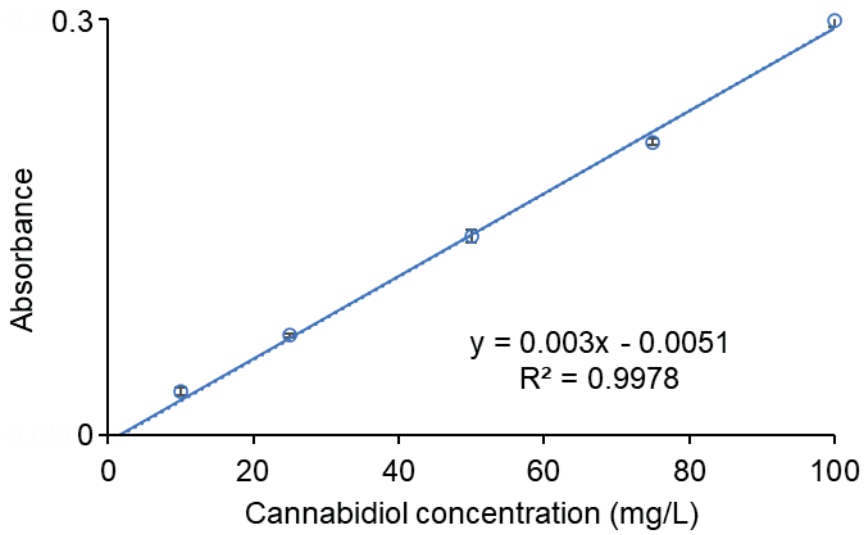

Figure 63: Cannabidiol calibration curve in ethanol:milliQ water (50:50, v/v) from 0 to 100 mg/L of the drug measured at 275 nm with the equation and the linear regression coefficient. The calibration line was calculated by linear regression (n = 3).

In contrast to reaction yield, for CBD encapsulation, the drug loading percentages were much higher in both formulations than the results obtained using olivetol (Fig. 64). The values for CBD were 10.4% for γ-CD-MOFs KCl and KNO_3, in comparison with the previous 7% and 6% with OLV. This fact could be explained since to maintain the same molar ratio as with the olivetol, the amount of cannabidiol added during the synthesis was adjusted as it was explained in the experimental section 3.3.6. This amount of CBD was higher due to the differences in molecular weight of both compounds (OLV: 180.24 g/mol and CBD: 314.47 g/mol). Thus, these differences in the initial amount of each drug during the synthesis affected the drug loading percentages results since they are expressed in terms of mass.

However, if these values are expressed in function of molar weight, the results are comparable for both drugs (Table 15). These values were recalculated following equation 2 using mols instead of mass. Therefore, the substitution of OLV by CBD did not alter the results in terms of drug encapsulation efficiency after the optimization with olivetol, validating the use of OLV as an analogue of CBD in this experimental approach. Furthermore, these drug loading values were in agreement with reported studies about γ-CD-MOFs when other compounds were employed [220–222].

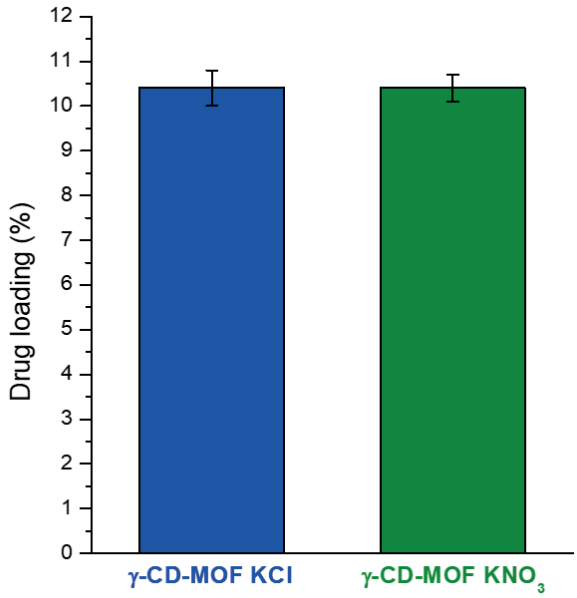

Figure 64: Drug loading percentage of cannabidiol in γ-CD-MOF KCl and γ-CD-MOF KNO_3 with their respective standard deviations.

Table 15: Comparison of drug encapsulation percentage for each formulation with their standard deviations between CBD and OLV after the optimization using DoE.

Encapsulated drug	MOF sample	Drug encapsulation in terms of molar weight (%)
CBD	γ-CD-MOF KCl	35 ± 1
	γ-CD-MOF KNO_3	36 ± 1
OLV	γ-CD-MOF KCl	38 ± 4
	γ-CD-MOF KNO_3	35 ± 2

4.4.3. γ-CD-MOFs AND CANNABIDIOL INTERACTION: ATR-FTIR ANALYSIS

FTIR analysis showed the characteristic peaks in both γ-CD-MOF KCl and KNO_3 formulations and these spectra agreed with previous reported studies of these MOFs, and they matched with the characteristic peaks in the γ-CD spectrum, confirming the presence of the organic ligand in the crystals (Fig. 65) [107]. Besides, these results are comparable to previous infrared analysis when OLV was used (sections 4.1.1 and 4.3.5). The spectrum of cannabidiol showed the characteristic bands of this drug according to the literature at 690-850 cm^{-1}, 883 cm^{-1}, 1019 cm^{-1}, 1145-1376 cm^{-1}, 1440 cm^{-1}, 1585 cm^{-1}, 1628 cm^{-1}, 2829 cm^{-1}, 2855 cm^{-1}, 2920 cm^{-1}, 2965 cm^{-1} and 3400 cm^{-1} (Fig. 65) [253,254]. The region from 690 cm^{-1} and 850 cm^{-1} correspond to CH out of plane deformations. The peak at 883 cm^{-1} was related to $=CH_2$ wagging, from the $-C=CH_2$ group. The wide peak at 1019 cm^{-1} corresponded to vibrations between the carbon atoms in the aliphatic chain. The region from 1145 cm^{-1} to 1376 cm^{-1} contained the stretching vibrations between the carbon and oxygen atoms of the C–OH groups that are presented in the CBD molecule. At 1440 cm^{-1}, in plane scissoring vibrations from CH_2 and CH_3 aliphatic groups could be observed. The peak at 1585 cm^{-1} was related to skeletal stretching vibrations of -C=C- in the aromatic rings. Meanwhile, the peak at 1628 cm^{-1} derived from the stretching vibrations of the unsaturated carbon atoms. The wide region with peaks at 2829 cm^{-1}, 2855 cm^{-1}, 2920 cm^{-1} and 2965 cm^{-1} corresponded to the symmetric and antisymmetric stretching vibrations of C–H bond of CH_2 and CH_3 groups. The peak at 3400 cm^{-1} was assigned to stretching vibrations between oxygen and hydrogen atoms of the hydroxyl groups. A direct comparison between the infrared spectra of CBD and both γ-CD-MOF formulations revealed that the single peak at 1640 cm^{-1} showed a double peak at 1585 and 1628 cm^{-1} that it was not in the raw γ-CD spectrum, and it may correspond to the skeletal stretching -C=C- vibration of the drug and the stretching vibrations of the unsaturated carbon atoms (Fig. 65). These results supported the interaction between γ-CD-MOFs and cannabidiol, and they are in agreement with drug quantification. These interactions could occur through intermolecular forces such as Van der Waals forces as before with OLV and in previous literature where other compounds were encapsulated into CD-MOFs such as curcumin [216]. Thus, these results also agreed with previous infrared analysis when OLV was used (sections 4.1.1 and 4.3.5).

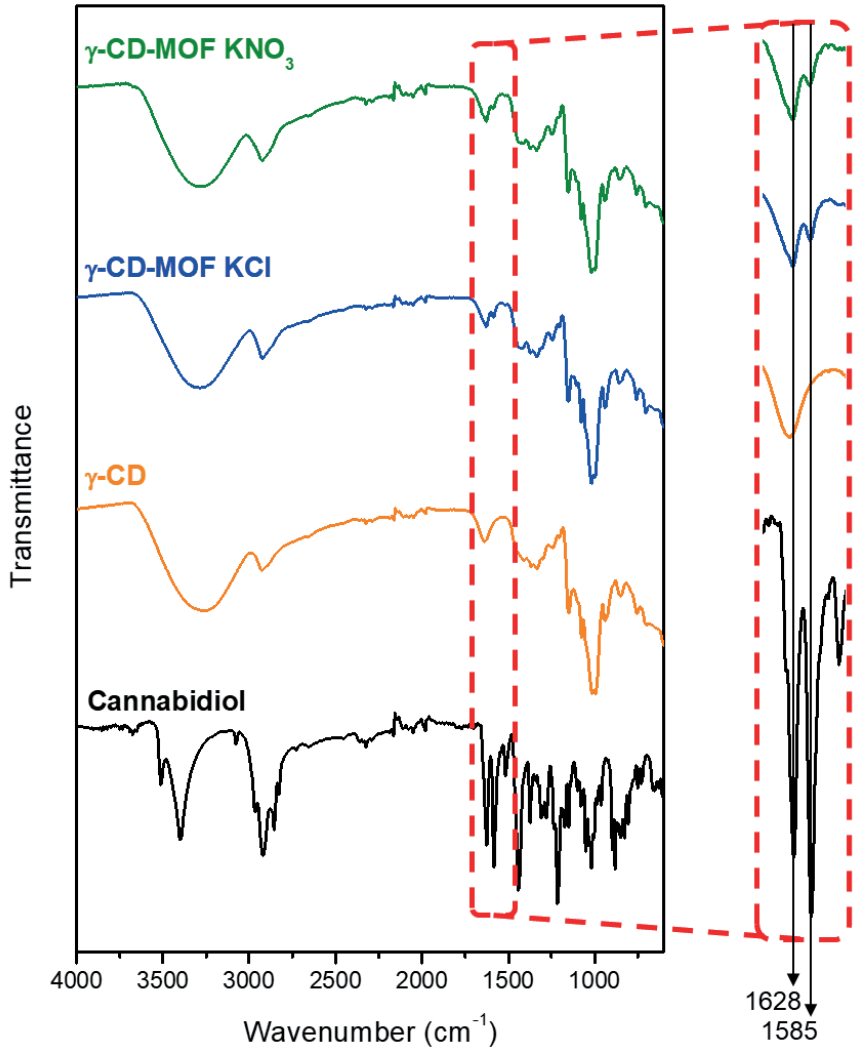

Figure 65: Attenuated Total Reflection-Fourier Transform Infrared Spectroscopy spectra of: cannabidiol (black), γ-CD (orange), cannabidiol loaded γ-CD-MOF KCl (blue) and γ-CD-MOF KNO_3 (green) from 4000 cm^{-1} to 600 cm^{-1}, and magnified comparison in the region of interest from 1700 cm^{-1} to 1500 cm^{-1} marking the double peak at 1585 and 1628 cm^{-1}.

5. CONCLUSIONS

The results obtained in the studies previously described lead to the following conclusions:

- The present work shows that MOFs based on γ-cyclodextrin and potassium ions, perform as an effective drug delivery system of olivetol. OLV was used as an analogue compound of cannabinoids for its encapsulation in these CD-MOFs by using either impregnation or co-crystallization methods. A microwave-assisted methodology was used to produce a fast preparation, using different potassium sources such as the conventional KOH, as well as alternative KCl and KNO_3 never used before. SEM and PXRD analysis revealed a trigonal morphology when the alternative potassium compounds were employed, against the typical cubic structures obtained with KOH. This fact may be due to the different pH of respective initial solutions.
- With respect to the olivetol loading, it was demonstrated olivetol to be loaded into MOFs as drug delivery systems when co-crystallization method was used, solving the problem of its poor encapsulation when the impregnation method was performed. FTIR analysis corroborated the success of this encapsulation. Therefore, the MOFs preparation method with alternative potassium sources and using the co-crystallization process resulted in γ-CD-MOFs with a strong potential as drug carriers for cannabinoids compounds, including CBD. Moreover, this method may become an alternative for drug delivery systems of unstable molecules in an alkaline or acid solution.
- DPPC liposomes were also synthetized as drug delivery system of olivetol as analogue of cannabidiol. This synthesis was performed following the thin-film hydration method and mechanical dispersion using the rotary evaporator and sonication respectively. DPPC liposomes in presence or absence of drug showed a similar morphology and size distribution below 200 nm, even though liposomes without drug was closer to a normal distribution than the formulations with OLV. It could be explained because olivetol is encapsulated in the liposome bilayer, thus increasing the rigidity of the vesicles. In any case, the synthesis method was found to be useful to produce stable DPPC liposomes independent of olivetol presence, making them suitable as drug delivery systems for the *in vitro* application.
- To assess the tooth surface layer penetration of the drug loaded into both delivery systems, an *in vitro* experimental study using bovine teeth, with synchrotron-source infrared spectroscopy observations and principal component analysis for data treatment was developed. Corresponding spectral data from enamel and dentin

regions revealed a similar behaviour by the analysis using PCA. PC1 grouped the samples according to the drug presence in both tissues due to a reduction in the intensity of all spectral bands. This fact is explained by the high organic matter content hindering the crystallinity of the carbonates and phosphates groups of HAP. Meanwhile, PC2 grouped the samples according to the depth in the enamel structure due to the typical mineral gradient of this tissue, this component grouped the samples according to the carrier presence in the dentin because the less crystallinity and more widder phosphate band v_3 PO_4^{3-}. Thus, the analysis of both regions was consistent between each other. Moreover, no differences were observed between OLV and CBD behaviour, thus validating the hypothesis of OLV application as CBD analogue in this *in vitro* experiment. Therefore, it was possible to trace the penetration of the drug in the tooth structure using these techniques and to know that the carriers helped in the delivery process making it more efficient, even though the olivetol loading in the MOFs' formulations was lower than in the liposomes.

- Considering these differences in terms of OLV encapsulation between both drug delivery systems, an experimental design was developed using a response surface methodology to optimize the synthesis and encapsulation techniques of γ-CD-MOFs KCl and KNO_3. The effect of four independent variables (olivetol concentration, methanol content, incubation time and incubation temperature) in the process was investigated. Two models per potassium salt were obtained for predicting reaction yield and drug encapsulation of the formulations. Reaction yield response followed a quadratic model while drug encapsulation response adjusted to a 2FI model for both salts. In all the cases, models showed a suitable fitting following statistical analysis. Reaction yield and drug encapsulation were maximized for each formulation. The models for predicting both responses showed a good agreement between the experimental and predicted values. In comparison with previous results obtained before this optimization, both reaction yields doubled the initials values, meanwhile drug encapsulation also increased in the optimized formulations (by 20% for KCl and 46% for KNO_3). In addition, these formulations were characterized showing that the new optimal conditions did not compromise the structure of the olivetol loaded γ-CD-MOFs. Thus, the application of experimental design capabilities has been successfully implemented. Moreover, drug release of these optimal formulations was also assessed. Both release behaviours were fast, showing a continuous release over

the first hour in PBS buffer, with more than 50% of the OLV released after this time. Then, the accumulative release of olivetol reached a maximum of 89% of drug after 19 hours when γ-CD-MOFs KCl was employed, and only the 65% of olivetol was quantified after 48 hours for γ-CD-MOFs KNO_3.

- After the optimization, OLV was substituted by cannabidiol using the optimal conditions in MOFs' formulations to validate its use as a CBD analogue in the experimental approach. Both γ-CD-MOFs formulations showed the same rectangular shape as elongated prisms and the EDX analysis confirmed the presence of potassium in these structures. Concerning the crystallinity, both formulations using CBD showed the same characteristics peaks that may correspond to a triclinic, tetragonal o trigonal space groups, so the structural properties were not compromised when olivetol was substituted by cannabidiol. Moreover, reaction yield values followed the predictions of the values from DoE when olivetol was used for the optimization of the formulations. The substitution of OLV by CBD did not alter the results in terms of drug encapsulation efficiency after the optimization with olivetol, validating the use of OLV as a CBD analogue.

Thus, new formulations based on cannabinoids loaded in γ-CD-MOFs and DPPC liposomes were developed using OLV as CBD analogue. The *in vitro* application of these formulations showed promising results, whereby these both drug delivery systems emerge as a new perspective to combat dentin hypersensitivity. Considering that OLV content in MOFs was lower than in liposomes, the methodology for MOFs' synthesis was optimized using DoE, and then the use of olivetol as a CBD analogue was also validated.

6. FUTURE PERSPECTIVES

Considering the results discussed in the presented thesis, further insights could be explored from the laboratory to the final market. Regarding basic research, more characterization techniques could be performed in order to obtain a complete description about these γ-CD-MOFs. These techniques may include nitrogen adsorption-desorption porosimetry analysis to gain information about the external and internal surface textural properties of the material, such as the specific surface area, pore volume or pore size distribution. For liposomes' formulations, a better drug quantification procedure could be developed using high-performance liquid chromatography techniques to assess if all the drug is encapsulated in the bilayer, as well as the validation using CBD to verify if OLV could be also used as an analogue in this drug delivery system.

Then, *in vitro* studies using cell cultures that mimic de soft tissues in the oral cavity could be carried out to assess the potential analgesic and anti-inflammatory effect of the formulations. Next step, it would be *in vivo* experiments using an animal model to verify the efficacy against this pain, and if these results are promising clinical trials in humans could be developed. Considering that the materials that comprise both formulations are biocompatible the approval of the different institutions and ethic committees for these *in vivo* studies could be obtained more easily.

Thinking in the formulation of a final product that includes these cannabidiol loaded γ-CD-MOFs, a liquid or gel formulation based on water would not be suitable since the degradation of the material under these conditions will be very fast, as it was already showed in the release study of this thesis. Therefore, a powder or a spray product seems to be more appropriate. However, due to the editability of these MOFs, a surface functionalization could be carried out to improve its stability in an aqueous environment, without compromising their properties nor the drug. In case of DPPC liposomes, a liquid formulation such as a mouthwash could work since liposomes are already synthetized in aqueous solution. Nevertheless, its stability and aggregation should be evaluated.

Finally, another important aspect is to verify whether scaling up the production of the formulation from the laboratory level to the industrial level is technically and economically possible. This is a key aspect for the final product to reach the market since many times laboratory experiments give very different results to the real application ones.

In any case, this research will lead to the development of important advances in drug delivery technologies and in the field of oral health.

7. BIBLIOGRAPHY

[1] J. Baranova, D. Büchner, W. Götz, M. Schulze, E. Tobiasch, Tooth Formation: Are the Hardest Tissues of Human Body Hard to Regenerate?, *Int. J. Mol. Sci*. 2020, Vol. 21, Page 4031. 21 (2020) 4031. https://doi.org/10.3390/IJMS21114031.

[2] M. McCollum, P.T. Sharpe, Evolution and development of teeth, *J. Anat*. 199 (2001) 153–159. https://doi.org/10.1017/S0021878201008123.

[3] M.A. Wahbi, H.S. Al Sharief, H. Tayeb, A. Bokhari, Minimally invasive use of coloured composite resin in aesthetic restoration of periodontially involved teeth: Case report, *Saudi Dent. J.* 25 (2013) 83–89. https://doi.org/10.1016/J.SDENTJ.2013.02.001.

[4] M. Lemmons, D. Beebe, Oral Anatomy and Physiology, *Wiggs's Vet. Dent. Princ. Pract.* (2018) 1–24. https://doi.org/10.1002/9781118816219.CH1.

[5] P. Lucas, P. Constantino, B. Wood, B. Lawn, Dental enamel as a dietary indicator in mammals, *BioEssays*. 30 (2008) 374–385. https://doi.org/10.1002/BIES.20729.

[6] B. Hashemi-Beni, M. Khoroushi, M.R. Foroughi, S. Karbasi, A.A. Khademi, Tissue engineering: Dentin – pulp complex regeneration approaches (A review), *Tissue Cell*. 49 (2017) 552–564. https://doi.org/10.1016/J.TICE.2017.07.002.

[7] B.L. Foster, Methods for studying tooth root cementum by light microscopy, *Int. J. Oral Sci.* 2012 43. 4 (2012) 119–128. https://doi.org/10.1038/ijos.2012.57.

[8] S.S. Legge, A.M. Hardin, The Pulp Cavity and Its Contents, *A Companion to Dent. Anthropol.* (2015) 189–203. https://doi.org/10.1002/9781118845486.CH14.

[9] M. Shahmoradi, L.E. Bertassoni, H.M. Elfallah, M. Swain, Fundamental Structure and Properties of Enamel, *Dentin and Cementum*, (2014) 511–547. https://doi.org/10.1007/978-3-642-53980-0_17.

[10] B. Co, Medical gallery of Blausen Medical 2014, *WikiJournal Med*. 1 (2014). https://doi.org/10.15347/WJM/2014.010.

[11] N. Mlakar, Z. Pavlica, M. Petelin, J. Štrancar, P. Zrimšek, A. Pavlič, Animal and human dentin microstructure and elemental composition, *Cent. Eur. J. Med*. 2014 93. 9 (2014) 468–476. https://doi.org/10.2478/S11536-013-0295-X.

[12] C. Xu, X. Yao, M.P. Walker, Y. Wang, Chemical/molecular structure of the dentin-enamel junction is dependent on the intratooth location, *Calcif. Tissue Int*. 84 (2009) 221–228. https://doi.org/10.1007/S00223-008-9212-8/FIGURES/6.

[13] H.E. Schroeder, M.A. Listgarten, The junctional epithelium: From strength to defense, *J. Dent. Res*. 82 (2003) 158–161. https://doi.org/10.1177/154405910308200302.

[14] M. Hannig, The Importance of the Salivary Pellicle, *Oral Biofilms Mod. Dent. Mater*. (2021) 9–17. https://doi.org/10.1007/978-3-030-67388-8_2.

[15] C. Hannig, M. Hannig, The oral cavity—a key system to understand substratum-dependent bioadhesion on solid surfaces in man, *Clin. Oral Investig*. 2009 132. 13 (2009) 123–139. https://doi.org/10.1007/S00784-008-0243-3.

[16] D.D. Chawhuaveang, O.Y. Yu, I.X. Yin, W.Y.H. Lam, M.L. Mei, C.H. Chu, Acquired salivary pellicle and oral diseases: A literature review, *J. Dent. Sci*. 16 (2021) 523–

529. https://doi.org/10.1016/J.JDS.2020.10.007.

[17] W.L. Siqueira, W. Custodio, E.E. McDonald, New insights into the composition and functions of the acquired enamel pellicle, *J. Dent. Res*. 91 (2012) 1110–1118. https://doi.org/10.1177/0022034512462578.

[18] R.S. Lacruz, S. Habelitz, J.T. Wright, M.L. Paine, Dental enamel formation and implications for oral health and disease, *Physiol. Rev*. 97 (2017) 939–993. https://doi.org/10.1152/PHYSREV.00030.2016/ASSET/IMAGES/LARGE/Z9J003172 8020018.JPEG.

[19] E. Beniash, C.A. Stifler, C.Y. Sun, G.S. Jung, Z. Qin, M.J. Buehler, P.U.P.A. Gilbert, The hidden structure of human enamel, *Nat. Commun*. 2019 101. 10 (2019) 1–13. https://doi.org/10.1038/s41467-019-12185-7.

[20] H. Zhou, J. Lee, Nanoscale hydroxyapatite particles for bone tissue engineering, *Acta Biomater*. 7 (2011) 2769–2781. https://doi.org/10.1016/J.ACTBIO.2011.03.019.

[21] C. de C.A. Lopes, P.H.J.O. Limirio, V.R. Novais, P. Dechichi, Fourier transform infrared spectroscopy (FTIR) application chemical characterization of enamel, dentin and bone, *Appl. Spectrosc. Rev*. 53 (2018) 747–769. https://doi.org/10.1080/05704928.2018.1431923.

[22] C. Xu, R. Reed, J.P. Gorski, Y. Wang, M.P. Walker, The Distribution of Carbonate in Enamel and its Correlation with Structure and Mechanical Properties, *J. Mater. Sci*. 47 (2012) 8035–8043. https://doi.org/10.1007/S10853-012-6693-7.

[23] E. Garskaite, K.A. Gross, S.W. Yang, T.C.K. Yang, J.C. Yang, A. Kareiva, Effect of processing conditions on the crystallinity and structure of carbonated calcium hydroxyapatite (CHAp), *CrystEngComm*. 16 (2014) 3950–3959. https://doi.org/10.1039/c4ce00119b.

[24] S. Kannan, A. Rebelo, J.M.F. Ferreira, Novel synthesis and structural characterization of fluorine and chlorine co-substituted hydroxyapatites, *J. Inorg. Biochem*. 100 (2006) 1692–1697. https://doi.org/10.1016/J.JINORGBIO.2006.06.005.

[25] H. Pan, J. Tao, X. Yu, L. Fu, J. Zhang, X. Zeng, G. Xu, R. Tang, Anisotropic demineralization and oriented assembly of hydroxyapatite crystals in enamel: Smart structures of biominerals, *J. Phys. Chem. B*. 112 (2008) 7162–7165. https://doi.org/10.1021/JP802739F/SUPPL_FILE/JP802739F-FILE002.PDF.

[26] S. Elsharkawy, A. Mata, Hierarchical Biomineralization: from Nature's Designs to Synthetic Materials for Regenerative Medicine and Dentistry, *Adv. Healthc. Mater*. 7 (2018) 1800178. https://doi.org/10.1002/ADHM.201800178.

[27] K.J. Chun, H.H. Choi, J.Y. Lee, Comparison of mechanical property and role between enamel and dentin in the human teeth, *J. Dent. Biomech*. 5 (2014) 1–7. https://doi.org/10.1177/1758736014520809.

[28] M. Haapasalo, W. Qian, I. Portenier, T. Waltimo, Effects of Dentin on the Antimicrobial Properties of Endodontic Medicaments, *J. Endod*. 33 (2007) 917–925. https://doi.org/10.1016/J.JOEN.2007.04.008.

[29] M. Goldberg, A.B. Kulkarni, M. Young, A. Boskey, Dentin: Structure, Composition and Mineralization: The role of dentin ECM in dentin formation and mineralization, *Front. Biosci. (Elite Ed)*. 3 (2011) 711. https://doi.org/10.2741/e281.

[30] S. Opsahl Vital, C. Gaucher, C. Bardet, P.S. Rowe, A. George, A. Linglart, C. Chaussain, Tooth dentin defects reflect genetic disorders affecting bone mineralization, *Bone*. 50 (2012) 989–997. https://doi.org/10.1016/J.BONE.2012.01.010.

[31] A.J. Ortiz-Ruiz, J. de D. Teruel-Fernández, L.A. Alcolea-Rubio, A. Hernández-Fernández, Y. Martínez-Beneyto, F. Gispert-Guirado, Structural differences in enamel and dentin in human, bovine, porcine, and ovine teeth, *Ann. Anat. - Anat. Anzeiger*. 218 (2018) 7–17. https://doi.org/10.1016/J.AANAT.2017.12.012.

[32] A.A. Kunin, A.Y. Evdokimova, N.S. Moiseeva, Age-related differences of tooth enamel morphochemistry in health and dental caries, *EPMA J*. 6 (2015) 1–11. https://doi.org/10.1186/S13167-014-0025-8/TABLES/4.

[33] A.F. Reis, M. Giannini, A. Kavaguchi, / Carlos, J. Soares, S.R.P. Line, Comparison of Microtensile Bond Strength to Enamel and Dentin of Human, Bovine, and Porcine Teeth, *J Adhes Dent*. 6 (2004) 117–121.

[34] G.H. Yassen, J.A. Platt, A.T. Hara, Bovine teeth as substitute for human teeth in dental research: a review of literature, *J. Oral Sci*. 53 (2011) 273–282. https://doi.org/10.2334/JOSNUSD.53.273.

[35] F. Wegehaupt, D. Gries, A. Wiegand, T. Attin, Is bovine dentine an appropriate substitute for human dentine in erosion/abrasion tests?, *J. Oral Rehabil.* 35 (2008) 390–394. https://doi.org/10.1111/J.1365-2842.2007.01843.X.

[36] C.H.R. Camargo, M. Siviero, S.E.A. Camargo, S.H.G. de Oliveira, C.A.T. Carvalho, M.C. Valera, Topographical, Diametral, and Quantitative Analysis of Dentin Tubules in the Root Canals of Human and Bovine Teeth, *J. Endod.* 33 (2007) 422–426. https://doi.org/10.1016/J.JOEN.2006.12.011.

[37] S.R. Kwon, S.R. Kurti, U. Oyoyo, Y. Li, Effect of various tooth whitening modalities on microhardness, surface roughness and surface morphology of the enamel, *Odontology*. 103 (2015) 274–279. https://doi.org/10.1007/S10266-014-0163-4/FIGURES/6.

[38] S. Suzuki, T. Takamizawa, A. Imai, A. Tsujimoto, K. Sai, M. Takimoto, W.W. Barkmeier, M.A. Latta, M. Miyazaki, Bond durability of universal adhesive to bovine enamel using self-etch mode, *Clin. Oral Investig*. 22 (2018) 1113–1122. https://doi.org/10.1007/S00784-017-2196-X/FIGURES/5.

[39] F.Z.M. Soares, A. Follak, L.S. da Rosa, A.F. Montagner, T.L. Lenzi, R.O. Rocha, Bovine tooth is a substitute for human tooth on bond strength studies: A systematic review and meta-analysis of *in vitro* studies, *Dent. Mater.* 32 (2016) 1385–1393. https://doi.org/10.1016/J.DENTAL.2016.09.019.

[40] C. Babot-Marquillas, M.J. Sánchez-Martín, J. Rodríguez-Martínez, J. Estelrich, M.A. Busquets, M. Valiente, Flash tooth whitening: A friendly formulation based on a nanoencapsulated reductant, *Colloids Surfaces B Biointerfaces*. 195 (2020) 111241. https://doi.org/10.1016/j.colsurfb.2020.111241.

[41] C. Wang, Y. Li, X. Wang, L. Zhang, Tiantang, B. Fu, The Enamel Microstructures of Bovine Mandibular Incisors, *Anat. Rec. Adv. Integr. Anat. Evol. Biol.* 295 (2012) 1698–1706. https://doi.org/10.1002/AR.22543.

[42] M. Goldberg, M. Grootveld, E. Lynch, Undesirable and adverse effects of tooth-whitening products: A review, *Clin. Oral Investig.* 14 (2010) 1–10. https://doi.org/10.1007/s00784-009-0302-4.

[43] J. won Kim, J.C. Park, Dentin hypersensitivity and emerging concepts for treatments, *J. Oral Biosci.* 59 (2017) 211–217. https://doi.org/10.1016/J.JOB.2017.09.001.

[44] P.I. Idon, O.A. Sotunde, T.O. Ogundare, Beyond the Relief of Pain: Dentin Hypersensitivity and Oral Health-Related Quality of Life, *Front. Dent*. 16 (2019) 325. https://doi.org/10.18502/FID.V16I5.2272.

[45] K. Yadav, A. Sofat, R. Gambhir, V. Galhotra, Dentin hypersensitivity following tooth preparation: A clinical study in the spectrum of gender, *J. Nat. Sci. Biol. Med.* 5 (2014) 21. https://doi.org/10.4103/0976-9668.127277.

[46] O. Braimoh, N. Ilochonwu, Dentin hypersensitivity among undergraduates in a university community, *Saudi J. Oral Sci.* 1 (2014) 90. https://doi.org/10.4103/1658-6816.138473.

[47] C.H. Splieth, A. Tachou, Epidemiology of dentin hypersensitivity, *Clin. Oral Investig*. 17 (2013) 3. https://doi.org/10.1007/S00784-012-0889-8.

[48] I.C.C.M. Porto, A.K.M. Andrade, M.A.J.R. Montes, Diagnosis and treatment of dentinal hypersensitivity, *J. Oral Sci*. 51 (2009) 323–332. https://doi.org/10.2334/JOSNUSD.51.323.

[49] A. Davari, E. Ataei, H. Assarzadeh, Dentin Hypersensitivity: Etiology, Diagnosis and Treatment; A Literature Review, *J. Dent.* 14 (2013) 136. /pmc/articles/PMC3927677/ (accessed December 31, 2021).

[50] P. Dowell, M. Addy, Dentine hypersensitivity--a review. Aetiology, symptoms and theories of pain production., *J. Clin. Periodontol*. 10 (1983) 341–50. http://www.ncbi.nlm.nih.gov/pubmed/6309917 (accessed November 13, 2018).

[51] J. Rodríguez-Martínez, M. Valiente, M.J. Sánchez-Martín, Tooth whitening: From the established treatments to novel approaches to prevent side effects, *J. Esthet. Restor. Dent.* 31 (2019) 431–440. https://doi.org/10.1111/jerd.12519.

[52] M. Lin, G.M. Genin, F. Xu, T.J. Lu, Thermal Pain in Teeth: Electrophysiology Governed by Thermomechanics, *Appl. Mech. Rev.* 66 (2014) 0308011. https://doi.org/10.1115/1.4026912.

[53] A. Scherman, P.L. Jacobsen, Managing dentin hypersensitivity: what treatment to recommend to patients., *J. Am. Dent. Assoc*. 123 (1992) 57–61. https://doi.org/10.14219/JADA.ARCHIVE.1992.0107.

[54] M.Z. Hossain, M.M. Bakri, F. Yahya, H. Ando, S. Unno, J. Kitagawa, The Role of Transient Receptor Potential (TRP) Channels in the Transduction of Dental Pain, *Int. J. Mol. Sci.* 2019, Vol. 20, Page 526. 20 (2019) 526. https://doi.org/10.3390/IJMS20030526.

[55] S. Poulsen, M. Errboe, O. Hovgaard, H.W. Worthington, Potassium nitrate toothpaste for dentine hypersensitivity., *Cochrane Database Syst. Rev*. (2001) CD001476. https://doi.org/10.1002/14651858.CD001476.

[56] V. Camilotti, J. Zilly, P. do Monte Ribeiro Busato, C.A. Nassar, P.O. Nassar, Desensitizing treatments for dentin hypersensitivity: a randomized, split-mouth clinical trial, *Braz. Oral Res*. 26 (2012) 263–268. https://doi.org/10.1590/S1806-83242012000300013.

[57] P.M. Bartold, Dentinal hypersensitivity: A review, *Aust. Dent. J*. 51 (2006) 212–218. https://doi.org/10.1111/j.1834-7819.2006.tb00431.x.

[58] C.M. Marto, A. Baptista Paula, T. Nunes, M. Pimenta, A.M. Abrantes, A.S. Pires, M. Laranjo, A. Coelho, H. Donato, M.F. Botelho, M. Marques Ferreira, E. Carrilho, Evaluation of the efficacy of dentin hypersensitivity treatments—A systematic review and follow-up analysis, *J. Oral Rehabil*. 46 (2019) 952–990. https://doi.org/10.1111/joor.12842.

[59] W.-H. Lan, H.-C. Liu, C.-P. Lin, The combined occluding effect of sodium fluoride varnish and Nd:YAG laser irradiation on human dentinal tubules, *J. Endod*. 25 (1999) 424–426. https://doi.org/10.1016/S0099-2399(99)80271-4.

[60] L. Fiorillo, L. Laino, R. De Stefano, C. D'amico, S. Bocchieri, G. Amoroso, G. Isola, G. Cervino, Dental Whitening Gels: Strengths and Weaknesses of an Increasingly Used Method, *Gels* 2019, Vol. 5, Page 35. 5 (2019) 35. https://doi.org/10.3390/GELS5030035.

[61] P. Charakorn, L.L. Cabanilla, W.C. Wagner, W.-C. Foong, J. Shaheen, R. Pregitzer, D. Schneider, The Effect of Preoperative Ibuprofen on Tooth Sensitivity Caused by In-office Bleaching, *Oper. Dent*. 34 (2009) 131–135. https://doi.org/10.2341/08-33.

[62] E. Paula, S. Kossatz, D. Fernandes, A. Loguercio, A. Reis, The Effect of Perioperative Ibuprofen Use on Tooth Sensitivity Caused by In-Office Bleaching, *Oper. Dent.* 38 (2013) 601–608. https://doi.org/10.2341/12-107-C.

[63] S.C. Vaez, A.L. Faria-e-Silva, A.D. Loguércio, M.T.G. Fernandes, F.P.S. Nahsan, S.C. Vaez, A.L. Faria-e-Silva, A.D. Loguércio, M.T.G. Fernandes, F.P.S. Nahsan, Preemptive use of etodolac on tooth sensitivity after in-office bleaching: a randomized clinical trial, *J. Appl. Oral Sci.* 26 (2018). https://doi.org/10.1590/1678-7757-2016-0473.

[64] M. Rezende, K. Chemin, S.C. Vaez, A.C. Peixoto, J. de F. Rabelo, S.S.L. Braga, A.L. Faria-e-Silva, G.R. da Silva, C.J. Soares, A.D. Loguercio, A. Reis, Effect of topical application of dipyrone on dental sensitivity reduction after in-office dental bleaching: A randomized, triple-blind multicenter clinical trial, *J. Am. Dent. Assoc*. (2018). https://doi.org/10.1016/J.ADAJ.2017.11.003.

[65] C. Goicoechea García, M.I. Martín Fontelles, Sistemas cannabinoide y opioide en los mecanismos y el control del dolor, Reumatol. *Clínica*. 5 (2009) 5–8. https://doi.org/10.1016/J.REUMA.2009.04.006.

[66] F. Coppla, M. Rezende, E. de Paula, P. Farago, A. Loguercio, S. Kossatz, A. Reis, Combination of Acetaminophen/Codeine Analgesics Does Not Avoid Bleaching-Induced Tooth Sensitivity: A Randomized, Triple-Blind Two-Center Clinical Trial,

Oper. Dent. 43 (2018) E53–E63. https://doi.org/10.2341/17-092-C.

[67] K. Hargreaves, P. Abbott, Drugs for pain management in dentistry, S14 Aust. Dent. J. Medicat. Suppl. 50 (2005). http://patologiabucal.com/index_htm_files/manejo del dolor.pdf (accessed April 23, 2018).

[68] M. Rezende, E. Bonafé, L. Vochikovski, P.V. Farago, A.D. Loguercio, A. Reis, S. Kossatz, Pre- and postoperative dexamethasone does not reduce bleaching-induced tooth sensitivity: A randomized, triple-masked clinical trial, *J. Am. Dent. Assoc*. 147 (2016) 41–49. https://doi.org/10.1016/J.ADAJ.2015.07.003.

[69] F. Carrouel, S. Viennot, L. Ottolenghi, C. Gaillard, D. Bourgeois, Nanoparticles as Anti-Microbial, Anti-Inflammatory, and Remineralizing Agents in Oral Care Cosmetics: A Review of the Current Situation, *Nanomater*. 2020, Vol. 10, Page 140. 10 (2020) 140. https://doi.org/10.3390/NANO10010140.

[70] P.J. Robson, Therapeutic potential of cannabinoid medicines, *Drug Test. Anal*. 6 (2014) 24–30. https://doi.org/10.1002/dta.1529.

[71] M. Ben Amar, Cannabinoids in medicine: A review of their therapeutic potential, *J. Ethnopharmacol.* 105 (2006) 1–25. https://doi.org/10.1016/J.JEP.2006.02.001.

[72] B. Hurgobin, M. Tamiru-Oli, M.T. Welling, M.S. Doblin, A. Bacic, J. Whelan, M.G. Lewsey, Recent advances in *Cannabis sativa* genomics research, *New Phytol.* 230 (2021) 73–89. https://doi.org/10.1111/NPH.17140.

[73] S. Chandra, H. Lata, M.A. ElSohly, Propagation of Cannabis for Clinical Research: An Approach Towards a Modern Herbal Medicinal Products Development, *Front. Plant Sci.* 11 (2020) 958. https://doi.org/10.3389/FPLS.2020.00958/BIBTEX.

[74] G. Appendino, G. Chianese, O. Taglialatela-Scafati, Cannabinoids: Occurrence and Medicinal Chemistry, *Curr. Med. Chem*. 18 (2011) 1085–1099. https://doi.org/10.2174/092986711794940888.

[75] G. Lafaye, L. Karila, L. Blecha, A. Benyamina, Cannabis, cannabinoids, and health, *Dialogues Clin. Neurosci*. 19 (2017) 309. https://doi.org/10.31887/DCNS.2017.19.3/GLAFAYE.

[76] K. Hayakawa, K. Mishima, M. Fujiwara, Therapeutic Potential of Non-Psychotropic Cannabidiol in Ischemic Stroke, *Pharm.* 2010, Vol. 3, Pages 2197-2212. 3 (2010) 2197–2212. https://doi.org/10.3390/PH3072197.

[77] H.C. Lu, K. Mackie, Review of the Endocannabinoid System, *Biol. Psychiatry Cogn. Neurosci. Neuroimaging.* 6 (2021) 607–615. https://doi.org/10.1016/J.BPSC.2020.07.016.

[78] H. Lowe, N. Toyang, B. Steele, J. Bryant, W. Ngwa, The Endocannabinoid System: A Potential Target for the Treatment of Various Diseases, *Int. J. Mol. Sci.* 2021, Vol. 22, Page 9472. 22 (2021) 9472. https://doi.org/10.3390/IJMS22179472.

[79] L. Bellocchio, C. Cervino, R. Pasquali, U. Pagotto, The Endocannabinoid System and Energy Metabolism, *J. Neuroendocrinol.* 20 (2008) 850–857. https://doi.org/10.1111/J.1365-2826.2008.01728.X.

[80] F. Borrelli, G. Aviello, B. Romano, P. Orlando, R. Capasso, F. Maiello, F. Guadagno, S. Petrosino, F. Capasso, V. Di Marzo, A.A. Izzo, Cannabidiol, a safe and non-

psychotropic ingredient of the marijuana plant *Cannabis sativa*, is protective in a murine model of colitis, *J. Mol. Med*. 87 (2009) 1111–1121. https://doi.org/10.1007/S00109-009-0512-X/FIGURES/7.

[81] S. Burstein, Cannabidiol (CBD) and its analogs: a review of their effects on inflammation, *Bioorg. Med. Chem*. 23 (2015) 1377–1385. https://doi.org/10.1016/J.BMC.2015.01.059.

[82] S. Atalay, I. Jarocka-karpowicz, E. Skrzydlewskas, Antioxidative and anti-inflammatory properties of cannabidiol, *Antioxidants*. 9 (2020) 1–20. https://doi.org/10.3390/antiox9010021.

[83] S. Pisanti, A.M. Malfitano, E. Ciaglia, A. Lamberti, R. Ranieri, G. Cuomo, M. Abate, G. Faggiana, M.C. Proto, D. Fiore, C. Laezza, M. Bifulco, Cannabidiol: State of the art and new challenges for therapeutic applications, *Pharmacol. Ther*. 175 (2017) 133–150. https://doi.org/10.1016/J.PHARMTHERA.2017.02.041.

[84] A.I. Fraguas-Sánchez, A.I. Torres-Suárez, Medical Use of Cannabinoids, *Drugs* 2018 7816. 78 (2018) 1665–1703. https://doi.org/10.1007/S40265-018-0996-1.

[85] R.G. Pertwee, Cannabidiol as a potential medicine, *Cannabinoids as Ther*. (2005) 47–65. https://doi.org/10.1007/3-7643-7358-X_3.

[86] N. Noreen, F. Muhammad, B. Akhtar, F. Azam, M.I. Anwar, Is cannabidiol a promising substance for new drug development? A review of its potential therapeutic applications, *Crit. Rev. Eukaryot. Gene Expr*. 28 (2018) 73–86. https://doi.org/10.1615/CritRevEukaryotGeneExpr.2018021528.

[87] C. Muller, P. Morales, P.H. Reggio, Cannabinoid ligands targeting TRP channels, *Front. Mol. Neurosci*. 11 (2019) 487. https://doi.org/10.3389/FNMOL.2018.00487/BIBTEX.

[88] N. Koch, O. Jennotte, Y. Gasparrini, F. Vandenbroucke, A. Lechanteur, B. Evrard, Cannabidiol aqueous solubility enhancement: Comparison of three amorphous formulations strategies using different type of polymers, *Int. J. Pharm*. 589 (2020) 119812. https://doi.org/10.1016/J.IJPHARM.2020.119812.

[89] M.P. Di Bello, E. Bloise, S.E. Mazzetto, G. Mele, Formulation and Chemical Stability in Aqueous Media of Cannabidiol Embedded in Cardanol-Based Nanovesicles, *ACS Sustain. Chem. Eng.* 5 (2017) 8870–8875. https://doi.org/10.1021/ACSSUSCHEMENG.7B01658.

[90] S.A. Millar, R.F. Maguire, A.S. Yates, S.E. O'Sullivan, Towards Better Delivery of Cannabidiol (CBD), *Pharm.* 2020, Vol. 13, Page 219. 13 (2020) 219. https://doi.org/10.3390/PH13090219.

[91] L.F. Cuba, F.G. Salum, K. Cherubini, M.A.Z. Figueiredo, Cannabidiol: an alternative therapeutic agent for oral mucositis?, *J. Clin. Pharm. Ther*. 42 (2017) 245–250. https://doi.org/10.1111/jcpt.12504.

[92] M.H. Napimoga, B.B. Benatti, F.O. Lima, P.M. Alves, A.C. Campos, D.R. Pena-dos-Santos, F.P. Severino, F.Q. Cunha, F.S. Guimarães, Cannabidiol decreases bone resorption by inhibiting RANK/RANKL expression and pro-inflammatory cytokines during experimental periodontitis in rats, *Int. Immunopharmacol.* 9 (2009) 216–

222. https://doi.org/10.1016/J.INTIMP.2008.11.010.

[93] S. Naheed, Medication dispensing system, US 2017/0021025A1, 2015. https://patents.google.com/patent/US20170021025A1/en (accessed February 3, 2022).

[94] G. Anastassov, L. Changoer, Oral care composition comprising cannabinoids, US 2016/0166498A1, 2015. https://patents.google.com/patent/US20160166498A1/en (accessed April 17, 2022).

[95] D.S. Nam, E. Kwon, Sedative laced toothpaste, US 2020/0206126 A1, 2019. https://patents.google.com/patent/US11026881B2/en (accessed February 3, 2022).

[96] H. Lowe, N. Toyang, B. Steele, J. Bryant, W. Ngwa, K. Nedamat, The Current and Potential Application of Medicinal Cannabis Products in Dentistry, *Dent. J.* 2021, Vol. 9, Page 106. 9 (2021) 106. https://doi.org/10.3390/DJ9090106.

[97] N.J. Himmel, D.N. Cox, Transient receptor potential channels: current perspectives on evolution, structure, function and nomenclature, *Proc. R. Soc. B.* 287 (2020). https://doi.org/10.1098/RSPB.2020.1309.

[98] B. Nilius, G. Appendino, G. Owsianik, The transient receptor potential channel TRPA1: from gene to pathophysiology, *Pflügers Arch. - Eur. J. Physiol*. 464 (2012) 425–458. https://doi.org/10.1007/s00424-012-1158-z.

[99] J.D. Levine, N. Alessandri-Haber, TRP channels: Targets for the relief of pain, *Biochim. Biophys. Acta - Mol. Basis Dis*. 1772 (2007) 989–1003. https://doi.org/10.1016/J.BBADIS.2007.01.008.

[100] A.R. Son, Y.M. Yang, J.H. Hong, S.I. Lee, Y. Shibukawa, D.M. Shin, Odontoblast TRP channels and thermo/mechanical transmission, *J. Dent. Res*. 88 (2009) 1014–1019. https://doi.org/10.1177/0022034509343413.

[101] I. Weyer-Menkhoff, J. Lötsch, Human pharmacological approaches to TRP-ion-channel-based analgesic drug development, *Drug Discov. Today*. 23 (2018) 2003–2012. https://doi.org/10.1016/J.DRUDIS.2018.06.020.

[102] K. Lee, B.M. Lee, C.K. Park, Y.H. Kim, G. Chung, Ion Channels Involved in Tooth Pain, *Int. J. Mol. Sci.* 2019, Vol. 20, Page 2266. 20 (2019) 2266. https://doi.org/10.3390/IJMS20092266.

[103] J. Elikkottil, J. Elikottil, P. Gupta, K. Gupta, The analgesic potential of cannabinoids., *J. Opioid Manag*. 5 (2009) 341–57. http://www.ncbi.nlm.nih.gov/pubmed/20073408.

[104] P. Taslimi, İ. Gulçin, Antioxidant and anticholinergic properties of olivetol, *J. Food Biochem.* 42 (2018). https://doi.org/10.1111/jfbc.12516.

[105] F. Taura, S. Tanaka, C. Taguchi, T. Fukamizu, H. Tanaka, Y. Shoyama, S. Morimoto, Characterization of olivetol synthase, a polyketide synthase putatively involved in cannabinoid biosynthetic pathway, *FEBS Lett*. 583 (2009) 2061–2066. https://doi.org/10.1016/J.FEBSLET.2009.05.024.

[106] T.J. Raharjo, W. Te Chang, Y.H. Choi, A.M.G. Peltenburg-Looman, R. Verpoorte,

Olivetol as product of a polyketide synthase in *Cannabis sativa* L, *Plant Sci*. 166 (2004) 381–385. https://doi.org/10.1016/J.PLANTSCI.2003.09.027.

[107] M.P. Abuçafy, B.L. Caetano, B.G. Chiari-Andréo, B. Fonseca-Santos, A.M. do Santos, M. Chorilli, L.A. Chiavacci, Supramolecular cyclodextrin-based metal-organic frameworks as efficient carrier for anti-inflammatory drugs, *Eur. J. Pharm. Biopharm.* (2018). https://doi.org/10.1016/j.ejpb.2018.02.009.

[108] B. Kumar, K. Jalodia, P. Kumar, H.K. Gautam, Recent advances in nanoparticle-mediated drug delivery, *J. Drug Deliv. Sci. Technol.* 41 (2017) 260–268. https://doi.org/10.1016/j.jddst.2017.07.019.

[109] J. Safari, Z. Zarnegar, Advanced drug delivery systems: Nanotechnology of health design A review, *J. Saudi Chem. Soc.* 18 (2014) 85–99. https://doi.org/10.1016/J.JSCS.2012.12.009.

[110] K. Park, Controlled drug delivery systems: past forward and future back, *J. Control. Release*. 190 (2014) 3–8. https://doi.org/10.1016/J.JCONREL.2014.03.054.

[111] Y. Zhang, T. Sun, C. Jiang, Biomacromolecules as carriers in drug delivery and tissue engineering, *Acta Pharm. Sin. B.* 8 (2018) 34–50. https://doi.org/10.1016/J.APSB.2017.11.005.

[112] A.Z. Wilczewska, K. Niemirowicz, K.H. Markiewicz, H. Car, Nanoparticles as drug delivery systems, *Pharmacol. Reports.* 64 (2012) 1020–1037. https://doi.org/10.1016/S1734-1140(12)70901-5.

[113] J.K. Patra, G. Das, L.F. Fraceto, E.V.R. Campos, M.D.P. Rodriguez-Torres, L.S. Acosta-Torres, L.A. Diaz-Torres, R. Grillo, M.K. Swamy, S. Sharma, S. Habtemariam, H.S. Shin, Nano based drug delivery systems: recent developments and future prospects, *J. Nanobiotechnology* 2018 161. 16 (2018) 1–33. https://doi.org/10.1186/S12951-018-0392-8.

[114] A.C. Anselmo, S. Mitragotri, An overview of clinical and commercial impact of drug delivery systems, *J. Control. Release*. 190 (2014) 15–28. https://doi.org/10.1016/J.JCONREL.2014.03.053.

[115] C. Zylberberg, S. Matosevic, Pharmaceutical liposomal drug delivery: a review of new delivery systems and a look at the regulatory landscape, *Drug Deliv.* 23 (2016) 3319–3329. https://doi.org/10.1080/10717544.2016.1177136.

[116] N.D. James, R.J. Coker, D. Tomlinson, J.R.W. Harris, M. Gompels, A.J. Pinching, J.S.W. Stewart, Liposomal doxorubicin (Doxil): An effective new treatment for Kaposi's sarcoma in AIDS, *Clin. Oncol.* 6 (1994) 294–296. https://doi.org/10.1016/S0936-6555(05)80269-9.

[117] D. Sharma, A.A.E. Ali, L.R. Trivedi, An Updated Review on: Liposomes as drug delivery system, *PharmaTutor.* 6 (2018) 50–62. https://doi.org/10.29161/PT.V6.I2.2018.50.

[118] H.J. Hsu, J. Bugno, S.R. Lee, S. Hong, Dendrimer-based nanocarriers: a versatile platform for drug delivery, *Wiley Interdiscip. Rev. Nanomedicine Nanobiotechnology.* 9 (2017) e1409. https://doi.org/10.1002/WNAN.1409.

[119] S. Hossen, M.K. Hossain, M.K. Basher, M.N.H. Mia, M.T. Rahman, M.J. Uddin, Smart

nanocarrier-based drug delivery systems for cancer therapy and toxicity studies: A review, *J. Adv. Res*. 15 (2019) 1–18. https://doi.org/10.1016/J.JARE.2018.06.005.

[120] D.B. Warheit, B.R. Laurence, K.L. Reed, D.H. Roach, G.A.M. Reynolds, T.R. Webb, Comparative Pulmonary Toxicity Assessment of Single-wall Carbon Nanotubes in Rats, *Toxicol. Sci.* 77 (2004) 117–125. https://doi.org/10.1093/TOXSCI/KFG228.

[121] S.T. Yang, J. Luo, Q. Zhou, H. Wang, Pharmacokinetics, Metabolism and Toxicity of Carbon Nanotubes for Biomedical Purposes, *Theranostics*. 2 (2012) 271. https://doi.org/10.7150/THNO.3618.

[122] S. Jain, V. Jain, S.C. Mahajan, Lipid Based Vesicular Drug Delivery Systems, *Adv. Pharm.* 2014 (2014). https://doi.org/10.1155/2014/574673.

[123] Z. Wang, X. Deng, J. Ding, W. Zhou, X. Zheng, G. Tang, Mechanisms of drug release in pH-sensitive micelles for tumour targeted drug delivery system: A review, *Int. J. Pharm.* 535 (2018) 253–260. https://doi.org/10.1016/J.IJPHARM.2017.11.003.

[124] H. Dhyani, M.A. Ali, S.P. Pal, S. Srivastava, P.R. Solanki, B.D. Malhotra, P. Sen, Mediator-free biosensor using chitosan capped CdS quantum dots for detection of total cholesterol, *RSC Adv*. 5 (2015) 45928–45934. https://doi.org/10.1039/C5RA07012K.

[125] R. Liu, T. Yu, Z. Shi, Z. Wang, The preparation of metal-organic frameworks and their biomedical application, *Int. J. Nanomedicine*. 11 (2016) 1187–1200. https://doi.org/10.2147/IJN.S100877.

[126] Y. Han, W. Liu, J. Huang, S. Qiu, H. Zhong, D. Liu, J. Liu, Cyclodextrin-Based Metal-Organic Frameworks (CD-MOFs) in Pharmaceutics and Biomedicine, *Pharmaceutics.* (2018). https://doi.org/10.3390/pharmaceutics10040271.

[127] B. Liu, Y. He, L. Han, V. Singh, X. Xu, T. Guo, F. Meng, X. Xu, P. York, Z. Liu, J. Zhang, Microwave-Assisted Rapid Synthesis of γ-Cyclodextrin Metal-Organic Frameworks for Size Control and Efficient Drug Loading, *Cryst. Growth Des*. 17 (2017) 1654–1660. https://doi.org/10.1021/acs.cgd.6b01658.

[128] L. Chen, X. Zhang, X. Cheng, Z. Xie, Q. Kuang, L. Zheng, The function of metal–organic frameworks in the application of MOF-based composites, *Nanoscale Adv. 2* (2020) 2628–2647. https://doi.org/10.1039/D0NA00184H.

[129] Y.R. Lee, J. Kim, W.S. Ahn, Synthesis of metal-organic frameworks: A mini review, *Korean J. Chem. Eng*. 2013 309. 30 (2013) 1667–1680. https://doi.org/10.1007/S11814-013-0140-6.

[130] S. He, L. Wu, X. Li, H. Sun, T. Xiong, J. Liu, C. Huang, H. Xu, H. Sun, W. Chen, R. Gref, J. Zhang, Metal-organic frameworks for advanced drug delivery, *Acta Pharm. Sin. B.* (2021). https://doi.org/10.1016/J.APSB.2021.03.019.

[131] A.S. Narang, D. Delmarre, D. Gao, Stable drug encapsulation in micelles and microemulsions, *Int. J. Pharm.* 345 (2007) 9–25. https://doi.org/10.1016/J.IJPHARM.2007.08.057.

[132] C. Chretien, J.C. Chaumeil, Release of a macromolecular drug from alginate-impregnated microspheres, *Int. J. Pharm.* 304 (2005) 18–28. https://doi.org/10.1016/J.IJPHARM.2005.06.030.

[133] Y. Sun, L. Zheng, Y. Yang, X. Qian, T. Fu, X. Li, Z. Yang, H. Yan, C. Cui, W. Tan, Metal–Organic Framework Nanocarriers for Drug Delivery in Biomedical Applications, *Nano-Micro Lett.* 12 (2020) 1–29. https://doi.org/10.1007/s40820-020-00423-3.

[134] U. Mueller, M. Schubert, F. Teich, H. Puetter, K. Schierle-Arndt, J. Pastré, Metal–organic frameworks—prospective industrial applications, *J. Mater. Chem.* 16 (2006) 626–636. https://doi.org/10.1039/B511962F.

[135] Y. He, W. Zhou, G. Qian, B. Chen, Methane storage in metal–organic frameworks, *Chem. Soc. Rev.* 43 (2014) 5657–5678. https://doi.org/10.1039/C4CS00032C.

[136] J. Meng, X. Liu, C. Niu, Q. Pang, J. Li, F. Liu, Z. Liu, L. Mai, Advances in metal–organic framework coatings: versatile synthesis and broad applications, *Chem. Soc. Rev*. 49 (2020) 3142–3186. https://doi.org/10.1039/C9CS00806C.

[137] V.P. Torchilin, Multifunctional nanocarriers, *Adv. Drug Deliv. Rev*. 58 (2006) 1532–1555. https://doi.org/10.1016/j.addr.2006.09.009.

[138] H. Cai, Y.L. Huang, D. Li, Biological metal–organic frameworks: Structures, host–guest chemistry and bio-applications, *Coord. Chem. Rev*. (2019). https://doi.org/10.1016/j.ccr.2017.12.003.

[139] C.M. Doherty, D. Buso, A.J. Hill, S. Furukawa, S. Kitagawa, P. Falcaro, Using Functional Nano- and Microparticles for the Preparation of Metal–Organic Framework Composites with Novel Properties, *Acc. Chem. Res*. 47 (2013) 396–405. https://doi.org/10.1021/AR400130A.

[140] C.-Y. Sun, C. Qin, X.-L. Wang, Z.-M. Su, Metal-organic frameworks as potential drug delivery systems, *Expert Opinion on Drug Delivery* 10 (2012) 89–101. https://doi.org/10.1517/17425247.2013.741583.

[141] T. Rajkumar, D. Kukkar, K.H. Kim, J.R. Sohn, A. Deep, Cyclodextrin-metal–organic framework (CD-MOF): From synthesis to applications, *J. Ind. Eng. Chem*. 72 (2019) 50–66. https://doi.org/10.1016/J.JIEC.2018.12.048.

[142] G. Crini, Review: A History of Cyclodextrins, *Chem. Rev.* 114 (2014) 10940–10975. https://doi.org/10.1021/CR500081P.

[143] G. Varan, C. Varan, N. Erdoğar, A.A. Hıncal, E. Bilensoy, Amphiphilic cyclodextrin nanoparticles, *Int. J. Pharm.* 531 (2017) 457–469. https://doi.org/10.1016/J.IJPHARM.2017.06.010.

[144] C. dos Santos, P. Buera, F. Mazzobre, Novel trends in cyclodextrins encapsulation. Applications in food science, *Curr. Opin. Food Sci.* 16 (2017) 106–113. https://doi.org/10.1016/J.COFS.2017.09.002.

[145] P. Horcajada, R. Gref, T. Baati, P.K. Allan, G. Maurin, P. Couvreur, G. Férey, R.E. Morris, C. Serre, Metal–Organic Frameworks in Biomedicine, *Chem. Rev*. 112 (2011) 1232–1268. https://doi.org/10.1021/CR200256V.

[146] I. Roy, J.F. Stoddart, Cyclodextrin Metal–Organic Frameworks and Their Applications, *Acc. Chem. Res.* (2021). https://doi.org/10.1021/acs.accounts.0c00695.

[147] R.A. Smaldone, R.S. Forgan, H. Furukawa, J.J. Gassensmith, A.M.Z. Slawin, O.M. Yaghi, J.F. Stoddart, Metalorganic frameworks from edible natural products,

Angew. Chemie - Int. Ed. 49 (2010) 8630–8634. https://doi.org/10.1002/anie.201002343.

[148] L. Jacquamet, J. Ohana, J. Joly, F. Borel, M. Pirocchi, P. Charrault, A. Bertoni, P. Israel-Gouy, P. Carpentier, F. Kozielski, D. Blot, J.L. Ferrer, Automated Analysis of Vapor Diffusion Crystallization Drops with an X-Ray Beam, *Structure*. 12 (2004) 1219–1225. https://doi.org/10.1016/J.STR.2004.04.019.

[149] S.L. Griffin, M.L. Briuglia, J.H. ter Horst, R.S. Forgan, Assessing Crystallisation Kinetics of Zr Metal–Organic Frameworks through Turbidity Measurements to Inform Rapid Microwave-Assisted Synthesis, *Chem. – A Eur. J.* 26 (2020) 6910–6918. https://doi.org/10.1002/CHEM.202000993.

[150] J.S. Choi, W.J. Son, J. Kim, W.S. Ahn, Metal–organic framework MOF-5 prepared by microwave heating: Factors to be considered, *Microporous Mesoporous Mater*. 116 (2008) 727–731. https://doi.org/10.1016/J.MICROMESO.2008.04.033.

[151] V. Singh, T. Guo, H. Xu, L. Wu, J. Gu, C. Wu, R. Gref, J. Zhang, Moisture resistant and biofriendly CD-MOF nanoparticles obtained via cholesterol shielding, *Chem. Commun*. 53 (2017) 9246–9249. https://doi.org/10.1039/C7CC03471G.

[152] A. Hamedi, A. Anceschi, A. Patrucco, M. Hasanzadeh, A γ-cyclodextrin-based metal–organic framework (γ-CD-MOF): a review of recent advances for drug delivery application, *Journal of Drug Targeting*. 30 (2021) 381-393. https://doi.org/10.1080/1061186X.2021.2012683.

[153] X. Li, T. Guo, L. Lachmanski, F. Manoli, M. Menendez-Miranda, I. Manet, Z. Guo, L. Wu, J. Zhang, R. Gref, Cyclodextrin-based metal-organic frameworks particles as efficient carriers for lansoprazole: Study of morphology and chemical composition of individual particles, *Int. J. Pharm*. 531 (2017) 424–432. https://doi.org/10.1016/J.IJPHARM.2017.05.056.

[154] K.J. Hartlieb, D.P. Ferris, J.M. Holcroft, I. Kandela, C.L. Stern, M.S. Nassar, Y.Y. Botros, J.F. Stoddart, Encapsulation of Ibuprofen in CD-MOF and Related Bioavailability Studies, *Mol. Pharm.* 14 (2017) 1831–1839. https://doi.org/10.1021/ACS.MOLPHARMACEUT.7B00168/SUPPL_FILE/MP7B00168_SI_002.CIF.

[155] T.T. Pham, C. Jaafar-Maalej, C. Charcosset, H. Fessi, Liposome and niosome preparation using a membrane contactor for scale-up, *Colloids Surfaces B Biointerfaces.* 94 (2012) 15–21. https://doi.org/10.1016/J.COLSURFB.2011.12.036.

[156] J. Chen, W.L. Lu, W. Gu, S.S. Lu, Z.P. Chen, B.C. Cai, X.X. Yang, Drug-in-cyclodextrin-in-liposomes: a promising delivery system for hydrophobic drugs, *Expert Opinion on Drug Delivery*. 11 (2014) 565–577. https://doi.org/10.1517/17425247.2014.884557.

[157] D. Yadav, K. Sandeep, D. Pandey, R.K. Dutta, Liposomes for Drug Delivery, *J Biotechnol Biomater.* 7 (2017) 276. https://doi.org/10.4172/2155-952X.1000276.

[158] B. Ozbakir, B.J. Crielaard, J.M. Metselaar, G. Storm, T. Lammers, Liposomal corticosteroids for the treatment of inflammatory disorders and cancer, *J. Control. Release*. 190 (2014) 624–636. https://doi.org/10.1016/J.JCONREL.2014.05.039.

[159] G. Gregoriadis, Liposomes and mRNA: Two technologies together create a COVID-19 vaccine, *Med. Drug Discov.* 12 (2021) 100104. https://doi.org/10.1016/J.MEDIDD.2021.100104.

[160] R. Lordan, A. Tsoupras, I. Zabetakis, Phospholipids of Animal and Marine Origin: Structure, Function, and Anti-Inflammatory Properties, *Mol.* 2017, Vol. 22, Page 1964. 22 (2017) 1964. https://doi.org/10.3390/MOLECULES22111964.

[161] B. Maherani, E. Arab-Tehrany, A. Kheirolomoom, F. Cleymand, M. Linder, Influence of lipid composition on physicochemical properties of nanoliposomes encapsulating natural dipeptide antioxidant l-carnosine, *Food Chem*. 134 (2012) 632–640. https://doi.org/10.1016/J.FOODCHEM.2012.02.098.

[162] Z. Wang, Y. Ma, H. Khalil, R. Wang, T. Lu, W. Zhao, Y. Zhang, J. Chen, T. Chen, Fusion between fluid liposomes and intact bacteria: study of driving parameters and *in vitro* bactericidal efficacy, *Int. J. Nanomedicine*. 11 (2016) 4025. https://doi.org/10.2147/IJN.S55807.

[163] H. Zhang, Thin-Film Hydration Followed by Extrusion Method for Liposome Preparation, *Methods Mol. Biol.* 1522 (2017) 17–22. https://doi.org/10.1007/978-1-4939-6591-5_2.

[164] Y. Wang, S. Tu, A.N. Pinchuk, M.P. Xiong, Active drug encapsulation and release kinetics from hydrogel-in-liposome nanoparticles, *J. Colloid Interface Sci*. 406 (2013) 247–255. https://doi.org/10.1016/J.JCIS.2013.05.081.

[165] J. Li, X. Wang, T. Zhang, C. Wang, Z. Huang, X. Luo, Y. Deng, A review on phospholipids and their main applications in drug delivery systems, *Asian J. Pharm. Sci*. 10 (2015) 81–98. https://doi.org/10.1016/J.AJPS.2014.09.004.

[166] M.K. Riaz, M.A. Riaz, X. Zhang, C. Lin, K.H. Wong, X. Chen, G. Zhang, A. Lu, Z. Yang, Surface Functionalization and Targeting Strategies of Liposomes in Solid Tumor Therapy: A Review, *Int. J. Mol. Sci.* 2018, Vol. 19, Page 195. 19 (2018) 195. https://doi.org/10.3390/IJMS19010195.

[167] H. Barani, M. Montazer, A Review on Applications of Liposomes in Textile Processing, *Journal of Liposome Research*. 18 (2008) 249–262. https://doi.org/10.1080/08982100802354665.

[168] G.R. Anyarambhatla, D. Needham, Enhancement of the Phase Transition Permeability of DPPC Liposomes by Incorporation of MPPC: A New Temperature-Sensitive Liposome for use with Mild Hyperthermia, *Journal of Liposome Research*. 9 (2008) 491–506. https://doi.org/10.3109/08982109909035549.

[169] L. Qiao, A. Ge, M. Osawa, S. Ye, Structure and stability studies of mixed monolayers of saturated and unsaturated phospholipids under low-level ozone, *Phys. Chem. Chem. Phys.* 15 (2013) 17775–17785. https://doi.org/10.1039/C3CP52484A.

[170] J. Tang, F.P. Resurreccion, Electromagnetic basis of microwave heating, *Dev. Packag. Prod. Use Microw. Ovens.* (2009) 3-38e. https://doi.org/10.1533/9781845696573.1.3.

[171] A.R. Yadav, S.K. Mohite, A Brief Review: Microwave Chemistry and its Applications, *Res. J. Pharm. Dos. Forms Technol.* 12 (n.d.) 191–197.

https://doi.org/10.5958/0975-4377.2020.00033.6.

[172] M.S.H. Akash, K. Rehman, Ultraviolet-Visible (UV-VIS) Spectroscopy, *Essentials Pharm. Anal*. (2020) 29–56. https://doi.org/10.1007/978-981-15-1547-7_3.

[173] W. Mäntele, E. Deniz, UV–VIS absorption spectroscopy: Lambert-Beer reloaded, *Spectrochim. Acta Part A Mol. Biomol. Spectrosc.* 173 (2017) 965–968. https://doi.org/10.1016/J.SAA.2016.09.037.

[174] K. Akhtar, S.A. Khan, S.B. Khan, A.M. Asiri, Scanning Electron Microscopy: Principle and Applications in Nanomaterials Characterization, *Handb. Mater. Charact.* (2018) 113–145. https://doi.org/10.1007/978-3-319-92955-2_4.

[175] T.J. Deerinck, T.M. Shone, E.A. Bushong, R. Ramachandra, S.T. Peltier, M.H. Ellisman, High-performance serial block-face SEM of nonconductive biological samples enabled by focal gas injection-based charge compensation, *J. Microsc.* 270 (2018) 142–149. https://doi.org/10.1111/JMI.12667.

[176] M. Scimeca, S. Bischetti, H.K. Lamsira, R. Bonfiglio, E. Bonanno, Energy Dispersive X-ray (EDX) microanalysis: A powerful tool in biomedical research and diagnosis, *Eur. J. Histochem.* 62 (2018) 89–99. https://doi.org/10.4081/EJH.2018.2841.

[177] A.A. Bunaciu, E. gabriela Udriştioiu, H.Y. Aboul-Enein, X-Ray Diffraction: Instrumentation and Applications, *Critical Reviews in Analytical Chemistry*. 45 (2015) 289–299. https://doi.org/10.1080/10408347.2014.949616.

[178] C. Berthomieu, R. Hienerwadel, Fourier transform infrared (FTIR) spectroscopy, *Photosynth. Res*. 101 (2009) 157–170. https://doi.org/10.1007/S11120-009-9439-X/FIGURES/6.

[179] S.E. Glassford, B. Byrne, S.G. Kazarian, Recent applications of ATR FTIR spectroscopy and imaging to proteins, *Biochim. Biophys. Acta - Proteins Proteomics.* 1834 (2013) 2849–2858. https://doi.org/10.1016/J.BBAPAP.2013.07.015.

[180] C.Y. Tang, Z. Yang, Transmission Electron Microscopy (TEM), *Membr. Charact.* (2017) 145–159. https://doi.org/10.1016/B978-0-444-63776-5.00008-5.

[181] M. Almgren, K. Edwards, G. Karlsson, Cryo transmission electron microscopy of liposomes and related structures, *Colloids Surfaces A Physicochem. Eng. Asp*. 174 (2000) 3–21. https://doi.org/10.1016/S0927-7757(00)00516-1.

[182] P.A. Hassan, S. Rana, G. Verma, Making Sense of Brownian Motion: Colloid Characterization by Dynamic Light Scattering, *Langmuir* 31 (2014) 3-12. https://doi.org/10.1021/la501789z.

[183] D.A. Duncan, Synchrotron-based Spectroscopy In On-Surface Polymerization of Covalent Networks, E*ncycl. Interfacial Chem. Surf. Sci. Electrochem*. (2018) 436–445. https://doi.org/10.1016/B978-0-12-409547-2.13768-0.

[184] T.K. Sham, M.L. Rivers, A Brief Overview of Synchrotron Radiation, *Rev. Mineral. Geochemistry.* 49 (2002) 117–147. https://doi.org/10.2138/GSRMG.49.1.117.

[185] K. Héberger, Chemoinformatics—multivariate mathematical–statistical methods for data evaluation, *Med. Appl. Mass Spectrom.* (2008) 141–169. https://doi.org/10.1016/B978-044451980-1.50009-4.

[186] S.D. Sarker, L. Nahar, Applications of High Performance Liquid Chromatography in the Analysis of Herbal Products, *Evidence-Based Valid. Herb. Med*. (2015) 405–425. https://doi.org/10.1016/B978-0-12-800874-4.00019-2.

[187] S. Beg, S. Swain, M. Rahman, M.S. Hasnain, S.S. Imam, Application of Design of Experiments (DoE) in Pharmaceutical Product and Process Optimization, *Pharmaceutical Quality by Design*, (2019) 43-64. https://doi.org/10.1016/b978-0-12-815799-2.00003-4.

[188] S.N. Politis, P. Colombo, G. Colombo, D.M. Rekkas, Design of experiments (DoE) in pharmaceutical development, *Drug Dev. Ind. Pharm.* 43 (2017) 889–901. https://doi.org/10.1080/03639045.2017.1291672.

[189] I. Khatib, M.Y.T. Chow, J. Ruan, D. Cipolla, H.K. Chan, Modeling of a spray drying method to produce ciprofloxacin nanocrystals inside the liposomes utilizing a response surface methodology: Box-Behnken experimental design, *Int. J. Pharm*. 597 (2021) 120277. https://doi.org/10.1016/j.ijpharm.2021.120277.

[190] M.A. Bezerra, R.E. Santelli, E.P. Oliveira, L.S. Villar, L.A. Escaleira, Response surface methodology (RSM) as a tool for optimization in analytical chemistry, *Talanta.* 76 (2008) 965–977. https://doi.org/10.1016/j.talanta.2008.05.019.

[191] J.M. Amigo, Practical issues of hyperspectral imaging analysis of solid dosage forms, *Anal. Bioanal. Chem.* 2010 3981. 398 (2010) 93–109. https://doi.org/10.1007/S00216-010-3828-Z.

[192] H. Abdi, L.J. Williams, Principal component analysis, *Wiley Interdiscip. Rev. Comput. Stat.* 2 (2010) 433–459. https://doi.org/10.1002/WICS.101.

[193] Å. Rinnan, F. van den Berg, S.B. Engelsen, Review of the most common pre-processing techniques for near-infrared spectra, *TrAC Trends Anal. Chem*. 28 (2009) 1201–1222. https://doi.org/10.1016/J.TRAC.2009.07.007.

[194] M. Najlah, A.S. Suliman, I. Tolaymat, S. Kurusamy, V. Kannappan, A.M.A. Elhissi, W. Wang, Development of injectable PEGylated liposome encapsulating disulfiram for colorectal cancer treatment, *Pharmaceutics.* 11 (2019) 1–16. https://doi.org/10.3390/pharmaceutics11110610.

[195] I.R. Silva, T. Kronenberger, E.C.L. Gomes, I.C. César, R.B. Oliveira, V.G. Maltarollo, Improving the solubility of an antifungal thiazolyl hydrazone derivative by cyclodextrin complexation, *Eur. J. Pharm. Sci*. 156 (2021) 105575. https://doi.org/10.1016/J.EJPS.2020.105575.

[196] N.A. Khan, S.H. Jhung, Synthesis of metal-organic frameworks (MOFs) with microwave or ultrasound: Rapid reaction, phase-selectivity, and size reduction, *Coord. Chem. Rev.* 285 (2015) 11–23. https://doi.org/10.1016/j.ccr.2014.10.008.

[197] H. Guo, Y. Zhu, S. Wang, S. Su, L. Zhou, H. Zhang, Combining coordination modulation with acid-base adjustment for the control over size of metal-organic frameworks, *Chem. Mater*. 24 (2012) 444–450. https://doi.org/10.1021/cm202593h.

[198] D. Ke, J.F. Feng, D. Wu, J.B. Hou, X.Q. Zhang, B.J. Li, S. Zhang, Facile stabilization of a cyclodextrin metal-organic framework under humid environment: Via hydrogen

sulfide treatment, *RSC Adv.* 9 (2019) 18271–18276. https://doi.org/10.1039/c9ra03079d.

[199] R.T. Downs, M. Hall-Wallace, The American Mineralogist crystal structure database, *Am. Mineral*. 88 (2003) 247–250.

[200] S. Graulis, D. Chateigner, R.T. Downs, A.F.T. Yokochi, M. Quirós, L. Lutterotti, E. Manakova, J. Butkus, P. Moeck, A. Le Bail, Crystallography Open Database - An open-access collection of crystal structures, *J. Appl. Crystallogr*. 42 (2009) 726–729. https://doi.org/10.1107/S0021889809016690.

[201] S. Gražulis, A. Merkys, A. Vaitkus, M. Okulič-Kazarinas, Computing stoichiometric molecular composition from crystal structures, *J. Appl. Crystallogr*. 48 (2015) 85–91. https://doi.org/10.1107/S1600576714025904.

[202] S. Gražulis, A. Daškevič, A. Merkys, D. Chateigner, L. Lutterotti, M. Quirós, N.R. Serebryanaya, P. Moeck, R.T. Downs, A. Le Bail, Crystallography Open Database (COD): An open-access collection of crystal structures and platform for world-wide collaboration, *Nucleic Acids Res.* 40 (2012) 420–427. https://doi.org/10.1093/nar/gkr900.

[203] A. Merkys, A. Vaitkus, J. Butkus, M. Okulič-Kazarinas, V. Kairys, S. Gražulis, COD::CIF::Parser: An error-correcting CIF parser for the Perl language, *J. Appl. Crystallogr*. 49 (2016) 292–301. https://doi.org/10.1107/S1600576715022396.

[204] M. Quirós, S. Gražulis, S. Girdzijauskaitė, A. Merkys, A. Vaitkus, Using SMILES strings for the description of chemical connectivity in the Crystallography Open Database, *J. Cheminform*. 10 (2018) 1–17. https://doi.org/10.1186/s13321-018-0279-6.

[205] A. Vaitkus, A. Merkys, S. Gražulis, Validation of the Crystallography Open Database using the Crystallographic Information Framework, *J. Appl. Crystallogr.* 54 (2021) 661–672. https://doi.org/10.1107/s1600576720016532.

[206] N. Motakef-Kazemi, S.A. Shojaosadati, A. Morsali, In situ synthesis of a drug-loaded MOF at room temperature, *Microporous Mesoporous Mater*. (2014). https://doi.org/10.1016/j.micromeso.2013.11.036.

[207] M. Al Haydar, H.R. Abid, B. Sunderland, S. Wang, Metal organic frameworks as a drug delivery system for flurbiprofen, *Drug Des. Devel. Ther.* (2017). https://doi.org/10.2147/DDDT.S145716.

[208] R.S. Forgan, R.A. Smaldone, J.J. Gassensmith, H. Furukawa, D.B. Cordes, Q. Li, C.E. Wilmer, Y.Y. Botros, R.Q. Snurr, A.M.Z. Slawin, J.F. Stoddart, Nanoporous carbohydrate metal-organic frameworks, *J. Am. Chem. Soc.* 134 (2012) 406–417. https://doi.org/10.1021/ja208224f.

[209] T. Dong, Y. He, K.M. Shin, Y. Inoue, Formation and characterization of inclusion complexes of poly(butylene succinate) with α- and γ-cyclodextrins, *Macromol. Biosci*. 4 (2004) 1084–1091. https://doi.org/10.1002/mabi.200400054.

[210] M. Wei, A.E. Tonelli, Compatiblization of polymers via coalescence from their common cyclodextrin inclusion compounds, *Macromolecules.* 34 (2001) 4061–4065. https://doi.org/10.1021/ma010235a.

[211] Y. Xiong, L. Wu, T. Guo, C. Wang, W. Wu, Y. Tang, T. Xiong, Y. Zhou, W. Zhu, J. Zhang, Crystal Transformation of β-CD-MOF Facilitates Loading of Dimercaptosuccinic Acid, *AAPS PharmSciTech*. 20 (2019) 1–9. https://doi.org/10.1208/s12249-019-1422-z.

[212] M. Kumar Trivedi, A. Branton, Characterisation of Physical, Spectral and Thermal Properties of Biofield treated Resorcinol, *Org. Chem. Curr. Res*. 04 (2015). https://doi.org/10.4172/2161-0401.1000146.

[213] X. Ren, H. Cai, H. Du, J. Chang, The preparation and characterization of pyrolysis bio-oil-resorcinol-aldehyde resin cold-set adhesives for wood construction, *Polymers*. 9 (2017). https://doi.org/10.3390/polym9060232.

[214] D.J. Prasad Reddy, A.V. Rajulu, V. Arumugam, M.D. Naresh, M. Muthukrishnan, Effects of resorcinol on the mechanical properties of soy protein isolate films, *J. Plast. Film Sheeting.* 25 (2009) 221–233. https://doi.org/10.1177/8756087910365030.

[215] H. Gu, Olivetol-cyclodextrin complexes and regio-selective process for preparing delta 9-tetrahydrocannabinol, WO2004092101A3, 2004. https://patents.google.com/patent/WO2004092101A3.

[216] Z. Moussa, M. Hmadeh, M.G. Abiad, O.H. Dib, D. Patra, Encapsulation of curcumin in cyclodextrin-metal organic frameworks: Dissociation of loaded CD-MOFs enhances stability of curcumin, *Food Chem*. (2016). https://doi.org/10.1016/j.foodchem.2016.06.013.

[217] M.L. Briuglia, C. Rotella, A. McFarlane, D.A. Lamprou, Influence of cholesterol on liposome stability and on *in vitro* drug release, *Drug Deliv. Transl. Res.* 5 (2015) 231–242. https://doi.org/10.1007/s13346-015-0220-8.

[218] Y. Jia, H. Joly, A. Omri, Liposomes as a carrier for gentamicin delivery: Development and evaluation of the physicochemical properties, *Int. J. Pharm*. 359 (2008) 254–263. https://doi.org/10.1016/j.ijpharm.2008.03.035.

[219] S. Kaddah, N. Khreich, F. Kaddah, C. Charcosset, H. Greige-Gerges, Cholesterol modulates the liposome membrane fluidity and permeability for a hydrophilic molecule, *Food Chem. Toxicol.* 113 (2018) 40–48. https://doi.org/10.1016/J.FCT.2018.01.017.

[220] G. Zhang, F. Meng, Z. Guo, T. Guo, H. Peng, J. Xiao, B. Liu, V. Singh, S. Gui, P. York, W. Qian, L. Wu, J. Zhang, Enhanced stability of vitamin A palmitate microencapsulated by γ-cyclodextrin metal-organic frameworks, *J. Microencapsul.* 35 (2018) 249–258. https://doi.org/10.1080/02652048.2018.1462417.

[221] Y. Chen, K. Tai, P. Ma, J. Su, W. Dong, Y. Gao, L. Mao, J. Liu, F. Yuan, Novel γ-cyclodextrin-metal–organic frameworks for encapsulation of curcumin with improved loading capacity, physicochemical stability and controlled release properties, *Food Chem*. 347 (2021). https://doi.org/10.1016/j.foodchem.2020.128978.

[222] Z. Hu, S. Li, S. Wang, B. Zhang, Q. Huang, Encapsulation of menthol into cyclodextrin metal-organic frameworks: Preparation, structure characterization and evaluation of complexing capacity, *Food Chem*. 338 (2021) 127839.

https://doi.org/10.1016/j.foodchem.2020.127839.

[223] L. Bachmann, R. Diebolder, R. Hibst, D.M. Zezell, Infrared absorption bands of enamel and dentin tissues from human and bovine teeth, *Appl. Spectrosc. Rev.* 38 (2003) 1–14. https://doi.org/10.1081/ASR-120017479.

[224] M. Anwar Alebrahim, C. Krafft, W. Sekhaneh, B. Sigusch, J. Popp, ATR-FTIR and Raman spectroscopy of primary and permanent teeth, *Biomed. Spectrosc. Imaging.* 3 (2014) 15–27. https://doi.org/10.3233/bsi-130059.

[225] F. Taube, M. Marczewski, J.G. Norén, Deviations of inorganic and organic carbon content in hypomineralised enamel, *J. Dent*. 43 (2015) 269–278. https://doi.org/10.1016/j.jdent.2014.09.003.

[226] J. Gan, S. Liu, L. Zhou, Y. Wang, J. Guo, C. Huang, Effect of Nd:YAG laser irradiation pretreatment on the long-term bond strength of etch-and-rinse adhesive to dentin, *Oper. Dent.* 42 (2017) 62–72. https://doi.org/10.2341/15-268-L.

[227] C.A.M. France, N. Sugiyama, E. Aguayo, Establishing a preservation index for bone, dentin, and enamel bioapatite mineral using ATR-FTIR, *J. Archaeol. Sci. Reports*. 33 (2020) 102551. https://doi.org/10.1016/J.JASREP.2020.102551.

[228] J.D. McGuire, M.P. Walker, V. Dusevich, Y. Wang, J.P. Gorski, Enamel organic matrix: potential structural role in enamel and relationship to residual basement membrane constituents at the dentin enamel junction, *Connect. Tissue Res.* 55 (2014) 33. https://doi.org/10.3109/03008207.2014.923883.

[229] S. González-López, C. Torres-Rodríguez, V. Bolaños-Carmona, P. Sanchez-Sanchez, A. Rodríguez-Navarro, P. Álvarez-Lloret, M. Domingo Garcia, Effect of 30 % hydrogen peroxide on mineral chemical composition and surface morphology of bovine enamel, *Odontology*. 104 (2016) 44–52. https://doi.org/10.1007/s10266-014-0189-7.

[230] H.F. Shurvell, Spectra- Structure Correlations in the Mid- and Far-Infrared, *Handbook of Vibrational Spectroscopy,* (2006). https://doi.org/10.1002/0470027320.s4101.

[231] P. Fattibene, A. Carosi, V. De Coste, A. Sacchetti, A. Nucara, P. Postorino, P. Dore, A comparative EPR, infrared and Raman study of natural and deproteinated tooth enamel and dentin, *Phys. Med. Biol.* 50 (2005) 1095–1108. https://doi.org/10.1088/0031-9155/50/6/004.

[232] I.H. Kim, J.S. Son, B.K. Min, Y.K. Kim, K.H. Kim, T.Y. Kwon, A simple, sensitive and non-destructive technique for characterizing bovine dental enamel erosion: attenuated total reflection Fourier transform infrared spectroscopy, *Int. J. Oral Sci*. 2016 81. 8 (2016) 54–60. https://doi.org/10.1038/ijos.2015.58.

[233] N. Pleshko, A. Boskey, R. Mendelsohn, Novel infrared spectroscopic method for the determination of crystallinity of hydroxyapatite minerals, *Biophys. J.* 60 (1991) 786–793. https://doi.org/10.1016/S0006-3495(91)82113-0.

[234] T. Sakae, Variations in Dental Enamel Crystallites and Micro-Structure, *J. Oral Biosci.* 48 (2006) 85–93. https://doi.org/10.1016/S1349-0079(06)80021-6.

[235] N. Raghavendra Naveen, M. Kurakula, B. Gowthami, Process optimization by

response surface methodology for preparation and evaluation of methotrexate loaded chitosan nanoparticles, *Mater. Today Proc.* 33 (2020) 2716–2724. https://doi.org/10.1016/J.MATPR.2020.01.491.

[236] A. Gutiérrez-Serpa, A.I. Jiménez-Abizanda, F. Jiménez-Moreno, J. Pasán, V. Pino, Core-shell microparticles formed by the metal-organic framework CIM-80(Al) (Silica@CIM-80(Al)) as sorbent material in miniaturized dispersive solid-phase extraction, *Talanta*. 211 (2020) 120723. https://doi.org/10.1016/j.talanta.2020.120723.

[237] L. Lindfors, S. Forssén, J. Westergren, U. Olsson, Nucleation and crystal growth in supersaturated solutions of a model drug, *J. Colloid Interface Sci.* 325 (2008) 404–413. https://doi.org/10.1016/J.JCIS.2008.05.034.

[238] R. Androsch, M.L. Di Lorenzo, Crystal Nucleation in Glassy Poly(l-lactic acid), *Macromolecules*. 46 (2013) 6048–6056. https://doi.org/10.1021/MA401036J.

[239] J. McGinty, N. Yazdanpanah, C. Price, J.H. ter Horst, J. Sefcik, CHAPTER 1 Nucleation and Crystal Growth in Continuous Crystallization, *Handb. Contin. Cryst*. (2020) 1–50. https://doi.org/10.1039/9781788013581-00001.

[240] W.R. Bauer, W. Nadler, Stationary flow, first passage times, and macroscopic Fick's first diffusion law: Application to flow enhancement by particle trapping, *J. Chem. Phys.* 122 (2005) 1–13. https://doi.org/10.1063/1.1940056.

[241] S.B. Ünal, F. Erdoğdu, H.I. Ekiz, Effect of temperature on phosphate diffusion in meats, *J. Food Eng.* 76 (2006) 119–127. https://doi.org/10.1016/j.jfoodeng.2005.04.041.

[242] B.T. Smith, Remington education: physical pharmacy, 1st ed., Pharmaceutical Press, London, 2015.

[243] F. Ravera, L. Liggieri, A. Steinchen, Sorption kinetics considered as a renormalized diffusion process, *J. Colloid Interface Sci.* 156 (1993) 109–116. https://doi.org/10.1006/JCIS.1993.1088.

[244] S. Wang, X. Yang, W. Lu, N. Jiang, G. Zhang, Z. Cheng, W. Liu, Spray drying encapsulation of CD-MOF nanocrystals into Eudragit® RS microspheres for sustained drug delivery, *J. Drug Deliv. Sci. Technol.* 64 (2021) 102593. https://doi.org/10.1016/j.jddst.2021.102593.

[245] Z. Li, G. Yang, R. Wang, Y. Wang, J. Wang, M. Yang, C. Gong, Y. Yuan, γ-Cyclodextrin metal–organic framework as a carrier to deliver triptolide for the treatment of hepatocellular carcinoma, *Drug Deliv. Transl. Res*. (2021) 15–17. https://doi.org/10.1007/s13346-021-00978-7.

[246] Y. Wei, C. Chen, S. Zhai, M. Tan, J. Zhao, X. Zhu, L. Wang, Q. Liu, T. Dai, Enrofloxacin/florfenicol loaded cyclodextrin metal-organic-framework for drug delivery and controlled release, *Drug Deliv.* 28 (2021) 372–379. https://doi.org/10.1080/10717544.2021.1879316.

[247] H. Li, J. Zhu, C. Wang, W. Qin, X. Hu, J. Tong, L. Yu, G. Zhang, X. Ren, Z. Li, J. Zhang, Paeonol loaded cyclodextrin metal-organic framework particles for treatment of acute lung injury via inhalation, *Int. J. Pharm.* 587 (2020) 119649.

https://doi.org/10.1016/j.ijpharm.2020.119649.

[248] K.J. Hartlieb, A.W. Peters, T.C. Wang, P. Deria, O.K. Farha, J.T. Hupp, J.F. Stoddart, Functionalised cyclodextrin-based metal–organic frameworks, *Chem. Commun*. 53 (2017) 7561–7564. https://doi.org/10.1039/C7CC03345A.

[249] H. Li, M.R. Hill, R. Huang, C. Doblin, S. Lim, A.J. Hill, R. Babarao, P. Falcaro, Facile stabilization of cyclodextrin metal–organic frameworks under aqueous conditions via the incorporation of C60 in their matrices, *Chem. Commun*. 52 (2016) 5973–5976. https://doi.org/10.1039/C6CC01620K.

[250] H. Li, N. Lv, X. Li, B. Liu, J. Feng, X. Ren, T. Guo, D. Chen, J. Fraser Stoddart, R. Gref, J. Zhang, Composite CD-MOF nanocrystals-containing microspheres for sustained drug delivery, *Nanoscale.* 9 (2017) 7454–7463. https://doi.org/10.1039/C6NR07593B.

[251] I. Kritskiy, T. Volkova, A. Surov, I. Terekhova, γ-Cyclodextrin-metal organic frameworks as efficient microcontainers for encapsulation of leflunomide and acceleration of its transformation into teriflunomide, *Carbohydr. Polym.* 216 (2019) 224–230. https://doi.org/10.1016/j.carbpol.2019.04.037.

[252] Y. Wei, C. Chen, S. Zhai, M. Tan, J. Zhao, X. Zhu, L. Wang, Q. Liu, T. Dai, Enrofloxacin/florfenicol loaded cyclodextrin metal-organic-framework for drug delivery and controlled release, *Drug Delivery*. 28 (2021) 372–379. https://doi.org/10.1080/10717544.2021.1879316.

[253] R.A. Vlad, P. Antonoaea, N. Todoran, D.L. Muntean, E.M. Rédai, O.A. Silași, A. Tătaru, M. Bîrsan, S. Imre, A. Ciurba, Pharmacotechnical and analytical preformulation studies for cannabidiol orodispersible tablets, *Saudi Pharm. J.* 29 (2021) 1029–1042. https://doi.org/10.1016/J.JSPS.2021.07.012.

[254] N. Geskovski, G. Stefkov, O. Gigopulu, S. Stefov, C.W. Huck, P. Makreski, Mid-infrared spectroscopy as process analytical technology tool for estimation of THC and CBD content in Cannabis flowers and extracts, *Spectrochim. Acta Part A Mol. Biomol. Spectrosc.* 251 (2021) 119422. https://doi.org/10.1016/J.SAA.2020.119422.

ANNEXES: SUBMITTED PAPERS

Predicting cannabinoid release system: encapsulation of a cannabidiol precursor into γ-cyclodextrin metal-organic frameworks

Jorge Rodríguez-Martínez[1(¥)], María-Jesús Sánchez-Martín*[1(¥)], Oscar López-Patarroyo[1], Manuel Valiente[1]

[1] GTS Research Group, Department of Chemistry, Faculty of Science, Universitat Autònoma de Barcelona, 08193 Bellaterra, Spain.

[(¥)] Shared co-first authorship

*Co-first author and author for correspondence: mariajesus.sanchez@uab.cat

Telephone: +34 93 581 4638

Abstract

γ-Cyclodextrin-metal-organic frameworks (γ-CD-MOFs) are developed as a new promising and biocompatible material, which shows a great potential for drug delivery system (DDS) applications. γ-CD-MOFs were successfully synthesized using microwave-assisted technique from different potassium sources (KOH, KCl and KNO_3). The encapsulation of olivetol (OLV) into these materials was investigated as an innovative model of DDS for cannabinoids. Loading of OLV in γ-CD-MOFs was performed by impregnation and co-crystallization methods. Scanning electron microscopy (SEM) and X-ray powder diffraction (XRPD) were employed to study the structural properties of γ-CD-MOF samples, showing the typical cubic crystals in case of KOH and trigonal morphologies in case of KCl and KNO_3. Olivetol content was determined using UV-Vis spectrophotometry and its interaction with γ-CD-MOFs was investigated by Attenuated Total Reflection-Fourier Transform Infrared Spectroscopy analysis (ATR-FTIR). OLV content was significantly higher when KCl or KNO_3 were employed in combination with a co-crystallization method, while the drug encapsulation using KOH and the impregnation method was really poor. Therefore, it can be proposed that γ-CD-MOFs could be considered a novel strategy for DDS of cannabinoids.

Keywords

γ-Cyclodextrin-metal-organic frameworks (γ-CD-MOFs), cannabidiol (CBD), cannabinoids, drug delivery systems (DDS), olivetol (OLV).

Graphical abstract

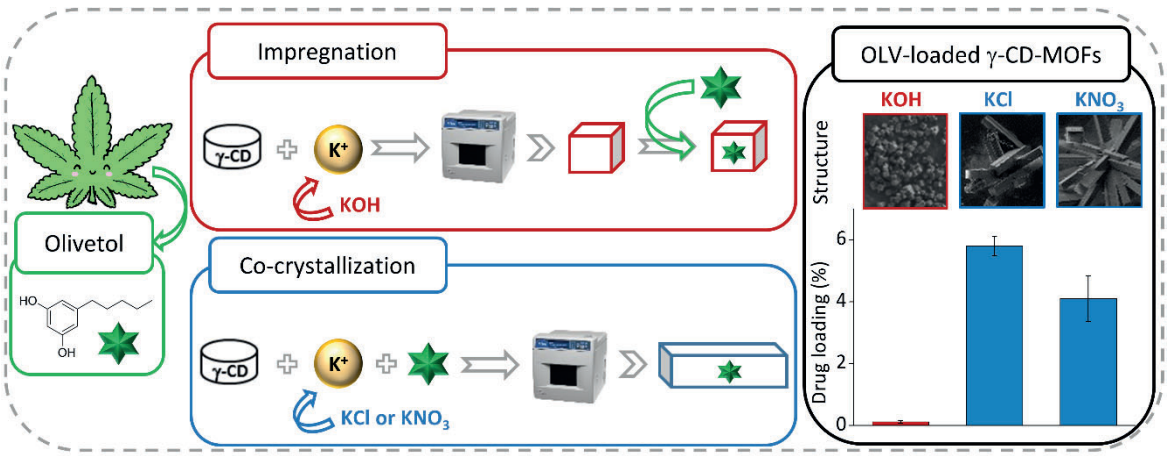

1. Introduction

Metal-organic frameworks (MOFs) have emerged in several applications such as gas storage, catalysis, pollutant-removal agents and drug delivery systems (DDS) [1]. These materials are made of metal ions and organic ligands linked in an infinite extended one-two-three dimensional networks [2]. This packing confers crystallinity and extraordinary properties to MOFs such as high surface areas, ultrahigh porosity and thermal stability making them promising for plenty applications as already mentioned above [3]. Moreover, the parameters that define these properties could be modified by the selection of the linkers and the control of the different steps during the synthesis procedure [4]. Another aspect to take into account is the formation of the host-guest complexes. This encapsulation process depends on the drug to encapsulate and on the medium. In fact, there are a lot of methodologies for this purpose, like direct impregnation, vaporization, direct contact pressure or co-crystallization techniques [5]. Furthermore, the procedure should be selected properly in order not to affect the properties of the MOFs.

Within the uses of MOFs, the application of these materials in biomedical field has been growing over the last years since they could act as drug delivery systems in order to improve the characteristics of the encapsulated agent and to target its pharmaceutical effect [6]. Nevertheless, biocompatibility is a key aspect in these cases and the components that comprise the MOFs should show low toxicity [7,8]. In recent years, γ-cyclodextrin-metal-organic frameworks (γ-CD-MOFs) have arisen as promising biocompatible candidates due to their relevance in pharmacy and biomedicine [9]. These types of MOFs are made of γ-cyclodextrin as the organic ligand and the selected metal linker. γ-CD presents a hydrophobic inner cavity where non-polar compounds could be encapsulated and a hydrophilic outer surface allowing its solubility in aqueous solutions [10]. Besides, the encapsulation capacity of γ-CD-MOFs is higher than in the γ-CD alone and, according to reported studies; these MOFs improve the physicochemical and biopharmaceutical characteristics of the encapsulated drug and control its release process [11,12]. In order to perform the synthesis of these materials, the vapor diffusion technique is the most conventional and well-known method but it requires at least several days to obtain γ-CD-MOFs [13]. Therefore, new methodologies are being developed in order to solve this difficulty, such as the analytical microwave-assisted technique, obtaining homogeneous crystal structures with editable size and a suitable reaction yield [14,15]. Moreover, the synthesis time has been reduced from days to hours using this technique instead of the vapor diffusion method. Thus, microwave technique emerges as a fast and efficient methodology in the synthesis of these frameworks. CD-MOFs based on α-CD, β-CD or γ-CD using potassium nitrate were developed for menthol encapsulation [16]. The obtained crystals presented uniform size, ordered structures and regular shape, showing a better thermal stability than alone CDs. This study could be useful in the design of efficient materials in the food industry. Moreover, other study has made an attempt to improve the encapsulation of the insoluble drug, honokiol, into the pores of γ-CD-MOFs using supercritical carbon dioxide for its activation [17]. The resulting DDS improved the solubility and bioavailability of the drug and the activation of the MOFs maximized its potential encapsulation capability.

Cannabidiol (CBD) is the main non-psychotropic cannabinoid of the *Cannabis sativa* plant. This compound is the main component responsible of the medical benefits of cannabis. Cannabidiol and other natural cannabinoids act on the endocannabinoid system [18]. This system regulates several physiological processes in the body related to cognition and brain function, pain pathways in the brain, immune and hematopoietic systems. Therefore, CBD presents interesting

properties such as its analgesic, anti-inflammatory and immunomodulatory effects [19]. Because of that, this compound has been employed in several studies over the last few years for the treatment of diseases such as Alzheimer or cancer [20,21]. These promising effects in a lot of different diseases are due to the capacity of CBD to interact not only with the corresponding endocannabinoid receptors but also with a wide spectrum of others receptors [22]. However, CBD also presents some limitations that compromise its plenty applications. This compound is insoluble in water, it presents low chemical stability and it gets oxidized in alkali media [23]. Consequently, numerous materials for CBD encapsulation have been developed to minimize these weaknesses, including inclusion complexes of cyclodextrins, lipid carriers and microparticles, among others [24]. Poly(lactic-co-glycolic acid) spherical microparticles were used for CBD encapsulation improving the administration of the drug and showing a useful formulation to be combined with conventional chemotherapy against ovarian cancer [25]. In other study, the preparation of stable inclusion complex of CBD with three native cyclodextrins increased significantly the water solubility and *in vitro* anticancer activity of cannabidiol compared with free drug thanks to the encapsulation of the CBD into the inner cavity of cyclodextrins [26]. Similarly, nanostructured lipid carriers formulations loaded with CBD were developed and characterized as a promising delivery system to enhance the bioavailability of cannabidiol for the treatment of neuropathic pain [27]. Even though there are several studies on the encapsulation of cannabidiol into different carriers, investigations on CBD being loaded into γ-CD-MOFs have not been reported. Nevertheless, cannabidiol is not a very affordable product, therefore analogues or precursors of this compound could be used instead of CBD for multiple experimental approaches. Olivetol (OLV), also known as 5-pentylresorcinol, is a natural organic compound found in certain species of plants [28] and itis an intermediate involved in the cannabinoid biosynthesis in *C. sativa.* This compound leads to the different cannabinoids, including CBD becoming an important metabolite in cannabinoid biosynthesis [29]. In fact, it is used in various methods to produce synthetic analogues of cannabinoids [30]. Chemically, OLV structure is found in cannabinoids, so OLV could be used as an analogue of CBD as it could mimic its interactions with the drug delivery systems.

The aim of this study is to develop CD-MOFs for olivetol encapsulation as a model of cannabinoid drug delivery system. CD-MOFs are prepared using γ-CD and three different potassium sources depending on the followed synthesis method. The characterization of the drug delivery systems is performed and the encapsulation efficiency of OLV into γ-CD-MOFs is determined. For the first time, γ-CD-MOFs are used for olivetol encapsulation and it could be useful in the development of CD-MOFs as promising drug delivery systems with analgesic effect in pharmacy and biomedical field.

2. Materials and methods

2.1. Reagents

Olivetol (95%) and γ-cyclodextrin (98%) were purchased from Carbosynth Ltd (Compton, United Kingdom). Potassium hydroxide (85.5%) and potassium nitrate (99.2%) were purchased from VWR BDH Chemicals (Oud-Heverlee, Belgium). Dichloromethane (99.5%) and ethanol (96%) were purchased from Scharlau (Sentmenat, Spain). Potassium chloride (99.0%) was purchased from Sigma-Aldrich (St. Louis, MO, USA). Polyethylene glycol 20000 was purchased from Merk (Darmstadt, Germany). Methanol (99.8%) and acetic acid (99.9%) were purchased from Fisher Scientific (Madrid, Spain). MilliQ water was purified through a Millipore purification system from Millipore (Milford, MA, USA).

2.2. Preparation of the samples

A fast synthesis of γ-CD-MOFs with microwave irradiation was performed using a modified method [1]. This reported method offers the advantages of simple, rapid, inexpensive, relatively green, and efficient non-conventional heating and high yield [12]. Briefly, γ-CD (324 mg) and KOH (112 mg) were mixed in milliQ water (10 mL). The molar ratio of KOH to γ-CD was 1:8. Then, 6 mL of methanol were added. This initial solution was treated at 50 ºC in the analytical microwave (CEM Corporation Matthews, North Carolina, USA) for 10 min and a power of 600 w. After that process, 256 mg of PEG 20000 were added for one hour to trigger the precipitation of the crystals at room temperature. In order to remove the unreacted material, the crystals were washed first with 10 mL of methanol and then with 10 mL more of ethanol in a centrifuge at 3000 rpm for 5 min. Next, γ-CD-MOFs were left under vacuum and dried overnight at 50 ºC. Herein, preliminary alkaline γ-CD-MOFs (pH = 12) were obtained. Since cannabinoids get oxidized in alkali media, a neutralization of the γ-CD-MOFs was needed. For this step, the crystals were treated with a mixture of 5.2 mL of ethanol and 0.8 mL of acetic acid. The suspension was then shaken at 290 rpm for 2 hours and the precipitates were collected by centrifugation (3000 rpm for 5 min). Once again, the powder was left to dry overnight under vacuum at 50 ºC. Afterwards, an activation of the γ-CD-MOFs was performed using a solvent exchange method with dichloromethane in order to remove guest molecules from chemicals used in the synthetic procedure. γ-CD-MOFs were mixed with 10 mL of dichloromethane at 290 rpm for 3 days. Every 24 hours the solvent was replaced by centrifugation (3000 rpm for 5 min). Finally, the samples were dried overnight under vacuum at 50 ºC. γ-CD-MOFs were kept under vacuum at room temperature until its use and the reaction yields were also calculated.

Impregnation and co-crystallization methods were performed to load olivetol into γ-CD-MOFs. In case of impregnation, 30.8 mg of MOF samples were added to 20 mL of OLV 360 mg/mL solution in ethanol in order to obtain a 1:2 molar ratio of γ-CD-MOFs:OLV respectively. The suspensions were incubated for 24 hours at 37 ºC under stirring conditions (290 rpm). After the incubation time, the crystals were washed with 10 mL of ethanol in a centrifuge at 3000 rpm for 5 minutes in order to remove the drug that did not interact with the γ-CD-MOFs. Finally, the samples were dried and kept under vacuum at room temperature until its use.

The co-crystallization method is similar to that described before. In this case, the potassium sources were KCl or KNO_3 instead of KOH, adding 149 mg or 202 mg respectively, to maintain the 1:2 molar ratio. The change in the potassium source is because of in the co-crystallization the drug is loaded on the initial solution where the synthesis takes place, and the pH of the medium must be neutral from the beginning to avoid olivetol oxidation. Additionally, 30 mg of OLV were also diluted in the initial solution. This amount of drug was selected in order to keep the same molar ratio between MOF and olivetol as in the impregnation method. In this method, the incubation time with PEG 20000 was 24 hours instead of one hour, but the neutralization and activation steps were not needed. Finally, the washes were the same as before and the resultant samples were left overnight under vacuum at 50 ºC and kept under vacuum at room temperature until its use. It should be noted that MOFs were not obtained when KCl or KNO_3 were employed following the same synthesis procedure as for KOH.

The γ-CD-MOFs loaded by impregnation method was named as γ-CD-MOF-1, loaded or not with OLV. In the case of co-crystallization technique, MOFs were named as γ-CD-MOF-2 and γ-CD-MOF-3, for KCl and KNO_3 as potassium sources respectively.

2.3. Drug release and quantification

The quantification of the drug encapsulation into the MOFs was determined as follows: 15 mg of MOF sample were added to 5 mL of a mixture of milliQ water and ethanol (1:1, v/v). The mixture was incubated at room temperature under stirring conditions (290 rpm) for 24 hours to promote the degradation of the crystals and release the encapsulated OLV. To determine the amount of olivetol, the solution was measured by UV-Vis spectrophotometry (Thermo Fisher Scientific, Massachusetts, USA). The UV detection was performed at 275 nm that is the characteristic peak of OLV and the reference was a mixture of milliQ water and ethanol (1:1, v/v). A calibration curve of different known concentrations of olivetol in milliQ water and ethanol solutions (1:1, v/v) was also performed from 0 to 100 mg/L of the drug (Fig. A.1) to determine the concentration of olivetol in the samples.

The drug loading for each MOF was calculated following equation 1:

$$Drug\ loading\ (\%) = \frac{Encapsulated\ OLV\ into\ CD{-}MOFs\ (mg)}{Total\ Weight\ of\ coplexation\ powder\ (mg)} \cdot 100 \qquad [1]$$

All determinations of the loaded drug in each MOF sample were performed by triplicate.

2.4. Scanning electron microscope and Energy-Dispersive X-ray Spectroscopy

The morphology and elemental composition of the MOF samples were analysed by Scanning Electron Microscopy (SEM) and Energy Dispersive X-ray Spectroscopy (EDX) with a Zeiss Merlin FE-SEM equipped with an EDX Oxford INCA X-Max Detector. The images were taken with the Secondary Electron Detector with a low voltage of 1 - 2 kV and the EDX measurements were taken at 10 kV. This microscope has a unique charge compensation system that allows the high-resolution imaging of non-conductive samples, electrons which accumulate on the sample surface are swept away by a fine jet of nitrogen. All the experiments were performed at room temperature.

2.5. X-ray powder diffraction analysis

The crystallinity of the MOFs samples was characterized by X-ray powder diffraction (XRPD) using a Malvern Panalytical X'Pert PRO MPD (Material Powder Diffractometer). The MPD is suitable for the analysis of polycrystalline samples at room temperature. This diffractometer has a vertical theta-theta goniometer (240 mm radius). The XRD analysis was carried in transmission mode using a capillary spinner and the sample were filled inside borosilicate glass capillaries with outer diameter of 0.7 mm. A focusing mirror was used for the incident beam and a lineal X'Celerator detector for the diffracted beam. The samples were irradiated with a ceramic X-ray tube with Cu Kα anode (l = 1.5406 Å), tube voltage of 45 kV, tube current of 40 mA in a step size scan mode (0.03º min^{-1}) and analysed over a 2θ angle range of 2.5 - 35º.

2.6. Attenuated Total Reflection-Fourier Transform Infrared Spectroscopy analysis

Infrared Spectroscopy spectra of samples were obtained using an Infrared Spectrophotometer Tensor 27 equipped with an Attenuated Total Reflectance module Specac Golden Gate (ATR-FTIR, Bruker, Ettlingen, Germany). The ATR accessory allows direct recording of samples thus facilitating the recording of IR spectra on liquid or solid samples regardless of their physical nature. To measure the powder samples 64 scans were carried out in wavenumber from 4000 cm^{-1} to 600 cm^{-1} at a resolution of 4 cm^{-1} and at room temperature. For the background the own diamond window of the equipment was used.

3. Results and discussion

3.1. Structural properties of γ-CD-MOFs

The crystal morphology and element distribution of different γ-CD-MOFs compared with native γ-CD were determined by SEM and EDX analysis. In case of γ-CD-MOF-1, the final morphology of the crystals matched very well with the previously reported morphology of the same material (Fig. 1A) [9]. The SEM images of γ-CD-MOF-1 showed that they presented cubic-shaped with a size average of 2 μm, while the morphology of the raw γ-CD alone was completely amorphous when the same technique was performed (Fig. A.2). Moreover, the EDX detector in the SEM equipment was used to the elemental qualitative analysis of γ-CD-MOF-1 and it confirmed the presence of potassium in the cubic structures (Table A.1). Thus, the cubic crystals were the material of interest. Furthermore, the size average of the structures was reduced in comparison with the γ-CD-MOFs obtained with conventional methodologies, such as vapor diffusion method (Fig. A.3). This fact demonstrated the high capabilities of the microwave technique to achieve narrow size distributions and control of the morphology in the MOFs synthesis. Indeed, this is a key point when the final application of the structures is as drug delivery systems. In the case of olivetol loaded γ-CD-MOF-1, similar size and cubic shape were observed in comparison with the unloaded ones (Fig. 1B). Therefore, the morphology of the MOF structures was stable after the encapsulation with the drug.

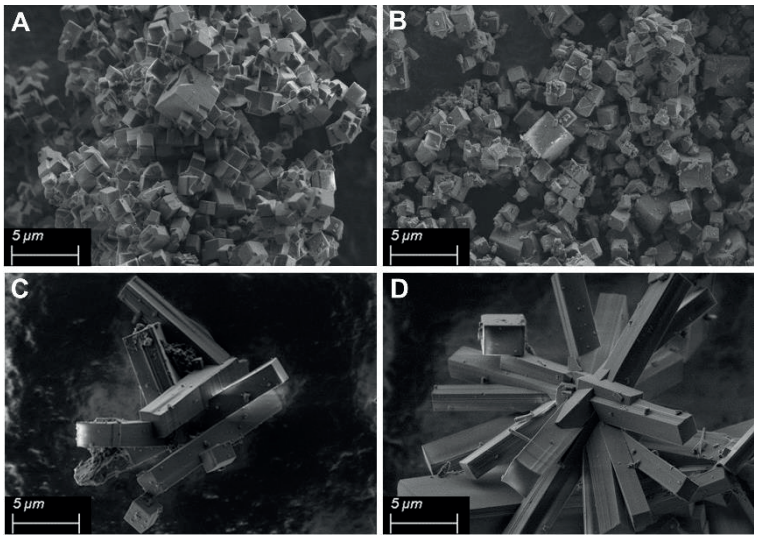

Figure 1. Scanning electron microscopy images of unloaded γ-CD-MOF-1 (A), olivetol loaded γ-CD-MOF-1 (B), γ-CD-MOF-2 (C) and γ-CD-MOF-3 (D) with a low voltage of 2 kV, 5000x of magnification and a working distance of 4.7 mm.

In case of γ-CD-MOF-2 and γ-CD-MOF-3, the resultant crystals presented a different morphology when they were compared with γ-CD-MOF-1 and the reported ones. Co-crystallization of γ-CD-MOFs with OLV showed a rectangular shape as elongated prims and a bigger and less homogeneous size than in the synthesis with KOH. The differences in size and homogeneity may be due to the incubation time with PEG during the synthesis process. Since in γ-CD-MOF-1 the incubation time was 1 hour, in the co-crystallization it took 24 hours to get the precipitation of the crystals. It was reported that if enough amount of time is allowed for crystallization, larger particles will obtain but also small ones because synthesis during a short time may be also possible [14]. Therefore, the size will not be homogeneous and bigger crystals will be obtained. Differences observed in shape between MOFs obtained by co-crystallization (γ-CD-MOF-2 and γ-CD-MOF-3) and γ-CD-MOF-1 may be due to the use of the potassium salts instead of KOH as

metal source. The change of this reagent modifies an important solution parameter such as pH. For γ-CD-MOF-1, the pH of the initial solution was 12 and in the co-crystallization the pH was 7. It is reported that the pH control of the environment of the reaction medium in MOFs synthesis allows you to control the size and the morphology of the resulting crystals [31]. Moreover, the totality of studies that synthetize γ-CD-MOF use alkali media in order to get the classic cubic shapes regardless of metal source. The fact that both KCl and KNO_3 led the same elongated prisms morphologies supports this pH-dependent theory. Besides that, EDX analysis also showed the presence of potassium in the MOFs obtained by co-crystallization (Table A.1), confirming the interaction between the metal ion and the organic ligand to form this material.

Further characterization was performed using X-ray diffraction. The crystallinity of γ-CD-MOF-1 before and after the encapsulation experiments with the drug was measured by XRPD. According to reported studies about the synthesis of γ-CD-MOFs using KOH, the characteristic peaks in X-ray diffraction patterns of these materials are located in the next angles: 4º, 5.7º, 7º, 13.3º and 16.6º [32]. These positions correspond to body-centered cubic crystals of space group *I*432. XRPD results showed that the diffractogram of the unloaded MOFs presented the same peaks in comparison with the standard reference of these crystals (Fig. 2 and fig. A.4). Therefore, the crystalline phase obtained for γ-CD-MOF-1 coincided with the typical cubic unit of these materials. Comparing the data before and after the encapsulation experiment with olivetol, the crystallinity of MOFs loaded with the drug changed with respect to the unloaded crystals. The intensity of the peaks of the γ-CD-MOF-1 with OLV was significantly reduced compared to those of the unloaded MOFs (Fig. 2). This partial loss of crystallinity of the MOFs may result from the filling of pores with olivetol, the high degree of disorder of the drug and the presence of a low percentage of water in the ethanol solution used in these experiments [33]. However, the peak positions in the diffractograms were similar in both cases indicating that MOF crystals were stable after the encapsulation with olivetol [34]. Moreover, no new diffraction peaks appeared into the olivetol loaded MOFs, suggesting that the encapsulated drug is in an amorphous state. Taking into account SEM and XRPD results, we can conclude that the morphology of the γ-CD-MOF-1 was stable after the encapsulation with the drug, in spite of the partial loss of crystallinity. For γ-CD-MOF-2 and γ-CD-MOF-3, important changes were observed in the diffraction patterns (Fig. 2). The partial loss of crystallinity was observed again in the co-crystallization MOFs with a similar intensity in the diffraction peaks as in the previous case of OLV loaded γ-CD-MOF-1, probably due to the encapsulation of the drug. Furthermore, the characteristics positions peaks were located in different angles: 5.3º, 7.4º, 10.5º, 11.5º, 12.1º, 14.2º, 14.9º, 15.8º and 16.7º. These peaks did not correspond with the diffraction pattern described before for the conventional CD-MOFs synthetized with KOH, despite the metal linker has not changed. Moreover, they did not match with the peaks of raw γ-CD or any simulated references (Fig. A.4). A possible explanation for that is the pH of the initial solution during the MOF synthesis, as described before for SEM results. Since for γ-CD-MOF-1 the pH of the initial solution was around 12 due to the use of potassium hydroxide, for γ-CD-MOF-2 and γ-CD-MOF-3 the potassium salts led the initial solution to a neutral pH. It is reported that the body-centered cubic CD-MOFs were grown from solutions of basic salts, such as hydroxides and carbonates. Although this alkali media is not enough to deprotonate the hydroxyl groups of γ-CD, it seems to facilitate the growing of this type of crystals [35]. Moreover, previous studies about CD-MOFs have reported trigonal crystals with several spaces groups (*R*32, *I*4, *P*1 or $P3_2$) different from *I*432 [4,35]. In these CD-MOFs, the metal sources were not the typical potassium hydroxide. Therefore, the metal linker and the pH of the initial solution could be causes of the different morphology and diffraction pattern observed for

the CD-MOFs. This fact would explain the new diffraction patterns in γ-CD-MOF-2 and γ-CD-MOF-3 that did not match with the cubic space group *I*432 correlating to the trigonal morphology observed in their respective SEM images.

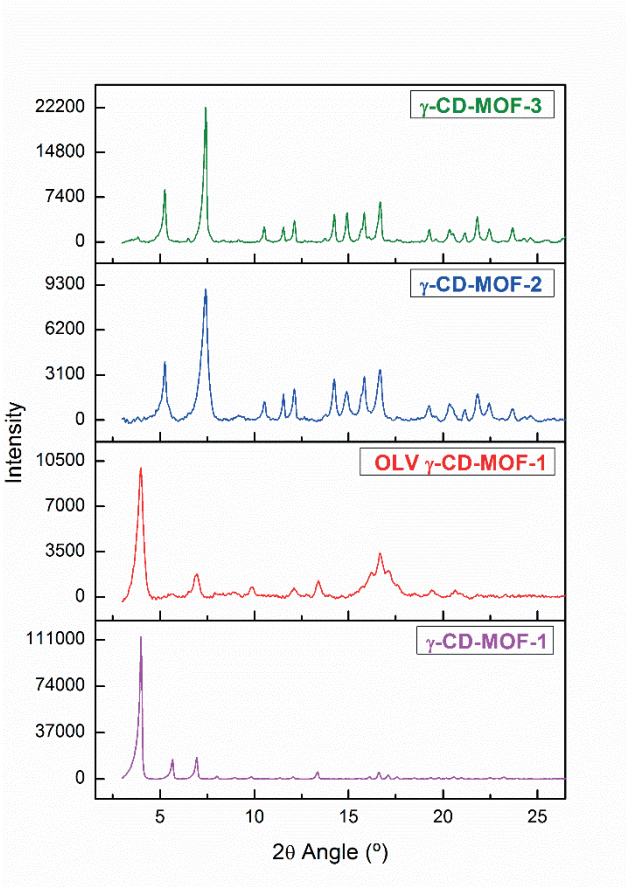

Figure 2. X-ray powder diffraction patterns of unloaded γ-CD-MOF-1 (pink), olivetol loaded γ-CD-MOF-1 (red), γ-CD-MOF-2 (blue) and γ-CD-MOF-3 (green).

3.2. Reaction synthesis yield and Olivetol content in γ-CD-MOFs

In the synthesis process of the γ-CD-MOF-1 using KOH, the reaction yield matched well with the values described in reported studies [12,36]. Nevertheless, in co-crystallization syntheses (γ-CD-MOF-2 and γ-CD-MOF-3) similar reaction yields were obtained but much lower than for the γ-CD-MOF-1 (Table 1). These differences are due to the pH change, as typical cubic CD-MOFs growing is favoured in alkali solutions [35]. As it was reported in the previous section, γ-CD-MOF-2 and γ-CD-MOF-3 presented different morphology and diffraction pattern, so the kinetics for the precipitation of the crystals should not be the same as for the γ-CD-MOF-1 crystal formation because of the different pH values due to the alternative potassium sources. In fact, this could also explain the absence of MOFs using KCl or KNO_3 but following the procedure of conventional synthesis with KOH.

Table 1. Reaction synthesis yield of γ-CD-MOF-1, γ-CD-MOF-2 and γ-CD-MOF-3 with their respective standard deviations.

MOF sample	*Reaction yield (%)*	*σ*
γ-CD-MOF-1	59.44	0.03
γ-CD-MOF-2	30.98	0.06
γ-CD-MOF-3	34.65	0.04

Not only reaction yields have changed depending on the potassium source but also the drug loading content (Fig. 3). For OLV γ-CD-MOF-1 the drug content was really poor using the impregnation method to perform the encapsulation. This could be explained due to the hybrid polarity behaviour of OLV. Olivetol dissolves perfectly in organic solvents but it is partially miscible in aqueous solutions. According to that, OLV would tend to be more comfortable on a hydrophobic environment like the inner cavities of the MOFs, than in the ethanol solution used for the encapsulation that is a relatively polar organic solvent. However, this hybrid polarity behaviour may cause that olivetol could interact with both hydrophobic and hydrophilic environments and the drug is not strongly attracted to the inner cavities of the MOFs, affecting its encapsulation efficiency. In the case of the co-crystallization process, the drug loading was higher than the impregnation method, showing γ-CD-MOF-2 slightly more OLV content than γ-CD-MOF-3 (Fig. 3). This efficiency in the co-crystallization could be explained by the formation of crystals itself. γ-CD-MOF-2 and γ-CD-MOF-3 precipitation may directly trap the drug into the MOF cavities, regardless the hybrid polarity behaviour of OLV. Moreover, drug loading values of co-crystallization synthesis were in agreement with reported studies about γ-CD-MOFs obtaining encapsulation percentages from 2% to 10% for different compounds [11,16,37].

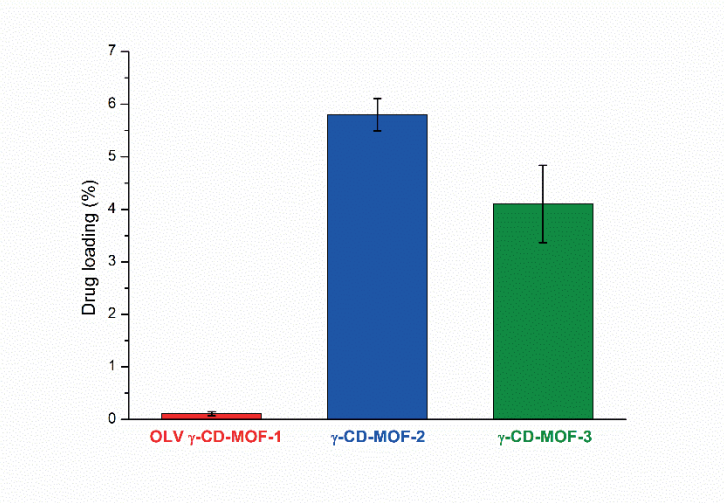

Figure 3. Drug loading percentage of olivetol in γ-CD-MOF-1, γ-CD-MOF-2 and γ-CD-MOF-3 with their respective standard deviations.

3.3. Characterization of γ-CD-MOFs and olivetol interaction: ATR-FTIR analysis

FTIR spectroscopy is a useful tool to detect the bonding changes between functional groups of the MOFs, the drug and the resulting interactions of both components. There were characteristic peaks in all γ-CD-MOF samples at 1078 cm^{-1}, 1152 cm^{-1}, 1336 cm^{-1}, 2700 – 2995 cm^{-1} and 3000 – 3670 cm^{-1} (Fig. 4A). These peaks were in agreement with previous reported literature of γ-CD-MOFs [9,38–40]. Moreover, these regions in the MOF spectra also coincided with the characteristic peaks in the γ-CD spectrum, showing the presence of the organic linker in the crystals. At 1078 cm^{-1}, an antisymmetric stretching vibration mode derived from the C–O–C groups in aliphatic ethers can be observed. These ether groups are presented in the γ-CD structure. The units of γ-CD are α-d-glucopyranose molecules with intra-monomeric ether bonds 1 → 5. These units are linked to each other through inter-monomeric ether bonds 1 → 4. The peak at 1152 cm^{-1} was assigned to the stretching vibration between carbon and oxygen atoms in C–OH groups of the two secondary alcohols that are in each unit of α-d-glucopyranose. The peak at 1336 cm^{-1} was related to the contribution of alkane groups and the band from 2700 –

2995 cm^{-1} were the contributions of the C–H antisymmetric and symmetric stretching vibrations of CH_2 and CH_3 in aliphatic compounds. These regions may come from the CH_2 group in the hydroxymethyl side chain in each α-d-glucopyranose unit of γ-CD. A wide band ranging from 3000 – 3670 cm^{-1} was assigned to stretching vibrations of the hydroxyl groups, the ones that are secondary alcohols groups but also the primary alcohol in the hydroxymethyl side chain in each α-d-glucopyranose unit. In addition to these characteristic bands of γ-CD-MOFs, the peak observed at 1640 cm^{-1} may be due to the hydroxyl groups of water molecules that still remained into the cavities of the MOFs after the drying process. The spectrum of olivetol showed the characteristic peaks of this drug according to the literature at 690 cm^{-1}, 830 cm^{-1}, 1145 cm^{-1}, 1210 cm^{-1}, 1310 cm^{-1}, 1376 cm^{-1}, 1477 cm^{-1}, 1600 cm^{-1}, 1628 cm^{-1}, 2858 cm^{-1}, 2929 cm^{-1} and 3240 cm^{-1} (Fig. 4A) [41–43]. At 690 cm^{-1} and 830 cm^{-1} wavenumbers, two peaks from CH out of plane deformations were observed because of the triple substitution in one, three and five carbon positions in the benzene ring of the OLV. The four peaks at 1145 cm^{-1}, 1210 cm^{-1}, 1310 cm^{-1} and 1376 cm^{-1} corresponded to the stretching vibrations between the carbon and oxygen atoms of the two C–OH groups that are presented in the drug molecule. Moreover, phenols absorb near 1350 cm^{-1} due to the OH deformation and give a second band due to C–OH stretching near 1210 cm^{-1}, and in this case, the two hydroxyl groups are in the benzene ring of the drug. At 1477 cm^{-1} and the double peak at 1600 and 1628 cm^{-1}, two regions of stretching vibrations derived from the interactions between the carbon atoms in the aromatic ring of the olivetol structure and the skeletal stretching vibration of -C=C- could be observed. The peaks at 2858 cm^{-1} and 2929 cm^{-1} were related to the antisymmetric stretching vibrations of C–H bond of CH_2 and CH_3 groups that are presented in the pentyl chain of the molecule. The wide peak at 3240 cm^{-1} was assigned to stretching vibrations between oxygen and hydrogen atoms of the two hydroxyls groups in the aromatic ring. A direct comparison between the infrared spectra of OLV and γ-CD-MOF-1 before and after the encapsulation process with the drug did not show any differences (Fig. 4A). This could be due to the poor encapsulation of the drug in γ-CD-MOF-1 that it was not enough to observe perceptible changes. Nevertheless, γ-CD-MOF-2 and γ-CD-MOF-3 spectra showed in the peak at 1640 cm^{-1} a double peak at 1600 and 1628 cm^{-1} corresponding to the skeletal stretching -C=C- vibration of OLV (Fig. 4B). It was observed that the 1640 cm^{-1} peak in MOFs is partially occluded by this OLV signal. These results confirmed the interaction between γ-CD-MOFs and olivetol in the co-crystallization, because if this interaction did not take place, OLV would have been removed during the washing steps with the organic solvents. Moreover, this interaction in γ-CD-MOF-2 and γ-CD-MOF-3 was in agreement with the quantification of the drug explained before, that showed a high OLV encapsulation in the co-crystallization samples. In accordance with previous literature, the interaction between OLV and γ-CD-MOFs may take place through the two phenolic hydroxyl groups of the olivetol structure and the inner cavity of the γ-CD molecules. It has been described that cyclodextrin molecules provide their cavities as a non-polar field, in which OLV is complexed through its hydroxyl groups and non-covalent interactions [44]. Furthermore, a study that encapsulates curcumin in γ-CD-MOFs to improve the stability of this compound concluded that the interaction between curcumin and the MOFs is through the phenolic hydroxyl group of the curcumin [45]. Therefore, based on the infrared results of this investigation and previous reported studies, the interactions between olivetol and γ-CD-MOFs may be due to Van der Waals forces and hydrophobic effects between the different atoms of the olivetol structure and the inner parts of the non-polar MOF cavities, since shifts on wavenumbers are due to changes on vibrations through the molecules involved and there were not significant shifts in the spectra.

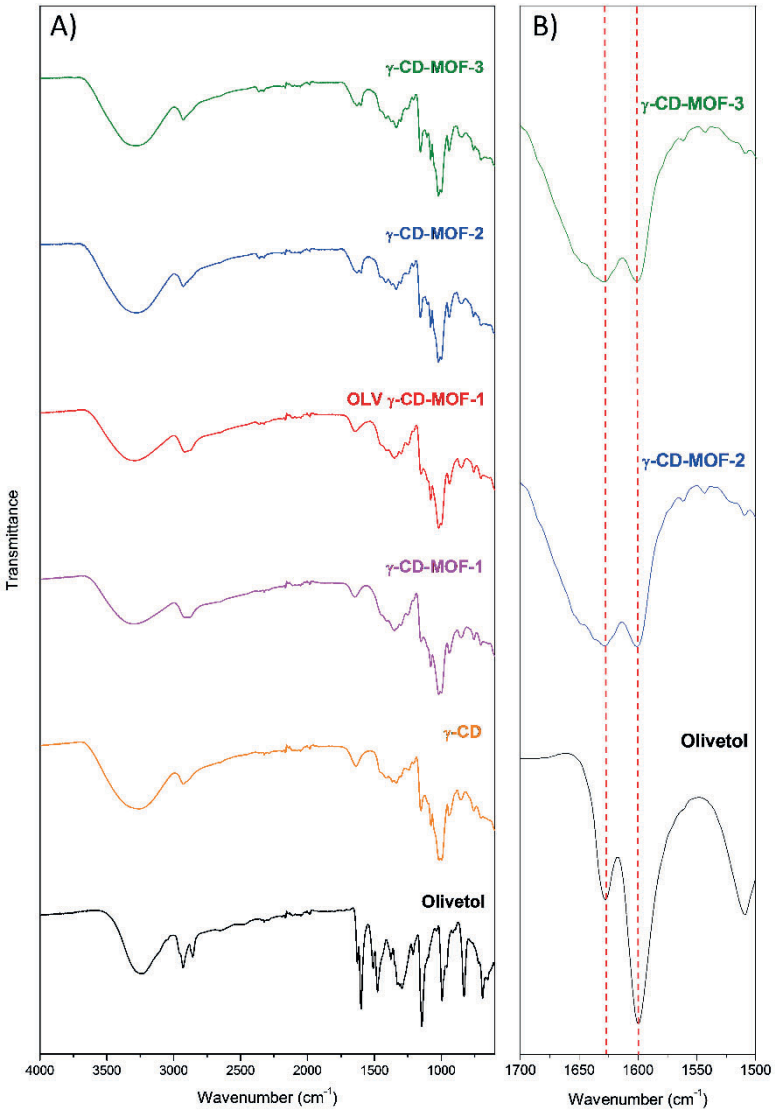

Figure 4. Attenuated Total Reflection-Fourier Transform Infrared Spectroscopy spectra of: olivetol (black), γ-CD (orange), unloaded γ-CD-MOF-1 (pink), olivetol loaded γ-CD-MOF-1 (red), γ-CD-MOF-2 (blue) and γ-CD-MOF-3 (green) from 4000 cm^{-1} to 600 cm^{-1} (A). Magnified comparison of olivetol (black), γ-CD-MOF-2 (blue) and γ-CD-MOF-3 (green) spectra (B) in the region of interest from 1700 cm^{-1} to 1500 cm^{-1} marking the double peak at 1600 and 1628 cm^{-1}.

4. Conclusions

The present work shows that MOFs based on γ-cyclodextrin and potassium ions serve as an effective drug delivery system of olivetol. OLV was used as a guest model compound of cannabinoids for its encapsulation into these CD-MOFs using impregnation and co-crystallization methods. Microwave technique was used to get a fast synthesis using different potassium sources such as the conventional KOH, as well as KCl and KNO_3 as innovative approach. SEM and PXRD analysis revealed a trigonal morphology and a different diffraction pattern when the alternative potassium compounds were employed, in comparison with the typical cubic structures obtained with KOH. This fact could be explained due to the different pH of the initial solutions. It was demonstrated that olivetol could be loaded into these carriers by co-crystallization method, solving the problem of its poor encapsulation when the impregnation method was performed. FTIR analysis corroborated the success of this encapsulation. Therefore, the combination of alternative potassium sources and the co-crystallization process resulted in

γ-CD-MOFs with a strong potential as drug carriers for cannabinoids compounds, including CBD. Moreover, these materials may become alternative drug delivery systems of unstable molecules in an alkaline or acid solution. Nevertheless, further studies would be convenient to optimize the different crystal precipitation parameters during the co-crystallization process in order to obtain suitable materials for biomedical applications.

5. Acknowledgments

The Spanish *Ministerio de Economía y Competitividad* is acknowledged for the financial support provided (Project: CTM2015-65414-C2-1-R). Jorge Rodríguez-Martínez acknowledges the FI-2018 fellowship from *Agència de Gestió d'Ajuts Universitaris i de Recerca (Generalitat de Catalunya).*

References

[1] B. Liu, Y. He, L. Han, V. Singh, X. Xu, T. Guo, F. Meng, X. Xu, P. York, Z. Liu, J. Zhang, Microwave-Assisted Rapid Synthesis of γ-Cyclodextrin Metal-Organic Frameworks for Size Control and Efficient Drug Loading, Cryst. Growth Des. 17 (2017) 1654–1660. https://doi.org/10.1021/acs.cgd.6b01658.

[2] B. Liu, H. Li, X. Xu, X. Li, N. Lv, V. Singh, J.F. Stoddart, P. York, X. Xu, R. Gref, J. Zhang, Optimized synthesis and crystalline stability of γ-cyclodextrin metal-organic frameworks for drug adsorption, Int. J. Pharm. 514 (2016) 212–219. https://doi.org/10.1016/j.ijpharm.2016.09.029.

[3] H. Cai, Y.L. Huang, D. Li, Biological metal–organic frameworks: Structures, host–guest chemistry and bio-applications, Coord. Chem. Rev. 378 (2019) 207–221. https://doi.org/10.1016/J.CCR.2017.12.003.

[4] R.A. Smaldone, R.S. Forgan, H. Furukawa, J.J. Gassensmith, A.M.Z. Slawin, O.M. Yaghi, J.F. Stoddart, Metalorganic frameworks from edible natural products, Angew. Chemie - Int. Ed. 49 (2010) 8630–8634. https://doi.org/10.1002/anie.201002343.

[5] I. Kritskiy, T. Volkova, A. Surov, I. Terekhova, γ-Cyclodextrin-metal organic frameworks as efficient microcontainers for encapsulation of leflunomide and acceleration of its transformation into teriflunomide, Carbohydr. Polym. 216 (2019) 224–230. https://doi.org/10.1016/j.carbpol.2019.04.037.

[6] Y. Sun, L. Zheng, Y. Yang, X. Qian, T. Fu, X. Li, Z. Yang, H. Yan, C. Cui, W. Tan, Metal–Organic Framework Nanocarriers for Drug Delivery in Biomedical Applications, Nano-Micro Lett. 12 (2020) 1–29. https://doi.org/10.1007/s40820-020-00423-3.

[7] V.P. Torchilin, Multifunctional nanocarriers, Adv. Drug Deliv. Rev. 58 (2006) 1532–1555. https://doi.org/10.1016/j.addr.2006.09.009.

[8] X. Unamuno, E. Imbuluzqueta, F. Salles, P. Horcajada, M.J. Blanco-Prieto, Biocompatible porous metal-organic framework nanoparticles based on Fe or Zr for gentamicin vectorization, Eur. J. Pharm. Biopharm. 132 (2018) 11–18. https://doi.org/10.1016/J.EJPB.2018.08.013.

[9] M.P. Abuçafy, B.L. Caetano, B.G. Chiari-Andréo, B. Fonseca-Santos, A.M. do Santos, M. Chorilli, L.A. Chiavacci, Supramolecular cyclodextrin-based metal-organic frameworks as efficient carrier for anti-inflammatory drugs, Eur. J. Pharm. Biopharm. (2018). https://doi.org/10.1016/j.ejpb.2018.02.009.

[10] A.R. Khan, P. Forgo, K.J. Stine, V.T. D'Souza, Methods for selective modifications of cyclodextrins, Chem. Rev. 98 (1998) 1977–1996. https://doi.org/10.1021/cr970012b.

[11] Y. Chen, K. Tai, P. Ma, J. Su, W. Dong, Y. Gao, L. Mao, J. Liu, F. Yuan, Novel γ-cyclodextrin-metal–organic frameworks for encapsulation of curcumin with improved loading capacity, physicochemical stability and controlled release properties, Food Chem. 347 (2021). https://doi.org/10.1016/j.foodchem.2020.128978.

[12] Y. Han, W. Liu, J. Huang, S. Qiu, H. Zhong, D. Liu, J. Liu, Cyclodextrin-Based Metal-Organic Frameworks (CD-MOFs) in Pharmaceutics and Biomedicine, Pharmaceutics. (2018). https://doi.org/10.3390/pharmaceutics10040271.

[13] J. Qiu, X. Li, R. Gref, A. Vargas-Berenguel, Carbohydrates in metal organic frameworks: Supramolecular assembly and surface modification for biomedical applications, Elsevier Inc., 2020. https://doi.org/10.1016/b978-0-12-816984-1.00022-6.

[14] N.A. Khan, S.H. Jhung, Synthesis of metal-organic frameworks (MOFs) with microwave or ultrasound: Rapid reaction, phase-selectivity, and size reduction, Coord. Chem. Rev. 285 (2015) 11–23. https://doi.org/10.1016/j.ccr.2014.10.008.

[15] K. Pintado-Palomino, O. Peitl Filho, E.D. Zanotto, C. Tirapelli, A clinical, randomized, controlled study on the use of desensitizing agents during tooth bleaching, J. Dent. 43 (2015) 1099–1105. https://doi.org/10.1016/J.JDENT.2015.07.002.

[16] Z. Hu, S. Li, S. Wang, B. Zhang, Q. Huang, Encapsulation of menthol into cyclodextrin metal-organic frameworks: Preparation, structure characterization and evaluation of complexing capacity, Food Chem. 338 (2021) 127839. https://doi.org/10.1016/j.foodchem.2020.127839.

[17] Y. He, X. Hou, J. Guo, Z. He, T. Guo, Y. Liu, Y. Zhang, J. Zhang, N. Feng, Activation of a gamma–cyclodextrin–

based metal–organic framework using supercritical carbon dioxide for high–efficient delivery of honokiol, Carbohydr. Polym. 235 (2020) 115935. https://doi.org/10.1016/j.carbpol.2020.115935.

[18] N. Noreen, F. Muhammad, B. Akhtar, F. Azam, M.I. Anwar, Is cannabidiol a promising substance for new drug development? A review of its potential therapeutic applications, Crit. Rev. Eukaryot. Gene Expr. 28 (2018) 73–86. https://doi.org/10.1615/CritRevEukaryotGeneExpr.2018021528.

[19] S. Atalay, I. Jarocka-karpowicz, E. Skrzydlewskas, Antioxidative and anti-inflammatory properties of cannabidiol, Antioxidants. 9 (2020) 1–20. https://doi.org/10.3390/antiox9010021.

[20] S.A. Millar, R.F. Maguire, A.S. Yates, S.E. O'Sullivan, Towards Better Delivery of Cannabidiol (CBD), Pharm. 2020, Vol. 13, Page 219. 13 (2020) 219. https://doi.org/10.3390/PH13090219.

[21] A.I. Fraguas-Sánchez, A. Fernández-Carballido, R. Simancas-Herbada, C. Martin-Sabroso, A.I. Torres-Suárez, CBD loaded microparticles as a potential formulation to improve paclitaxel and doxorubicin-based chemotherapy in breast cancer, Int. J. Pharm. 574 (2020) 118916. https://doi.org/10.1016/j.ijpharm.2019.118916.

[22] R.A. Ross, Anandamide and vanilloid TRPV1 receptors, Br. J. Pharmacol. 140 (2003) 790–801. https://doi.org/10.1038/sj.bjp.0705467.

[23] A.I. Fraguas-Sánchez, A. Fernández-Carballido, C. Martin-Sabroso, A.I. Torres-Suárez, Stability characteristics of cannabidiol for the design of pharmacological, biochemical and pharmaceutical studies, J. Chromatogr. B. 1150 (2020) 122188. https://doi.org/10.1016/J.JCHROMB.2020.122188.

[24] C. Itin, D. Barasch, A.J. Domb, A. Hoffman, Prolonged oral transmucosal delivery of highly lipophilic drug cannabidiol, Int. J. Pharm. 581 (2020). https://doi.org/10.1016/j.ijpharm.2020.119276.

[25] A.I. Fraguas-Sánchez, A.I. Torres-Suárez, M. Cohen, F. Delie, D. Bastida-Ruiz, L. Yart, C. Martin-Sabroso, A. Fernández-Carballido, PLGA nanoparticles for the intraperitoneal administration of CBD in the treatment of ovarian cancer: *In vitro* and *in Ovo* assessment, Pharmaceutics. 12 (2020) 1–19. https://doi.org/10.3390/pharmaceutics12050439.

[26] P. Lv, D. Zhang, M. Guo, J. Liu, X. Chen, R. Guo, Y. Xu, Q. Zhang, Y. Liu, H. Guo, M. Yang, Structural analysis and cytotoxicity of host-guest inclusion complexes of cannabidiol with three native cyclodextrins, J. Drug Deliv. Sci. Technol. 51 (2019) 337–344. https://doi.org/10.1016/j.jddst.2019.03.015.

[27] A.P. Matarazzo, L.M.S. Elisei, F.C. Carvalho, R. Bonfílio, A.L.M. Ruela, G. Galdino, G.R. Pereira, Mucoadhesive nanostructured lipid carriers as a cannabidiol nasal delivery system for the treatment of neuropathic pain, Eur. J. Pharm. Sci. 159 (2021). https://doi.org/10.1016/j.ejps.2020.105698.

[28] P. Taslimi, İ. Gulçin, Antioxidant and anticholinergic properties of olivetol, J. Food Biochem. 42 (2018). https://doi.org/10.1111/jfbc.12516.

[29] T.J. Raharjo, W. Te Chang, Y.H. Choi, A.M.G. Peltenburg-Looman, R. Verpoorte, Olivetol as product of a polyketide synthase in *Cannabis sativa* L, Plant Sci. 166 (2004) 381–385. https://doi.org/10.1016/J.PLANTSCI.2003.09.027.

[30] A. Brizzi, F. Aiello, S. Boccella, M.G. Cascio, L. De Petrocellis, M. Frosini, F. Gado, A. Ligresti, L. Luongo, P. Marini, C. Mugnaini, F. Pessina, F. Corelli, S. Maione, C. Manera, R.G. Pertwee, V. Di Marzo, Synthetic bioactive olivetol-related amides: The influence of the phenolic group in cannabinoid receptor activity, Bioorganic Med. Chem. 28 (2020) 115513. https://doi.org/10.1016/j.bmc.2020.115513.

[31] H. Guo, Y. Zhu, S. Wang, S. Su, L. Zhou, H. Zhang, Combining coordination modulation with acid-base adjustment for the control over size of metal-organic frameworks, Chem. Mater. 24 (2012) 444–450. https://doi.org/10.1021/cm202593h.

[32] D. Ke, J.F. Feng, D. Wu, J.B. Hou, X.Q. Zhang, B.J. Li, S. Zhang, Facile stabilization of a cyclodextrin metal-organic framework under humid environment: Via hydrogen sulfide treatment, RSC Adv. 9 (2019) 18271–18276. https://doi.org/10.1039/c9ra03079d.

[33] N. Motakef-Kazemi, S.A. Shojaosadati, A. Morsali, In situ synthesis of a drug-loaded MOF at room temperature, Microporous Mesoporous Mater. (2014). https://doi.org/10.1016/j.micromeso.2013.11.036.

[34] M. Al Haydar, H.R. Abid, B. Sunderland, S. Wang, Metal organic frameworks as a drug delivery system for flurbiprofen, Drug Des. Devel. Ther. (2017). https://doi.org/10.2147/DDDT.S145716.

[35] R.S. Forgan, R.A. Smaldone, J.J. Gassensmith, H. Furukawa, D.B. Cordes, Q. Li, C.E. Wilmer, Y.Y. Botros, R.Q. Snurr, A.M.Z. Slawin, J.F. Stoddart, Nanoporous carbohydrate metal-organic frameworks, J. Am. Chem. Soc. 134 (2012) 406–417. https://doi.org/10.1021/ja208224f.

[36] I. Roy, J.F. Stoddart, Cyclodextrin Metal–Organic Frameworks and Their Applications, Acc. Chem. Res. (2021). https://doi.org/10.1021/acs.accounts.0c00695.

[37] G. Zhang, F. Meng, Z. Guo, T. Guo, H. Peng, J. Xiao, B. Liu, V. Singh, S. Gui, P. York, W. Qian, L. Wu, J. Zhang, Enhanced stability of vitamin A palmitate microencapsulated by γ-cyclodextrin metal-organic frameworks, J. Microencapsul. 35 (2018) 249–258. https://doi.org/10.1080/02652048.2018.1462417.

[38] T. Dong, Y. He, K.M. Shin, Y. Inoue, Formation and characterization of inclusion complexes of poly(butylene succinate) with α- and γ-cyclodextrins, Macromol. Biosci. 4 (2004) 1084–1091. https://doi.org/10.1002/mabi.200400054.

[39] M. Wei, A.E. Tonelli, Compatiblization of polymers via coalescence from their common cyclodextrin inclusion compounds, Macromolecules. 34 (2001) 4061–4065. https://doi.org/10.1021/ma010235a.

[40] Y. Xiong, L. Wu, T. Guo, C. Wang, W. Wu, Y. Tang, T. Xiong, Y. Zhou, W. Zhu, J. Zhang, Crystal Transformation

of β-CD-MOF Facilitates Loading of Dimercaptosuccinic Acid, AAPS PharmSciTech. 20 (2019) 1–9. https://doi.org/10.1208/s12249-019-1422-z.

[41] M. Kumar Trivedi, A. Branton, Characterisation of Physical, Spectral and Thermal Properties of Biofield treated Resorcinol, Org. Chem. Curr. Res. 04 (2015). https://doi.org/10.4172/2161-0401.1000146.

[42] D.J. Prasad Reddy, A.V. Rajulu, V. Arumugam, M.D. Naresh, M. Muthukrishnan, Effects of resorcinol on the mechanical properties of soy protein isolate films, J. Plast. Film Sheeting. 25 (2009) 221–233. https://doi.org/10.1177/8756087910365030.

[43] X. Ren, H. Cai, H. Du, J. Chang, The preparation and characterization of pyrolysis bio-oil-resorcinol-aldehyde resin cold-set adhesives for wood construction, Polymers (Basel). 9 (2017). https://doi.org/10.3390/polym9060232.

[44] OLIVETOL-CYCLODEXTRIN COMPLEXES AND REGIO-SELECTIVE PROCESS FOR PREPARING DELTA 9-TETRAHYDROCANNABINOL, (2006).

[45] Z. Moussa, M. Hmadeh, M.G. Abiad, O.H. Dib, D. Patra, Encapsulation of curcumin in cyclodextrin-metal organic frameworks: Dissociation of loaded CD-MOFs enhances stability of curcumin, Food Chem. (2016). https://doi.org/10.1016/j.foodchem.2016.06.013.

Appendices – Supporting information

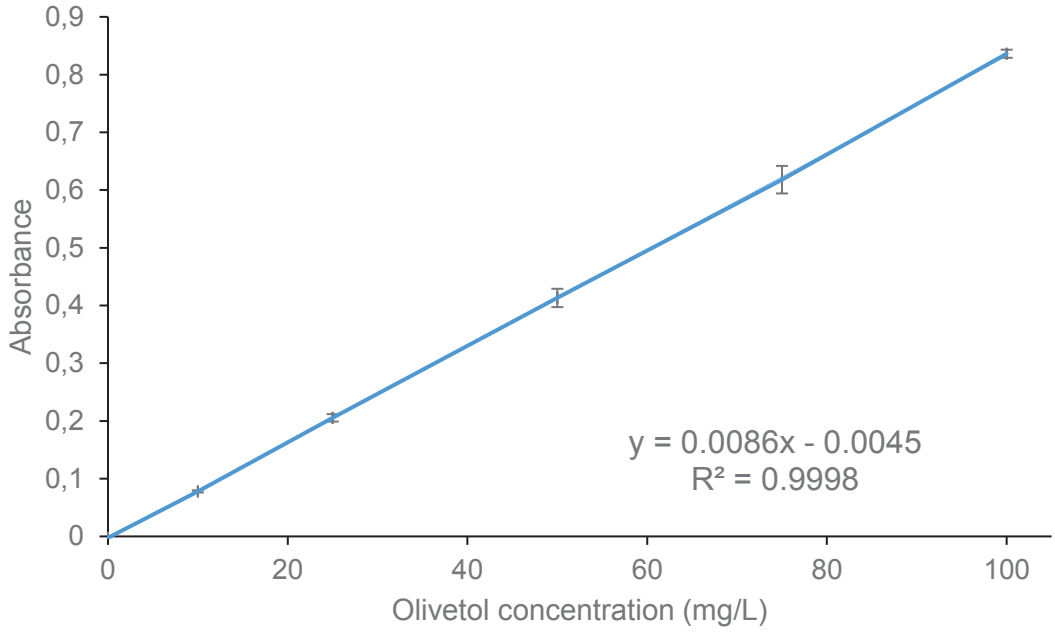

Figure A.1. Olivetol calibration curve in ethanol:milliQ water (50:50, v/v) from 0 to 100 mg/L of the drug measured at 275 nm with the equation and the linear regression coefficient. The calibration line was calculated by linear regression.

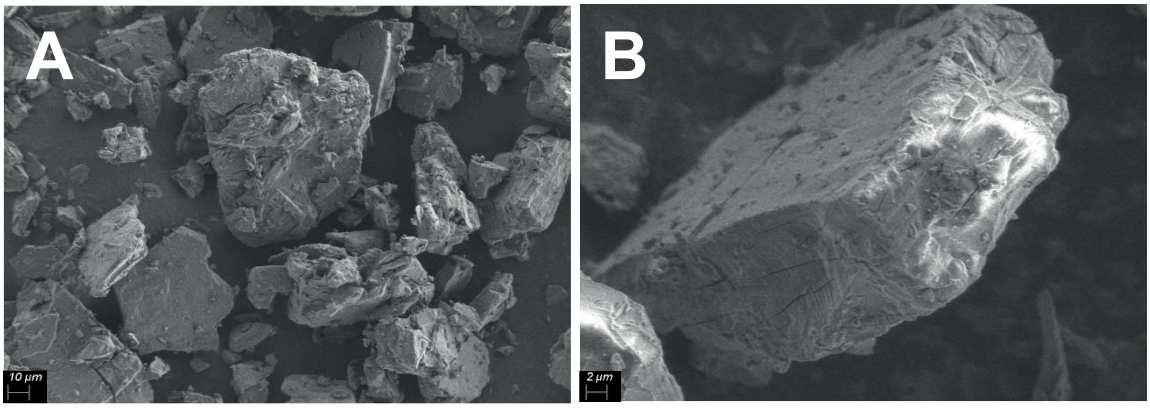

Figure A.2. Scanning electron microscopy images of raw γ-CD with a low voltage of 2 kV, 1000x (A) and 5000x (B) of magnification and a working distance of 5.6 mm.

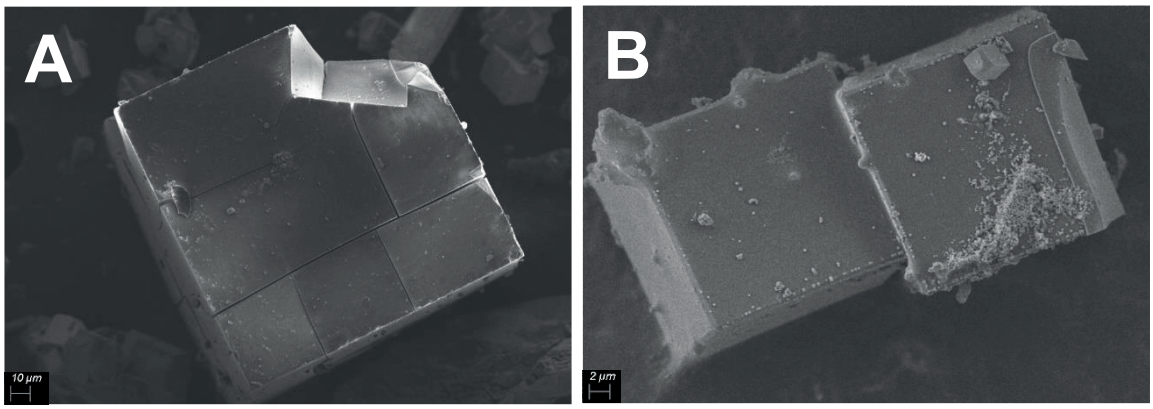

Figure A.3. Scanning electron microscopy images of γ-CD-MOFs obtained by vapor diffusion method with a low voltage of 3 kV, 1000x (A) and 5000x (B) of magnification and a working distance of 5 mm.

Table A.1. Qualitative analysis of potassium using energy-dispersive X-ray spectroscopy in γ-CD-MOF-1, γ-CD-MOF-2, γ-CD-MOF-3 and γ-CD-MOF obtained by vapor diffusion method samples.

MOF sample	Atomic percentage of potassium (%)
γ-CD-MOF-1	6
γ-CD-MOF-2	5
γ-CD-MOF-3	5
γ-CD-MOF by vapor diffusion method	7

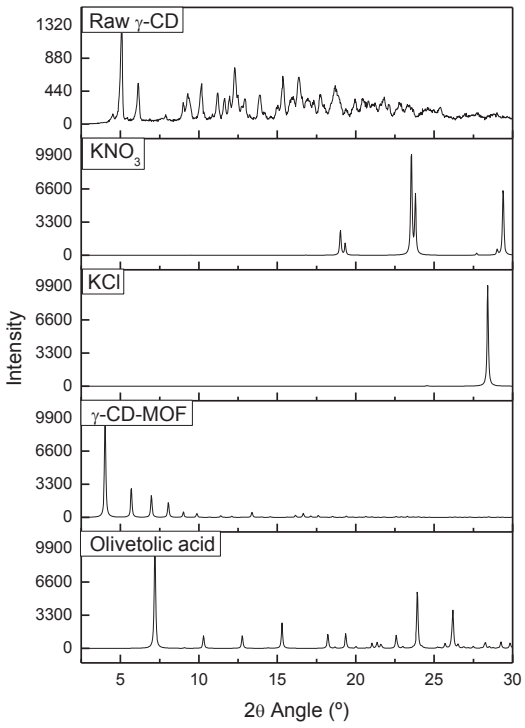

Figure A.4. X-ray powder diffraction pattern of raw γ-CD and simulated references of olivetolic acid, γ-CD-MOF, KCl and KNO_3 from Crystallography Open Database (COD) (Downs and Hall-Wallace, 2003; Graulis et al., 2009; Gražulis et al., 2015, 2012; Merkys et al., 2016; Quirós et al., 2018; Vaitkus et al., 2021).

References

Downs, R.T., Hall-Wallace, M., 2003. The American Mineralogist crystal structure database. Am. Mineral. 88, 247–250.

Graulis, S., Chateigner, D., Downs, R.T., Yokochi, A.F.T., Quirós, M., Lutterotti, L., Manakova, E., Butkus, J., Moeck, P., Le Bail, A., 2009. Crystallography Open Database - An open-access collection of crystal structures. J. Appl. Crystallogr. 42, 726–729. https://doi.org/10.1107/S0021889809016690

Gražulis, S., Daškevič, A., Merkys, A., Chateigner, D., Lutterotti, L., Quirós, M., Serebryanaya, N.R., Moeck, P., Downs, R.T., Le Bail, A., 2012. Crystallography Open Database (COD): An open-access collection of crystal structures and platform for world-wide collaboration. Nucleic Acids Res. 40, 420–427. https://doi.org/10.1093/nar/gkr900

Gražulis, S., Merkys, A., Vaitkus, A., Okulič-Kazarinas, M., 2015. Computing stoichiometric molecular composition from crystal structures. J. Appl. Crystallogr. 48, 85–91. https://doi.org/10.1107/S1600576714025904

Merkys, A., Vaitkus, A., Butkus, J., Okulič-Kazarinas, M., Kairys, V., Gražulis, S., 2016. COD::CIF::Parser: An error-correcting CIF parser for the Perl language. J. Appl. Crystallogr. 49, 292–301. https://doi.org/10.1107/S1600576715022396

Quirós, M., Gražulis, S., Girdzijauskaitė, S., Merkys, A., Vaitkus, A., 2018. Using SMILES strings for the description of chemical connectivity in the Crystallography Open Database. J. Cheminform. 10, 1–17. https://doi.org/10.1186/s13321-018-0279-6

Vaitkus, A., Merkys, A., Gražulis, S., 2021. Validation of the Crystallography Open Database using the Crystallographic Information Framework. J. Appl. Crystallogr. 54, 661–672. https://doi.org/10.1107/s1600576720016532

A methodology to control cannabinoid delivery by using Metal-Organic Frameworks. Experimental design for optimization of drug encapsulation and yield.

Jorge Rodríguez-Martínez[1(¥)], María-Jesús Sánchez-Martín*[1(¥)], Serena Iaconelli[2], Manuel Valiente[1]

[1] GTS Research Group, Department of Chemistry, Faculty of Science, Universitat Autònoma de Barcelona, 08193 Bellaterra, Spain.
[2] Department of Chemistry, University of Rome "La Sapienza", Piazzale Aldo Moro 5, 00185 Rome, Italy.

[(¥)] Shared co-first authorship

*Co-first author and author for correspondence: mariajesus.sanchez@uab.cat

Telephone: +34 93 581 4638

Abstract

Drug delivery systems (DDS) have been developed to prevent low chemical stability and poor water solubility of cannabidiol (CBD). Metal-organic frameworks (MOFs) have been already applied as DDS, but not as carriers for cannabinoids. Moreover, formulation optimization is a critical process in MOFs synthesis and drug encapsulation in terms of final quality attributes, time and economic value. Herein, γ-cyclodextrin-MOFs (γ-CD-MOFs) were synthesized using microwave-assisted technique and two potassium sources, KCl and KNO_3. For drug encapsulation, a co-crystallization method was employed and olivetol (OLV) was used as a CBD precursor. Response surface methodology (RSM) based on a face-centered Central Composite Design (CCD) was used to optimize the drug encapsulation and reaction yield through the evaluation of four independent variables: incubation temperature, incubation time, methanol content and olivetol concentration. Optimal conditions were established as 30 ºC, 15 hours, 23% and 3.1 mg/mL for KCl and 27 ºC, 18.5 hours, 28% and 3.1 mg/mL for KNO_3. The experimental values were 60% and 69% of reaction yield and 7% and 6% of drug encapsulation, for KCl and KNO_3 respectively. The experimental results were properly fitted with a quadratic model for reaction yield and two-factor interaction (2FI) model for drug encapsulation. After optimization, existing results from previous studies were improved. Optimized formulations were characterized showing that the new conditions did not compromise γ-CD-MOFs nature.

Keywords

γ-Cyclodextrin metal-organic frameworks (γ-CD-MOFs), cannabidiol (CBD), design of experiments (DoE), drug delivery systems (DDS), optimization, response surface methodology (RSM).

Graphical abstract

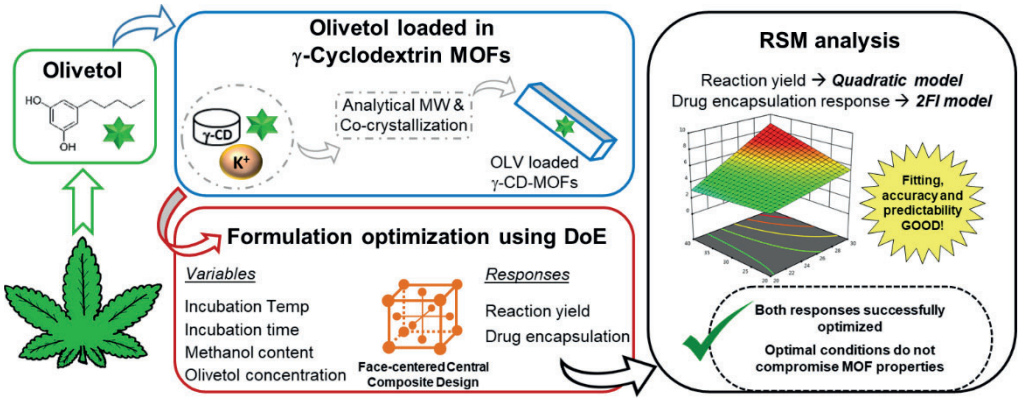

1. Introduction

Cannabidiol (CBD) is the main non-psychotropic compound in *Cannabis sativa* plant. This compound has been employed for industrial and health areas for decades and currently applications are growing, especially for biomedical and pharmaceutical purposes. CBD presents attractive properties such as analgesic, anti-inflammatory and immunomodulatory effects [1]. For this reason, cannabidiol has been used as a treatment against several diseases like cancer or epilepsy and in symptomatic relief of peripheral neuropathy with topical application [2–4]. This compound presents low chemical stability and it is easily degraded [5]. Besides, CBD is poor soluble in aqueous solutions, an important factor to consider especially in biomedical field where the final application environment is the physiological medium [6]. Therefore, researchers have been developing several strategies to overcome these difficulties and protect the compound until the final target, such as drug delivery systems (DDS) [7]. Another aspect to consider of CBD is its cost since it is not an easy affordable reagent the use of analogues or precursors of cannabidiol could be suitable for experimental approaches. Olivetol (OLV) can be an alternative, as it is an important metabolite in cannabinoids biosynthesis and chemically its structure is contained in the structure of several cannabinoids, including CBD [8].

DDS are engineered technologies that can deliver therapeutic agents in proper dosage to a targeted location. They have become very popular in the last decades since they overcome the limitations of the conventional drug administration such as toxicity, poor distribution and low efficacy [9]. There are plenty DDS like liposomes, carbon nanotubes or nanoparticles and their uses depend on the purpose of each research and the final application that profit from the different strengths of each DDS [10–13]. Other DDS that have been considered good candidates are Metal-organic frameworks (MOFs) [14,15]. However, MOFs as carriers for cannabinoids has been scarce applied in any area, including as DDS in biomedicine and pharmaceutical field.

MOFs are materials based on an organic ligand linked to a metal ion through coordination bonds in an infinite and one-two-three dimension extended network that present crystallinity [16]. These materials have promising properties like ultrahigh porosity, thermal stability and high surface areas [14]. Besides, MOFs are editable materials and their characteristics could be modify varying same parameters during the synthesis process [17,18]. Due to these properties, MOFs have emerged as potential materials since they have been employed in several applications such as catalysis, gas storage, environmental field and biomedicine [19,20]. In this last area, an important aspect to take into account is the biocompatibility of the components that comprise the MOF that should show low toxicity [21]. A class of MOFs that have arisen since some years ago due to its biocompatibility are γ-cyclodextrin metal-organic frameworks (γ-CD-MOFs) [22]. These materials have γ-CD as organic ligand and alkali-metals cations as the metal linker. γ-CD is a cyclic oligosaccharide based on eight subunits of glucopyranose that present a hydrophilic outer surface due to the hydroxyl groups of the glucopyranose and a hydrophobic inner cavity where non-polar compounds could be encapsulated [23]. Regarding the metal linker, Li^+, Na^+, Rb^+ and Cs^+ have been used from their corresponding basic salts but potassium ions are the most widely employed especially from KOH [24]. Nearly all the alkali metal salts investigated form these conventional γ-CD-MOFs with an extended body-centered cubic structure with the space group *I432* [25]. Over the last years, these MOFs have been obtained following different techniques being the vapor diffusion method one of the earliest one [22]. Hydrothermal and solvothermal methods are also common techniques that apply temperature and/or pressure to the solution that contains the organic ligand and the metal linker. Nevertheless, these methods usually take a lot of time for the whole process and the size of the

crystals is not homogeneous [26]. Recently, microwave-assisted methods have been developed showing a good reaction yields and a fast synthesis thank to the efficient heating of the microwave irradiation [27]. Regarding the encapsulation technology, the compounds could be encapsulated in different ways. Impregnation method is the most common strategy where the molecules are encapsulated into the MOFs post-synthesis through a suitable solvent [28]. During co-crystallization technique, the guest molecule is in the initial solution from the beginning of the process and the encapsulation takes place at the same time as the formation of the MOFs [29]. Considering the synthetic solution pH of the conventional γ-CD-MOFs is highly alkaline, compounds that are not stable at alkali conditions could not be encapsulated in these conventional γ-CD-MOFs using a co-crystallization method or without a post-synthesis neutralization step even when an impregnation method is employed. Therefore, the application of these materials may be limited in these cases.

Due to the MOF adaptability, the different steps in the synthesis process and the encapsulation technology play crucial roles in the final properties of the γ-CD-MOFs [17]. Therefore, reactant concentrations, incubation temperatures, reaction times, pH and solvents could be adjusted in order to get the desired characteristics. However, the optimization of all these variables at the same time in a formulation is not always affordable in terms of money and time [30,31]. Hence, a suitable option would be the use of an experimental design approach. Design of experiments (DoE) is a statistical method widely used in pharmaceutical science that allows reliable results with many variables [32–35]. DoE helps in establishing cause-and-effect relationships between the input factors and the output responses [31,36]. In experimental design, the information obtained from a set of experiments is employed to build a model. This model will establish these relationships among the factors and responses and it will be able to predict new values for the responses by introducing changes in the input factors [37]. Besides, experiments under optimal conditions could be planned using DoE. There are different statistical methods that could be applied in experimental design, but one of the most relevant and used is the response surface methodology (RSM), such as Central Composite Design (CCD) [38–41]. RSM is a multivariate statistical method that has been widely applied to the modelling, simulation and optimization of complex processes [42,43]. Multivariate analysis usually reduces the number of experiments needed to optimize the process than those obtained by conventional strategies, providing a lot of information at the same time [44–46]. Nevertheless, the selection of the range of the input factors is important to obtain the optimal conditions [42]. In addition, RSM methods consider the interactions between the studied factors and they could perform a more accurate optimization [47].

During laboratory experiments, it has been observed that multiple variables affect MOFs' synthesis. In this context, a CCD was used to explore the best conditions to obtain γ-CD-MOFs using KCl and KNO_3 as potassium sources, maintaining a neutral pH to avoid the oxidation of the drug. The analytical microwave technique and a co-crystallization method were employed in the MOF synthesis process and OLV encapsulation. Pursuing this goal, methanol content of the initial solution, drug content, incubation time and temperature were selected as input factors of the design. Reaction yield and drug encapsulation were the responses to be optimized. The design was performed two times, one per salt as implicit factor. For the first time, experimental design is applied to γ-CD-MOFs and the encapsulation of cannabinoids. Thus, this research implements the capabilities of experimental design in an innovative cannabidiol precursor γ-CD-MOFs formulation, bringing this statistical tool closer to the MOFs field.

2. Materials and methods

2.1. Reagents

Potassium hydroxide (85.5%) and potassium nitrate (99.2%) were purchased from VWR BDH Chemicals (Oud-Heverlee, Belgium). Potassium chloride (99.0%) was purchased from Sigma-Aldrich (St. Louis, MO, USA). Methanol (99.8%) and acetic acid (99.9%) were purchased from Fisher Scientific (Madrid, Spain). Dichloromethane (99.5%) and ethanol (96%) were purchased from Scharlau (Sentmenat, Spain). Polyethylene glycol 20000 was purchased from Merk (Darmstadt, Germany). Olivetol (95%) and γ-cyclodextrin (98%) were purchased from Carbosynth Ltd (Compton, United Kingdom). MilliQ water was purified through a Millipore purification system from Millipore (Milford, MA, USA).

2.2. Preparation of the samples

A fast and modified method using microwave irradiation was performed for γ-CD-MOFs synthesis [27]. Besides, a co-crystallization method was performed to load olivetol into γ-CD-MOFs.

Briefly, KCl and KNO_3 were employed as two potassium sources adding 149 mg or 202 mg respectively, and 324 mg of γ-CD to have a molar ratio of 1:8 of potassium source to organic ligand. These compounds were mixed in 16 mL of an initial solution based on milliQ water and methanol, varying the percentage of organic solvent (20, 30 and 40%). Besides, different amounts of OLV were also diluted in this initial solution to have three final concentrations of the drug (1.3, 2.2 and 3.1 mg/mL). This initial solution was treated at 50 ºC in the analytical microwave (CEM Corporation Matthews, North Carolina, USA) for 10 min and a power of 600 w. Next, 256 mg of PEG 20000 were added to trigger the precipitation of the crystals for three different incubation times (5, 15 and 25 hours) and at three different incubation temperatures (20, 25 and 30 ºC). In order to remove the unreacted material, the crystals were washed first with 10 mL of methanol and then with 10 mL more of ethanol in a centrifuge at 3000 rpm for 5 min. Finally, γ-CD-MOFs were dried and kept under vacuum at room temperature until its use and the reaction yields were calculated.

2.3. Drug release and quantification

The quantification of the OLV content into the MOFs was performed mixing 15 mg of MOF sample in 5 mL of a mixture of milliQ water and ethanol (1:1, v/v). Then, an incubation step took place at room temperature under stirring conditions (250 rpm) for 24 hours. In this way, the degradation of the crystals and the release of the drug were favoured. The resultant solutions were measured by UV-Vis spectrophotometry (Thermo Fisher Scientific, Massachusetts, USA) at 275 nm where the characteristic peak of OLV could be found. A mixture of milliQ water and ethanol (1:1, v/v) was used as the reference and a calibration curve of different known concentrations of OLV in the same solution was prepared from 0 to 100 mg/L.

The drug encapsulation for each MOF was calculated following equation 1:

$$Drug\ encapsulation\ (\%) = \frac{Encapsulated\ OLV\ into\ CD-MOFs\ (mg)}{Total\ Weight\ of\ coplexation\ powder\ (mg)} \cdot 100 \quad [1]$$

All determinations were performed by triplicate.

2.4. Experimental design and optimization

A face-centered Central Composite Design (CCD) was used for applying the response surface methodology (RSM). The effect of four independent variables (input factors) on two dependent variables (output responses) was estimated. The central point value and the range of the four independent variables studied are shown in Table 1. These ranges were defined from a preliminary screening study (not shown).

Table 1: List of independent variables and their corresponding levels.

Independent variables	Unit	Symbol	Levels		
			-1	0	+1
Incubation temperature	ºC	A	20	25	30
Incubation time	hours	B	5	15	25
Methanol content	%	C	20	30	40
Olivetol concentration	mg/mL	D	1.3	2.2	3.1

The design consisted of 27 experiments including three central points (Table 2). The design was performed two times, one per potassium salt (KCl and KNO_3) as implicit factor, and the experiments were randomly performed. Reaction yield (%) and drug encapsulation (%) were selected as dependent variables (Y_1 and Y_2 respectively).

Table 2: Experimental design matrix.

Run	Coded variables			
	A	B	C	D
1	20	25	20	1.3
2	30	25	20	3.1
3	25	15	30	2.2
4	30	5	40	1.3
5	20	5	20	1.3
6	20	15	30	2.2
7	20	5	20	3.1
8	25	15	30	2.2
9	20	5	40	1.3
10	25	15	30	1.3
11	30	5	20	1.3
12	25	25	30	2.2
13	20	25	40	3.1
14	30	25	20	1.3
15	25	15	40	2.2
16	30	25	40	1.3
17	25	15	20	2.2
18	20	5	40	3.1
19	25	15	30	2.2
20	30	5	40	3.1
21	30	15	30	2.2

22	25	5	30	2.2
23	20	25	40	1.3
24	30	25	40	3.1
25	30	5	20	3.1
26	20	25	20	3.1
27	25	15	30	3.1

The experimental results were fitted with a quadratic model for reaction yield response and two-factor interaction (2FI) model for drug encapsulation response in both potassium salts. These multiple factorial regression analyses are based in the following equations (eq. 2-3):

$$Y_{1\,(Quadratic)} = \beta_0 + \beta_1 A + \beta_2 B + \beta_3 C + \beta_4 D + \beta_5 AB + \beta_6 AC + \beta_7 AD + \beta_8 BC + \beta_9 BD + \beta_{10} CD + \beta_{11} A^2 + \beta_{12} B^2 + \beta_{13} C^2 + \beta_{14} D^2 \quad [2]$$

$$Y_{2\,(2FI)} = \beta_0 + \beta_1 A + \beta_2 B + \beta_3 C + \beta_4 D + \beta_5 AB + \beta_6 AC + \beta_7 AD + \beta_8 BC + \beta_9 BD + \beta_{10} CD \quad [3]$$

Where Y_1 and Y_2 are the dependent variables analysed (Y_1 reaction yield and Y_2 drug encapsulation); β_0 is a constant coefficient; β_1, β_2, β_3 and β_4 are the coefficients for linear effect; β_5, β_6, β_7, β_8, β_9 and β_{10} are the coefficients for interaction effect; β_{11}, β_{12}, β_{13} and β_{14} are the coefficients for quadratic effect; and A, B, D and D are the independent variables. The linear terms evaluate the effect of one factor over the response, the interaction terms analyse the effect of two factors at the same time and the quadratic terms determine a non-linear response. Statistical analysis for experimental data was performed through Design Expert Software version 11.1.0.1 (Stat-Ease Inc., Minneapolis, USA). The best fitting for each design was selected through comparison of different statistical parameters including multiple correlation coefficient (R^2), adjusted R^2, predicted R^2 and lack-of-fit. The level of significance was considered at p-value < 0.05.

To optimize the formulation of γ-CD-MOFs, reaction yield and drug encapsulation responses were maximized, in order to improve the results of previous studies with these MOFs, where reaction yield was around 31% and 35% and drug encapsulation 5.8% and 4.1%, for KCl and KNO_3 respectively.

2.5. Characterization techniques

The morphology of the γ-CD-MOFs was evaluated by Scanning Electron Microscopy (SEM) with a Zeiss Merlin FE-SEM. Secondary Electron Detector with a low voltage of 1 - 2 kV was employed to take the images. Electrons that accumulate on the sample surface were swept away with nitrogen. All measurements were performed at room temperature.

The crystallinity of the γ-CD-MOFs was determined by X-ray powder diffraction (XRPD) using a Malvern Panalytical X'Pert PRO MPD (Material Powder Diffractometer). The XRD analysis was carried at room temperature in transmission mode using a capillary spinner. The sample were filled inside borosilicate glass capillaries with outer diameter of 0.7 mm. The samples were irradiated with a ceramic X-ray tube with Cu K_α anode (l = 1.5406 Å), tube voltage of 45 kV, tube

current of 40 mA in a step size scan mode (0.03º min^{-1}) and analysed over a 2θ angle range of 2.5 - 35º.

Infrared Spectroscopy spectra of samples were obtained using an Infrared Spectrophotometer Tensor 27 equipped with an Attenuated Total Reflectance module Specac Golden Gate (ATR-FTIR, Bruker, Ettlingen, Germany). To measure the powder samples 64 scans were carried out in wavenumber from 4000 cm^{-1} to 600 cm^{-1} at a resolution of 4 cm^{-1} and at room temperature. For the background, the own diamond window of the equipment was used.

3. Results and discussion

3.1. Model fitting

A total of 27 runs were performed per potassium salt, varying the four inputs factors at three different levels. Reaction yield (Y_1) and drug encapsulation (Y_2) were the two studied responses for this experimental design. The design layout with the experimental values of the responses is shown in Table A.1 (Online Resource 1). Runs 4, 12, 16 and 20 were removed from the analysis. In case of runs 4, 16 and 20 not enough product could be obtained from the reaction due to the experimental conditions and the values of the responses were not consistent. For run 12, the values did not fit with the design and the statistics parameters became worse. Excluding these mentioned four runs, reaction yield and drug encapsulation values varied from 0.1% to 75.5% and 1.1% to 7.7% respectively. These data were employed for the experimental design analysis using Design Expert Software. ANOVA was performed for the calculations of coefficients of the polynomial equations. Results showed that quadratic and 2FI models could be used to represent the data for the reaction yield (Y_1) and drug encapsulation (Y_2) respectively in both potassium salts. The equations for the responses (eq. 4-7) explain their interactions with the independent variables (incubation temperature, A; incubation time, B; methanol content, C; olivetol concentration, D). In all the cases, the terms of the equations that presented a non-significant p-value (p-value > 0.05) were removed from the final equations in order to improve the fitting. Here below, the final reduced equations in terms of coded factors with only significant model terms are shown:

For potassium chloride:

$$Y_{1\,(Reaction\ yield)} = 32.76 - 16.21A + 5.98B - 22.15C + 18.13D + 2.52AB - 7.45AC - 12.40B^2 \quad [4]$$

$$Y_{2\,(Drug\ encapsulation)} = 6.06 + 1.62A - 0.0958B + 0.5353C - 0.6819AB - 0.4832BC \quad [5]$$

For potassium nitrate:

$$Y_{1\,(Reaction\ yield)} = 41.07 - 12.96A + 8.66B - 21.25C + 18.30D - 5.37AC + 4BD - 8.56C^2 - 8.58D^2 \quad [6]$$

$$Y_{2\,(Drug\ encapsulation)} = 5.33 + 1.85A - 0.5220B + 0.5917C + 0.3250D - 1.17AB + 1.04AC - 0.4231AD - 0.5622BC + 0.5289CD \quad [7]$$

The equations in terms of coded factors can be used to make predictions about the response for given levels of each factor. These equations are useful for identifying the relative impact of the factors by comparing the factor coefficients. A positive value in the coefficients means that there

is a synergistic effect on that response and a negative value indicates an antagonistic effect [47,48].

In all the models for both responses, statistic parameters showed a good fitting with the experimental results (Table 3). The significance of the factors was determined based on the F-values and/or p-values with 95% confidence level. The model F-values implied that selected models were significant and there was only a 0.01% chance these F-values could occur due to noise. The values of coefficient of determination (R^2) were reasonable high; values close to unity indicate a better fitting of model to experimental results. Besides, the predicted R^2 were in agreement with the adjusted ones, since in all the cases the difference between these two values was less than 0.2. Predicted *versus* actual values distributions (Online Resource 1: Fig. A.2) also show a high compatibility of these data, since the points are closely following the diagonal. Moreover, adequate precision measures the signal-to-noise ratio and a ratio greater than four is desirable, in order to use the model to navigate the design space. The lack of fit expresses the residual error compared to the pure error. Non-significant lack of fit (p-value > 0.05) for the selected models indicated its accuracy and the low error. Therefore, based on the statistical analysis, the effect of the factors on responses could be explained using a quadratic polynomial model and a 2FI model for reaction yield and drug encapsulation respectively.

Table 3: Statistics summary of the quadratic and 2FI response surface models for reaction yield and drug encapsulation responses in each potassium salt.

	Response			
	KCl		KNO_3	
	Reaction yield	Drug encapsulation	Reaction yield	Drug encapsulation
Model	Quadratic	2FI	Quadratic	2FI
F-value	92.89	11.79	31.19	23.34
Model p-values	< 0.0001	< 0.0001	< 0.0001	< 0.0001
R^2	0.9775	0.7762	0.9469	0.9417
Adjusted R^2	0.9669	0.7103	0.9165	0.9014
Predicted R^2	0.9561	0.6487	0.8507	0.7851
Adequate precision	31.92	11.97	21.10	16.99
Lack of fit p-values	0.9477	0.9651	0.5966	0.2461

Furthermore, the residuals were studied to validate the adequacy of the different models through the analysis of the normal plots and the residuals *versus* the predicted responses graphs (Fig. 1). The difference between the real response and the predicted one determines the residual value. In all the cases, the residuals were distributed in a straight line according to their normal probability. In figure 1, the distribution of the residuals *versus* predicted responses was totally random suggesting that the models were suitable and that the models showed independence and constant variance assumption.

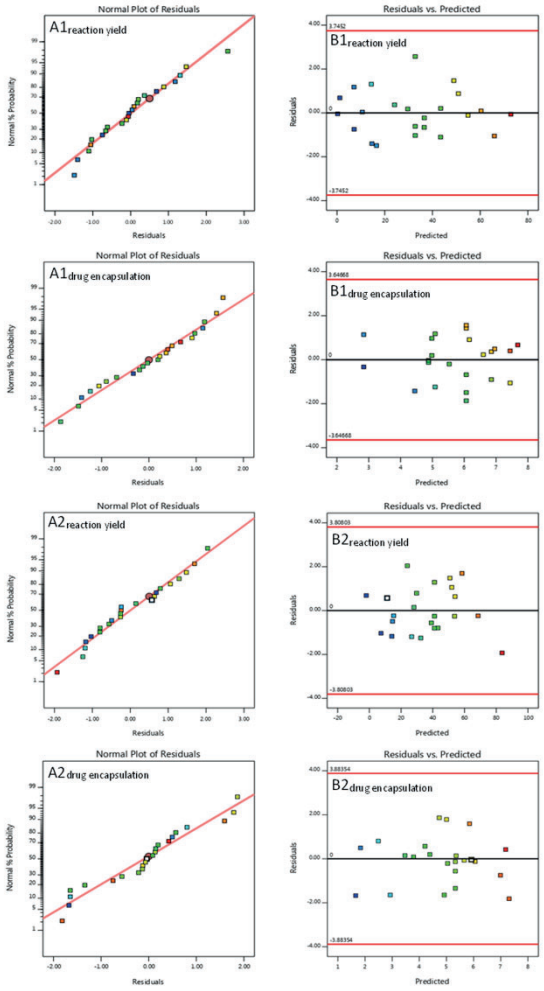

Fig. 1: Normal probability plots of the residual (A) and residual *versus* predicted response graphs (B) for KCl (1) reaction yield and drug encapsulation and for KNO_3 (2) reaction yield and drug encapsulation.

3.2. Reaction yield

The selected factors in this study were adjusted following a quadratic polynomial for reaction yield response in both potassium salts (eq. 4 and 6). After removing non-significant terms, it could be observed that the linear contributions of all the factors presented the same behaviour for KCl and KNO_3. The incubation time (B) and olivetol concentration (D) increased the reaction yield. Meanwhile, the incubation temperature (A) and methanol content (C) showed an antagonistic effect. For KCl, the interaction of A with B increased this response, but the one of A with C and the quadratic contribution of B reduced the reaction yield. For KNO_3, the interaction of B with D showed an agonistic effect, whereas the interaction of A with C and the quadratic contributions of C and D minimised this response. Some of these main and interactions effects are shown using contour plots and three-dimensional response surface plots (Fig. 2). These plots give a visual representation of this response and its relationship with the different factors.

The increment of incubation time (B) and olivetol concentration (D) increased the reaction yield. The first parameter could be explained based on crystallization kinetics, since nucleation and crystal growth [49]. These parameters are time-dependent and if the time is too short, crystal formation could not occur [50]. Therefore, the MOFs reaction yield is increasing in function of the time with the development of the crystallization process. The fact that the concentration of

the drug had a positive effect in the reaction yield may be due to an increase in the solutes concentration of the initial solution, promoting its supersaturation. The supersaturation is directly proportional to the concentration. Therefore, if the concentration is higher than the solubility, the solution is supersaturated and the crystallization process takes place [51]. The increment of olivetol could contribute to reach the supersaturation point of the initial solution, obtaining more precipitate. On the other hand, incubation temperature (A) and methanol content (C) presented a negative effect over the reaction yield. The concept of supersaturation could be also useful to explain the antagonistic effect of the incubation temperature. This parameter also depends on solubility, being inversely proportional. Increasing the temperature, the solubility also increases, decreasing the supersaturation [51]. Hence, the solution becomes under-saturated and the crystallization process does not occur. The fact that the methanol content has a negative effect over the reaction yield may be related to olivetol solubility. Since olivetol is an organic compound, it is more soluble in organic solvents than in aqueous solutions. Therefore, the higher the methanol content, the greater the amount of soluble drug in the same mixture, keeping away from the supersaturation and making more difficult the crystallization process.

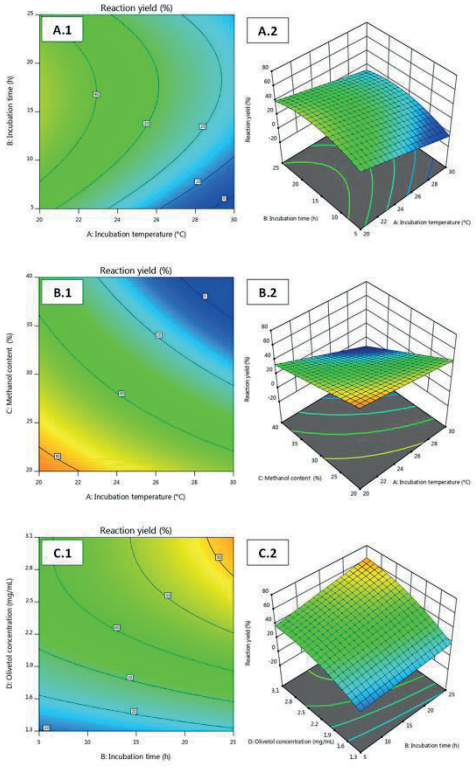

Fig. 2: Contour plots (1) and three-dimensional response surface plots (2) for reaction yield response in both salts: KCl (A and B) and KNO_3 (C).

3.3. Drug encapsulation

The effects of the factors on the drug encapsulation were studied through a 2FI polynomial for both potassium salts (eq. 5 and 7). After eliminating non-significant terms for KCl, the linear contribution of incubation temperature (A) and methanol content (C) increased the drug encapsulation. However, these responses were reduced due to the antagonistic effects observed by the linear contribution of incubation time (B) and by the interactions of A with B and B with C. In case of KNO_3, same contributions described before for KCl were observed presenting the same behaviour. Besides, the linear contribution of olivetol concentration (D),

the interactions of A with C and C with D showed an agonistic effect, while the interaction of A with D decreased the drug encapsulation. Some of these main interactions effects are shown using contour plots and three-dimensional response surface plots (Fig. 3). These plots give a visual representation of this response and its relationship with the different factors.

Incubation temperature (A), methanol content (C) and olivetol concentration (D) have a positive effect over the drug encapsulation. The behaviour of these factors could be described in terms of diffusion. The first state of Fick's law relates diffusion to concentration. This law postulates that the flux goes from a region of high concentration to regions of low concentration, being proportional to the concentration gradient [52]. Thus, olivetol molecules diffuse from the solution to the MOFs pores due to drug concentration gradient. According to Fick, diffusion is also directly proportional to the diffusion coefficient and this coefficient depends on the temperature. The relationship between this coefficient and the temperature could be explained by the Einstein equation, where a positive effect in temperature increases the thermal energy of molecules, raising its diffusion rate [53]. Besides, diffusion process is closely related to solute dissolution rate, when the dissolution rate is higher, the diffusion also increases [54]. Thus, raising the methanol content of the initial solution, more olivetol molecules will be dissolved due to the non-polar behaviour of the drug. In this way, more olivetol will be available for the diffusion into the pores, increasing the encapsulation process. The incubation time (B) contributes with a negative effect for drug encapsulation. With the time, the diffusion process is taking place from the solution where the drug is highly concentrated to the empty pores of the MOFs. However, when the drug concentration is higher in the carriers than in the medium, the diffusion transport starts in the opposite direction, trying to reach the equilibrium and decreasing the drug encapsulation [55].

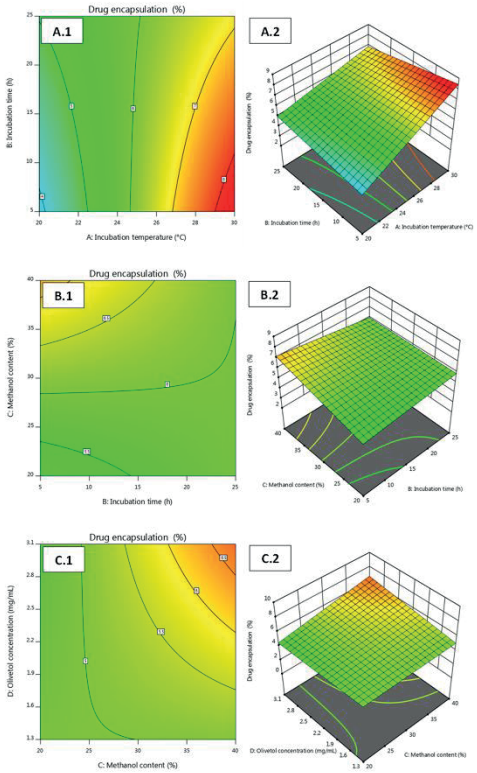

Fig. 3: Contour plots (1) and three-dimensional response surface plots (2) for drug encapsulation response in both salts: KCl (A and B) and KNO_3 (C).

3.4. Reponses optimization and verification of the models

Optimization of the independent variables was done by setting goals for each response using Design Expert software. All four independent variables were incorporated in the optimization at their design space, except the incubation time for KCl. This variable was targeted to 15 hours, considering the practical experimental conditions. The challenge of this study was maximized both responses. However, since their behaviour was the opposite, reaction yield response was targeted to 55% to be able to maximize the encapsulation. This value was selected to improve previous results of reaction yield of these CD-MOFs, which was around 35%. Besides, this number is like the one obtained when the conventional KOH is employed as potassium source. Numerical optimization values were selected using desirability function (D), where D values ranging between 0 and 1, being 0 for low desirable conditions and 1 for high desirable ones. Following this criteria, different solutions of optimal conditions were obtained with different desirability values. The solution that showed the highest desirability value was selected as optimized synthesis conditions for each potassium salt (Table 4).

Table 4: Optimized synthesis conditions for each potassium salt with its desirability value.

Potassium salt	Incubation temperature (ºC)	Incubation time (hours)	Methanol content (%)	Olivetol concentration (mg/mL)	Desirability
KCl	30	15	23.1	3.1	0.945
KNO_3	26.9	18.6	27.9	3.1	0.815

Considering the practical experimental conditions, the conditions were set to 30 ºC, 15 hours, 23% and 3.1 mg/mL for KCl and 27 ºC, 18.5 hours, 28% and 3.1 mg/mL for KNO_3.The selected optimal conditions were verified by performing the experiments under these conditions in two independent replicates per salt. The results are shown in Table 5. Validation of the experimental design was done by comparing predicted and experimental values. The obtained data were inside the limits of the 95% prediction interval in all the cases and the values of the errors found to be within an acceptable range. This means that the experimental results were comparable to the predicted results that illustrate the preciseness of the design. Moreover, the experimental results for reaction yield were even better than the predicted values. Therefore, the generated models showed sufficient accuracy and predictability for optimizing the reaction yield and drug encapsulation in the experimental conditions mentioned above. Besides, the values of both responses have been improved for both potassium salts in comparison with previous experimental results. Reaction yield values have doubled, while drug encapsulation has increased by 20% for KCl and 46% for KNO_3.

Table 5: Experimental and predicted values of both responses at optimized conditions for each salt (PI = prediction interval).

Potassium salt	Response	Predicted value	Experimental value	95% PI low	95% PI high	Error
KCl	Reaction yield (%)	55	60 ± 2	46	64	5
	Drug encapsulation (%)	7.3	7.0 ± 0.7	5.5	9.1	0.3
KNO_3	Reaction yield (%)	55	69 ± 3	39	71	14
	Drug encapsulation (%)	5.6	6.0 ± 0.4	4.4	6.7	0.4

3.5. Characterization of the optimal formulations

The morphology and the crystallinity of the optimal formulations were studied using SEM and PXRD analysis (Fig. 4.a). Both γ-CD-MOFs formulations showed a rectangular shape as elongated prims. The length of most of the crystals was around 2 to 50 μm, but there were also crystal sizes out of this range. This fact may be due to the long time during the incubation step that was 15 and 18.5 hours for KCl and KNO_3 respectively. It was reported that if enough amount of time is allowed during a crystallization process, the size of the resulting crystals would not be homogeneous [56]. Concerning the diffraction patterns, both formulations showed the same characteristics peaks that were in different angles: 5.3º, 7.4º, 10.5º, 11.5º, 12.1º, 14.2º, 14.9º, 15.8º and 16.7º. Besides, the sharp peaks in the diffraction patterns revealed a high crystallinity of the MOFs, despite the improvement in the drug encapsulation following the optimal conditions. These peaks positions may correspond to a triclinic, tetragonal o trigonal space groups such as *R*32, *I*4, *P*1 or *P*32, that were already reported in CD-MOFs where the metal sources were not the typical potassium hydroxide [57]. These diffraction patterns would be correlated to the rectangular prism morphologies observed in their respective SEM analysis. Considering these SEM and PXRD results, it is remarkable to mention that the new optimal conditions did not compromise the morphology and the crystallinity of these γ-CD-MOFs.

FTIR analysis showed the characteristic peaks in both γ-CD-MOF formulations at 1078 cm^{-1}, 1152 cm^{-1}, 1336 cm^{-1}, 2700 – 2995 cm^{-1} and 3000 – 3670 cm^{-1} (Fig. 4.b). These peaks were in agreement with previous reported studies of these MOFs and they matched with the characteristic peaks in the γ-CD spectrum, confirming the presence of the organic ligand in the crystals [58]. At 1078 cm^{-1} and 1152 cm^{-1}, stretching vibrations derived from -C-O-C- and C–OH bonds in cyclodextrin sugars could be observed respectively. The peak at 1336 cm^{-1} and the band from 2700 – 2995 cm^{-1} were related to the contributions of alkane groups. The wide band from 3000 – 3670 cm^{-1} was assigned to stretching vibrations of the hydroxyl groups from the cyclodextrin molecules. Besides, the peak observed at 1640 cm^{-1} could be due to the water molecules that remained into the cavities of the MOFs after the drying process. The spectrum of olivetol showed its characteristic peaks according to the literature at 3240 cm^{-1}, 2929 cm^{-1}, 2858 cm^{-1} and a double peak with two peaks at 1628 cm^{-1} and 1600 cm^{-1}. These peaks correspond to the -OH stretching vibration, -CH symmetric and antisymmetric stretching in the aliphatic chain and the -C=C- stretching vibration from the aromatic ring respectively (Fig. 4.b) [59]. A direct comparison between the infrared spectra of OLV and both γ-CD-MOFs revealed that the single peak at 1640 cm^{-1} showed a double peak at 1600 and 1628 cm^{-1} that it was not in the raw γ-CD spectrum and it may correspond to the skeletal stretching -C=C- vibration of the drug (Fig. 4.B). It means that olivetol is interacting with the γ-CD-MOFs as it is also reported in the results for the drug encapsulation response. These interactions could occur through Van der Waals forces and hydrophobic effects, due to there were not significant shifts in the spectra.

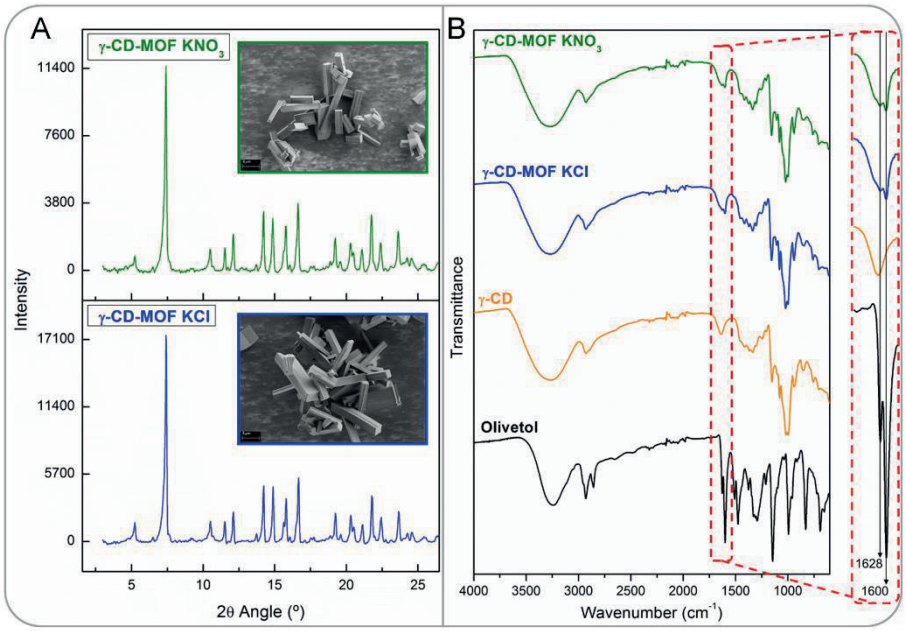

Fig. 4: Scanning electron microscopy images and X-ray powder diffraction patterns of optimal γ-CD-MOF formulations using KCl (blue) and KNO_3 (green) as potassium sources (a). Attenuated Total Reflection-Fourier Transform Infrared Spectroscopy spectra of: olivetol (black), γ-CD (orange), optimal γ-CD-MOF formulations using KCl (blue) and KNO_3 (green) as potassium sources from 4000 cm^{-1} to 600 cm^{-1}, showing a magnification of the double peak at 1600 and 1628 cm^{-1} (b).

4. Conclusions

In the present work, olivetol-loaded γ-CD-MOFs were successfully prepared with KCl and KNO_3 as potassium sources, using the analytical microwave for a fast synthesis and a co-crystallization process for the drug encapsulation. The effect of four independent variables in the synthesis was investigated using RSM. Two models per potassium salt were obtained for predicting reaction yield and drug encapsulation of the formulations. Reaction yield response followed a quadratic model while drug encapsulation response adjusted to a 2FI model for both salts. In all the cases, models showed a suitable fitting following statistical analysis. Reaction yield and drug encapsulation were maximized for each formulation. The models for predicting both responses showed a good agreement between the experimental and predicted values, demonstrating the application of experimental design for optimization purposes. A comparison with previous studies, our results show both the reaction yields obtained being twice as high as in those studies and drug encapsulation has increased in the optimized formulations (by 20% for KCl and 46% for KNO_3). These formulations were characterized showing that the new optimal conditions did not compromise the structure of the olivetol loaded γ-CD-MOFs. Finally, the application of experimental design capabilities such as RSM, scarcely used to optimize our CD-MOFs, has been successfully implemented.

5. Conflict of Interest

The authors declare not to have competing financial interests or personal relationships to influence the work reported in this paper.

6. Acknowledgments and Funding Information

The Spanish *Ministerio de Economía y Competitividad*, is acknowledged for the financial support provided (Project: CTM2015-65414-C2-1-R). Jorge Rodríguez-Martínez acknowledges the FI-

2018 fellowship *from Agència de Gestió d'Ajuts Universitaris i de Recerca* (*Generalitat de Catalunya*). Serena Iaconelli acknowledges 1/2020 Erasmus+ grant from European Commission. The authors acknowledge Professor Federico Marini from University of Rome "La Sapienza" for his support.

References

[1] S. Atalay, I. Jarocka-Karpowicz, E. Skrzydlewska, Antioxidative and Anti-Inflammatory Properties of Cannabidiol, Antioxidants 2020, Vol. 9, Page 21. 9 (2019) 21. https://doi.org/10.3390/ANTIOX9010021.

[2] H. Li, Y. Liu, D. Tian, L. Tian, X. Ju, L. Qi, Y. Wang, C. Liang, Overview of cannabidiol (CBD) and its analogues: Structures, biological activities, and neuroprotective mechanisms in epilepsy and Alzheimer's disease, Eur. J. Med. Chem. 192 (2020) 112163. https://doi.org/10.1016/J.EJMECH.2020.112163.

[3] M. Ożarowski, T.M. Karpiński, A. Zielińska, E.B. Souto, K. Wielgus, Cannabidiol in Neurological and Neoplastic Diseases: Latest Developments on the Molecular Mechanism of Action, Int. J. Mol. Sci. 2021, Vol. 22, Page 4294. 22 (2021) 4294. https://doi.org/10.3390/IJMS22094294.

[4] D.H. Xu, B.D. Cullen, M. Tang, Y. Fang, The Effectiveness of Topical Cannabidiol Oil in Symptomatic Relief of Peripheral Neuropathy of the Lower Extremities, Curr. Pharm. Biotechnol. 21 (2019) 390–402. https://doi.org/10.2174/1389201020666191202111534.

[5] A.I. Fraguas-Sánchez, A. Fernández-Carballido, C. Martin-Sabroso, A.I. Torres-Suárez, Stability characteristics of cannabidiol for the design of pharmacological, biochemical and pharmaceutical studies, J. Chromatogr. B Anal. Technol. Biomed. Life Sci. 1150 (2020) 122188. https://doi.org/10.1016/j.jchromb.2020.122188.

[6] S.A. Millar, R.F. Maguire, A.S. Yates, S.E. O'Sullivan, Towards Better Delivery of Cannabidiol (CBD), Pharm. 2020, Vol. 13, Page 219. 13 (2020) 219. https://doi.org/10.3390/PH13090219.

[7] N.M. Francke, F. Schneider, K. Baumann, H. Bunjes, Formulation of Cannabidiol in Colloidal Lipid Carriers, Mol. 2021, Vol. 26, Page 1469. 26 (2021) 1469. https://doi.org/10.3390/MOLECULES26051469.

[8] L.J. Kearsey, N. Prandi, V. Karuppiah, C. Yan, D. Leys, H. Toogood, E. Takano, N.S. Scrutton, Structure of the *Cannabis sativa* olivetol-producing enzyme reveals cyclization plasticity in type III polyketide synthases, FEBS J. 287 (2020) 1511–1524. https://doi.org/10.1111/FEBS.15089.

[9] G. Tiwari, R. Tiwari, B. Sriwastawa, L. Bhati, S. Pandey, P. Pandey, S.K. Bannerjee, Drug delivery systems: An updated review, Int. J. Pharm. Investig. 2 (2012) 2. https://doi.org/10.4103/2230-973X.96920.

[10] M. Alavi, N. Karimi, M. Safaei, Application of Various Types of Liposomes in Drug Delivery Systems, Adv. Pharm. Bull. 7 (2017) 3. https://doi.org/10.15171/APB.2017.002.

[11] B.R.C. de Menezes, K. Faquine Rodrigues, B.C. da Silva Fonseca, R. Guimarães Ribas, T.L. do Amaral Montanheiro, G. Patrocínio Thim, Recent advances in the use of carbon nanotubes as smart biomaterials, J. Mater. Chem. B. 7 (2019) 1343–1360. https://doi.org/10.1039/C8TB02419G.

[12] M.J. Mitchell, M.M. Billingsley, R.M. Haley, M.E. Wechsler, N.A. Peppas, R. Langer, Engineering precision nanoparticles for drug delivery, Nat. Rev. Drug Discov. 2020 202. 20 (2020) 101–124. https://doi.org/10.1038/s41573-020-0090-8.

[13] M. Malakouti-Nejad, H. Bardania, F. Aliakbari, A. Baradaran-Rafii, E. Elahi, D. Monti, D. Morshedi, Formulation of nanoliposome-encapsulated bevacizumab (Avastin): Statistical optimization for enhanced drug encapsulation and properties evaluation, Int. J. Pharm. 590 (2020) 119895. https://doi.org/10.1016/j.ijpharm.2020.119895.

[14] C.-Y. Sun, C. Qin, X.-L. Wang, Z.-M. Su, Metal-organic frameworks as potential drug delivery systems, Expert Opin. Drug Deliv. (2013). https://doi.org/10.1517/17425247.2013.741583.

[15] C. Carrillo-Carrión, Nanoscale metal–organic frameworks as key players in the context of drug delivery: evolution toward theranostic platforms, Anal. Bioanal. Chem. 412 (2020) 37–54. https://doi.org/10.1007/s00216-019-02217-y.

[16] H.-C. "Joe" Zhou, Susumu Kitagawa, Metal–Organic Frameworks (MOFs), Chem. Soc. Rev. 43 (2014) 5415–5418. https://doi.org/10.1039/C4CS90059F.

[17] R.S. Forgan, Metal-Organic Frameworks: Edible Frameworks, Encycl. Inorg. Bioinorg. Chem. (2014) 1–13. https://doi.org/10.1002/9781119951438.EIBC2192.

[18] W. Gong, L. Zhang, Y. Yu, B. Lin, Y. Wang, M. Guo, Y. Cao, A novel fluorescent strategy based on double modifications of metal organic framework material CAU-10-NH2 for low background and high sensitivity determination of H2S, Talanta. 229 (2021) 122271. https://doi.org/10.1016/j.talanta.2021.122271.

[19] C. Pettinari, F. Marchetti, N. Mosca, G. Tosi, A. Drozdov, Application of metal − organic frameworks, Polym. Int. 66 (2017) 731–744. https://doi.org/10.1002/PI.5315.

[20] K. Dong, Y. Zhang, L. Zhang, Z. Wang, J. Ren, X. Qu, Facile preparation of metal–organic frameworks-based hydrophobic anticancer drug delivery nanoplatform for targeted and enhanced cancer treatment, Talanta. 194 (2019) 703–708. https://doi.org/10.1016/j.talanta.2018.10.101.

[21] Namita Singh, Somayah qutub, N. M. Khashab, Biocompatibility and Biodegradability of Metal Organic Frameworks for Biomedical Applications, J. Mater. Chem. B. (2021). https://doi.org/10.1039/D1TB01044A.

[22] Y. Han, W. Liu, J. Huang, S. Qiu, H. Zhong, D. Liu, J. Liu, Cyclodextrin-Based Metal-Organic Frameworks (CD-

MOFs) in Pharmaceutics and Biomedicine, Pharmaceutics. (2018). https://doi.org/10.3390/pharmaceutics10040271.

[23] P. Saokham, T. Loftsson, γ-Cyclodextrin, Int. J. Pharm. 516 (2017) 278–292. https://doi.org/10.1016/J.IJPHARM.2016.10.062.

[24] I. Roy, J.F. Stoddart, Cyclodextrin Metal–Organic Frameworks and Their Applications, Acc. Chem. Res. (2021). https://doi.org/10.1021/acs.accounts.0c00695.

[25] T. Rajkumar, D. Kukkar, K.H. Kim, J.R. Sohn, A. Deep, Cyclodextrin-metal–organic framework (CD-MOF): From synthesis to applications, J. Ind. Eng. Chem. 72 (2019) 50–66. https://doi.org/10.1016/J.JIEC.2018.12.048.

[26] P.S. Sharanyakanth, M. Radhakrishnan, Synthesis of metal-organic frameworks (MOFs) and its application in food packaging: A critical review, Trends Food Sci. Technol. 104 (2020) 102–116. https://doi.org/10.1016/J.TIFS.2020.08.004.

[27] B. Liu, Y. He, L. Han, V. Singh, X. Xu, T. Guo, F. Meng, X. Xu, P. York, Z. Liu, J. Zhang, Microwave-Assisted Rapid Synthesis of γ-Cyclodextrin Metal-Organic Frameworks for Size Control and Efficient Drug Loading, Cryst. Growth Des. 17 (2017) 1654–1660. https://doi.org/10.1021/acs.cgd.6b01658.

[28] M. Shen, D. Liu, T. Ding, Cyclodextrin-metal-organic frameworks (CD-MOFs): main aspects and perspectives in food applications, Curr. Opin. Food Sci. 41 (2021) 8–15. https://doi.org/10.1016/J.COFS.2021.02.008.

[29] S. He, L. Wu, X. Li, H. Sun, T. Xiong, J. Liu, C. Huang, H. Xu, H. Sun, W. Chen, R. Gref, J. Zhang, Metal-organic frameworks for advanced drug delivery, Acta Pharm. Sin. B. (2021). https://doi.org/10.1016/J.APSB.2021.03.019.

[30] Z. Kazemi, S.M. Taghizadeh, S.T. Keshavarz, F. Lahootifard, Effect of composition on mechanical and physicochemical properties of mucoadhesive buccal films containing buprenorphine hydrochloride: From design of experiments to optimal formulation, J. Drug Deliv. Sci. Technol. 56 (2020) 101578. https://doi.org/10.1016/J.JDDST.2020.101578.

[31] J. Gil-Chávez, S.S.P. Padhi, U. Hartge, S. Heinrich, I. Smirnova, Optimization of the spray-drying process for developing aquasolv lignin particles using response surface methodology, Adv. Powder Technol. 31 (2020) 2348–2356. https://doi.org/10.1016/j.apt.2020.03.027.

[32] S.N. Politis, P. Colombo, G. Colombo, D.M. Rekkas, Design of experiments (DoE) in pharmaceutical development, Drug Dev. Ind. Pharm. 43 (2017) 889–901. https://doi.org/10.1080/03639045.2017.1291672.

[33] I. Khatib, M.Y.T. Chow, J. Ruan, D. Cipolla, H.K. Chan, Modeling of a spray drying method to produce ciprofloxacin nanocrystals inside the liposomes utilizing a response surface methodology: Box-Behnken experimental design, Int. J. Pharm. 597 (2021) 120277. https://doi.org/10.1016/j.ijpharm.2021.120277.

[34] S. Mandani, B. Rezaei, A.A. Ensafi, P. Rezaei, Ultrasensitive electrochemical molecularly imprinted sensor based on AuE/Ag-MOF@MC for determination of hemoglobin using response surface methodology, Anal. Bioanal. Chem. 413 (2021) 4895–4906. https://doi.org/10.1007/s00216-021-03453-x.

[35] M. Lakehal Senhaji, A. Hafnaoui, M. Khouloud, A. El Agri, A. Boulahna, M. El Asri, Formulation of anti-dust coating agent for monoammonium phosphate fertilizer using experimental design, Chemom. Intell. Lab. Syst. 216 (2021) 104375. https://doi.org/10.1016/J.CHEMOLAB.2021.104375.

[36] S. Beg, S. Swain, M. Rahman, M.S. Hasnain, S.S. Imam, Application of Design of Experiments (DoE) in Pharmaceutical Product and Process Optimization, Elsevier Inc., 2019. https://doi.org/10.1016/b978-0-12-815799-2.00003-4.

[37] B. Singh, R. Kumar, N. Ahuja, Optimizing Drug Delivery Systems Using Systematic "Design of Experiments." Part I: Fundamental Aspects, Crit. Rev. Ther. Drug Carr. Syst. 22 (2005) 27–105. https://doi.org/10.1615/CRITREVTHERDRUGCARRIERSYST.V22.I1.20.

[38] M.A. Bezerra, R.E. Santelli, E.P. Oliveira, L.S. Villar, L.A. Escaleira, Response surface methodology (RSM) as a tool for optimization in analytical chemistry, Talanta. 76 (2008) 965–977. https://doi.org/10.1016/j.talanta.2008.05.019.

[39] M. Blanco, J. Coello, M.J. Sánchez, Experimental design for optimization of peroxide formulation stability and cost, J. Surfactants Deterg. 9 (2006) 341–347. https://doi.org/10.1007/s11743-006-5012-1.

[40] A.A. Asgharinezhad, H. Ebrahimzadeh, Magnetic porous carbon nanocomposite derived from cobalt based-metal-organic framework for extraction and determination of homo and hetero-polycyclic aromatic hydrocarbons, Talanta. 233 (2021) 122526. https://doi.org/10.1016/j.talanta.2021.122526.

[41] M. Nazari, F. Yaripour, S. Shifteh, Systematic evaluation and optimization of crystallization conditions for an ethanol-templated ZSM-5 zeolite using response surface methodology, Adv. Powder Technol. (2021). https://doi.org/10.1016/j.apt.2021.10.018.

[42] M. Yahya, Y.W. Chen, H.V. Lee, C.C. Hock, W.H.W. Hassan, A New Protocol for Efficient and High Yield Preparation of Nanocellulose from Elaeis guineensis Biomass: A Response Surface Methodology (RSM) Study, J. Polym. Environ. 27 (2019) 678–702. https://doi.org/10.1007/s10924-019-01373-7.

[43] M. Hashemzehi, V. Pirouzfar, H. Nayebzadeh, A. Alihosseini, Application of response surface methodology to optimize high active Cu-Zn-Al mixed metal oxide fabricated via microwave-assisted solution combustion method, Adv. Powder Technol. 31 (2020) 1470–1479. https://doi.org/10.1016/j.apt.2020.01.010.

[44] I. Niizawa, B.Y. Espinaco, S.E. Zorrilla, G.A. Sihufe, Natural astaxanthin encapsulation: Use of response surface methodology for the design of alginate beads, Int. J. Biol. Macromol. 121 (2019) 601–608. https://doi.org/10.1016/j.ijbiomac.2018.10.044.

[45] B.P.M. Duarte, A.C. Atkinson, J.F.O. Granjo, N.M.C. Oliveira, Optimal design of mixture experiments for general blending models, Chemom. Intell. Lab. Syst. 217 (2021) 104400. https://doi.org/10.1016/J.CHEMOLAB.2021.104400.
[46] J.M. Jafari, H. Abdollahi, R. Tauler, Bilinear and trilinear modelling of three-way data obtained in two factor designed metabolomics studies, Chemom. Intell. Lab. Syst. 197 (2020) 103917. https://doi.org/10.1016/J.CHEMOLAB.2019.103917.
[47] N. Raghavendra Naveen, M. Kurakula, B. Gowthami, Process optimization by response surface methodology for preparation and evaluation of methotrexate loaded chitosan nanoparticles, in: Mater. Today Proc., Elsevier Ltd, 2020: pp. 2716–2724. https://doi.org/10.1016/j.matpr.2020.01.491.
[48] A. Gutiérrez-Serpa, A.I. Jiménez-Abizanda, F. Jiménez-Moreno, J. Pasán, V. Pino, Core-shell microparticles formed by the metal-organic framework CIM-80(Al) (Silica@CIM-80(Al)) as sorbent material in miniaturized dispersive solid-phase extraction, Talanta. 211 (2020) 120723. https://doi.org/10.1016/j.talanta.2020.120723.
[49] L. Lindfors, S. Forssén, J. Westergren, U. Olsson, Nucleation and crystal growth in supersaturated solutions of a model drug, J. Colloid Interface Sci. 325 (2008) 404–413. https://doi.org/10.1016/J.JCIS.2008.05.034.
[50] R. Androsch, M.L. Di Lorenzo, Crystal Nucleation in Glassy Poly(l-lactic acid), Macromolecules. 46 (2013) 6048–6056. https://doi.org/10.1021/MA401036J.
[51] J. McGinty, N. Yazdanpanah, C. Price, J.H. ter Horst, J. Sefcik, CHAPTER 1 Nucleation and Crystal Growth in Continuous Crystallization, Handb. Contin. Cryst. (2020) 1–50. https://doi.org/10.1039/9781788013581-00001.
[52] W.R. Bauer, W. Nadler, Stationary flow, first passage times, and macroscopic Fick's first diffusion law: Application to flow enhancement by particle trapping, J. Chem. Phys. 122 (2005) 1–13. https://doi.org/10.1063/1.1940056.
[53] S.B. Ünal, F. Erdoğdu, H.I. Ekiz, Effect of temperature on phosphate diffusion in meats, J. Food Eng. 76 (2006) 119–127. https://doi.org/10.1016/j.jfoodeng.2005.04.041.
[54] B.T. Smith, Remington education: physical pharmacy, Pharmaceutical Press, 2015.
[55] F. Ravera, L. Liggieri, A. Steinchen, Sorption kinetics considered as a renormalized diffusion process, J. Colloid Interface Sci. 156 (1993) 109–116. https://doi.org/10.1006/JCIS.1993.1088.
[56] N.A. Khan, S.H. Jhung, Synthesis of metal-organic frameworks (MOFs) with microwave or ultrasound: Rapid reaction, phase-selectivity, and size reduction, Coord. Chem. Rev. 285 (2015) 11–23. https://doi.org/10.1016/j.ccr.2014.10.008.
[57] R.A. Smaldone, R.S. Forgan, H. Furukawa, J.J. Gassensmith, A.M.Z. Slawin, O.M. Yaghi, J.F. Stoddart, Metalorganic frameworks from edible natural products, Angew. Chemie - Int. Ed. 49 (2010) 8630–8634. https://doi.org/10.1002/anie.201002343.
[58] M.P. Abuçafy, B.L. Caetano, B.G. Chiari-Andréo, B. Fonseca-Santos, A.M. do Santos, M. Chorilli, L.A. Chiavacci, Supramolecular cyclodextrin-based metal-organic frameworks as efficient carrier for anti-inflammatory drugs, Eur. J. Pharm. Biopharm. (2018). https://doi.org/10.1016/j.ejpb.2018.02.009.
[59] M. Kumar Trivedi, A. Branton, Characterisation of Physical, Spectral and Thermal Properties of Biofield treated Resorcinol, Org. Chem. Curr. Res. 04 (2015). https://doi.org/10.4172/2161-0401.1000146.

Appendices – Supporting information

Table A.1: Experimental values of reaction yield and drug encapsulation responses for each potassium salt. Highlighted runs were removed from the analysis.

Run	Response values			
	KCl		KNO_3	
	Reaction yield (%)	Drug encapsulation (%)	Reaction yield (%)	Drug encapsulation (%)
	Y_1	Y_2	Y_1	Y_2
1	35.9	5.6	36.5	4.5
2	60.6	6.3	67.4	3.8
3	30.5	5.0	48.3	5.3
*4**	*0.2*	*0.4*	*0.3*	*0.3*
5	30.2	2.6	33.4	2.7
6	53.8	3.4	57.5	3.5
7	62.8	3.5	65.6	2.5
8	40.7	4.7	39.6	4.7
9	0.1	4.8	1.2	1.1

10	9.9	7.1	8.5	5.8
11	10.3	7.7	12.3	6.8
*12**	*44.2*	*6.5*	*44.5*	*7.1*
13	44.1	5.8	56.8	4.4
14	25.1	7.1	32.4	5.0
15	10.8	6.8	14.0	5.9
*16**	*0.2*	*1.1*	*0.5*	*1.9*
17	54.5	5.4	52.4	5.6
18	34.6	4.9	21.3	4.4
19	29.0	7.2	36.4	5.0
*20**	*0.5*	*4.5*	*0.6*	*13.5*
21	11.6	8.2	29.0	7.4
22	18.8	6.8	25.6	6.5
23	5.0	4.3	2.7	2.0
24	2.4	7.2	14.6	6.8
25	40.4	6.8	39.6	6.0
26	72.7	5.1	75.5	5.4
27	54.0	5.5	57.9	5.6

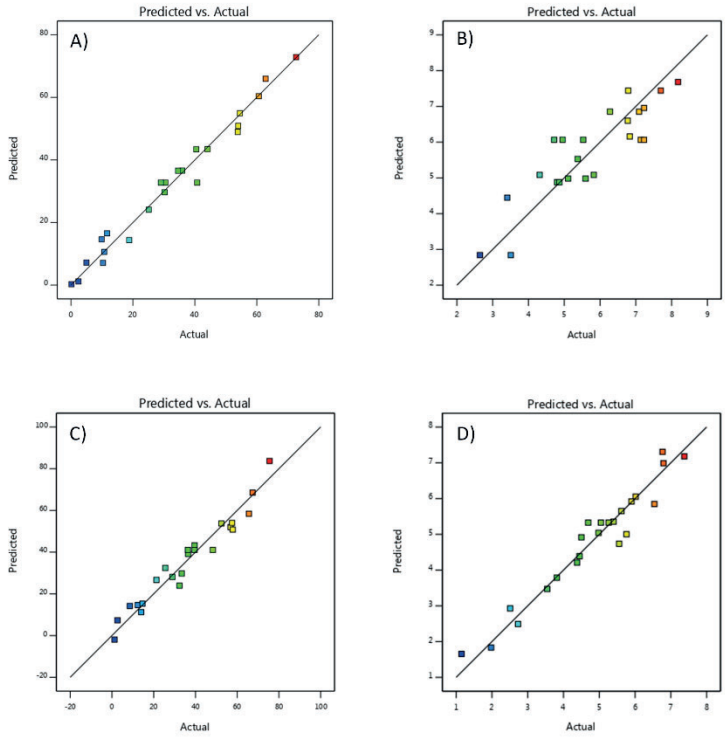

Fig. A.2: Predicted *versus* actual values for KCl reaction yield and drug encapsulation (A and B) and for KNO_3 reaction yield and drug encapsulation (C and D).

Synchrotron infrared micro-spectroscopy study using chemometrics: potential analgesic delivery systems loaded with cannabinoids for oral health

Jorge Rodríguez-Martínez[1(¥)], María-Jesús Sánchez-Martín*[1(¥)], Manuel Valiente[1]

[1] GTS Research Group, Department of Chemistry, Faculty of Science, Universitat Autònoma de Barcelona, 08193 Bellaterra, Spain.

[(¥)] Shared co-first authorship

*Co-first author and author for correspondence: mariajesus.sanchez@uab.cat

Telephone: +34 93 581 4638

Abstract

Dental or dentin hypersensitivity (DH) could be defined as a short and sharp pain derived from exposed dentin in response to different stimuli. Current strategies to avoid this discomfort are not totally effective and it is necessary to develop new treatments to avoid this sharp pain. Cannabidiol (CBD) is the main non-psychotropic component of *Cannabis sativa,* and it emerges as a promising candidate to avoid this pain since it can modulate receptors involved in the response caused by DH. However, CBD shows low chemical stability and poor aqueous solubility. The use of drug delivery systems (DDS) such as liposomes or metal-organic frameworks (MOFs) for its encapsulation or adsorption could overcome these disadvantages. In this study, olivetol (OLV), as a CBD analogue, was incorporated in γ-cyclodextrin-MOFs and 1,2-dipalmitoyl-sn-glycero-3-phosphocholine (DPPC) liposomes as potential analgesic delivery systems for DH treatment. Different techniques have been employed for their characterization. *In vitro* experiments using bovine teeth were performed to verify if the drug is able to reach the dentin, where it can flow to the pulp tissues and exert its analgesic effect; enamel and dentin regions were analysed by synchrotron radiation-based FTIR micro-spectroscopy. Principal component analysis (PCA) was used to process the spectroscopic data as a powerful chemometric tool and it revealed a similar behaviour in both regions. The studied DDS have been demonstrated to be an efficient way to carry the drug through dental tissues without compromising its structure. These DDS have been scarcely employed in oral health, being the first time in case of MOFs loaded with cannabinoids. Besides, OLV has been validated as a good analogue to study CBD behaviour.

Keywords

γ-Cyclodextrin-MOFs (γ-CD-MOFs), cannabinoids, dentin hypersensitivity (DH), DPPC liposomes (1,2-dipalmitoyl-sn-glycero-3-phosphocholine), principal component analysis (PCA), synchrotron FTIR micro-spectroscopy.

Graphical abstract

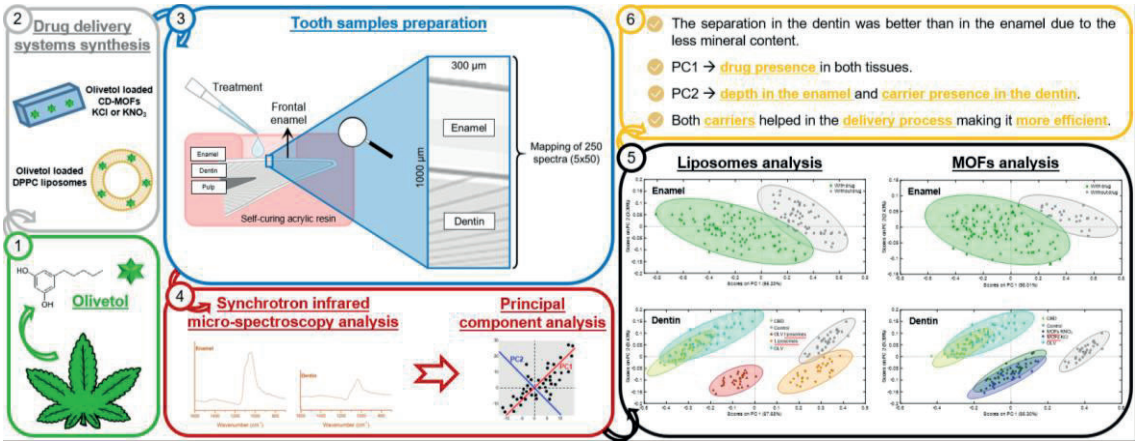

1. Introduction

Dental or dentin hypersensitivity (DH) could be defined as a short and sharp pain derived from exposed dentin in response to chemical, thermal, tactile or osmotic stimuli and it could appear when a tooth whitening treatment is applied or after periodontal surgery [1,2]. Several theories have been proposed to explain the origin of this pain, being Brannstorm's hydrodynamic theory the most accepted. However, DH mechanism is still uncertain. There are current strategies to avoid the discomfort associated with this dentin hypersensitivity, such as the use of potassium nitrate for nerve desensitization, the coverage of the exposed dentinal tubules with salts or adhesives and the application of analgesics and anti-inflammatory drugs for pain relieve [3]. Nevertheless, previous clinical studies using these treatments have shown that they are not totally effective, and current strategies still need to be improved [4,5]. Therefore, it is necessary to develop more effective, efficient and long-lasting treatments to avoid DH.

Cannabidiol (CBD) is the main non-psychotropic component of *Cannabis sativa*. According to reported studies, CBD has antioxidant, anti-inflammatory and immunomodulatory properties [6] . Despite its scarce use in dentistry, CBD has shown promising results in the treatment of serious diseases such as epilepsy, chronic pain or diabetes. Moreover, it is known that CBD can modulate the TRPA1 receptor expressed in dental pulp tissue that is believed to be involved in the response caused by DH [7,8]. Thus, CBD emerges as a promising candidate to avoid this discomfortbut it is also known for others less attractive characteristics such as its low solubility in aqueous solutions and high degradation easiness [9]. In order to solve these difficulties, previous studies have developed drug delivery systems (DDS) for the encapsulation of cannabinoids to protect this kind of compounds until the final target when they are used in medicine [10]. There are plenty DDS such as liposomes or metal-organic frameworks (MOFs), which are well-known drug delivery systems and used in pharmaceutical formulations. Liposomes are spherical vesicles consisting of one or more phospholipid bilayers surrounding a water space that present the ability to encapsulate different substances [11]. While lipophilic agents are entrapped in the bilayer, hydrophilic agents are enclosed in the aqueous core [12]. Besides, liposomes are able to fuse with the cell membrane and release the encapsulated drug [13]. MOFs are porous crystalline materials consisting of metal ions or clusters linked to organic ligands by coordination bonds [14]. As any crystals, MOFs present a repeating pattern of its unit cell building one, two or three-dimensional periodic networks [15]. An important and common advantage of liposomes and MOFs is that they are editable materials and their structure can be modified with different molecules to adapt them to their final application [16]. Due to all these characteristics, both systems have a wide range of application fields, such as gas storage, catalysis or drug delivery [17,18]. In the case of medical applications, it is necessary to take into account that the structures should be biocompatible and non-toxic for the biological tissues [19]. Therefore, the selection of the materials that comprise the DDS is very important. For liposomes, a quite studied phospholipid is 1,2-dipalmitoyl-sn-glycero-3-phosphocholine (DPPC) [20]. DPPC is a zwitterionic phospholipid which forms neutral or lightly negatively charged liposomes used as a model system to mimic the cell membrane [21]. Furthermore, DPPC is already in mammals as lung surfactant and it plays an important role in the study of liposomes and human bilayers [22–24]. Regarding MOFs, γ-cyclodextrin-MOFs (γ-CD-MOFs) have been reported as suitable materials in pharmacy and biomedicine due to its high biocompatibility since they are composed of γ-CD as organic ligand and usually potassium ions as metal linker [25]. γ-CD is a cyclic oligosaccharide of eight glucopyranose units with a hydrophilic external surface and a hydrophobic internal cavity where non-polar drugs could be encapsulated [26]. According to reported studies, γ-CD-MOFs have the capacity to increase the drug loading compared to γ-CD alone, to improve the physicochemical and biopharmaceutical characteristics of the drug and to control its release process [27,28]. Therefore, both systems present unique advantages for

applications in encapsulation and release of cannabinoids. MOFs have been scarce studied as carriers of CBD, but some researchers have developed some liposomal formulations with CBD for biological and medical applications such as cancer treatment [29,30]. However, there are not specific reports about the use of CD-MOFs and DPPC liposomes loaded with CBD for oral health application.

Dental structure has been studied using different characterization techniques such as Raman spectroscopy to study the changes in the tissues of teeth with periodontitis [31,32]. In previous works, Fourier Transform Infrared Spectroscopy, also known as FTIR Analysis, has been used to diagnose tooth structure alterations and pathologies. FTIR analysis is a non-invasive and non-destructive technique, obtaining a lot of information from a single spectrum about the chemical and physical properties [33]. Infrared spectroscopy is a very useful technique in dental research since it is able to study the tooth structure and its chemistry, organic and inorganic material and their interactions [34]. Nevertheless, conventional vibrational spectroscopic methods are not always enough accurate to assess modifications in dental composition, since tooth structure changes take place at micro and nano levels [35]. Thus, the addition of a synchrotron radiation light source to FTIR technique (synchrotron radiation-based FTIR microspectroscopy, SR-μFTIR) provide the high intensity, the spectral purity, the spatial and the energy resolution necessary to study dental structure at micro and nano levels [36]. However, analysis of spectral data obtained is quite challenging due to the high number of spectra, the fact that many of the spectral bands are overlapping and small changes could not be appreciated using visual comparison [37]. To solve these problems chemometrics have been used. This statistic and mathematic tool extracts information from multivariate chemical data and it has become a useful technique for faster analysis of huge amount of data for different applications [38]. A wide array of chemometrics is used for discrimination and classification of the dataset being principal component analysis (PCA) one of the most common applied in combination with FTIR spectroscopy [37]. PCA reduces the data to a low dimension and resolves small differences in the spectra trying to establish subgroups in the data [39].

Several researchers have already explored the large capabilities of the combination of synchrotron source infrared spectroscopy with chemometrics in dental field, such as the diagnostics and evaluation of formation of the biomimetic dentin/dental composite interface or dental caries assessment [33,40–42] . In this study, γ-CD-MOFs and DPPC liposomes containing olivetol (OLV) were synthetised and characterised as potential analgesic delivery systems for DH treatment. OLV was employed as an affordable CBD analogue, since it is a precursor in cannabidiol biosynthesis and they share part of the chemical structure [43]. In order to verify if the drug is able to cross the enamel and get into dentinal tubules, where it can flow to the pulp tissues and exert its analgesic effect, *in vitro* experiments using bovine teeth were developed. The primary component in the tooth is hydroxyapatite (HAP) that has well-defined bands in the infrared spectra (1600 - 700 cm^{-1}) and the spectrum of CBD and olivetol has several absorption bands in the infrared region. Therefore, it would be possible to trace the penetration of the drug in the tooth structure using this technique coupling it to the synchrotron radiation source allowing spectra with high signal-to-noise ratio to be obtained in small sample areas. Furthermore, the penetration patterns according to the delivery system were evaluated and how the γ-CD-MOFs and DPPC liposomes help in the release process. Besides, the effect of the different treatments over the tooth was assessed based on the changes in the HAP band. To process these infrared spectroscopic data, chemometrics were employed using PCA as a powerful tool that can identify subtle spectral differences from complicated datasets.

2. Materials and methods

2.1. Reagents

Chloroform (99.9%) and potassium nitrate (99.2%) were purchased from VWR BDH Chemicals (Oud-Heverlee, Belgium). Potassium chloride (99.0%), sodium azide (99.5%) and 2-[4-(2-hydroxyethyl)piperazin-1-yl]ethanesulfonic acid (99.5%, HEPES) were purchased from Sigma-Aldrich (St. Louis, MO, USA). 1,2-Dipalmitoyl-sn-glycero-3-phosphocholine (99%, DPPC) was purchased from Avanti Polar Lipids (Alabaster, AL, USA). Cannabidiol (99%) was purchased from Tocris Bioscience (Bristol, United Kingdom). Methanol (99.8%) was purchased from Fisher Scientific (Madrid, Spain). Ethanol (96%) was purchased from Scharlau (Sentmenat, Spain). Polyethylene glycol 20000 was purchased from Merk (Darmstadt, Germany). Olivetol (95%) and γ-cyclodextrin (98%) were purchased from Carbosynth Ltd (Compton, United Kingdom). MilliQ water was purified through a Millipore purification system from Millipore (Milford, MA, USA).

2.2. Drug delivery systems synthesis

A fast and modified method using microwave irradiation was performed for γ-CD-MOFs synthesis [44]. Besides, a co-crystallization method was used to load olivetol into γ-CD-MOFs. Briefly, KCl and KNO_3 were employed as two potassium sources adding 149 mg or 202 mg respectively, and 324 mg of γ-CD to have a molar ratio of 1:8, potassium source to organic ligand. These compounds were mixed in 16 mL of an initial solution based on 10 mL of milliQ water and 6 mL of methanol. Besides, 30 mg of OLV were also diluted in this initial solution. This mixture was treated at 50 ºC in the analytical microwave (CEM Corporation Matthews, North Carolina, USA) for 10 min and a power of 600 w. Next, 256 mg of PEG 20000 were added to trigger the precipitation of the crystals for 24 hours. In order to remove the unreacted material, the crystals were washed first with 10 mL of methanol and then with 10 mL of ethanol in a centrifuge at 3000 rpm for 5 min. Finally, γ-CD-MOFs were dried and kept under vacuum at room temperature until their use.

DPPC liposomes were obtained by hydration and mechanical dispersion [13]. Briefly, DPPC was dissolved in chloroform/methanol (2:1, v/v) at 100 mM. 0.25 mL of the DPPC solution plus a small volume of the chloroform/methanol mixture were introduced in a bottom round flask until a final volume from 4 to 7 mL. Then, it was evaporated using a rotary evaporator (Büchi, Flawil, Switzerland) maintaining the temperature of the bottom round flask above the phase transition temperature (T_m) of the phospholipid . In this study, T_m is 41 ºC for DPPC. When the monolayer of DPPC was obtained on the inside surface of the flask, 5 mL of HEPES buffer solution 20 mM (pH = 7.4) was added to the flask. Then, the suspension was sonicated for 15 minutes to obtain multilamellar vesicles (MLVs), maintaining the temperature of the bottom round flask above the T_m. The final concentration of DPPC was 5 mM and the liposomal preparations were stored at 4 ºC until their use In the same way, DPPC liposomes loaded with olivetol were prepared, using a DPPC:OLV molar ratio of 2:1. In this case, 3.75 mL of a stock solution of olivetol 600 mg/L in methanol were added to the DPPC solution into the bottom round flask before the solvent evaporation, in order to get the final desired concentration of the drug (2.5 mM for 2:1 ratio).

2.3. Characterization techniques

Morphology and crystallinity of MOFs samples were evaluated by Scanning Electron Microscopy (SEM) and X-ray powder diffraction (XRPD), respectively. SEM images were taken using a Zeiss Merlin FE-SEM with the Secondary Electron Detector with a low voltage of 2 kV, at

room temperature, 2000x of magnification and a working distance of 4.3 mm. The XRD analysis was carried out using a Malvern Panalytical X'Pert PRO MPD (Material Powder Diffractometer), in transmission mode using a capillary spinner and the sample were filled inside borosilicate glass capillaries with outer diameter of 0.7 mm. The samples were irradiated with a ceramic X-ray tube with Cu K_α anode (l = 1.5406 Å), tube voltage of 45 kV, tube current of 40 mA in a step size scan mode (0.03º min^{-1}) and analysed over a 2θ angle range of 2.5 - 35º.

Liposome dispersions were characterized by Cryo-transmission electron microscopy (Cryo-TEM) and Dynamic light scattering (DLS). Cryo-TEM images were taken using a JEM-2011 (Jeol, Japan), 5000x of magnification and samples were prepared by depositing 3 µL of the liposomes' solution on a copper grid covered with a carbon reinforced holey polymer film. Thin sample films (30 - 300 nm) were blotted with a filter paper and immersed into liquid ethane. Samples were kept below -179 °C and protected from atmospheric conditions during the whole process. All sample preparations were performed in a room at 25 °C and 70 % relative humidity. DLS analysis was performed with ZetaSizer Nanos ZS (Malvern Panalytical, Netherlands and United Kingdom) and sensitive avalanche photodiode detector (APD). Dynamic light scattering is used to measure particle size and molecular size. Measurements were made in disposable folded capillary cells (R.I.: 1.450 and absorption coefficient: 0.01) at 20 ºC using a laser with λ_0 = 632.8 nm and 175º angle. The viscosity of water was taken as 1.0031 cP and 1.330 of R.I.

2.4. Drug release and quantification

The quantification of the OLV content into the MOFs was performed mixing 15 mg of MOF sample in 5 mL of a mixture of Milli-Q water and ethanol (1:1, v/v). Then, an incubation step took place at room temperature under stirring conditions (250 rpm) for 24 hours to degrade the crystals and release the drug. For liposomes, the encapsulation of the drug was determined adapting a method previously described [45]. 0.17 mL of liposome suspension were added to 0.83 mL of ethanol (1:5, v/v). The mixture was sonicated for 5 minutes and mixed to promote the disruption of the liposomes and release the encapsulated olivetol. The resultant solutions were measured by UV-Vis spectrophotometry (Thermo Fisher Scientific, Massachusetts, USA) at 275 nm where the characteristic peak of OLV could be found. The reference was the same solution where each carrier was dissolved and a calibration curve of different known concentrations of OLV in the same solution was prepared from 0 to 100 mg/L for each carrier (Fig. A.1).

The drug encapsulation for each carrier was calculated following equation 1:

$$Drug\ encapsulation\ (\%) = \frac{Encapsulated\ OLV\ into\ the\ carrier\ (mg)}{Total\ Weight\ of\ OLV\ loaded\ carrier\ (mg)} \cdot 100 \quad [1]$$

All determinations were performed by triplicate.

2.5. Tooth samples preparation

Bovine incisors were cut by separating them from the roots using a diamond saw. Then, the specimens were cleaned and preserved in sodium azide solution (0.8%). Teeth were embedded in self-curing acrylic resin (Paladur, Germany) leaving the frontal enamel free of resin. Specimens were cut in half and its lateral surface was polished down to 1 µm particle size in order to obtain good reflection properties for the measurements using a sequence of silicon carbide paper. Then, teeth were treated with 0.1 mL of each treatment 3 times per day for 5 days, making sure that only the frontal enamel was in contact with each solution and not with the lateral surface (Table 1, Fig. A.2.A). Since MOFs' treatments are the only ones which are in powder, 1 mg of

each MOF formulation was mixed with 15 µL of HEPES buffer and then, the resultant solution was applied over the teeth.

Table 1: List with the different treatments applied over the dental samples.

Treatments' list
Control (HEPES buffer)
Cannabidiol (10 mg/mL)
Olivetol (10 mg/mL)
DPPC liposomes
DPPC liposomes loaded with olivetol
γ-CD-MOFs KCl loaded with olivetol
γ-CD-MOFs KNO_3 loaded with olivetol

2.6. Synchrotron radiation-based FTIR microspectroscopy (SR-µFTIR) measurements

Specular reflectance spectra were acquired using FTIR microscope in the reflection mode at MIRAS beamline of ALBA synchrotron (Cerdanyola del Vallès, Spain). Hyperion 3000 microscope coupled to a Vertex 70 spectrometer (Bruker, Germany) and an HgCdTe (MCT) detector was used. The 36x Schwarzschild magnification objective and condenser were used to focus the infrared light on the sample. A mapping of 300x1000 µm (wide x length) was made per each sample in the lateral surface from the outside of the enamel to the dentin. In each mapping, 250 spectra were measured having 5 spectra wide and 50 spectra length (Fig. A.2.B). For each spectrum, 64 scans were carried out from 4000 cm^{-1} to 600 cm^{-1} with 4 cm^{-1} spectral resolution and at room temperature, using 10x10 μm^2 of aperture size. The background was measured with a gold mirror reference. OPUS 7.5 (Bruker, Germany) was used to collect the spectra.

2.7. Principal component analysis (PCA)

PCA was applied to process the SR-µFTIR data using PLS toolbox 8.2.1 (20559) for use with MATLAB 9.1 (R2016b). This chemometric tool is able to extract the main variability correlating it with the chemical compounds that are in the sample and their distribution. In the spectral data obtained for this study, enamel and dentin are the two regions well differentiated in the mappings, being the most intense peak the ν_3 PO_4^{2-} for both regions. Due to the high variability of biological samples, the big mapping per sample were limited to two smaller mappings of 30 spectra having 5 spectra wide and 6 spectra length, one in the inner enamel and another in the inner dentin. The wavenumber range was also limited from 1600 to 700 cm^{-1} where the main bands of HAP are located. Before PCA, mean centering pre-processing was applied to all the spectra. Besides, in each region of the tooth, enamel and dentin, liposomes and MOFs treatments were analysed by separate.

3. Results and discussion

3.1. Drug delivery systems characterization and olivetol quantification

In order to evaluate the morphology and the crystal structure of the γ-CD-MOFs loaded with the drug, SEM and PXRD analysis were performed. The diffraction patterns of both γ-CD-MOFs KCl and γ-CD-MOFs KNO_3 presented their peaks at the same 2θ angles (Fig. 1.1): 5.3º, 7.4º, 10.5º, 11.5º, 12.1º, 14.2º, 14.9º, 15.8º and 16.7º. Peaks were quite narrow for both potassium salts, indicating high crystallinity, especially when KNO_3 was employed since their peaks were sharper and more intense. The space group of these diffraction patterns was not the typical *I*432 with a body-centered cubic unit cell. Previous studies have already shown trigonal spaces groups when the metal linker was not delivered by potassium hydroxide [46]. This PXRD analysis was in

agreement with SEM evaluation. The prism morphology of the crystals was the same for both potassium salts (Fig. 1.2). The size of these structures was quite heterogeneous, but most of them was around 2 to 50 µm. It could be explained due to the long incubation time to trigger the precipitation of the crystals that was 24 hours, since it is a key parameter in the kinetics that are involve in crystal growth [47]. Consequently, SEM and PXRD analysis showed crystalline CD-MOFs with prism shape, regardless the potassium salt.

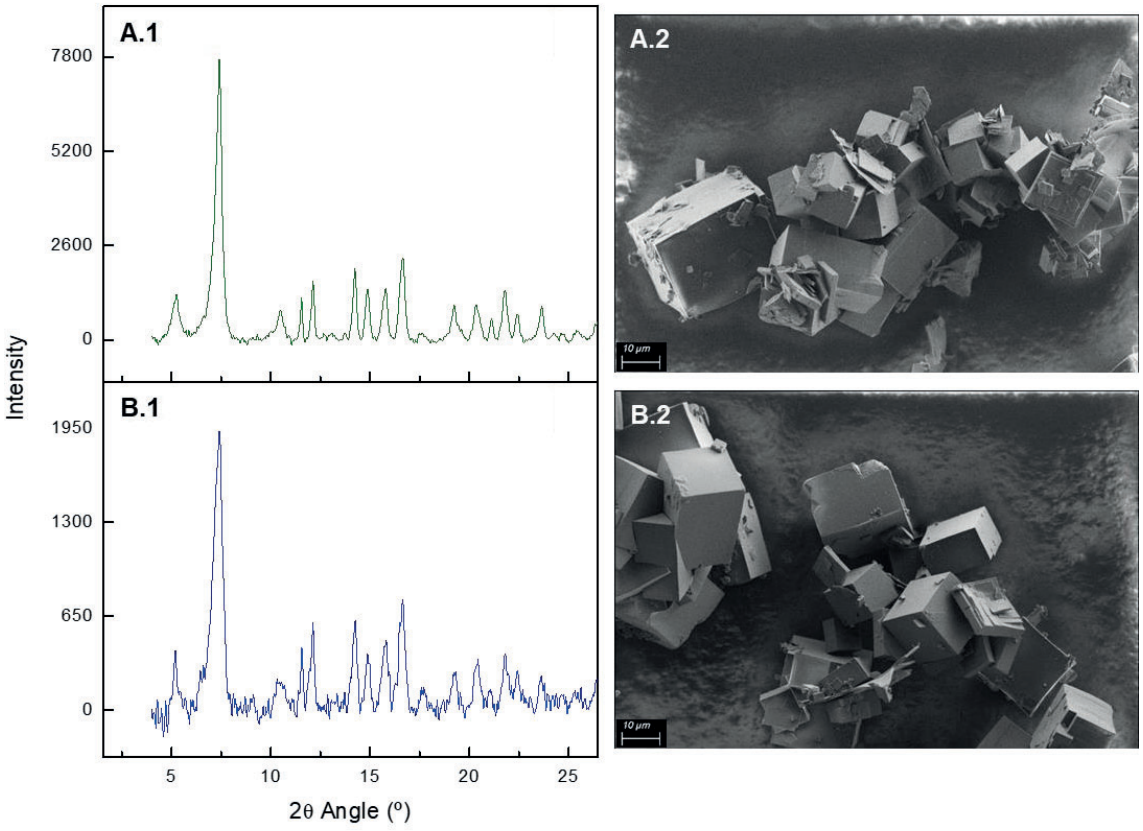

Figure 1: X-ray powder diffraction patterns (1) and scanning electron microscopy images (2) of OLV loaded γ-CD-MOF formulations using KNO_3 (A) and KCl (B) as potassium sources.

Regarding the liposomes' characterization, the size distribution is a key aspect to consider, even more when the final application is as drug delivery systems [48]. In order to get information about the size of DPPC liposomes and the physical stability of these systems after the encapsulation of olivetol, DLS and cryo-TEM analysis were performed. DPPC formulations loaded with the drug showed more polydispersity than empty DPPC liposomes with wider and more asymmetric peaks in DLS results (Fig. 2.A). These results were in agreement with cryo-TEM analysis where bigger liposomes and with several concentric lipidic bilayers could be observed in the samples with OLV (Fig. 2.B). The mean diameter of the liposomes was below 200 nm: 125 ± 52 nm for DPPC liposomes and 159 ± 67 nm for DPPC liposomes loaded with OLV. Mean diameter and standard deviation were similar in both liposomes' formulations. However, the size distribution observed in the liposomes without drug was closer to a normal distribution than the formulations with OLV, as well as the polydispersity index values were lower in the empty liposomes (0.3) than in the loaded ones (0.9). This fact means that the samples with low polydispersity index had homogeneous distribution of the vesicles of similar diameters without

aggregates [49]. It could be explained since olivetol is an organic compound and it is encapsulated in the bilayer increasing the rigidity of liposomes, such as the effect of cholesterol addition [50]. Cryo-TEM analysis corroborated these results. Anyway, the synthesis method was found to be useful for producing stable DPPC liposomes with and without olivetol of relatively controllable particle size.

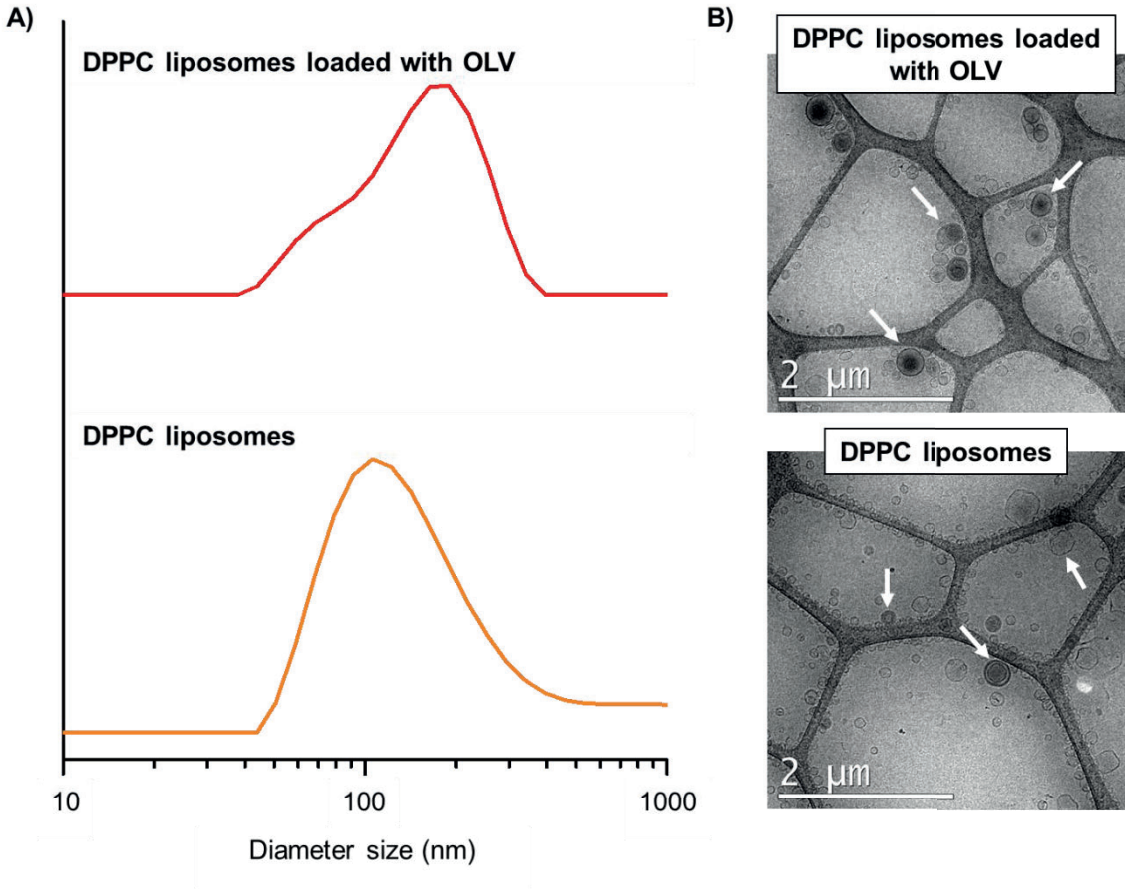

Figure 2: Size distribution by intensity (A) and cryo-TEM images (B) of OLV loaded DPPC liposomes and DPPC liposomes.

The UV-Vis spectrophotometry analysis confirmed the presence of olivetol in all the carriers (Table 2). For MOFs formulations, OLV encapsulation percentages were in the order of the values reported in previous studies using CD-MOFs for the encapsulation of different compounds [51–53]. For liposomes formulation, OLV encapsulation percentage was higher than the values for both MOFs. These percentages could not be compared between MOFs and liposomes, since the values are expressed in terms of mass and the weight of each carrier is different [46,53]. In order to verify if the amount of drug applied over the teeth in liposomes and MOFs formulations was comparable, the OLV amount per application was calculated based on the sample preparation process (section 2.5). This amount was of the same order for the three carriers (Table 2). Besides, the amount of drug applied without carrier as positive control was extremely high to study the efficiency when the carrier was used. In any case, the drug could be quantified in all the formulations, making them suitable as carriers for olivetol and for their application over the tooth structure.

Table 2: Olivetol encapsulation percentage for each formulation with their standard deviations and drug amount per application.

	OLV encapsulation (%)	OLV/CBD amount per application (μg)
DPPC loaded with olivetol MLV (molar ratio 2:1)	9.1 ± 0.1	36.8 ± 0.5
γ-CD-MOFs KCl loaded with olivetol	2.4 ± 0.3	24 ± 3
γ-CD-MOFs KNO_3 loaded with olivetol	1.6 ± 0.2	16 ± 2
CBD or OLV (10 mg/mL)	-	1000

3.2. Peaks assignment of enamel and dentin

Enamel and dentin are the main tissues that comprise the teeth. Enamel is composed of 96% of mineral content, while in the dentin it is reduced to approximately 70%. Regarding the organic matter, the enamel presents only 2% and in the dentin, it increases to 20%, predominating cross-linked type I collagen. The inorganic mineral that mainly composes both tissues is the carbonated calcium-deficient hydroxyapatite (HAP), which is a crystalline calcium phosphate [$Ca_{10}(PO_4)_6(OH)_2$] and carbonates impurities [CO_3^{2-}][52]. These carbonates could substitute two anion phosphate groups or two hydroxyl groups in HAP structure, being B-type or A-type carbonated apatite, respectively [54]. Bovine enamel and dentin reflection spectra are shown in Fig. 3 between 1600 and 700 cm^{-1} where the bands of carbonates and phosphates groups of HAP could be observed. Due to the high degree of crystallinity of the enamel, the bands that correspond to this mineral matrix are more intense than in the dentin tissue which has a low crystallinity, and the peaks appear weakly [55]. Antisymmetric stretching vibration of phosphates groups (v_3 PO_4^{3-}) appears as a wide band in the 1200-900 cm^{-1} region, in both enamel and dentin tissues with a maximum at 1045 and 1028 cm^{-1},respectively. These broad bands are attributed to triply degenerated v_3 PO_4^{3-} and its deconvolution is described as secondary phase vibrations of Ca-O-P, P-O, Ca-O and O-Ca-O vibrations, but they are not fully resolved [56]. The shoulder at 956 cm^{-1} corresponds to the symmetric stretching vibration of the same group (v_1 PO_4^{3-}) in both tissues, despite the band being more saturated in the enamel than in the dentin [57]. The peaks at 1403 and 1442 cm^{-1} match with antisymmetric stretching vibration of carbonate groups (v_3 CO_3^{2-}) and the one at 867 cm^{-1} with symmetric angular deformation (v_2 CO_3^{2-}) in both tissues. These peaks correspond to a mixture of A-type and B-type carbonated apatites, being B-type the one with more contribution since it is the predominant type in biological apatite [54]. Besides, organic matter (amide II) is detected at 1540 cm^{-1} in the dentin, since its percentage in this tissue is higher than in the enamel [58].

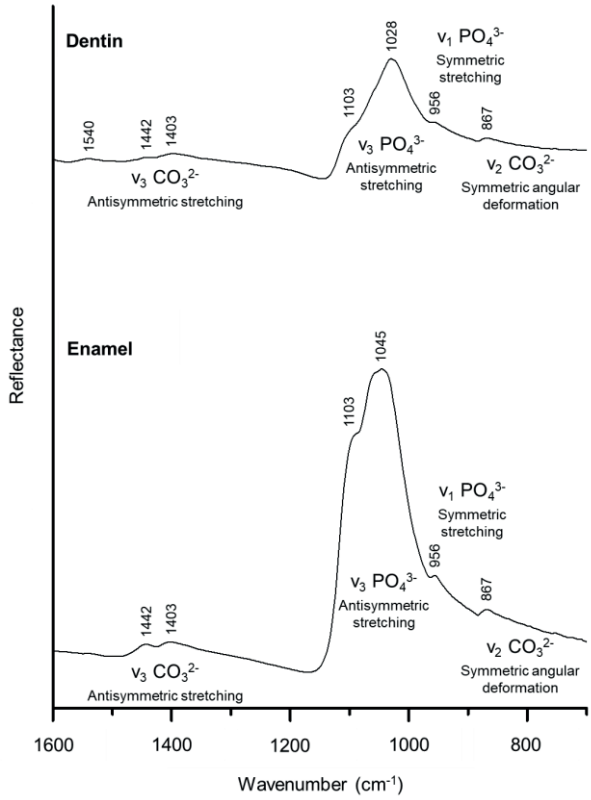

Figure 3: Average of the specular reflectance FTIR spectra of control enamel and dentin of bovine tooth and band assignment numbers (n=30).

3.3. Study of the treatments' effect over the enamel

In the present study, the enamel FTIR spectra of the different samples were analysed by PCA, where the weights of the main components were concentrated in the components 1 and 2 (PC1 and PC2) for both carriers. Liposomes and MOFs analysis had a PC1 of 95.20% and 96.01% versus PC2 of 3.39% and 2.43% accounting for a total of 98.59% and 98.44% of the variance, respectively (Fig. 4). The two carriers' analysis had a similar distribution in the enamel and only two groups could be distinguished along PC1 according to drug presence (Fig. 4.A). The group with drug included CBD, OLV and OLV loaded liposomes or MOFs (depending on the carrier analysis) and the group without drug comprised HEPES control for both carriers and also unloaded liposomes for liposomes analysis. Therefore, it revealed that both OLV loaded carriers may transport the drug, since these treatments were in the same group as CBD and OLV control treatments. Nevertheless, the separation between the groups that contained or not drug was not perfectly clear. This fact could be explained due to the large inorganic material content and high crystallinity of the enamel [59]. Because of these enamel properties, the signal of carbonates and phosphates groups of HAP was too high overlapping the possible vibrations peaks of organic material that can be present in the enamel, as the drugs and carriers employed in the different treatments [60]. For this same reason, no more differences related with the treatments could be observed between groups, since spectra were distributed according to the depth in the enamel structure along PC2 (Fig. 4.B).

Regarding the loading graphs (Fig. 4.C), PC1 comprised all the bands of carbonates and phosphates groups of HAP previously assigned for both liposomes and MOFs analysis in the positive part of the graphs. Taking into account the enamel structure properties, no contribution of drugs, liposomes or MOFs vibration peaks were expected to be distinguished, since their signals are not significant in comparison with the signal of the inorganic material of the enamel [61]. Thus, only changes over HAP structure could be noted. The treatments with drug (CBD, OLV, OLV loaded liposomes and MOFs) produced the decrease of the bands of carbonates and phosphates groups of HAP in comparison with the average of the spectra of the samples without drug, especially in the antisymmetric stretching vibration v_3 PO_4^{3-} (Fig. A.3.A). This fact could be explained due to the organic matter increment in the samples treated with drug, because the crystallinity of the enamel in these samples was worse detected than in the ones without any drug, since they have better reflective properties, and its infrared signal is higher [62]. Besides, shifts were not detected in the average of the spectra of the samples with and without drug for both carriers, so the treatments did not compromise carbonates and phosphates groups of HAP [63]. These results agreed with the distribution in scores graphs along PC1 (Fig. 4.A), where the group with drug is in the negative part of the component (less intense signal) and the group without drug in the positive part (more intense signal).

PC2 loadings profiles revealed in the positive part of the graphs, v_3 CO_3^{2-} and v_2 CO_3^{2-} peaks of carbonate groups from 1475 to 1380 cm^{-1} and 867 cm^{-1}, respectively (Fig. 4.C). A secondary phase vibration of v_3 PO_4^{3-} at 1113 cm^{-1} was observed. This vibration contributes to the shoulder at 1103 cm^{-1} of the peaks assignment, and it is related with the bandwidth [63]. Meanwhile, the maximum peak of v_3 PO_4^{3-} was in the negative part. This profile was in agreement with the distribution of the scores according to the depth in the enamel structure (Fig. 4.B). Enamel tissue presents heterogeneous distribution of the inorganic material, since its carbonate content increases from the outer to inner enamel, the phosphates decrease showing more crystallinity and more packing in the outer part [64–66]. Therefore, the fact that the scores in the positive part of the graph correspond to the inner parts of the enamel and the ones in the negative part to the outer region matched with the PC2 loading profiles for both carriers. This information is in accordance with the typical mineral gradient of the enamel, verifying that PC2 distributes the samples following the depth in this tissue.

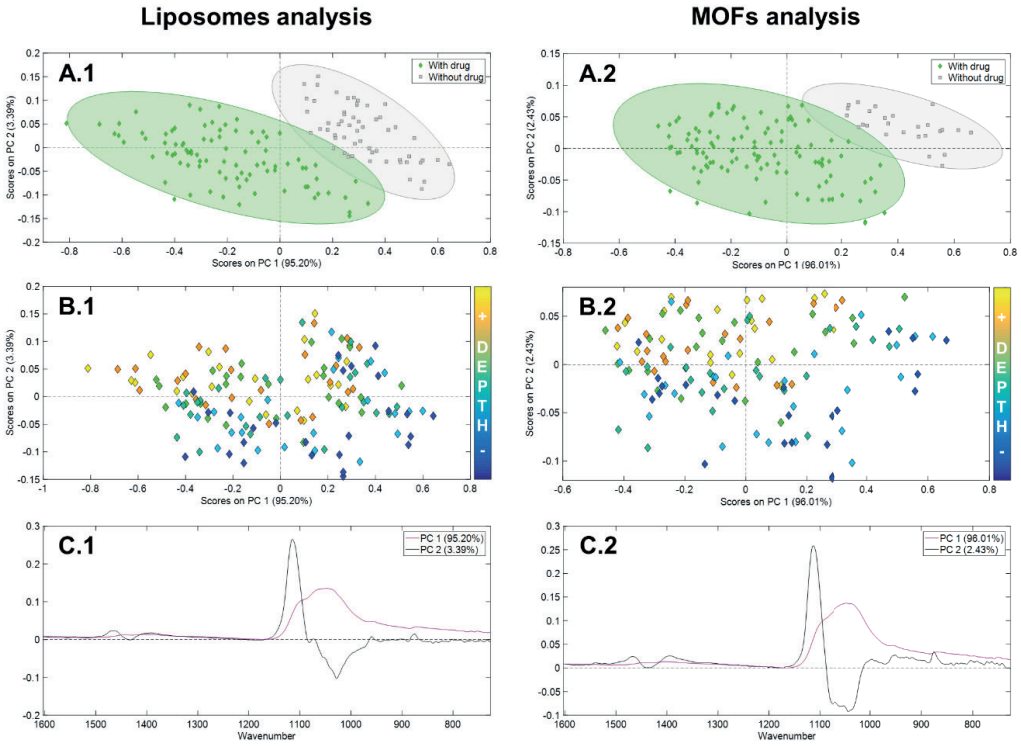

Figure 4: Principal Component Analysis of liposomes (1) and MOFs (2) in the enamel; scores plots grouping according to the drug presence (A); scores plots showing the distribution across the enamel depth (B); loadings profiles of PC1 and PC2 (C).

3.4. Study of the treatments' effect over the enamel

The analysis of the dentin was also performed using PCA for the different treatments. As in the enamel results, the weights of the main components were in the components 1 and 2 (PC1 and PC2) for both carriers. Liposomes and MOFs analysis had a PC1 of 87.68% and 86.30% versus PC2 of 8.43% and 9.39% accounting for a total of 96.11% and 95.69% of the variance, respectively (Fig. 5.A). In comparison to the enamel analysis, the separation between the groups in the dentin was much better and more consistent information can be obtained. This better separation of the different groups in the dentin may be due to the less mineral content and less crystal packing in this tissue, having the organic matter of the drug stronger presence improving the sample grouping [55]. Therefore, the signal of carbonates and phosphates groups of HAP decreases and the vibrations of the organic material could be distinguished. All the groups in both carriers' analysis had similar distribution in the scores' graphs along PC1 and PC2 (Fig. 5.A). Loaded liposomes and MOFs groups were closer to the samples treated with only drug (CBD and OLV) than the samples without treatment or unloaded carrier. Thus, it means that both carriers led the drug transport until the dentin tissue efficiently increasing the diffusion process, despite the drug concentration per application was much lower than in the CBD and OLV control groups (Table 2) [13]. Furthermore, CBD and OLV control groups are completely overlapped in this analysis, confirming that OLV could be used as CBD analogue in this experiment. Dentin analysis also revealed differences related to the presence of liposomes or MOFs along PC2. Meanwhile, the groups without any carrier were in the positive part of PC2, the groups with carrier were in the negative part of this component regardless the drug presence. Therefore, PC1 may group the samples according to the drug presence and PC2 according to the carrier presence in the dentin tissue. Moreover, these results from the dentin analysis verified and supported the previous results of the enamel.

PC1 loadings graphs included all the characteristic vibrations previously assigned in the dentin tissue for both carriers in the positive part of the profile (Fig. 5.B). As in the enamel analysis, drug vibrations did not appear since the contribution of the inorganic material was much more significant that the contribution of the drug. The comparison between the average of the spectra without drug with the average of the spectra with drug (CBD, OLV, OLV loaded liposomes and MOFs) revealed a reduction in the intensity of all the bands, related to a higher organic matter content in the dentin tissue that decreased the crystallinity and the signal of the bands (Fig. A.3.B) [67]. The only band that did not decrease is the one at 1540 cm^{-1} in case of the liposomes analysis, since this vibration may be related to the NH_3^+ deformation from the DPPC structure avoiding the loss of intensity of this peak despite the decrease in crystallinity due to the drug presence [68]. However, the main vibrations did not shift, so the chemical structure of the dentin was not changed. The loading profiles of PC1 were in agreement with the scores' graphs since the samples without drug were in the positive part of this component (more intense signal) and the samples with drug were in less positive values (less intense signal).

PC2 profiles comprised the wide band of the antisymmetric stretching vibration v_3 PO_4^{3-} in the negative part emphasising the shoulder at 1103 cm^{-1} of the peaks' assignment, while the rest of the peaks were in the positive half of this component (Fig. 5.B). This negative band gives information about the bandwidth and the groups that were in the more negative part of the scores' graphs correspond to treatments with liposomes and MOFs that contributed with the increase of the organic material in the dentin tissue, reducing the crystallinity and making the mentioned phosphate band widder when these groups were compared to the ones without any carrier [69]. This information agreed with scores distribution along PC2 where the samples without carrier were in the positive part and the samples with carrier in the negative half. The fact that rest of the bands were in the positive part means that the presence of any carrier did not affect these vibrations.

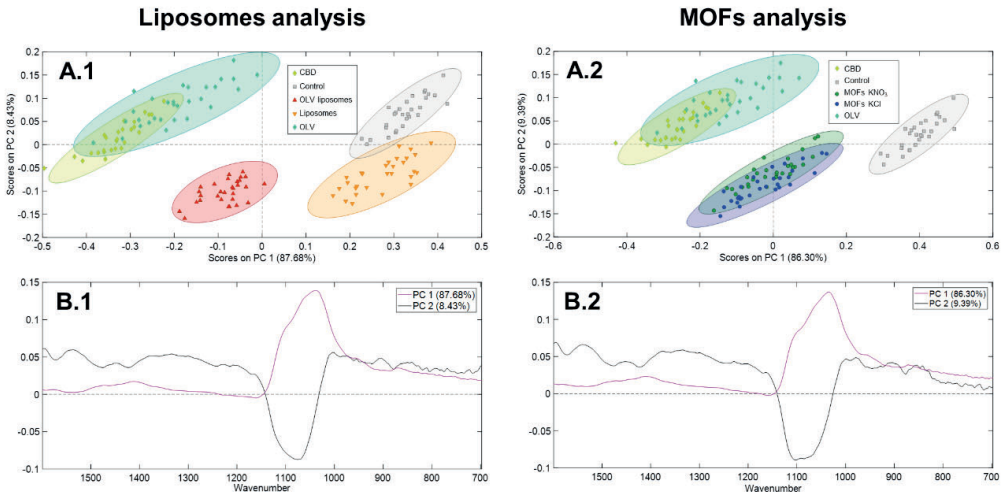

Figure 5: Principal Component Analysis of liposomes (1) and MOFs (2) in the dentin; scores plots grouping according to the drug presence and carrier presence (A); loadings profiles of PC1 and PC2 (B).

4. Conclusions

In the present study, olivetol loaded γ-CD-MOFs and DPPC liposomes were successfully prepared and characterised as potential analgesic delivery systems of CBD for DH treatment. *In vitro* experiments using bovine teeth were developed using SR-μFTIR and chemometrics to process the data. Enamel and dentin regions data were analysed using PCA, showing a similar behaviour.

PC1 grouped the samples according to the drug presence in both tissues due to a reduction in the intensity of all the bands. This fact was explained since a high organic matter content decreased the crystallinity of the carbonates and phosphates groups of HAP. Meanwhile, PC2 grouped the samples according to the depth in the enamel structure due to the typical mineral gradient of this tissue, this component grouped the samples according to the carrier presence in the dentin because the less crystallinity and more widder phosphate band v_3 PO_4^{3-}. Thus, the analysis of both regions was consistent between each other, despite the separation in the dentin was much better than in the enamel due to the less mineral content. Moreover, no differences were observed between OLV and CBD validating the hypothesis of OLV application as CBD analogue in this experimental approach. Besides, OLV loaded liposomes and MOFs targeted the drug transport in a more efficient way, since these groups were closer to the CBD and OLV control groups despite the drug concentration per application was much lower. Therefore, it was possible to trace the penetration of the drug in the tooth structure using these techniques and to know that the carriers helped in the delivery process making it more efficient. Besides, shifts in the HA bands were not observed meaning that the treatments did not affect the tooth structure. In conclusion, potential analgesic delivery systems loaded with cannabinoids for oral health were developed, leading the drug transport in an efficient way to cross the tooth structure.

5. Acknowledgments

The Spanish *Ministerio de Economía y Competitividad*, is acknowledged for the financial support provided (Project: CTM2015-65414-C2-1-R). Jorge Rodríguez-Martínez acknowledges the FI-2018 fellowship from *Agència de Gestió d'Ajuts Universitaris i de Recerca (Generalitat de Catalunya*). The SR-µFTIR experiment was performed at MIRAS beamline at ALBA Synchrotron (Cerdanyola del Vallès, Spain), with the collaboration of ALBA staff. This work has been funded by ALBA Synchrotron through granted proposal (grant reference: 2020024303).

References

[1] C.M. Marto, A. Baptista Paula, T. Nunes, M. Pimenta, A.M. Abrantes, A.S. Pires, M. Laranjo, A. Coelho, H. Donato, M.F. Botelho, M. Marques Ferreira, E. Carrilho, Evaluation of the efficacy of dentin hypersensitivity treatments—A systematic review and follow-up analysis, J. Oral Rehabil. 46 (2019) 952–990. https://doi.org/10.1111/joor.12842.

[2] J. Rodríguez-Martínez, M. Valiente, M.J. Sánchez-Martín, Tooth whitening: From the established treatments to novel approaches to prevent side effects, J. Esthet. Restor. Dent. 31 (2019) 431–440. https://doi.org/10.1111/jerd.12519.

[3] P.M. Bartold, Dentinal hypersensitivity: a review., Aust. Dent. J. 51 (2006) 212–8; quiz 276. http://www.ncbi.nlm.nih.gov/pubmed/17037886 (accessed November 13, 2018).

[4] Dentin Hypersensitivity: A Review of its Treatment Modalities, (2021). https://doi.org/10.21276/aimdr.2021.7.3.DE3.

[5] J. won Kim, J.C. Park, Dentin hypersensitivity and emerging concepts for treatments, J. Oral Biosci. 59 (2017) 211–217. https://doi.org/10.1016/J.JOB.2017.09.001.

[6] T. Soundara, S. Giacoppo, R. Iori, G. Rosalinda, D. Nicola, G. Grassi, F. Pollastro, P. Bramanti, E. Mazzon, Fitoterapia Anti-in fl ammatory and antioxidant effects of a combination of cannabidiol and moringin in LPS-stimulated macrophages, Fitoterapia. 112 (2016) 104–115. https://doi.org/10.1016/j.fitote.2016.05.008.

[7] C.H. Thiesen, R. Rodrigues Filho, L.H.M. Prates, N. Sartori, C.H. Thiesen, R. Rodrigues Filho, L.H.M. Prates, N. Sartori, The influence of desensitizing dentifrices on pain induced by in-office bleaching, Braz. Oral Res. 27 (2013) 517–523. https://doi.org/10.1590/S1806-83242013000600012.

[8] S. Atalay, I. Jarocka-Karpowicz, E. Skrzydlewska, Antioxidative and Anti-Inflammatory Properties of Cannabidiol, Antioxidants 2020, Vol. 9, Page 21. 9 (2019) 21. https://doi.org/10.3390/ANTIOX9010021.

[9] R.S. Borges, A.B.F. Silva, Chapter e12 - Cannabidiol as an Antioxidant, Elsevier Inc., 2017. https://doi.org/10.1016/B978-0-12-800756-3/00093-4.

[10] S.A. Millar, R.F. Maguire, A.S. Yates, S.E. O'sullivan, Towards better delivery of cannabidiol (Cbd), Pharmaceuticals. 13 (2020) 1–15. https://doi.org/10.3390/ph13090219.

[11] Z. Drulis-Kawa, A. Dorotkiewicz-Jach, Liposomes as delivery systems for antibiotics, Int. J. Pharm. 387 (2010)

187–198. https://doi.org/10.1016/j.ijpharm.2009.11.033.
[12] G. Bozzuto, A. Molinari, Liposomes as nanomedical devices, Int. J. Nanomedicine. 10 (2015) 975–999. https://doi.org/10.2147/IJN.S68861.
[13] C. Babot-Marquillas, M.J. Sánchez-Martín, J. Rodríguez-Martínez, J. Estelrich, M.A. Busquets, M. Valiente, Flash tooth whitening: A friendly formulation based on a nanoencapsulated reductant, Colloids Surfaces B Biointerfaces. 195 (2020) 111241. https://doi.org/10.1016/j.colsurfb.2020.111241.
[14] H. Cai, Y.L. Huang, D. Li, Biological metal–organic frameworks: Structures, host–guest chemistry and bio-applications, Coord. Chem. Rev. (2019). https://doi.org/10.1016/j.ccr.2017.12.003.
[15] M.D. Allendorf, V. Stavila, Crystal engineering, structure-function relationships, and the future of metal-organic frameworks, CrystEngComm. 17 (2015) 229–246. https://doi.org/10.1039/c4ce01693a.
[16] K. Sun, L. Li, X.L. Yu, L. Liu, Q. Meng, F. Wang, R. Zhang, Functionalization of mixed ligand metal-organic frameworks as the transport vehicles for drugs, J. Colloid Interface Sci. 486 (2017) 128–135. https://doi.org/10.1016/j.jcis.2016.09.068.
[17] L. Jiao, Y. Wang, H.L. Jiang, Q. Xu, Metal–Organic Frameworks as Platforms for Catalytic Applications, Adv. Mater. 30 (2018) 1703663. https://doi.org/10.1002/adma.201703663.
[18] B. Li, M. Chrzanowski, Y. Zhang, S. Ma, Applications of metal-organic frameworks featuring multi-functional sites, Coord. Chem. Rev. 307 (2016) 106–129. https://doi.org/10.1016/j.ccr.2015.05.005.
[19] R. Liu, T. Yu, Z. Shi, Z. Wang, The preparation of metal-organic frameworks and their biomedical application, Int. J. Nanomedicine. 11 (2016) 1187–1200. https://doi.org/10.2147/IJN.S100877.
[20] U. Bulbake, S. Doppalapudi, N. Kommineni, W. Khan, Liposomal Formulations in Clinical Use: An Updated Review, Pharmaceutics. 9 (2017) 12. https://doi.org/10.3390/pharmaceutics9020012.
[21] P.-W. Yang, T.-L. Lin, Y. Hu, U.-S. Jeng, Small-Angle X-ray Scattering Studies on the Structure of Mixed DPPC/diC(7)PC Micelles in Aqueous Solutions High pressure & low temperature system View project In-situ SAXS monitoring of supercrystal formation process View project CHINESE JOURNAL OF PHYSICS Small-Angle X-ray Scattering Studies on the Structure of Mixed DPPC/diC 7 PC Micelles in Aqueous Solutions, 2012. http://psroc.phys.ntu.edu.tw/cjp (accessed January 28, 2020).
[22] C. Zylberberg, S. Matosevic, Pharmaceutical liposomal drug delivery: a review of new delivery systems and a look at the regulatory landscape, Https://Doi.Org/10.1080/10717544.2016.1177136. 23 (2016) 3319–3329. https://doi.org/10.1080/10717544.2016.1177136.
[23] G. Smistad, J. Jacobsen, S.A. Sande, Multivariate toxicity screening of liposomal formulations on a human buccal cell line, Int. J. Pharm. 330 (2007) 14–22. https://doi.org/10.1016/j.ijpharm.2006.08.044.
[24] B.A. Holm, Z. Wang, E.A. Egan, R.H. Notter, Content of Dipalmitoyl Phosphatidylcholine in Lung Surfactant: Ramifications for Surface Activity, Pediatr. Res. 1996 395. 39 (1996) 805–811. https://doi.org/10.1203/00006450-199605000-00010.
[25] E. Gulcay, I. Erucar, Metal-organic frameworks for biomedical applications, in: Two-Dimensional Nanostructures Biomed. Technol., Elsevier, 2020: pp. 173–210. https://doi.org/10.1016/b978-0-12-817650-4.00006-1.
[26] G. Tiwari, R. Tiwari, A. Rai, Cyclodextrins in delivery systems: Applications, J. Pharm. Bioallied Sci. 2 (2010) 72. https://doi.org/10.4103/0975-7406.67003.
[27] Y. Han, W. Liu, J. Huang, S. Qiu, H. Zhong, D. Liu, J. Liu, Cyclodextrin-Based Metal-Organic Frameworks (CD-MOFs) in Pharmaceutics and Biomedicine, Pharmaceutics. (2018). https://doi.org/10.3390/pharmaceutics10040271.
[28] T. Higashi, D. Iohara, K. Motoyama, H. Arima, Supramolecular pharmaceutical sciences: A novel concept combining pharmaceutical sciences and supramolecular chemistry with a focus on cyclodextrin-based supermolecules, Chem. Pharm. Bull. 66 (2018) 207–216. https://doi.org/10.1248/cpb.c17-00765.
[29] M. Lodzki, B. Godin, L. Rakou, R. Mechoulam, R. Gallily, E. Touitou, Cannabidiol - Transdermal delivery and anti-inflammatory effect in a murine model, J. Control. Release. 93 (2003) 377–387. https://doi.org/10.1016/j.jconrel.2003.09.001.
[30] A. Sharma, A. Kumar, C. Li, P. Panwar Hazari, S.D. Mahajan, R. Aalinkeel, R.K. Sharma, M.T. Swihart, A cannabidiol-loaded Mg-gallate metal-organic framework-based potential therapeutic for glioblastomas, J. Mater. Chem. B. 9 (2021) 2505–2514. https://doi.org/10.1039/d0tb02780d.
[31] N.E. Pretorius, A. Power, M. Tennant, A. Forrest, D. Cozzolino, The use of vibrational spectroscopy in the geographic characterization of human teeth: a systematic review, Appl. Spectrosc. Rev. 55 (2020) 105–127. https://doi.org/10.1080/05704928.2018.1539006.
[32] E. Timchenko, P. Timchenko, L. Volova, O. Frolov, M. Zibin, I. Bazhutova, Raman spectroscopy of changes in the tissues of teeth with periodontitis, Diagnostics. 10 (2020) 1–12. https://doi.org/10.3390/diagnostics10110876.
[33] P. Sodata, J. Peerapattana, Application of near infrared spectroscopy with chemometrics for qualitative and quantitative dental caries assessment, Vib. Spectrosc. 111 (2020) 103170. https://doi.org/10.1016/j.vibspec.2020.103170.
[34] G. Jegova, R. Titorenkova, M. Rashkova, B. Mihailova, Raman and IR reflection micro-spectroscopic study of Er:YAG laser treated permanent and deciduous human teeth, J. Raman Spectrosc. 44 (2013) 1483–1490. https://doi.org/10.1002/jrs.4373.

[35] P. Dumas, G.D. Sockalingum, J. Sulé-Suso, Adding synchrotron radiation to infrared microspectroscopy: what's new in biomedical applications?, Trends Biotechnol. 25 (2007) 40–44. https://doi.org/10.1016/j.tibtech.2006.11.002.

[36] P. Seredin, D. Goloshchapov, Y. Ippolitov, J. Vongsvivut, Development of a new approach to diagnosis of the early fluorosis forms by means of FTIR and Raman microspectroscopy, Sci. Rep. 10 (2020) 1–12. https://doi.org/10.1038/s41598-020-78078-8.

[37] C.L. Song, S.G. Kazarian, Micro ATR-FTIR spectroscopic imaging of colon biopsies with a large area Ge crystal, Spectrochim. Acta - Part A Mol. Biomol. Spectrosc. 228 (2020) 117695. https://doi.org/10.1016/j.saa.2019.117695.

[38] I.S. Lurie, Capillary electrophoresis of illicit drug seizures, Forensic Sci. Int. 92 (1998) 125–136. https://doi.org/10.1016/S0379-0738(98)00012-7.

[39] E. Lipiec, K.R. Bambery, J. Lekki, M.J. Tobin, C. Vogel, D.R. Whelan, B.R. Wood, W.M. Kwiatek, SR-FTIR Coupled with Principal Component Analysis Shows Evidence for the Cellular Bystander Effect, Radiat. Res. 184 (2015) 73–82. https://doi.org/10.1667/RR13798.1.

[40] P. Seredin, D. Goloshchapov, Y. Ippolitov, J. Vongsvivut, Engineering of a Biomimetic Interface between a Native Dental Tissue and Restorative Composite and Its Study Using Synchrotron FTIR Microscopic Mapping, Int. J. Mol. Sci. 2021, Vol. 22, Page 6510. 22 (2021) 6510. https://doi.org/10.3390/IJMS22126510.

[41] P. Seredin, D. Goloshchapov, V. Kashkarov, Y. Ippolitov, I. Ippolitov, J. Vongsvivut, To the Question on the Use of Multivariate Analysis and 2D Visualisation of Synchrotron ATR-FTIR Chemical Imaging Spectral Data in the Diagnostics of Biomimetic Sound Dentin/Dental Composite Interface, Diagnostics 2021, Vol. 11, Page 1294. 11 (2021) 1294. https://doi.org/10.3390/DIAGNOSTICS11071294.

[42] S. Diez-García, M.-J. Jesús Sánchez-Martín, J.M. Amigo, M. Valiente, Combination of Two Synchrotron Radiation-Based Techniques and Chemometrics to Study an Enhanced Natural Remineralization of Enamel, Anal. Chem. (2022). https://doi.org/10.1021/ACS.ANALCHEM.1C05498.

[43] T.J. Raharjo, W. Te Chang, Y.H. Choi, A.M.G. Peltenburg-Looman, R. Verpoorte, Olivetol as product of a polyketide synthase in *Cannabis sativa* L, Plant Sci. 166 (2004) 381–385. https://doi.org/10.1016/J.PLANTSCI.2003.09.027.

[44] B. Liu, Y. He, L. Han, V. Singh, X. Xu, T. Guo, F. Meng, X. Xu, P. York, Z. Liu, J. Zhang, Microwave-Assisted Rapid Synthesis of γ-Cyclodextrin Metal-Organic Frameworks for Size Control and Efficient Drug Loading, Cryst. Growth Des. 17 (2017) 1654–1660. https://doi.org/10.1021/acs.cgd.6b01658.

[45] M. Najlah, A.S. Suliman, I. Tolaymat, S. Kurusamy, V. Kannappan, A.M.A. Elhissi, W. Wang, Development of injectable PEGylated liposome encapsulating disulfiram for colorectal cancer treatment, Pharmaceutics. 11 (2019) 1–16. https://doi.org/10.3390/pharmaceutics11110610.

[46] R.A. Smaldone, R.S. Forgan, H. Furukawa, J.J. Gassensmith, A.M.Z. Slawin, O.M. Yaghi, J.F. Stoddart, Metalorganic frameworks from edible natural products, Angew. Chemie - Int. Ed. 49 (2010) 8630–8634. https://doi.org/10.1002/anie.201002343.

[47] N.A. Khan, S.H. Jhung, Synthesis of metal-organic frameworks (MOFs) with microwave or ultrasound: Rapid reaction, phase-selectivity, and size reduction, Coord. Chem. Rev. 285 (2015) 11–23. https://doi.org/10.1016/j.ccr.2014.10.008.

[48] M.L. Briuglia, C. Rotella, A. McFarlane, D.A. Lamprou, Influence of cholesterol on liposome stability and on *in vitro* drug release, Drug Deliv. Transl. Res. 5 (2015) 231–242. https://doi.org/10.1007/s13346-015-0220-8.

[49] Y. Jia, H. Joly, A. Omri, Liposomes as a carrier for gentamicin delivery: Development and evaluation of the physicochemical properties, Int. J. Pharm. 359 (2008) 254–263. https://doi.org/10.1016/j.ijpharm.2008.03.035.

[50] S. Kaddah, N. Khreich, F. Kaddah, C. Charcosset, H. Greige-Gerges, Cholesterol modulates the liposome membrane fluidity and permeability for a hydrophilic molecule, Food Chem. Toxicol. 113 (2018) 40–48. https://doi.org/10.1016/J.FCT.2018.01.017.

[51] Y. Chen, K. Tai, P. Ma, J. Su, W. Dong, Y. Gao, L. Mao, J. Liu, F. Yuan, Novel γ-cyclodextrin-metal–organic frameworks for encapsulation of curcumin with improved loading capacity, physicochemical stability and controlled release properties, Food Chem. 347 (2021). https://doi.org/10.1016/j.foodchem.2020.128978.

[52] Z. Hu, S. Li, S. Wang, B. Zhang, Q. Huang, Encapsulation of menthol into cyclodextrin metal-organic frameworks: Preparation, structure characterization and evaluation of complexing capacity, Food Chem. 338 (2021) 127839. https://doi.org/10.1016/j.foodchem.2020.127839.

[53] G. Zhang, F. Meng, Z. Guo, T. Guo, H. Peng, J. Xiao, B. Liu, V. Singh, S. Gui, P. York, W. Qian, L. Wu, J. Zhang, Enhanced stability of vitamin A palmitate microencapsulated by γ-cyclodextrin metal-organic frameworks, J. Microencapsul. 35 (2018) 249–258. https://doi.org/10.1080/02652048.2018.1462417.

[54] E. Garskaite, K.A. Gross, S.W. Yang, T.C.K. Yang, J.C. Yang, A. Kareiva, Effect of processing conditions on the crystallinity and structure of carbonated calcium hydroxyapatite (CHAp), CrystEngComm. 16 (2014) 3950–3959. https://doi.org/10.1039/c4ce00119b.

[55] L. Bachmann, R. Diebolder, R. Hibst, D.M. Zezell, Infrared absorption bands of enamel and dentin tissues from human and bovine teeth, Appl. Spectrosc. Rev. 38 (2003) 1–14. https://doi.org/10.1081/ASR-120017479.

[56] M. Anwar Alebrahim, C. Krafft, W. Sekhaneh, B. Sigusch, J. Popp, ATR-FTIR and Raman spectroscopy of

primary and permanent teeth, Biomed. Spectrosc. Imaging. 3 (2014) 15–27. https://doi.org/10.3233/bsi-130059.
[57] F. Taube, M. Marczewski, J.G. Norén, Deviations of inorganic and organic carbon content in hypomineralised enamel, J. Dent. 43 (2015) 269–278. https://doi.org/10.1016/j.jdent.2014.09.003.
[58] J. Gan, S. Liu, L. Zhou, Y. Wang, J. Guo, C. Huang, Effect of Nd:YAG laser irradiation pretreatment on the long-term bond strength of etch-and-rinse adhesive to dentin, Oper. Dent. 42 (2017) 62–72. https://doi.org/10.2341/15-268-L.
[59] P. Fattibene, A. Carosi, V. De Coste, A. Sacchetti, A. Nucara, P. Postorino, P. Dore, A comparative EPR, infrared and Raman study of natural and deproteinated tooth enamel and dentin, Phys. Med. Biol. 50 (2005) 1095–1108. https://doi.org/10.1088/0031-9155/50/6/004.
[60] I.H. Kim, J.S. Son, B.K. Min, Y.K. Kim, K.H. Kim, T.Y. Kwon, A simple, sensitive and non-destructive technique for characterizing bovine dental enamel erosion: attenuated total reflection Fourier transform infrared spectroscopy, Int. J. Oral Sci. 2016 81. 8 (2016) 54–60. https://doi.org/10.1038/ijos.2015.58.
[61] C.A.M. France, N. Sugiyama, E. Aguayo, Establishing a preservation index for bone, dentin, and enamel bioapatite mineral using ATR-FTIR, J. Archaeol. Sci. Reports. 33 (2020) 102551. https://doi.org/10.1016/J.JASREP.2020.102551.
[62] J.D. McGuire, M.P. Walker, V. Dusevich, Y. Wang, J.P. Gorski, Enamel organic matrix: potential structural role in enamel and relationship to residual basement membrane constituents at the dentin enamel junction, Connect. Tissue Res. 55 (2014) 33. https://doi.org/10.3109/03008207.2014.923883.
[63] S. González-López, C. Torres-Rodríguez, V. Bolaños-Carmona, P. Sanchez-Sanchez, A. Rodríguez-Navarro, P. Álvarez-Lloret, M. Domingo Garcia, Effect of 30 % hydrogen peroxide on mineral chemical composition and surface morphology of bovine enamel., Odontology. 104 (2014) 44–52. https://doi.org/10.1007/S10266-014-0189-7.
[64] C. Xu, R. Reed, J.P. Gorski, Y. Wang, M.P. Walker, The Distribution of Carbonate in Enamel and its Correlation with Structure and Mechanical Properties, J. Mater. Sci. 47 (2012) 8035–8043. https://doi.org/10.1007/S10853-012-6693-7.
[65] M. Shahmoradi, L.E. Bertassoni, H.M. Elfallah, M. Swain, Fundamental Structure and Properties of Enamel, Dentin and Cementum, (2014) 511–547. https://doi.org/10.1007/978-3-642-53980-0_17.
[66] T. Sakae, Variations in Dental Enamel Crystallites and Micro-Structure, J. Oral Biosci. 48 (2006) 85–93. https://doi.org/10.1016/S1349-0079(06)80021-6.
[67] C. de C.A. Lopes, P.H.J.O. Limirio, V.R. Novais, P. Dechichi, Fourier transform infrared spectroscopy (FTIR) application chemical characterization of enamel, dentin and bone, Appl. Spectrosc. Rev. 53 (2018) 747–769. https://doi.org/10.1080/05704928.2018.1431923.
[68] H.F. Shurvell, Spectra- Structure Correlations in the Mid- and Far-Infrared, 2006. https://doi.org/10.1002/0470027320.s4101.
[69] N. Pleshko, A. Boskey, R. Mendelsohn, Novel infrared spectroscopic method for the determination of crystallinity of hydroxyapatite minerals, Biophys. J. 60 (1991) 786–793. https://doi.org/10.1016/S0006-3495(91)82113-0.

Appendices – Supporting information

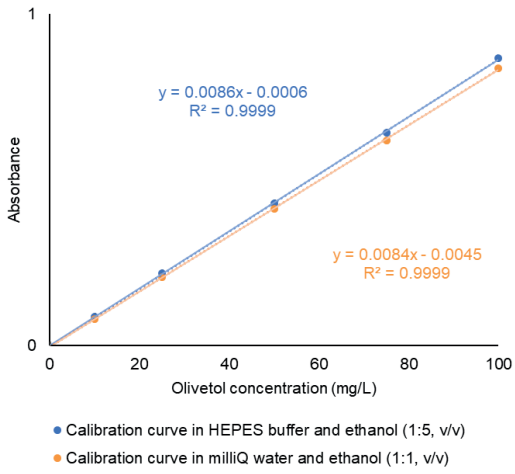

Figure A.1: Calibration curves of different known concentrations of olivetol from 0 to 100 mg/L in HEPES buffer and ethanol (1:5, v/v) (blue) and milliQ water and ethanol (1:1, v/v) (orange) media for the quantification of the drug in DPPC liposomes and MOFs, respectively.

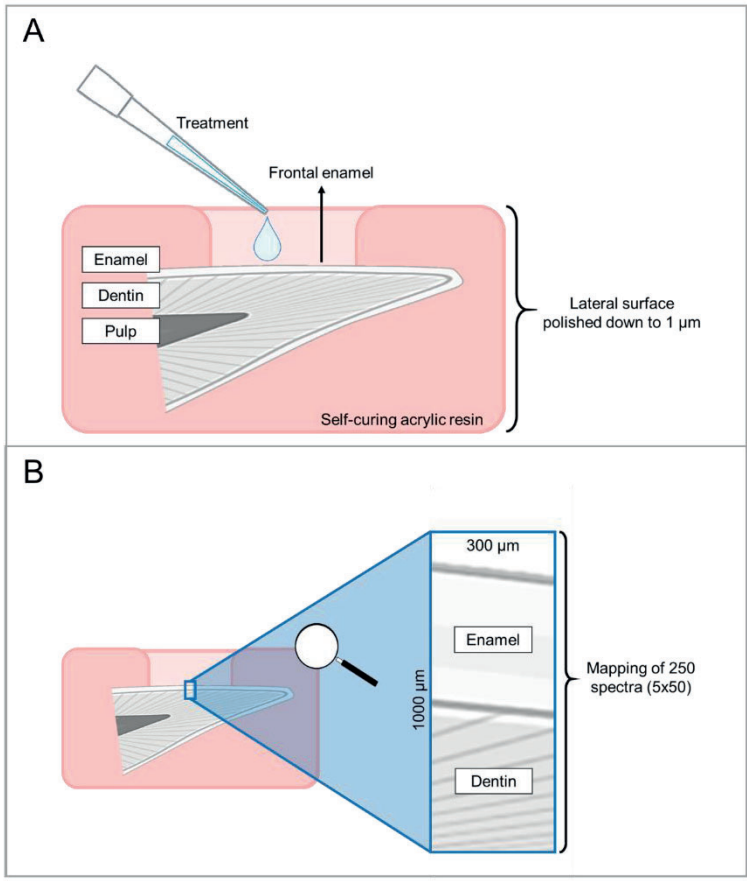

Figure A.2: Sample preparation and treatment application over the teeth diagram (A) and synchrotron source infrared spectroscopy measurements procedure (B).

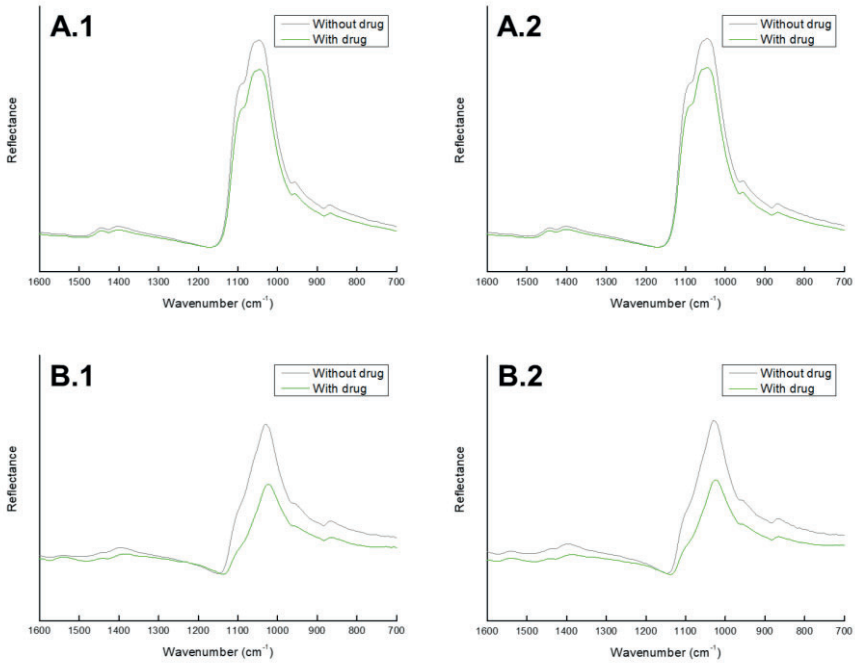

Figure A.3: Average of the spectra of the groups with and without drug for liposomes (1) and MOFs (2) in the enamel (A) and the dentin (B).

De familia de agricultores y ganaderos.

En cierto modo, no dejan de ser científicos rurales de la época, que sienten mucho amor y afición por lo que hacen, pero que también dedican mucho esfuerzo y sacrificio.

Todo lo que somos se lo debemos a ellos.

Villafañe (León, 1965)